Aalborg Universitet

AALBORG UNIVERSITY
DENMARK

Real-time Modelling, Diagnostics and Optimised MPPT for Residential PV Systems

Sera, Dezso

Publication date:
2009

Document Version
Publisher's PDF, also known as Version of record

Link to publication from Aalborg University

Citation for published version (APA):
Sera, D. (2009). *Real-time Modelling, Diagnostics and Optimised MPPT for Residential PV Systems*. Institut for Energiteknik, Aalborg Universitet.

General rights
Copyright and moral rights for the publications made accessible in the public portal are retained by the authors and/or other copyright owners and it is a condition of accessing publications that users recognise and abide by the legal requirements associated with these rights.

? Users may download and print one copy of any publication from the public portal for the purpose of private study or research.
? You may not further distribute the material or use it for any profit-making activity or commercial gain
? You may freely distribute the URL identifying the publication in the public portal ?

Take down policy
If you believe that this document breaches copyright please contact us at vbn@aub.aau.dk providing details, and we will remove access to the work immediately and investigate your claim.

Downloaded from vbn.aau.dk on: November 29, 2020

Real-time Modelling, Diagnostics and Optimised MPPT for Residential PV systems

by

Dezső Séra

Dissertation submitted to the Faculty of Engineering, Science & Medicine at Aalborg University
in partial fulfilment of the requirements for the degree of
Doctor of Philosophy in Electrical Engineering

Aalborg University
Institute of Energy Technology
Denmark, January 2009

AALBORG UNIVERSITY
Institute of Energy Technology
Pontoppidanstræde 101
DK-9220 Aalborg East
Phone: +45 9940 9240
Fax +45 9815 1411
http://www.iet.aau.dk

Copyright © Dezső Séra, 2009

Printed in Denmark by UniPrint

ISBN: 978-87-89179-76-6

This thesis has been typeset in LaTeX 2_ε.

Preface

This thesis is written under the research project *PSO-5854*, entitled *Real-time Modelling, Diagnostics and Optimised MPPT for Residential PV systems*, supported by the Danish Government and Energinet.dk, in collaboration with PowerLynx (Danfoss Solar). Acknowledgments are given to the above-mentioned institutions.

The research project was carried out under the supervision of Professor Remus Teodorescu from the Institute of Energy Technology, Aalborg University. First of all, I am deeply grateful to him for both the professional support and direction he gave me throughout the project period, as well as his open-mindedness and earnesty.

I would like to thank Professor Frede Blaabjerg, my co-supervisor in the first year of my PhD programme, for his guidance and advice during that period. I would also like to express my appreciation to Uffe Borup from Danfoss Solar for his helpful comments and suggestions during steering meetings. To Professor Yahia Baghzouz I would like to extend my gratitude for the support and consideration he gave me during my study abroad period at University of Nevada Las Vegas, USA. I am also thankful to Professor Vassilios Agelidis for his useful counsel and constructive criticism.

To Professor Maria Imecs, I would like to thank for all the support and guidance during the years at the Technical University of Cluj, Romania.

Particular thanks go to all my colleagues and especially to my fellow PhD students from the Institute of Energy Technology for the lively environment and camaraderie.

To Ashley Stewart, who incessantly proof-read my thesis: thank you very much for your assistance and for alleviating some of the strain of this thesis.

And finally, to my family, I would like to articulate my deepest gratitude for the unceasing confidence and encouragement which I have received from them throughout my life.

The errors and inconsistencies remain my own.

Aalborg, February 2009

Dezső Séra

Abstract

The work documented in this thesis has been focused into two main sections. The first part is centred around Maximum Power Point Tracking (MPPT) techniques for photovoltaic arrays, optimised for fast-changing environmental conditions, and is described in Chapter 2. The second part is dedicated to diagnostic functions as an additional tool to maximise the energy yield of photovoltaic arrays (Chapter 4). Furthermore, mathematical models of PV panels and arrays have been developed and built (detailed in Chapter 3) for testing MPPT algorithms, and for diagnostic purposes.

In Chapter 2 an overview of the today's most popular MPPT algorithms is given, and, considering their difficulty in tracking under variable conditions, a simple technique is proposed to overcome this drawback. The method separates the MPPT perturbation effects from environmental changes and provides correct information to the tracker, which is therefore not affected by the environmental fluctuations. The method has been implemented based on the Perturb and Observe ($P\&O$), and the experimental results demonstrate that it preserves the advantages of the existing tracker in being highly efficient during stable conditions, having a simple and generic nature, and has the benefit of also being efficient in fast-changing conditions. Furthermore, the algorithm has been successfully implemented on a commercial PV inverter, currently on the market. In Chapter 3, an overview of the existing mathematical models used to describe the electrical behaviour of PV panels is given, followed by the parameter determination for the five-parameter single-exponential model based on datasheet values, which has been used for the implementation of a PV simulator taking in account the shape, size ant intensity of partial shadow in respect to bypass diodes.

In order to eliminate the iterative calculations for parameter determinations, a simplified three-parameter model is used throughout Chapter 4, dedicated to diagnostic functions of PV panels. Simple analytic expressions for the model important parameters, which could reflect deviations from the normal (e.g. from datasheet or reference measurement) $I-V$ characteristic, is proposed.

A considerable part of this thesis is dedicated to the diagnostic functions of crystalline photovoltaic panels, aimed to detect failures related to increased series resistance and partial shadowing, the two major factors responsible for yield-reduction of residential photovoltaic systems.

Combining the model calculations with measurements, a method to detect changes in the panels' series resistance based on the slope of the $I - V$ curve in the vicinity of open-circuit conditions and scaled to Standard Test Conditions (STC) , is proposed. The results confirm the benefits of the proposed method in terms of robustness to irradiance changes and to partial shadows.

In order to detect partial shadows on PV panels, a method based on equivalent thermal voltage (V_t) monitoring is proposed. V_t is calculated using the simplified three-parameter model, based on experimental curve. The main advantages of the method are the simple expression for V_t, high sensitivity to even a relatively small area of partial shadow and very good robustness against changes in series resistance.

Finally, in order to quantify power losses due to different failures, e.g. partial shadows or increased series resistance, a model based approach has been proposed to estimate the panel rated power (in STC). Although it is known that the single-exponential model has low approximation precision at low irradiation conditions, using the previously determined parameters it was possible to achieve relatively good accuracy. The main advantage of the method is that it relies on already determined parameters (R_{sm}, V_t) based on measurements, therefore reducing the errors introduced by the limitation of the single-exponential model especially at low irradiation conditions.

Contents

List of Figures

List of Tables

List of Symbols and Abbreviations

A ..... Diode ideality (quality) factor. Characterises how closely the diode characteristics follows the ideal diode equation. Accounts for the recombination in the space-charge region, page 25

A_{meas} ..... Area under the measured $I - V$ curve, page 35

A_{sim} ..... Area under the simulated $I - V$ curve, page 35

CV ..... Constant Voltage MPPT method, page 14

FF ..... Fill factor, page 40

G ..... Irradiation (W/m^2), page 29

$I - V$ ..... Current-voltage, page v

I_0 ..... Dark saturation current of a PV cell, page 24

I_{01} ..... Dark saturation current of the first diode in the double-diode model, responsible for the diffusion current component, page 26

I_{02} ..... Dark saturation current of the second diode in the double-diode model, responsible for the recombination in the space charge region, page 26

I_{mp} ..... Current at the Maximum Power Point, page 12

I_{ph} ..... Photo-generated current, page 25

I_{sc} ..... Short-circuit current of the cell or module, page 27

$P - V$ ..... Power-voltage characteristic, page 29

PS ..... Partial shadow, page 40

$P\&O$ ..... Perturb and Observe, page v

P_k ..... Power sampled at the k-th sampling instance, page 15

$P_{PV\_meas\_mean}$ ... Mean of the measured PV power (over a specified time period), page 16

P_{k+1} ..... Power sampled at the $k+1$-th sampling instance, page 15

P_{mpB} ..... represents the base value for calculating dependency of rated power estimation on various irradiation conditions. It is a result of an estimation at irradiation conditions close to $1kW/m^2$ with temperature compensation to STC, page 57

P_{mp_mean} ..... Mean of the ideal (MPP) power (over a specified time period), page 16

P_{mp} ..... Power at MPP of the cell or module, page 27

R_s ..... Module internal series resistance, page 24

R_{oc} ..... Series resistance defined by the slope of the $I - V$ curve at open-circuit

conditions, page 41

R_{seAct} ..... Estimated series resistance based on the slope of the $I - V$ curve at open-circuit in actual environmental conditions., page 43

R_{seB} ..... Base value for calculating dependency of series resistance estimation on various irradiation conditions. It is a result of an estimation at irradiation conditions close to $1kW/m^2$ with temperature compensation to STC., page 45

R_{seSTC} ..... Estimated effective series resistance of the panel, with compensation for the environmental effects, page 45

R_{seSTC} ..... Estimated series resistance based on the slope of the $I - V$ curve at open-circuit in STC., page 43

R_{se} ..... The PV panel equivalent estimated series resistance, page 42

R_{sh} ..... Module shunt resistance, page 25

R_{sm} ..... Equivalent series resistance of the panel's model, page vi

R_{sm} ..... Series resistance as model parameter, page 43

T ..... Absolute temperature (^oK), page 25

T_p ..... MPPT perturbation period, page 15

T_{Act} ..... Actual temperature, page 45

T_{STC} ..... STC temperature, page 45

ThN ..... Negative threshold for the MPPT algorithm to change the perturbation direction, page ix

ThN ..... Negative threshold for the MPPT algorithm to change the perturbation direction, page 20

ThP ..... Threshold for the MPPT algorithm, over which it is considered that the last perturbation caused an increase of power, page ix

ThP ..... Threshold for the MPPT algorithm, over which it is considered that the last perturbation caused an increase of power, page 20

V_t ..... Thermal voltage of PV module, page vi

V_{br} ..... Breakdown voltage of the cell junction, page 28

$V_{dc}ref$ ..... MPPT voltage reference, page 19

V_{mp} ..... Voltage at the Maximum Power Point, page 12

V_{oc} ..... Open-circuit voltage of the PV panel or array, page 14

V_{tAct} ..... Thermal voltage calculated based on measurement taken in the actual environmental conditions., page 45

V_{tSTC} ..... Thermal voltage calculated based on STC measurement., page 45

ε_{Area} ..... Area fitting error between of the simulated characteristic to measured one, page 35

a ..... Fraction of the ohmic current in avalanche breakdown, page 28

dP ..... Change of power caused by the perturbation of the MPPT, page 15

$dP - P\&O$ ..... Optimised Perturb and Observe with additional dP calculation, page 16
dP_1 ..... Change of power caused by the perturbation of the MPPT plus the irradiance change, in the first half of the MPPT period, page 16
dP_2 ..... Change of power caused by the irradiance change, page 15
inc ..... Perturbation increment of the MPPT, page 15
k ..... Boltzmann's constant, page 24
k_i ..... Temperature coefficient of module short-circuit current, page 27
k_v ..... Temperature coefficient of module open-circuit voltage, page 27
m ..... Avalanche breakdown exponent, page 28
n_s ..... Number of series connected cells in the module, page 24
q ..... charge of an electron, page 24
DPGS ..... Distributed Power Generation Systems, page 4
IEA-PVPS ..... International Energy Agency-Photovoltaic Power Systems Programme, page 5
INC ..... Incremental Conductance MPPT method, page 12
LC ..... Inductance - Capacitance, page 9
MPP ..... Maximum Power Point, page 5
MPPT ..... Maximum Power Point Tracking, page v
STC ..... Standard Test Conditions - Testing conditions to measure photovoltaic cells or modules nominal output power. Irradiance level is $1000W/m^2$, with the reference air mass 1.5 solar spectral irradiance distribution and cell or module junction temperature of 25^oC., page vi

Part I

Report

Chapter 1

Introduction

This chapter presents the background and motivation of the work documented in this thesis, and includes a short overview of the current status of photovoltaic technology, focusing on grid connected photovoltaic systems. This is followed by project's objectives and limitations. Finally, an outline of the thesis is provided at the end of the chapter.

1.1 Background

Renewable energy generation has experienced consistent growth in the last two decades, motivated by the concerns of climate change and high oil prices, and supported by renewable energy legislation and incentives, with a close to $150 billion investment in 2007 [6].

Solar photovoltaics is one of the fastest growing energy technologies, with an average annual growth of about 40% in the past decade. [1,7–9]. The 2.6GW installed capacity in 2007 implies an increase of more than 50% compared to the previous year and has lead to a total capacity of 7.8GW photovoltaic power worldwide [1] (Fig. 1.1(a)). Similarly high grow rate has been registered in the past few decades for the wind power industry as well, with an approximately 30% increase in 2007 [10].

Despite the technological advances and governmental incentives, the cost of energy produced

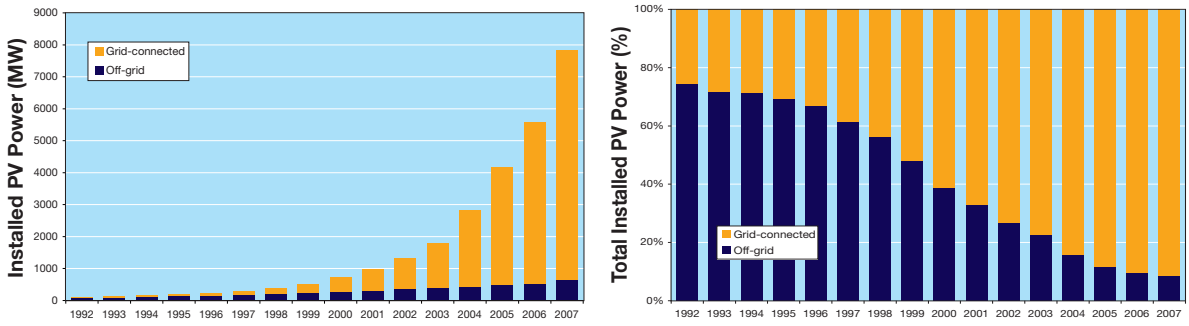

(a) (b)

Figure 1.1: *Cumulative installed (a) and percentage of grid connected and off-grid (b) PV power in the 'International Energy Agency - Photovoltaic Power Systems Programme' (IEA-PVPS) reporting countries [1].*

by grid connected PV systems is still relatively high and cannot compete yet with traditional wholesale electricity prices [9,11,12]. This motivates the research for creating not only improved solar panels but also more efficient power converters which can extract close to 100% of the available power from the photovoltaic array [5, 13–15].

1.1.1 Current status of photovoltaic technology

Photovoltaic solar electricity, together with solar thermal, has the highest potential of all the renewable energies, since solar energy is a practically unlimited resource, available everywhere [16].

Humanity have recognised the power in the sun's rays as early as the 3^{rd} century B.C., when magnifying glasses were used to light torches [17]. The photovoltaic effect was discovered by the French scientist Edmond Becquerel in 1839, but it was only explained in 1905 by a publication of Albert Einstein for which he won his Nobel-prize in 1921 [17]. The modern era of photovoltaics can be dated from 1954, when scientists at Bell Labs developed the first silicone PV cell [13,17]. From the end of the 1950s, solar cells for space applications have been produced. Terrestrial applications of photovoltaics started to spread at the beginning of the 1970s.

Today a large variety of photovoltaic generators from mW- range for scientific calculators, through several kW residential applications, to tens of MW- scale photovoltaic power plants, are in operation all over the world.

The vast majority, close to 90%, of photovoltaic modules are currently produced using wafer-based crystalline silicone [13, 18], but there are other emerging technologies which are gaining importance in the PV market. In recent years thin-film modules have earned share in the PV market, taking advantage of the photovoltaic-grade silicone shortage and consequently the higher prices in the PV market [9]. Concentrator PV technology tries to decrease the amount of semiconductor necessary, by using small-area high-efficiency cells and inexpensive polymer lenses to focus the light on the cell. This technology generally needs a sun-tracking system [9] and it is more suitable for medium to large PV systems [11] in areas with a high percentage of direct radiation [19].

Photovoltaic energy has the potential to play an important role in the transition towards a sustainable energy supply system in the 21^{st} century, to cover a significant share of the electricity needs of Europe [13], and is expected to be one of the key energy technologies of this century [16].

Grid connected photovoltaic systems

The terrestrial applications of photovoltaic systems are usually divided int four primary categories [1,7,8]: off-grid domestic systems, off-grid non-domestic installations, grid-connected distributed PV systems, and grid-connected centralised systems.

When terrestrial applications began, the main market for PV was remote industrial and household applications [16]. However the penetration of PV systems as Distributed Power Generation Systems (DPGS) , (i.e. power generators connected directly to the low-voltage grid of

the buildings) has increased dramatically in the last decades. The proportion of grid-connected PV systems installed - in the International Energy Agency-Photovoltaic Power Systems Programme (IEA-PVPS) reporting countries - rose from approximately 25% in 1992 to about 94% in 2007 [1, 9] (Fig. 1.1(b)).

The efficiency of a grid-connected (residential) PV system is higher than that of a stand-alone one, as it is not limited by battery storage capacity, and surplus electricity generated can always be fed into the utility grid [20]. This also saves the cost of battery storage [20].

PV plants in grid connected applications are tied to the grid via power conditioning units (inverters) of several technological concepts. These inverters play a key role in energy efficiency since their task is not only to convert the generated electricity to the desired frequency and voltage with the highest possible efficiency, but also to operate the PV array at the Maximum Power Point (MPP) . A classification of PV inverter topologies can be found in Publication 3.

1.1.2 Project motivations

Photovoltaic electricity generation offers the benefits of: clean, non-polluting energy generation, production of energy close to the consumer (in case of DPGS), the very little or no maintenance requirement, and of having a very long lifetime. Due to these advantages, today, the photovoltaic is one of the fastest growing market in the world [6]. However, PV power is still considered to be expensive, and the cost reduction of PV systems is subject to extensive research. From the point of view of power electronics, this goal can be approached by maximising the energy output of a given PV array. The inverter should ensure the highest possible conversion efficiency, while the requirement for the MPPT control (see Fig. 1.2) is to operate the PV array at the optimum working point (MPP) in all environmental conditions. A considerable amount of PV capacity today is installed in temperate climate zones, i.e. Central and Northern Europe, where passing clouds are often present on the sky, producing varying irradiation conditions for PV installations. Although modern PV inverters' MPPT efficiency is very high

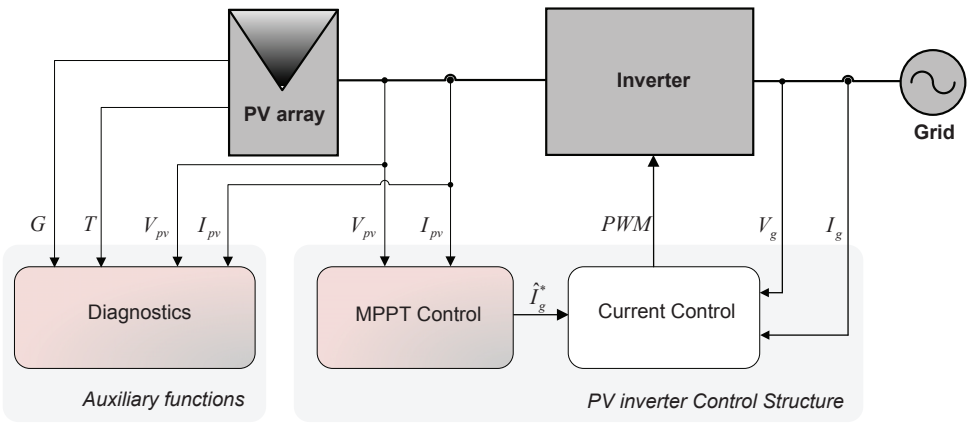

Figure 1.2: *Block diagram of PV system control structure with additional diagnostic functions.*

in stable conditions, further research is needed to achieve similar performance levels in variable conditions.

The 7.8GW installed capacity means an enormous number of photovoltaic panels, in the order of tens of millions, operating today. As the number of panels and operating time increases, the insuring of optimal operating conditions is becoming more crucial, in order to minimise production losses due to system failures or external reasons, such as dirt, or shadows. This creates the new challenge of performance monitoring and diagnostics for PV modules and arrays.

1.2 Project objectives

In accordance with the need to maximise the energy output of PV systems, the project has two main objectives:

- *to develop high efficiency MPPT strategies, suitable for fast changing environmental conditions typical to northern Europe, in order to increase efficiency during fluctuating conditions*
- *to develop diagnostic functions of the photovoltaic arrays, which, based on the electrical characteristics of the panels can provide information about the operational state of the system, enabling immediate remedy in case of faults*

1.3 Project limitations

Although there is a large number of PV inverter topologies present in the literature and on the market, only a single-stage topology is considered here, as is shown in Fig 1.2. The algorithm developed here can be used for different topologies and control structures, however, in that case, adaptation to the current topology or control structure might be necessary.

The experimental tests of the proposed MPP tracker have been carried out using programmable DC power supplies, which can only approximate the behaviour of a real PV array(Publication 1, 2).

As described in §1.1.1, there are a number of different PV cell materials and technologies in operation today. However, taking in account that close to 90% of the modules worldwide are based on flat-panel crystalline silicone cells, for modelling and diagnostic purposes only crystalline silicone cells were considered.

Although a typical grid-connected residential PV system implies several panels connected in series and/or parallel, the modelling and diagnostic methods developed in this thesis have been tested on (different) single panels, implying 2-4 bypass-diode protected submodules.

1.4 Main contributions

The main contributions of this thesis can be summarised as follows:

In Chapter 2 an improved MPPT method, suitable for fast changing environmental conditions is presented, based on the well-known *P&O* method. The International PHOTON Magazine test results of a commercial PV inverter using this method showed an MPPT efficiency of over 99%, with a particularly fast response, making it the best performing MPP tracker in a survey of the most important manufacturers of PV inverters worldwide in 2008. [21].

In Chapter 3 a real-time PV simulator implementation is proposed, which takes into consideration the size and shape of the shadow falling onto the panel, suitable for evaluating partial shadow effects on the output power of PV arrays. Additionally, simplified analytic formulae for determination of the panel model parameters based on the four-parameter model for diagnostic purposes, have been proposed.

In Chapter 4 simple analytic formulae for the panel's model parameters are proposed, enabling real-time parameter estimations for diagnostic functions of PV panels.

In the same chapter a simple method for estimating changes in PV panel's series resistance, with good robustness against environmental changes and other failures has been proposed. Experimental tests show good estimation accuracy for different panels with various values of added series resistance over a wide range of irradiations.

Another diagnostic function, aimed at detecting partial shadowing based on thermal voltage monitoring is proposed in Chapter 4. The method enables the detection of partial shadows with good sensitivity, while keeping strong robustness against changes in the panel's series resistance. The weak point of the method is that its sensitivity decreases in low irradiation conditions.

In the same chapter, a method for the panel's rated power estimation was proposed. The main benefit of this method is that it employs the previously estimated parameters based on measurements, and therefore it can quantify the overall effect of different failures, i.e. increased series resistance or a partial shadow in power loss.

1.5 Thesis outline

This thesis is divided into two main parts. **Part I** contains the report of the work carried out during the PhD project period, while **Part II** contains the relevant articles published throughout the project work. **Part I** is structured into 5 chapters, which are briefly presented in the following.

Chapter 2: Maximum Power Point Tracking for Photovoltaic Systems deals with MPPT control of grid-connected photovoltaic systems, focusing on rapidly changing environmental conditions, e.g. clouds, typical for Northern Europe. In the first part of the chapter, an overview of the most popular MPPT methods is given, with their advantages and disadvantages. In the second part, the problem of MPP tracking in fast changing irradiations is addressed. Furthermore, an MPPT method, suitable for rapidly changing environmental conditions, based on the Perturb&Observe, is presented. **Chapter 3: Modelling of PV cells and arrays** presents the most commonly used solar cell models and addresses the problem of model

parameter determination based on four- and five-parameter models.Simplified analytic formulae describing the four-parameter model for diagnostic purposes, are presented. Furthermore, the implementation of a PV simulator consisting of customisable series-parallel connected panels, suitable for testing MPPT algorithms and evaluating the effects of partial shadowing, with different shadow area and shape, is presented. **Chapter 4: Diagnostics of PV panels** deals with diagnostics of photovoltaic panels by means of analysis of their electrical characteristics. A method of series resistance estimation, robust to environmental changes, is presented, followed by partial shadowing detection through thermal voltage monitoring. Finally, temperature and rated power estimations for PV module are presented **Chapter 5: Conclusions** summarises the work which has been carried out throughout this project. The chapter ends with an outlook to further research which have been enabled by the work presented in this thesis.

1.5.1 List of publications derived from this thesis

1. D. Sera, T. Kerekes, R. Teodorescu, and F. Blaabjerg: "Improved MPPT method for rapidly changing environmental conditions", in Proc. of 2006 IEEE International Symposium on Industrial Electronics, 2006, vol. 2, pp. 1420-425.

2. D. Sera, R. Teodorescu, J. Hantschel, and M. Knoll: "Optimised maximum power point tracker for fast-changing environmental conditions", IEEE Transactions on Industrial Electronics, 2008, vol. 55, no. 7, pp. 2629-2637.

3. F. Iov, M. Ciobotaru, D. Sera, R. Teodorescu, and F. Blaabjerg: "Power electronics and control of renewable energy systems", in Proc. of 7th International Conference on Power Electronics and Drive Systems, PEDS '07. 2007, pp. P-6-P-28.

4. D. Sera, T. Kerekes, R. Teodorescu: "Teaching Maximum Power Point Trackers Using a Photovoltaic Array Model with Graphical User Interface", in Proc. of 3^{rd} IEE International Workshop on Teaching Photovoltaics, 2006.

5. D. Sera, R. Teodorescu, and P. Rodriguez: "PV panel model based on datasheet values", in Proc. of IEEE International Symposium on Industrial Electronics, ISIE 2007, pp. 2392-2396.

6. M. Valentini, A. Raducu, D. Sera, R. Teodorescu: "PV inverter test setup for European efficiency, static and dynamic MPPT efficiency evaluation", in Proc. of IEEE Optimisation of Electrical and Electronic Equipment, 2008. pp. 433-438.

7. M. Valentini, A. Raducu, and D. Sera: "Real time photovoltaic array simulator for testing grid-connected PV inverters", in Proc. of IEEE International Symposium on Industrial Electronics ISIE 2008.

8. D. Sera and Y. Baghzouz: "On the impact of partial shading on PV output power", in Proc. of the 2nd WSEAS/IASME International Conference on Renewable Energy Sources 2008.

9. D. Sera, R. Teodorescu, and P. Rodriguez: "Photovoltaic module diagnostics by series resistance monitoring and temperature and rated power estimation", in Proc. of the 34th Annual Conference of the IEEE Industrial Electronics Society, November 2008, pp. 2195-2199.

1.5.2 Tools used

In order to simulate the behaviour of different MPP trackers, the PV inverter control system has been implemented in Matlab/Simulink [22], while the electrical circuits (DC link, inverter, LC filter, Grid) have been modelled using either Simulink transfer functions, or the PLECS® toolbox for Simulink® [23]. For experimental tests the control system was implemented on the dSPACE® DS1103 PPC Controller Board [24] due to its high flexibility, considering its high computational capacity, the graphical user interface (Control Desk®), and good integration with Simulink®. The PV array has been simulated using Delta Elektronika SM300-5 [25] and SM300-10 [26] programmable DC supplies. The power has been delivered to the grid by the commercial voltage source inverter provided by Danfoss A/S [27].

Chapter 2

Maximum Power Point Tracking for Photovoltaic Systems

This chapter deals with MPPT control of grid connected photovoltaic systems, focusing on rapidly-changing environmental conditions (e.g. clouds), which is typical for Northern Europe. In the first part of the chapter an overview of the most popular MPPT methods is given, analysing their advantages and disadvantages. In the second part the problem of MPP tracking in fast-changing irradiation is addressed. Furthermore, a P&O based MPPT method, suitable for rapidly-changing environmental conditions, is presented.

2.1 Importance of MPPT for grid connected photovoltaic systems

As mentioned in Chapter 1, worldwide installed PV power capacity today is mostly dominated by grid-connected applications [1, 7, 8]. In these applications, the typical goal is to obtain the maximum possible power from the PV plant over the entire time of operation. Therefore, these systems need an MPPT, which always sets the system working point to the optimum, following the weather (i.e. solar irradiance and temperature) conditions. There are many MPPT strategies available in the literature, e.g [15, 28–36] for different converter topologies and environmental conditions (see Publication 3).

As the steady state MPPT efficiency at different irradiation levels is a figure of merit of a PV inverter, MPP trackers have been under continuous improvement. Today a commercial PV inverter has an MPPT efficiency of about 99% over a wide range of irradiation conditions. However, until recently, tracking in variable environmental conditions received little attention from manufacturers. In locations with variable cloudy conditions, fast dynamic MPP tracking can contribute a few additional percentage points to the energy yield [37]. In the last few years, test procedures for evaluating MPPT dynamic efficiencies have been proposed [5, 37–39]. In [37], Haeberlin et al. proposed a test procedure using a nearly rectangular variation of the irradiation, corresponding to variations of power from 20-100% of the rated value, with a sufficient stabilisation period (1-5 minutes) and a few intermediate stages of ≈100-200ms. However, in this thesis, a trapezoidal profile is used to test the tracking ability of the MPPT in varying environmental conditions, as rectangular variation of irradiation is seen by the MPPT

as a step change in conditions, and the new MPP is tracked *in stable conditions.*

2.2 Overview of most used MPPT algorithms

The **Perturb and Observe** is one of the so called 'hill-climbing' MPPT methods, which are based on the fact that, on the voltage-power characteristic, on the left of the MPP the variation of the power against voltage $dP/dV > 0$, while on the right, $dP/dV < 0$ (see Fig.2.1).

In Fig.2.1, if the operating voltage of the PV array is perturbed in a given direction and $dP/dV > 0$, it is known that the perturbation moved the array's operating point toward the MPP. The $P\&O$ algorithm would then continue to perturb the PV array voltage in the same direction. If $dP/dV < 0$, then the change in operating point moved the PV array away from the MPP, and the $P\&O$ algorithm reverses the direction of the perturbation [28] (Fig. 2.2).

The main advantage of the $P\&O$ method is that it is easy to implement, it has low computational demand, and it is very generic, i.e. applicable for most systems, as it does not require any information about the PV array, but only the measured voltage and current.

Because of this, the $P\&O$ today is perhaps the most-often used MPPT method [28, 40, 41]. The two main problems of the $P\&O$, frequently mentioned in the literature, are the oscillations around the MPP in steady state conditions, and poor tracking (possibly in the wrong direction, away from MPP) under rapidly-changing irradiations [15, 28, 36, 41–47]. Improvement methods for the dynamic performances of the $P\&O$ method, including variable step size and perturbation frequency have been reported in the literature [28, 43, 46, 47].

A similar hill-climbing MPPT algorithm is the **Incremental Conductance** (INC) [48], which intends to improve the $P\&O$ by replacing the derivative of the power versus voltage dP/dV used by the $P\&O$ with comparing the PV array instantaneous (I/V) and incremental (dI/dV) conductances, according to equations (2.1) and (2.2).

$$\frac{dP}{dV} = \frac{d(VI)}{dV} = V\frac{dI}{dV} + I \tag{2.1}$$

$$\left.\frac{dP}{dV}\right|_{\substack{I=I_{mp}\\V=V_{mp}}} = 0 \Rightarrow \left.\frac{dI}{dV}\right|_{\substack{I=I_{mp}\\V=V_{mp}}} = -\frac{I_{mp}}{V_{mp}} \tag{2.2}$$

where

- V_{mp} - MPP voltage of the array
- I_{mp} - MPP current of the array

It is a generally accepted property of the INC that it can find the distance to the MPP and can determine when the MPP has been reached and hence stop the perturbation [28, 45, 49], thus performing superiorly to the $P\&O$. However, as it has been pointed out already by the authors [48], in practice the equality in Eq. (2.2) is seldom obtained and therefore either a small marginal error has to be allowed [48] - which will limit the sensitivity of the tracker - or

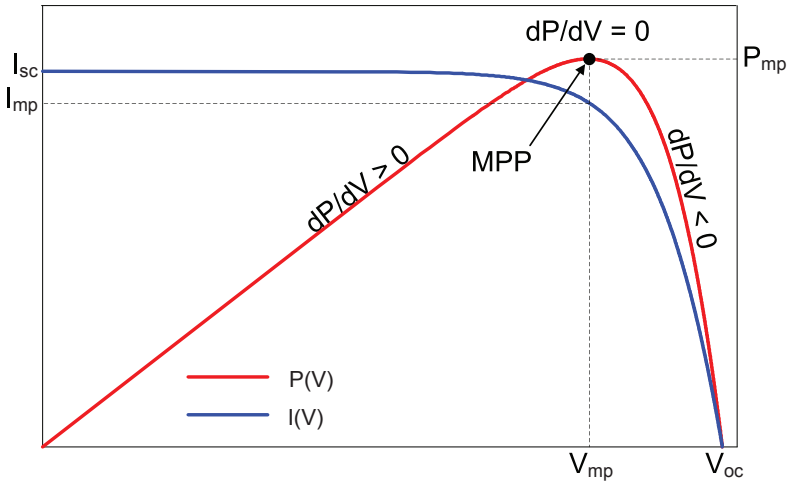

Figure 2.1: *Sign of dP/dV at different positions on the power characteristic of a PV module*

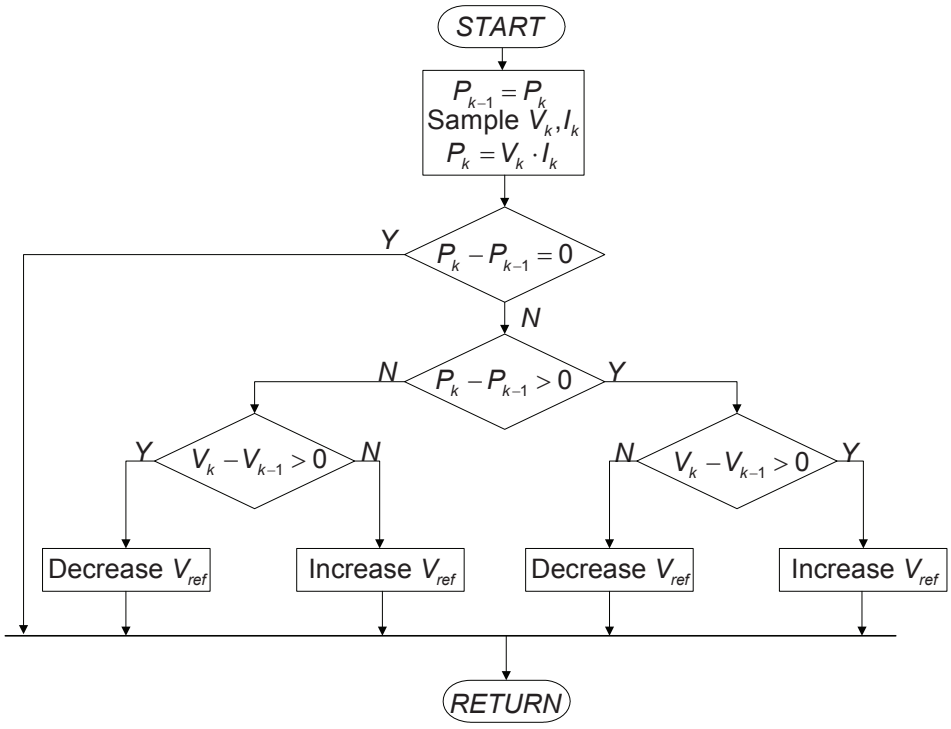

Figure 2.2: *The flowchart of the P&O algorithm*

it will show oscillations around the MPP. Although the INC method generally appears in the literature as a progress in efficiency compared to the $P\&O$ [28,40,45,49], it nonetheless shares its disadvantage in that it can track in wrong direction during rapidly-changing irradiations [43,46].

Another well-known MPPT method is the **Constant Voltage** (CV), which makes use of the fact that the PV array MPP voltage changes only slightly with irradiation. In this algorithm, the MPPT momentarily sets the PV array current to zero to allow the measurement of the open-circuit voltage. The operating voltage is set to a fixed percentage of the open-circuit voltage [28]. Although the ratio between the open-circuit voltage and MPP voltage (V_{oc}/V_{mp}) depends on the solar array parameters, a commonly used value for crystalline silicone panels is 76% [28, 50, 51]. This operating point is maintained for a set amount of time, after which the cycle is repeated. The main problem with this algorithm is that energy is wasted while the open-circuit voltage is measured, and the V_{mp} is not always at the fixed 76% of the V_{oc} [28].

A similar method to CV, called short-current pulse based MPPT, operates with current instead of voltage and makes use of the fact that the MPP current is a fixed ratio of the short-circuit current, with a value of $k \approx 0.92$ [52, 53]. The tracker then periodically short-circuits the PV array to measure the short-circuit current and then sets the operating point according to this measurement.

Several comparisons have been made for the above-mentioned algorithms: the $P\&O$, INC and CV, and it is generally concluded that, in high irradiation conditions, the INC produces the highest efficiency [28, 45, 48, 49]. On the other hand, as the irradiance decreases, the efficiency of the INC also decreases, and it has been shown in [45] and [54] that at irradiations below $300W/m^2$ the INC performs very poorly, and completely fails to track the MPP below irradiations of $50W/\ m^2$ [45]. The efficiency of the $P\&O$ also decreases with less irradiation, but it is able to track below $50W/m^2$ [45]. The CV method is generally considered the least efficient of the three [28], but, as the irradiance decreases, it shows improving performance, higher than both the $P\&O$ and INC. Because of this property, it is often used in combination with one of the hill-climbing methods [45, 54].

2.3 Maximum power point tracking in rapidly changing conditions

As was mentioned earlier, the $P\&O$ can track in the wrong direction under rapidly changing irradiation conditions. Irradiation can change relatively quickly due to weather conditions, e.g. passing clouds, and very fast changes (for small systems) corresponding to a variation of the rated power from 15% to 120% within $500ms$, were reported [55]. Nevertheless, the probability of such fast irradiation changes is extremely low [5]. The authors of [5], based on a measured irradiation data set of over a year with a $1Hz$ sampling rate, classified the irradiation changes regarding their rate and magnitude in 3 categories (Table 2.1).

If the change in the intensity of irradiation causes a bigger change in power than the one

Table 2.1: *Categories of irradiance changes [5].*

Time scale	Largest realistic variation (W/m^2)
Very fast (within 1 second)	27
Fast (within 5 seconds)	103
Slow (within 30 seconds)	441

caused by the increment in the voltage, the MPPT can get confused, as it will interpret the change in the power as an effect of its own action. This is illustrated in Figure 2.3.

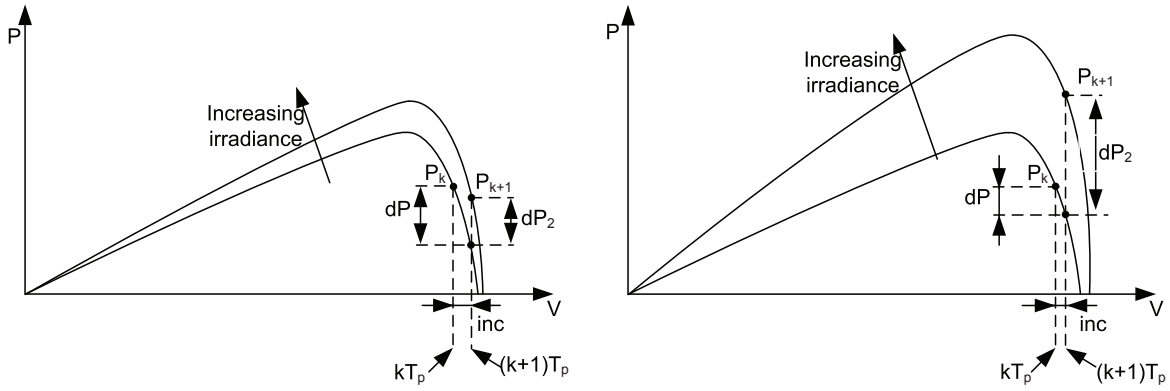

Figure 2.3: *In the case of slow irradiation changes, the P&O method is able to track in the right direction (a), but in case of rapidly-changing irradiation, it is unable to determine the right tracking direction (b)*

on Fig.2.3:

- T_p - the perturbation period of the MPPT
- P_k, P_{k+1} - the values of power measured at the k-th and the $k+1$-th sampling instances
- dP - the change in power, caused by the perturbation of the MPPT
- dP_2 - the change in power, caused by the increase in irradiation
- inc - the (voltage) perturbation increment of the MPPT

If $dP > dP_2$ the MPPT is able to interpret correctly the change in power between two sampling instances (Fig.2.3(a)), as the overall change in power will be dominated by the effect of the perturbation. On the other hand, if $dP < dP_2$, the MPPT is unable to determine the right direction of tracking as for example $P_{k+1} - P_k$ in Fig.2.3(b) is positive, regardless of the perturbation direction of the MPPT. In the case depicted in Fig. 2.3(a), the $P\&O$ would continue to increase the voltage reference until the irradiation change is stopped or dP becomes larger than dP_2.

In the following, an improvement, for increasing the $P\&O$ dynamic tracking performance, is proposed.

2.3.1 The proposed dP-P&O method

In Publication 1, the limitation of the Perturb&Observe algorithm of tracking under rapidly changing irradiation is addressed, and a simple improvement is proposed, called the $dP - P\&O$ method.

The $dP - P\&O$ performs an additional measurement of power in the middle of the MPPT sampling period without any perturbation, as illustrated in Fig. 2.4.

As shown in Fig. 2.4, the change of power between P_x and P_{k+1} reflects only the environmental changes, as no action has been taken by the MPPT. The difference between P_x and P_k (dP_1) contains the change in power caused by the perturbation of the MPPT, plus the environmental effect. Thereby, assuming that the rate of change in the irradiation is constant over one sampling period of the MPPT, the dP caused purely by the MPPT command can be calculated as:

$$\begin{aligned} dP = dP_1 - dP_2 &= (P_x - P_k) - (P_{k+1} - P_x) \\ &= 2P_x - P_{k+1} - P_k \end{aligned} \tag{2.3}$$

Introducing the above calculation of the power change caused by the action of the perturbation within one MPPT sampling instance, the flowchart of the classic $P\&O$ will change only by an additional element, as is shown in Fig. 2.5. The method has been implemented on a grid-connected inverter, using a control structure as presented in Fig. 2.6. The detailed description of the test conditions can be found in Publication 1.

The experimental results presented in Fig. 2.7 show that the $dP - P\&O$ is able to avoid misdirectional tracking in fast changing conditions, improving the overall performance of the $P\&O$. Applying the dynamic efficiency as calculated in Eq. (7) from Publication 1 on pg. 77, reproduced here:

$$\eta_{dynamic} = \frac{P_{PV\_meas\_mean}}{P_{mp\_mean}} \cdot 100 \tag{2.4}$$

the efficiency gain of the $dP - P\&O$ over the classical $P\&O$ has been calculated as 2.4% when the power feed-forward was switched on, and 5% without power feed-forward (considering the entire test period in which the trapezoidal irradiation profile was applied (2.7)).

2.3.2 Optimised dP-P&O

As reported in the previous section, accurately determining the dP allows tracking in the correct direction during irradiance changes. However, in order to track very fast changes of irradiation, the voltage perturbation may need to be increased. This would lead to oscillations around the MPP in steady-state conditions, degrading the overall performance. To overcome this drawback, the information regarding the change of output power due to external conditions, dP_2 is used. From the value of dP_2 it can be determined if the irradiation is stable, increasing

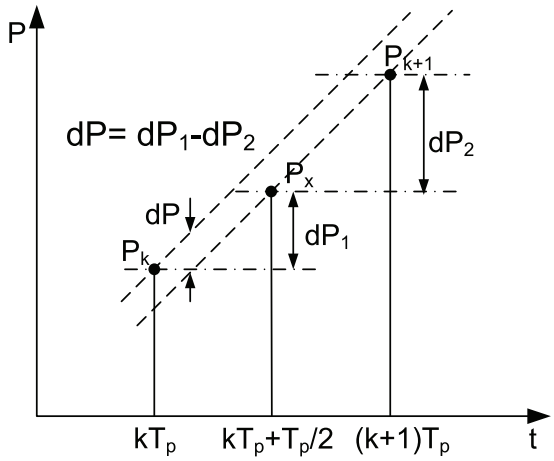

Figure 2.4: *Measurement of the power between two MPPT sampling instances*

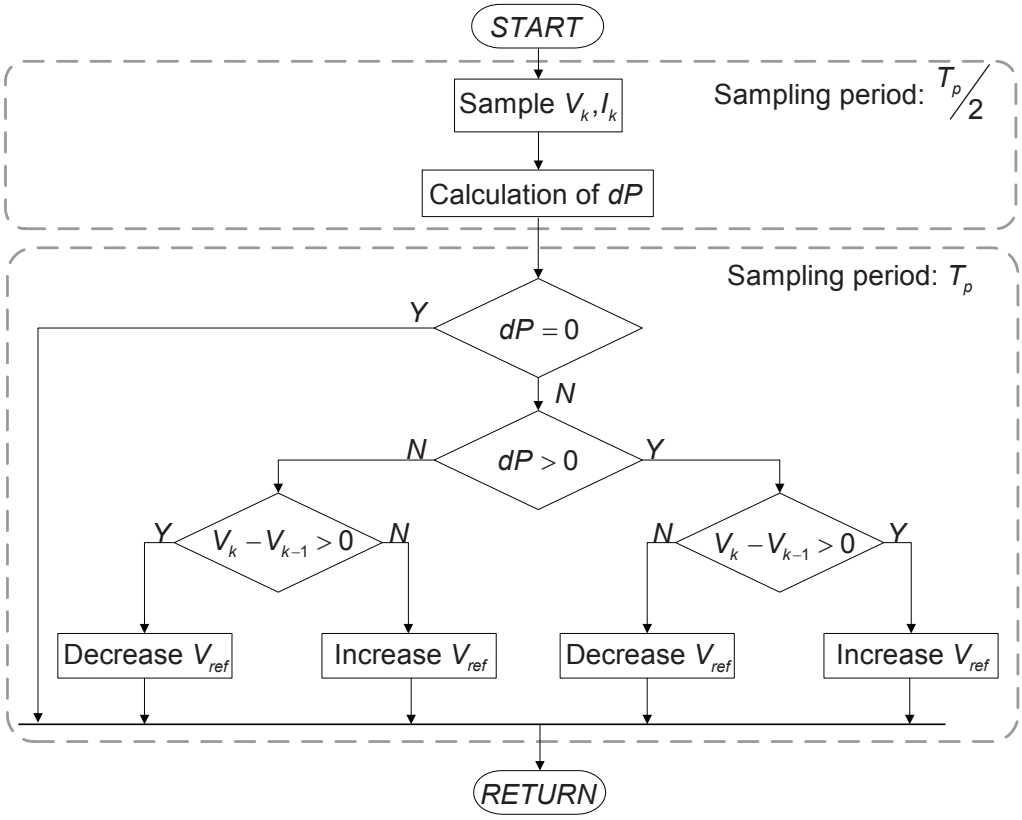

Figure 2.5: *The flowchart of the proposed dP-P&O algorithm.*

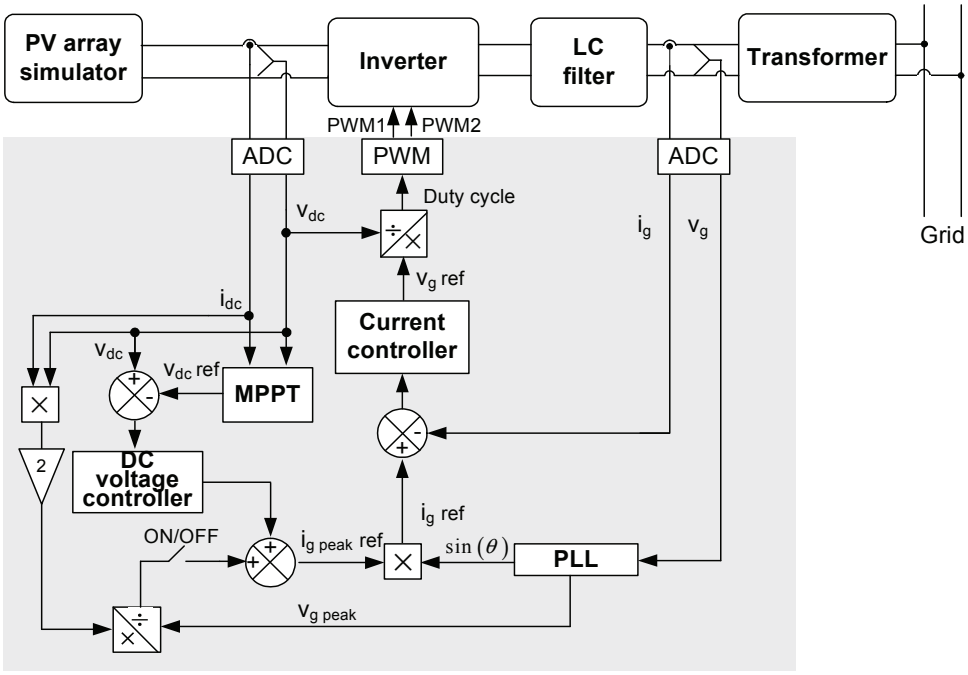

Figure 2.6: *MPPT and current control structure for a single phase PV inverter, used for testing the P&O and dP − P&O MPPT algorithms.*

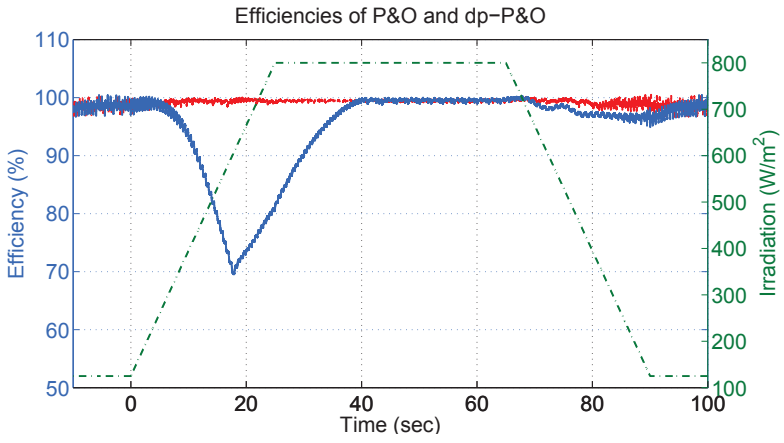

Figure 2.7: *Instantaneous efficiency plots of the classical P&O (blue) and the dP − P&O (red) methods at the same conditions, including control structure, sampling rate and voltage increment. A trapezoidal irradiation profile with a positive slope from 120W/m^2 to 800W/m^2 in 25 seconds, followed by a 40 seconds steady state period, and finally returning to 120W/m^2 irradiation in 25 seconds, have been used (Publication 1).*

or decreasing. Publication 2 presents an MPPT method employing the information about the irradiance change provided by the calculation in Eq. (2.3), which allows the use of optimised tracking strategy for the different cases; its flowchart is shown in Fig. 2.8.

In Fig. 2.8, if the change in power due to irradiation ($|dP_2|$) is smaller than the change of power due to the MPPT perturbation ($|dP|$), conditions are considered to be slowly-changing, and the system will use the basic $dP - P\&O$ algorithm, with small increment values, to reduce oscillations around the MPP.

If a fast rise in the irradiation was detected by dP_2 (Fig. 2.8), it means that the MPPT should increase the PV array's reference voltage, in order to follow the irradiance change. Therefore, in this situation, the MPPT switching strategy favours increasing the voltage reference. $V_{dc}ref$ in Fig. 2.6 is decreased only when the voltage was increased in the previous MPPT sampling instance *and* it caused a reduction of power $dP < ThN$. A negative threshold value ThN has been applied in order to avoid unnecessary switching around the MPP. If - due to the action of the MPPT in the last sampling period - dP becomes negative, the MPPT holds the voltage reference at the same level for one sampling period instead of decreasing it, unless the caused decrease of power became larger than the threshold ($|dP| > |ThN|$).

Both the basic and optimised $dP - P\&O$ methods were implemented and experimentally tested on a commercial PV inverter, the REFUSOL 11 K manufactured by REFU Elektronik GmbH, Germany [56]. The PHOTON Magazine test results of the REFUSOL 11 K with the $dP - P\&O$ show an MPPT efficiency of over 99% with a particularly fast response time, making it the best performing MPP tracker in a survey of the most important manufacturers of PV inverters worldwide in 2008 [21].

2.4 Summary

This chapter dealt with MPPT algorithms for photovoltaic systems. The most popular MPPT methods, the $P\&O$, the INC and the CV have been briefly presented. An improvement method to the classical $P\&O$ has been presented, called the $dP - P\&O$. It uses an additional measurement of power inside the MPPT algorithm, without perturbation, and uses this information to separate the effects of the environment from the tracker's perturbations. This avoids misdirectional tracking during fast-changing irradiations. Experimental results have been presented, showing considerable improvement in dynamic efficiency when compared to the classic $P\&O$. Furthermore, by identifying the environmental changes, it is possible to use optimised tracking for different operational conditions: stable, increasing or decreasing irradiation. By optimising the perturbation scheme for the different conditions, it can achieve faster tracking during irradiation changes, and more accuracy at steady state. Based on these considerations, an optimised dP-P&O method has also been proposed. Both the $dP - P\&O$ and optimised $dP - P\&O$ have been implemented on a commercial PV inverter, the REFUSOL 11 K, showing high efficiency during fast-changing irradiations.

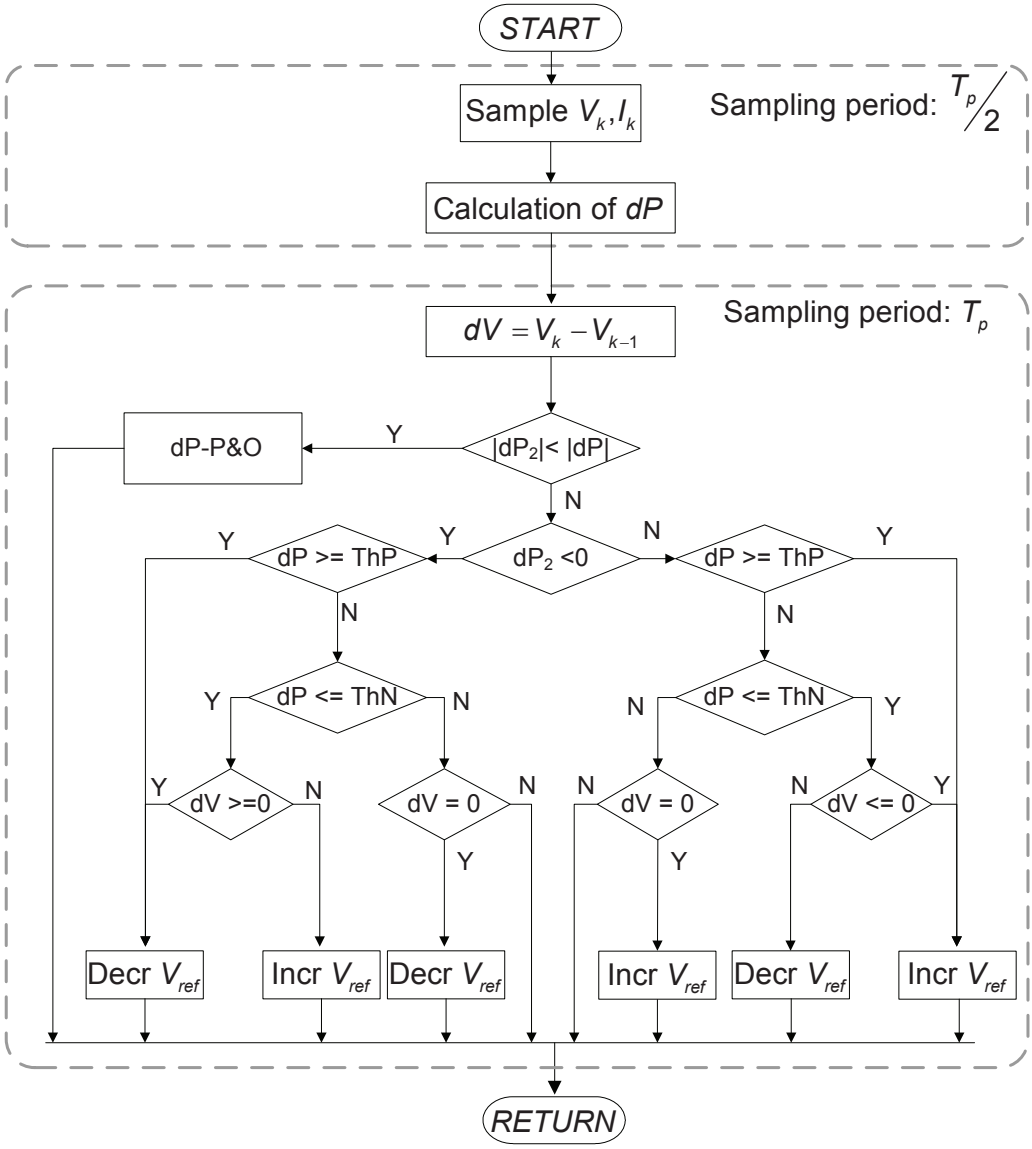

Figure 2.8: *Flowchart of the optimised $dP-P\&O$ method. ThN stands for the negative threshold for dP, while ThP represents the positive threshold for dP.*

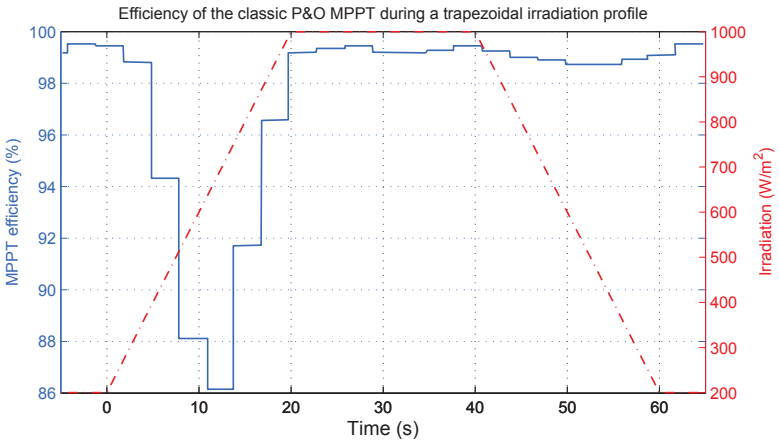

(a)

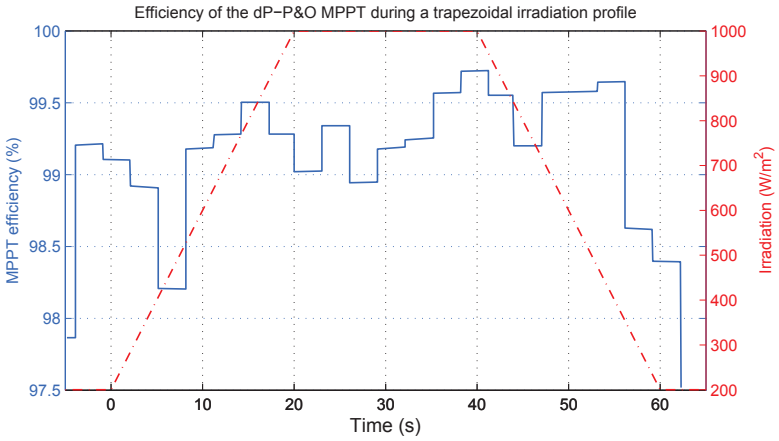

(b)

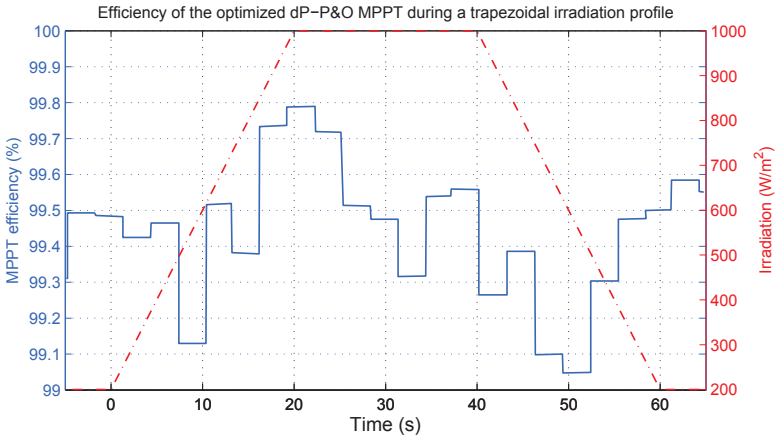

(c)

Figure 2.9: *Instantaneous efficiencies of the classical P&O (a), the $dP-P\&O$ (b), and optimised $dP-P\&O$ (c) during a trapezoidal irradiation profile. It can be seen that the average efficiency of the optimised $dP-P\&O$ during the entire test period is approximately* 99.4%, *which is approximately* 0.4% *higher than the basic $dP-P\&O$.*

Chapter 3

Modelling of PV cells and arrays

In this chapter the most commonly used solar cell models are introduced and the problem of model parameter determination based on the four and five parameter models is addressed. This is followed by the implementation of a PV simulator consisting of customisable series-parallel connected panels, suitable for testing MPPT algorithms and evaluating the effects of partial shadowing, with various shadow area and shape. Finally, simplified analytic formulae describing the four-parameter model for diagnostic purposes, are presented

3.1 Purpose of models

In this thesis, several models of PV modules and systems have been used and implemented for two distinct purposes, as described below.

PV system modelling: to model the behaviour of a PV system, composed of parallel connected arrays, which in turn are formed of series connected modules. The aim is to predict the behaviour and power output of such systems in various environmental conditions, and especially in the case of partial shadowing. Attention is paid to the shape and position of the shadow in respect with the position of the bypass diodes. The purpose of such a model is to gain an insight on the effects of partial shadowing, module mismatch, and cell or module failure on a PV system's output power and $I-V$ characteristics, and to test the performance of MPPT techniques in non-ideal conditions.

Diagnostics: to determine - based on its experimentally measured $I-V$ curve - the main characteristics of a PV system, such as the series resistances, presence of partial shadowing or malfunctioning cells, or bad connections. The aim is to obtain a simple model, which can have acceptable approximation quality, while having its parameters determined by simple analytical formulae, rather than complex iterative solutions, to which the five-, six-, or seven-parameter models would lead to. The purpose of this model is to post process the measured $I-V$ curve, calculate certain parameters (as described in the following), and to make an estimation of the module or array state of health from the deviation of these parameter from some predetermined values, e.g. those based on datasheet data or reference measurements. The model is not intended to be able to reproduce the measured $I-V$ curve, (which could have a complicated shape

depending on partial shadowing, discoloration of the protective plastic sheet, etc.), and therefore it can be kept simple.

3.2 PV cell models overview

There are two well-known and widely used models, both with different levels of complexity, depending on the purpose they are used for: the single-diode (often referred to as the single-exponential), and the two-diode (or double exponential) models. Both of these are based on the well-known Shockley diode equation [57]. The most common versions of these models are presented in the following.

The single diode simple model (or four-parameter model) described by Eq. (3.1) and its equivalent circuit diagram shown on Figure 3.1 consists of a constant current source, in parallel with a diode, which includes an ideality factor to account for the recombination in the space-charge region [58]. This model accounts for the losses due to the module's internal series resistance, as well as contacts and interconnections between cells and modules. It has a relatively good approximation precision and it is perhaps the most suitable model for the diagnostics of PV arrays, as it offers good compromise between approximation precision and simplicity.

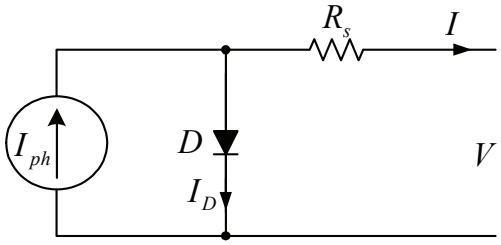

Figure 3.1: *Equivalent circuit of the single diode model with taking in account the series resistance of the module*

$$I = I_{ph} - I_0 \left(e^{\frac{V+IR_s}{V_t}} - 1 \right) \tag{3.1}$$

Where V_t is the module thermal voltage:

$$V_t = \frac{n_s AkT}{q} \tag{3.2}$$

where

- R_s - module internal series resistance (Ω)
- I_0 - dark saturation current (A)
- n_s - number of series connected cells in the module
- q - charge of an electron (C)
- k - Boltzmann's constant

- A - diode ideality factor
- T - temperature (^oK)
- I_{ph} - photo-generated current (A)

The single diode detailed model (or single-exponential five-parameter model) on Figure 3.2 also takes into account over the simple model the shunt resistance of the module, which models the losses due to the leakage currents across the junction and within the cell due to crystal imperfections and impurities [59].

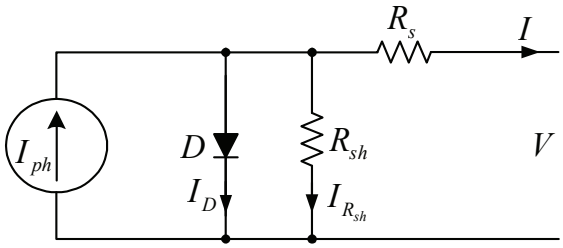

Figure 3.2: *Equivalent circuit of the single diode model, taking into account both the series and shunt resistances of the module.*

An additional term appears in the mathematical model, as shown in Eq. (3.3):

$$I = I_{ph} - I_o \left(e^{\frac{V+IR_s}{n_s V_t}} - 1 \right) - \frac{V + IR_s}{R_{sh}} \tag{3.3}$$

where

- R_{sh} - module shunt resistance (Ω)

The double diode model (or double-exponential model) considers an additional diode in the equivalent scheme to account for the losses due to the carrier recombination in the space charge region of the junction, and those due to surface recombination [57, 58, 60–62]. In this model the first diode is responsible for the diffusion current component [57].

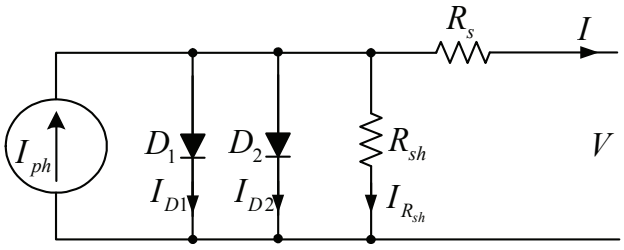

Figure 3.3: *Equivalent circuit of the double diode model, taking into account both the series and shunt resistances of the module.*

$$I = I_{ph} - I_{01} \left(e^{\frac{V+IR_s}{V_t}} - 1 \right) - I_{02} \left(e^{\frac{V+IR_s}{2V_t}} - 1 \right) - \frac{V + IR_s}{R_{sh}} \tag{3.4}$$

where

$$V_t = \frac{n_s kT}{q} \tag{3.5}$$

- I_{01} - Dark saturation current of the first diode modelling the diffusion current component
- I_{02} - Dark saturation current of the second diode modelling the recombination in the space charge region

The single-diode simple model is often called the four-parameter model, as it has four unknown parameters which need to be determined, before the model can be built: I_0, I_{ph}, A, and R_s.

The single diode detailed model, and in some cases the double diode model too, is often referred to as the five-parameters model. This, in addition to the previous case, has the module shunt resistance (R_{sh}) as the fifth parameter. In case of the double diode model, an additional parameter is introduced by the reverse saturation current of the second diode, but the diode ideality factors are considered to be known for both diodes, which are 1 and 2, respectively [61].

Nevertheless, different versions of this model are reported, considering the ideality (quality) factors of the diodes. Beier and Voss in [62] show through experimental measurements that the quality factor of the second diode often differs from the value 2. A similar approach is used in [63–65], and many others.

Some authors consider both diode quality factors as variable, fitting parameters [66,67]. The two latter versions of the double exponential model, although thought to offer higher fitting quality, lead to 6− and 7−parameter models, respectively, therefore considerably increasing the complexity of parameter calculations.

The double diode model is considered by many authors to be more accurate than the single diode model, e.g. [68,69], the latter is blamed for being imprecise particularly at low irradiation levels [58]. A similar approach is reported in [70].

However, it has been found that, when used for modelling the behaviour of many interconnected modules, e.g. PV systems, the single diode model is preferred by many of the authors in the literature, e.g. Bishop in [71], Araujo in [72], or the authors of [59,73–76].

One of the reasons could be that, in the case of modelling PV systems for the purpose of testing Maximum Power Point Tracking techniques, or a qualitative prediction about the effect of the partial shadowing or mismatched modules, the main objective and challenge is the modelling of the interactions between the cells and modules, rather than a very precise model of one single cell. Also, due to the inherent variations of the cells parameters, it is next to impossible to determine a very precise model for every single cell in a larger PV system. For this purpose, the single diode model's representation precision is considered to be sufficient.

The unknown parameters of the models have to be determined for the given type of cell, whose characteristics are to be reproduced by the model. A number of approaches for cells and module parameter determination can be adopted using the datasheet parameters or measured

$I-V$ curves, which are described in Chapter 4. For modelling purposes, a simple mathematical approach has been used in this work, which relies on parameters given in the panels' datasheet.

3.3 Parameter extraction using the five-parameter single diode model

Publication 5 addresses the development and implementation of a model for a photovoltaic module, including the forward and reverse characteristics, temperature and irradiance effects, with the panel datasheet parameters as input data, for use in a flexible PV simulator, as described on page 23.

The starting point is the module datasheet parameters, which contain the measured voltages and currents at the three key-points of the $I-V$ characteristic, and in general also the temperature coefficients of the short-circuit current and open-circuit voltage [77] as summarised in Table 3.1.

Using the information given by the product's datasheet, a system of equations can be built (Eq. (3.6)) and solved for the five unknown parameters I_0, I_{ph}, A, R_s, and R_{sh}.

$$\begin{cases} I_{oc} = 0 = I_{ph} - I_0 e^{\frac{V_{oc}}{V_t}} - \frac{V_{oc}}{R_{sh}} \\ I_{mp} = I_{ph} - I_0 e^{\frac{V_{mp}+I_{mp}R_s}{V_t}} - \frac{V_{mp}+I_{mp}R_s}{R_{sh}} \\ I_{sc} = I_{ph} - I_0 e^{\frac{I_{sc}R_s}{V_t}} - \frac{I_{sc}R_s}{R_{sh}} \\ \frac{dP}{dV}\Big|_{\substack{P=P_{mp} \\ V=V_{mp}}} = 0 \\ \frac{dI}{dV}\Big|_{\substack{I=I_{sc} \\ V=0}} = -\frac{1}{R_{sh}} \end{cases} \tag{3.6}$$

The structure of equation system (3.6) is described in detail in Publication 5, where the solution is also presented. Analytic formulae for determining the model's parameters could not be found, due to the transcendental nature of the equation system. Therefore, numerical methods have been used, which carry the downside of larger computational load, and the dependency on initial conditions.

As has been shown in Publication 5, taking the shunt resistance into consideration has a strong impact on the parameter' calculations, requiring iterative methods to determine the model parameters. On the other hand, the five-parameter model also suffers from the problem of the simple four-parameter model, namely that the model's parameters do not necessarily have physically meaningful values [58, 78–80].

Table 3.1: *Typical parameters given in the datasheet of a photovoltaic panel, based on STC measurements.*

I_{sc} -short-circuit current (A)	P_{mp} -power at the MPP (W)
V_{oc} -open-circuit voltage (V)	k_i -temperature coefficient of I_{sc} $(A/^\circ C)$
V_{mp} -voltage at the MPP (V)	k_v -temperature coefficient of V_{oc} $(V/^\circ C)$
I_{mp} -current at the MPP (A)	n_s -total number of cells in the module

3.4 Modelling the PV system

In this section, a digital PV simulator will be presented, built for the purpose of testing MPPT algorithms, and evaluating the effects of different shapes of partial shadows with respect to bypass diodes on the $I-V$ curve of the array. In the case of partial shadows, some cells can become reverse biased, moving their working point to the reverse part on the $I-V$ characteristic. In order to model this process, the reverse characteristic should be included in the cell's model. This can be done by completing Eq.(3.3) with Bishop's term [71] , which considers the reverse characteristic as a non-linear multiplication factor that affects the shunt resistance current [81].

$$I = I_{ph} - I_0 \left(e^{\frac{V+IR_s}{V_t}} - 1 \right) - \frac{V+IR_s}{R_{sh}} \left(1 + a \left(1 - \frac{V+IR_s}{n_s V_{br}} \right)^{-m} \right) \tag{3.7}$$

In Eq. (3.7), m is the avalanche breakdown exponent, a is the fraction of the ohmic current in the avalanche breakdown, and V_{br} is the cell junction breakdown voltage [71,81]. The parameters m and a have been determined empirically by Bishop in [71]. Although Bishop's approach is the most often used in the literature, it has been criticised of not being physically correct, as the avalanche current should affect the entire PN junction, not only the shunt paths [81]. The authors of [81] reported a model describing the reverse characteristic of the PV cell, considering the avalanche multiplication affecting the entire PN junction current.

It must be pointed out that this model does not have the ambition to high precision modelling of the PV cells' reverse characteristics. Due to the relatively large variability of reverse characteristics of PV cells, even within the same type and batch [82], this requires a more complex model, which is out of the scope of the present work. In Publication 8, the effect of partial shadowing on the output power is studied with emphasis on the different shapes of shadows in respect with the bypass diodes, when the reverse characteristic of the cells are modelled according to Eq. (3.7).

Equation (3.7) is suitable for describing the entire current-voltage characteristics of a photovoltaic cell. In order to include the effects of different irradiance and temperature conditions, the corresponding dependency of the parameters of (3.7) should be modelled. Most of the parameters' temperature dependency is straightforward, either being given in the datasheet (k_i for I_{sc}, k_v for V_{oc}), or considered independent of temperature (R_s, R_{sh}, a, m, V_{br}) as described in Publication 5.

However, the temperature dependence of the dark saturation current is less straightforward, and a number of approaches to express this function have been reported in the literature [74, 75, 83–85]. In this work a method similar to the one presented in [75] is used, with the essential difference being that, here, the dark saturation current is considered independent of irradiation, as opposed to the approach used in [75]. The method uses the expression of I_0 from the short-circuit current equation, and the temperature dependency is obtained by simply updating the parameters of Eq. (20) from Publication 5 with their corresponding temperature coefficients, as

reproduced here:

$$I_o(T) = \left(I_{sc}(T) - \frac{V_{oc}(T) - I_{sc}(T)\, R_s}{R_{sh}} \right) e^{-\frac{V_{oc}(T)}{V_t}} \tag{3.8}$$

In Fig. 3.4 'Reference 1' corresponds to the output of the model when the dark saturation current temperature function is expressed according to the authors of [86], and followed by the authors of [85] and [74], while 'Reference 2' identifies the output of the model using the dark saturation current temperature function given in [75].

3.4.1 Implementation of the PV simulator

The PV simulator has been implemented in Simulink®, using the principle shown in the block diagram in Fig. 3.5.

A PV system with a capacity of a few kW as described in Chapter 1, can contain thousands of cells, with series and parallel interconnections, and bypass diodes. Modelling the behaviour of every cell in such a system, even though it would offer a very high level of flexibility, is not feasible, as this would require enormous computational capacity, thereby certain simplifications are needed in order to create a useful model. The following assumptions have been made:

- All the cells in the system have identical physical properties, i.e. the same I-V characteristics. In reality, not all the cells are the same in a system, there are small deviations in their physical properties, which slightly reduce the overall output power [71].
- The irradiation is fully uniform over the system, except for the shadowed area, where the irradiation is smaller. In other words, two different irradiation levels were considered, and consequently two distinct models were used.
- The temperature was considered uniform over the entire system. In practice, variations of temperature can occur over the array, especially in facade applications [18].

In accordance with the above, the simulator contains two PV cell models, which generate the forward and reverse $I-V$ characteristics of the fully illuminated and shadowed cells, respectively. These cell characteristics are then combined to form the array's (only series connected cells and modules) $I-V$ curves, according to the specifications of the user.

The computation-intensive parts of the model are the generation of the characteristics of the cells and then the construction of the array's $I-V$ curves. However, this part is needed to run only when the environmental conditions are changing, hence it can be executed with low sampling rate. Therefore the model of the complex system is reduced to lookup tables, without requiring much computational resource, and is suitable for running in real-time, in order to control a hardware PV simulator (Publication 6 and 7). Figure 3.6 shows the measured and modelled $I-V$ characteristics of a PV module under various partial shadow conditions. Due to the ageing of the panel used, its behaviour is not identical to datasheet, therefore the environmental conditions (G and T) for the simulation have been adjusted in order to create the same short-circuit current and open-circuit voltage to the measurement.

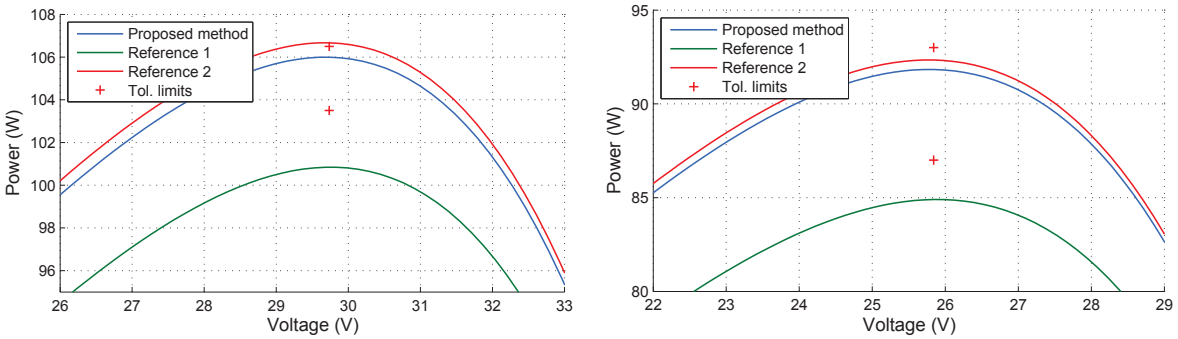

Figure 3.4: *P-V curves of the BPMSX120 [2] PV panel in the vicinity of MPP at $T = 50^oC$ (a) and $T = 75^oC$ sub3.4(b) using three different methods for calculating the dark saturation current dependency on temperature.*

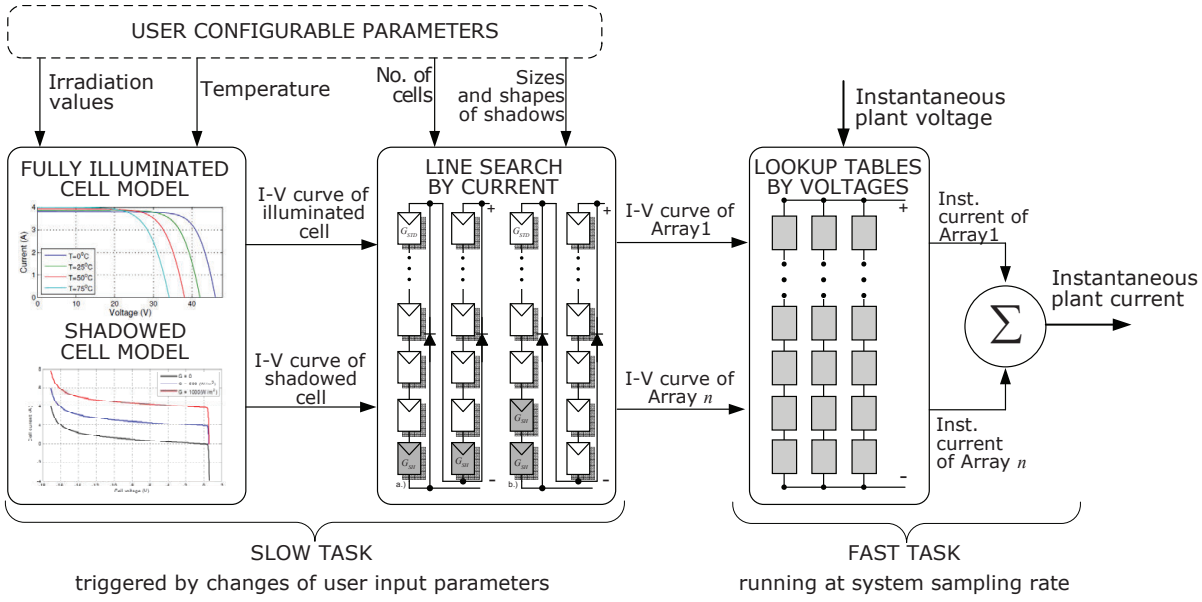

Figure 3.5: *Block diagram showing the implementation principles of the PV simulator.*

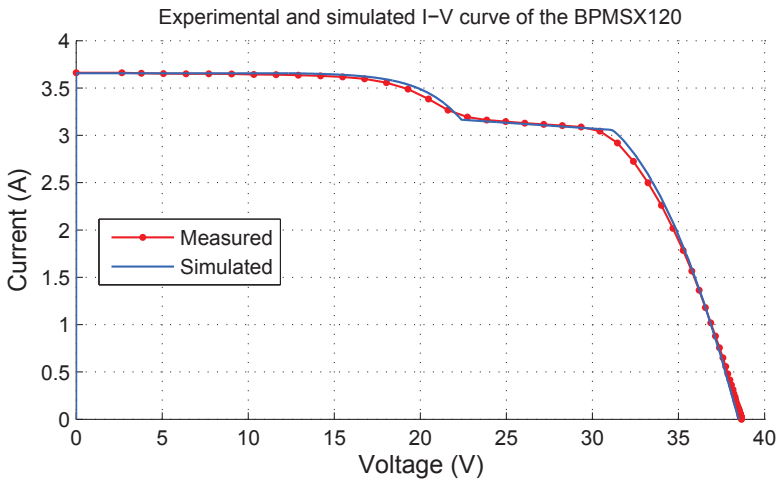

(a)

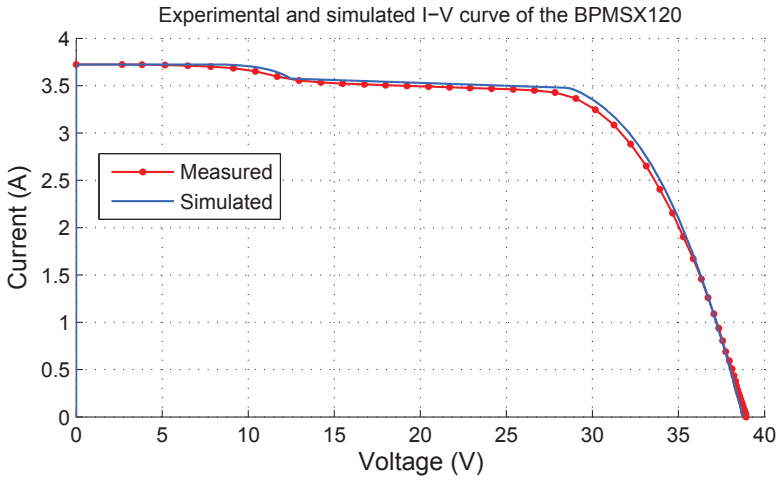

(b)

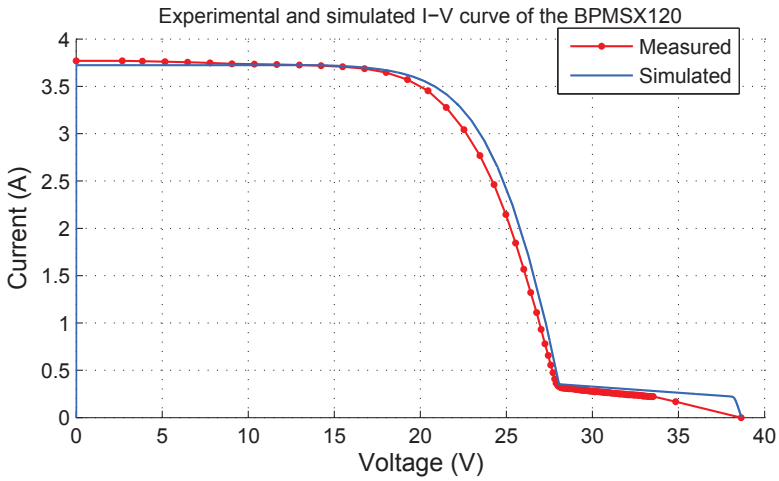

(c)

Figure 3.6: *Measured and simulated $I-V$ characteristics of a BPMSX120 panel, with one cell partially shadowed (a), with the same area of shadow affecting 2 cells (b), and with 2 cells entirely shadowed (c).*

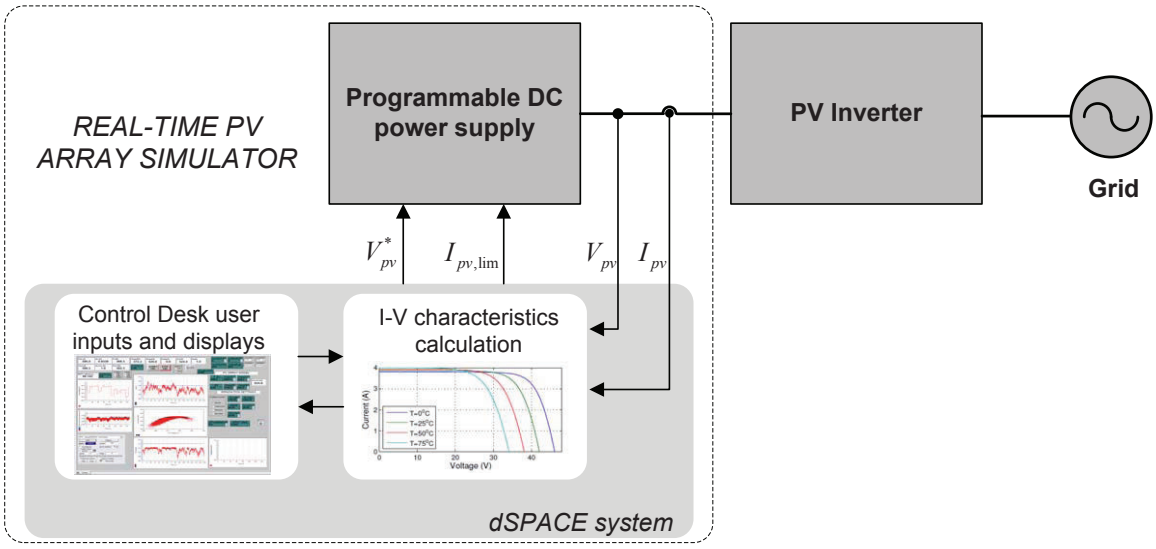

Figure 3.7: *Block diagram of the PV inverter test setup containing the dSpace real time simulator.*

3.5 Parameter extraction using the four-parameter model

As it has been previously described, for diagnostic purposes the simple 4-parameter model can be used, with the aim of finding analytical solutions for the parameters, suitable for online calculations. It should be emphasised that, as the model is a simplified one, the accuracy of the determined parameters is not as high as in case of a more detailed model.

The general expression of the photovoltaic panel's current as a function of voltage, using the four-parameter model can be expressed as in Eq.(3.1), reproduced here:

$$I = I_{ph} - I_0 \left(e^{\frac{V+IR_s}{V_t}} - 1 \right)$$

For calculating the panel's parameters, some simplifications to (3.1) have been made. As the dark saturation current in silicon devices (compared to the exponential term) is very small, the term '-1' can be neglected [73]. Another simplification, which has been made in order to obtain relatively simple and treatable equations approximates the photo-generated current I_{ph} with I_{sc} ($I_{ph} \approx I_{sc}$). It is common practice to ignore the difference between the photo-generated current and the short-circuit current, as it is generally very small [74, 75, 85, 87, 88]. This assumption can be considered valid for crystalline silicone cells, at moderate short-circuit currents (non-concentrator PV cells), where the losses in the series resistance at short-circuit conditions are not substantial.

In this case (3.1) becomes:

$$I = I_{sc} - I_0 \left(e^{\frac{V+IR_s}{V_t}} \right) \tag{3.9}$$

The calculation of the parameters in the following are based on (3.9). Using the simpli-

fication above, the four-parameter model can be reduced to a three-parameter one, with the number of equations and unknowns reduced to three, making the entire calculation relatively straightforward.

The following equations give the expression of the panel current on two of the three main points of the I-V characteristic: (the equation at short-circuit has been cancelled due to $I_{ph} \approx I_{sc}$).

At open-circuit conditions:

$$0 = I_{sc} - I_0 e^{\frac{V_{oc}}{V_t}} \tag{3.10}$$

and the current at MPP (I_{mp}) has the following form:

$$I_{mp} = I_{sc} - I_0 e^{\frac{V_{mp}+I_{mp}R_s}{V_t}} \tag{3.11}$$

In the third equation, the well-known relation of the derivative of the power with voltage at MPP is used:

$$\left.\frac{dP}{dV}\right|_{\substack{I=I_{mp}\\V=V_{mp}}} = 0 \tag{3.12}$$

The above equation can be expanded as follows:

$$\left.\frac{dP}{dV}\right|_{\substack{I=I_{mp}\\V=V_{mp}}} = \left.\frac{d\left(VI\right)}{dV}\right|_{\substack{I=I_{mp}\\V=V_{mp}}} = V\frac{dI}{dV} + I\Big|_{\substack{I=I_{mp}\\V=V_{mp}}} = 0 \tag{3.13}$$

which leads to the following:

$$\left.\frac{dI}{dV}\right|_{\substack{I=I_{mp}\\V=V_{mp}}} = -\frac{I_{mp}}{V_{mp}} \tag{3.14}$$

Considering the fact that $I(V)$ is a transcendent equation, and $I = f(I, V)$, the derivative of current with voltage can be expressed as:

$$dI = dI\,\frac{\partial f\left(I,V\right)}{\partial I} + dV\,\frac{\partial f\left(I,V\right)}{\partial V} \tag{3.15}$$

and therefore:

$$\frac{dI}{dV} = \frac{\frac{\partial}{\partial V} f\left(I,V\right)}{1 - \frac{\partial}{\partial I} f\left(I,V\right)} \tag{3.16}$$

Therefore, collecting Equations (3.10), (3.11) and executing the derivatives in (3.16), the three equations, forming the equation system for finding the panel model parameters, become:

$$\begin{cases} 0 = I_{sc} - I_0 e^{\frac{V_{oc}}{V_t}} \\ I_{mp} = I_{sc} - I_0 e^{\frac{V_{mp}+I_{mp}R_s}{V_t}} \\ \frac{I_{mp}}{V_{mp}} = \frac{I_0\, e^{\frac{V_{mp}+I_{mp}\,R_s}{V_t}}}{V_t\left(1+\frac{I_0\,R_s\,e^{\frac{V_{mp}+I_{mp}\,R_s}{V_t}}}{V_t}\right)} \end{cases} \tag{3.17}$$

Solving the above system of equations will result in the solution for I_0, R_s, and V_t as follows:

$$I_0(V_t) = \frac{I_{sc}}{e^{\frac{V_{oc}}{V_t}}} \tag{3.18}$$

$$R_s(V_t) = \frac{V_{oc} - V_{mp} + V_t \ln\left(\frac{I_{sc}-I_{mp}}{I_{sc}}\right)}{I_{mp}} \tag{3.19}$$

$$V_t = \frac{(2V_{mp} - V_{oc})\,(I_{sc} - I_{mp})}{I_{mp} - (I_{sc} - I_{mp}) \ln\left(\frac{I_{sc}-I_{mp}}{I_{sc}}\right)} \tag{3.20}$$

which contains only parameters given in the product datasheet or that are directly measurable.

In order to obtain a simpler result for V_t, an additional simplification can be done when differentiating the power with voltage at MPP. Instead of using Eq. (3.16), which takes into account that $I = f(I, V)$ (as $I(V)$ is transcendent), a simpler formula is used, which disregards at the derivation that $I = f(I, V)$. In other words, the first term on the right side of (3.15) is disregarded. Equation (3.11) can be revisited, multiplied with V_{mp} (in order to obtain P_{mp}), and simply differentiated with V_{mp}. This results in:

$$\left.\frac{dP}{dV}\right|_{MPP} = I_{sc} - \frac{I_{sc}\, e^{\frac{V_{mp}+I_{mp}\,R_s}{V_t}}}{e^{\frac{V_{oc}}{V_t}}}\left(\frac{V_{mp}}{V_t} + 1\right) = 0 \tag{3.21}$$

Inserting the expression of R_s from (3.19) into the above equation results in:

$$I_{sc} - (I_{sc} - I_{mp})\left(\frac{V_{mp}}{V_t} + 1\right) = 0 \tag{3.22}$$

Solving the above for V_t, results in the very simple expression:

$$V_t = \frac{(I_{sc} - I_{mp})\, V_{mp}}{I_{mp}} \tag{3.23}$$

The above formula gives a reasonable approximation precision, while avoiding the calculations of logarithmic functions, offering a simpler formulation for V_t, and at the same time decreasing the sensitivity to measurement errors of I_{sc} and I_{mp} when the difference between them is small, i.e. at low irradiation conditions. As is shown in Fig. 3.10, in most conditions the parameters found by the simplified expression provide fitting quality similar to those calculated starting with Eq. (3.20), with even smaller fitting errors in some cases.

The parameters determined in this section were not calculated with the purpose of finding the corresponding physical parameters of the photovoltaic module or cell, e.g. series resistance, dark saturation current or thermal voltage. In this context these values are treated as parameters of an exponential function, which has to fulfill the conditions given by (3.10), (3.11), and (3.12).

Conclusions regarding the state of health of the module can be made by comparing them to reference values, determined based on a controlled measurement, where the conditions of the measurement e.g. irradiation, temperature, partial shadowing are known, or datasheet values.

An alternative way to find the panel's model parameters using datasheet values and the same simple model, is the use of the $V(I)$ equations instead of the $I(V)$.

$$V = V_t \ln\left(\frac{I_{sc} - I}{I_0}\right) - iR_s, \tag{3.24}$$

The advantage of the $V(I)$ model is that it is algebraic, and the calculations are more straightforward. Using the same approach as in the previous section, the equation system for determining model parameters will take the form:

$$\begin{cases} V_{oc} = V_t \ln\left(\frac{I_{sc}}{I_0}\right) \\ V_{mp} = V_t \ln\left(\frac{I_{sc}-I_{mp}}{I_0}\right) - I_{mp}R_s \\ \frac{V_{mp}}{I_{mp}} = \frac{V_t}{I_{sc}-I_{mp}} + R_s \end{cases} \tag{3.25}$$

Solving the above system of equations will lead to the same results for the parameters I_0, R_s, and V_t as Equations (3.18), (3.19) and (3.20). The above equations can serve as a verification tool for the parameter determination presented previously.

In Fig. 3.8 the measured and simulated $I - V$ curves of three crystalline silicone PV panels can be seen. The curve denoted 'Simulated1' has been created using the simplified (3-parameter) model according to Eq. (3.9) with parameters calculated from Eq. (3.20). The curve 'Simulated2' is the result of the same model, but, in this case, V_t is calculated from Eq. (3.23). It should be pointed out that, as R_s is expressed in function of V_t, its value is also altered.

The plots on Fig. 3.8 and 3.9 show that both parameter sets offer relatively good fitting with experimental data, and the differences between them are rather small. In order to evaluate the fitting quality, the measured current data has been used as input to the model, and the fitting error has been calculated as:

$$\varepsilon_{Area} = \frac{|A_{meas} - A_{sim}|_{I>I_{mp}} + |A_{meas} - A_{sim}|_{I\leq I_{mp}}}{A_{meas}} 100 \tag{3.26}$$

In the above formula, A_{meas} and A_{sim} represent the area below the $I - V$ curve for the specified region. Equation (3.26) is based on the fact, that the measured and simulated curves cross each other only at the MPP (Fig. 3.8).Therefore this formula can provide a simple way to calculate the area fitting error of the models.

Although the fitting error increases as the irradiation decreases, it remains relatively low for both parameter sets (Fig. 3.10).

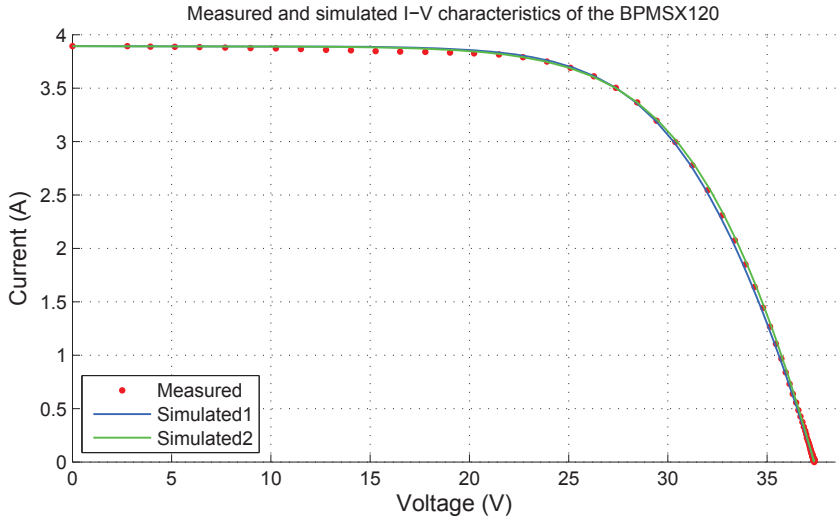

(a)

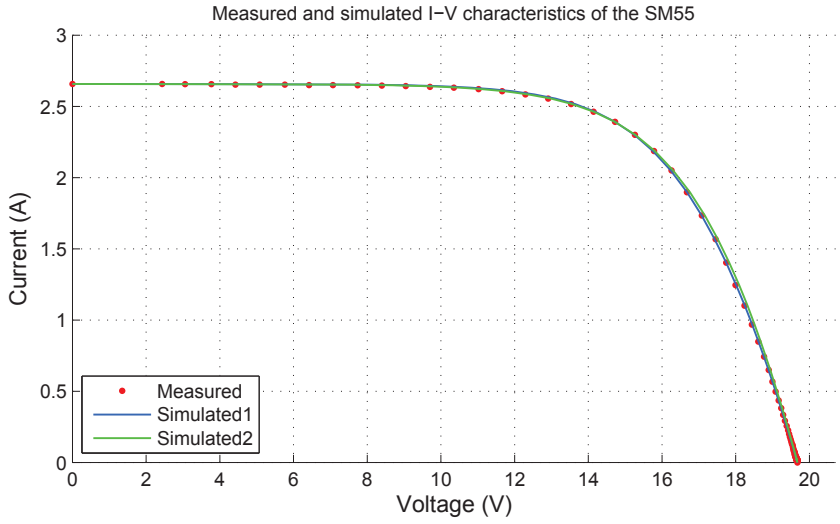

(b)

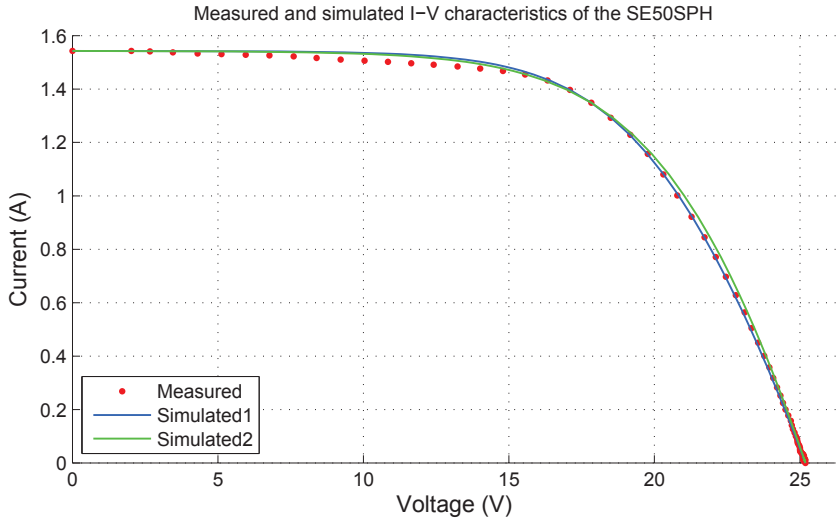

(c)

Figure 3.8: *Measured and simulated $I-V$ curves of three crystalline silicone panels, the BPMSX120 [2] (a), the SM55 [3] (b), and the SE50SPH [4], (c).* 'Simulated1' *has been created with single diode simple model using the parameters as calculated in Eq* (3.18), (3.20) *and* (3.19), *while* 'Simulated2' *has been created using the same model with the simplified expression of V_t (and consequently R_s).*

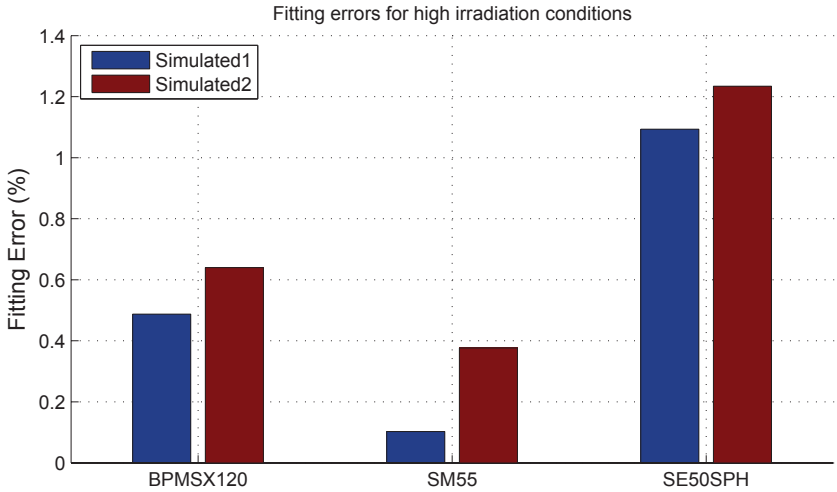

Figure 3.9: *Area fitting errors for three modules, when using the normal and simplified formulation of the parameters (measurements taken in high irradiation conditions).*

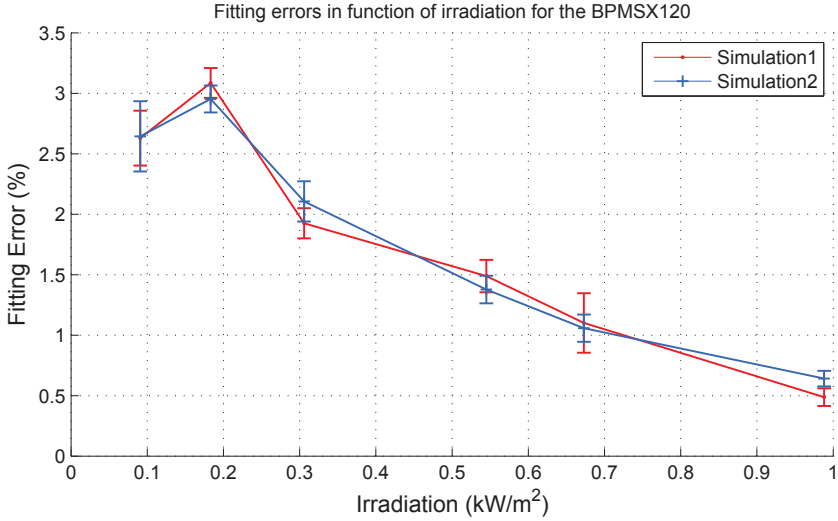

Figure 3.10: *Area fitting errors versus irradiation for the normal ('Simulated 1') and simplified ('Simulated 2') parameter sets. The data points represent the mean of the results based on 15 consecutive measurements, repeated every 12 seconds under the same conditions, and the vertical bars denote the standard deviations of the results over the respective set of measurements.*

3.6 Summary

This chapter gives a brief description of the mathematical modelling of PV cells and modules. The need for model parameter determination is addressed. In order to model the effects of partial shading on cells not protected by bypass diodes, the reverse characteristics have to be modelled. That requires incorporating the effects of the shunt resistance into the model [71, 81], which makes the model's parameter determination more complicated, requiring iterative methods to find the solutions.

Furthermore, a PV array model, as a tool for testing MPPT algorithms' efficiencies and evaluating the effects of different partial shadows, has been developed and implemented. It can be concluded that single diode five parameter model completed with Bishop's term is suitable to account for different environmental and partial shadowing conditions. However, in case when the model parameters have to be determined online, the lack of analytic solution is a limiting factor, despite of the theoretically higher precision capability of this model over that of the four-parameter model. Finally, parameter determination based on the simple four-parameter model for diagnostic purposes have been presented, with a proposed simplified analytic formula for finding the module's thermal voltage.

Chapter 4

Diagnostics of PV panels

This chapter deals with diagnostics of photovoltaic panels by means of analysis of their electrical characteristics. The chapter is divided into two main sections. The first part deals with parameter extraction (based on the single diode simple model) to be used for diagnostics purposes, and simple analytic formulae for the main parameters R_s and V_t are determined. In the second section the effects of various failures on these parameters are analysed, and diagnostic functions are proposed.

4.1 Introduction

Diagnostics of photovoltaic systems is gaining importance as an additional tool to increase the energy production of the PV system; they work by warning the user about failures or high failure risks, thereby minimising the time interval with reduced or no power production.

Diagnostics of a PV module implies determining some of its key parameters or characteristics, and, from their values, making an estimation about the health state and power producing capability of the system. A number of studies based on long-term monitoring of field data from PV systems are available [70, 89–94], which provide information about the main causes of performance degradations.

In Table 4.1 the main degradation factors which reduce the output power of PV systems has been summarised, based on data provided in [89–92, 94], as well as their possible effect on the PV module's electrical characteristic. The data presented in [91] and [92] indicate that degradation effects related to increased series resistance are the most frequent failure type in currently operating PV systems.

In Table 4.1, PS stands for partial shadow, and it represents distortions of the $I-V$ curve typical to ones caused by partial shadows. Section 4.3 deals with partial shadowing detection, which includes all the above-mentioned effects. Another large proportion of failures or performance degradations is related to the reduced amounts of light capable of reaching the surface of the PV cell. This can be caused by different factors, as are presented in Table 4.1. Except in the case when the reduced transparency of the covering layers is uniform, these types of problems generally result in non-uniform irradiation over the module, and thus have similar effects on the

Table 4.1: *Main fault types and their possible effect on the $I-V$ characteristics*

Type of failure	Possible effect on the $I-V$ curve
Corrosion [91, 92]	Increased R_s
Cell interconnect break [92]	Increased R_s, Decreased FF, PS
Decreased transparency of covering layers	
- Soiling	Decreased FF, PS
- Dust /Stain	Reduced peak power
- Discoloration of plastic encapsulates	Reduced peak power, decreased FF, PS
- Mismatches	Decreased FF, PS
Ageing of the semiconductor material	Reduced peak power, Decreased FF

I-V curve as a partial shadow.

As previously explained, diagnostics of PV modules and arrays also involve modelling. However, in this case, the main goal is to find simple analytic solutions, which can be executed in real-time, yet offer good fitting with the experimental data.

The determination of PV array parameters generally involves a sweep of the entire $I-V$ characteristic, from the short-circuit current to the open-circuit voltage, or using dark $I-V$ curves measurements [95].

In the literature many methods have been reported which aim to determine the parameters of a PV module or array, based on the experimental $I-V$ curve; most of them focus on finding a set of parameters which, inserted into a detailed model, would produce as close a fit as possible to the experimental curve. The parameters of the module are considered to be found with the solution set, which offer the best fitting with the experimental data. Such an approach is used by the authors of [58, 66, 67, 73, 95]. Generally a complex (5, 6, or 7-parameter) model is used and a good correlation with experimental data is achieved.

However, for the purpose of diagnostics, these methods may be criticised for, first of all, being computationally expensive, as they use iterative methods to find the optimum set of solutions. The other possible flaw of these methods is that they are considered to be valid in all irradiation and temperature conditions, and experimental results in environmental conditions different from the original measurements on which the parameter extraction is based, were not shown. Also, given the fact that even the detailed models found in the literature are still only approximations of the real physical process in the cells, [62,96] a high precision determination of some parameters of an approximate model seems to be impractical.

When looking at the determination of a panel's parameters from the diagnostics point of view, it is necessary to select some key parameters which would reflect changes in the panel's health state, relevant to energy yield. Although, as mentioned previously, there are many works dealing with parameter extraction for photovoltaic modules, there are few articles which drew conclusions about the state of health of the panel, based on the found set of parameters.

The parameter which garners the most attention is the panel's series resistance, which is well-known to have a direct impact on the fill-factor and the peak power of the module [70, 72, 88, 93].

The increase of series resistance has been identified as the main reason for module performance degradation [91, 92].

4.2 Series resistance monitoring

According to the IEC 60891 standard [97], in order to measure a PV panel's series resistance, two consecutive measurements are needed at different irradiation intensities, but at the same spectral distribution and temperature. This is often very difficult to achieve in natural ambient conditions. One method presented in [88] aims to overcome this problem by measuring only one I-V curve, and calculating the other one, using a model of the PV panels. However, the translation of the measurement data to other irradiation conditions in [88] does not consider the change of V_{oc} and V_{mp} with irradiance, which is likely to introduce additional uncertainty into the estimation, especially at low irradiation levels. Other methods seek to estimate the internal series resistance using dark I-V curve measurements, and model fitting, e.g. [67]. The shortcoming of the latter method is that, in case of a larger system, in order to measure the dark $I-V$ curve, a large DC power source is needed, which is generally not available in case of a residential rooftop installation.

In [72], a method for experimental determination of a solar cell's series resistance is presented. Using the four-parameter single diode model, and based on the area of the measured $I-V$ curve, an analytic solution for the cell's series resistance is shown. The advantage of this method that it does not require iterative calculations, and the integration process used to calculate the area under the $I-V$ curve has the effect of smoothing measurement data errors [72]. However, this method was intended mostly for solar cells with light concentrators, as some of the assumptions made while developing the formula are valid for high short-circuit currents [72].

A detailed analysis of the effects of series resistance and diode ideality factors based on field data, is presented in [70] and [93]. The series resistance and diode quality factors are identified using multiple $I-V$ curve measurements. Based on a series of measurements taken at different irradiance conditions, the series resistance has been identified as the intercept of the line defined by the slope of the $I-V$ curve at open-circuit conditions (noted R_{oc} in [70]) as $1/I_{sc}$ goes to zero (Fig.4.1(b)). The shortcoming of this method could be the necessity of a rather large number of measurements in different irradiation conditions, which are than normalised to the STC temperature, as described in [70, 93].

In this work, as mentioned in § 3.5, the focus is on the estimation of an equivalent series resistance, robust to environmental conditions, which can be used to indicate if there has been a significant deviation from predetermined values, either found by reference measurement or using datasheet parameters.

4.2.1 Equivalent series resistance estimation based on the slope of the $I-V$ curve at open-circuit

It is well-known that a forward biased p-n junction's current increases exponentially with the junction voltage, and the slope of the current tends to infinite, being limited only by the junction's internal series resistance. Therefore, for sufficiently large forward voltage, the slope of the current will be determined solely by the junction's series resistance. In the case of a photovoltaic module, its effective series resistance is composed by the junction's internal resistance, metallic contacts and interconnections [59].

Under natural conditions for a solar module, according to its equivalent circuit (Fig. 3.1) the highest forward bias (and highest current) for the junction is at the open-circuit voltage. That is the operating point where the slope of the $I-V$ curve is the closest to being determined solely by the series resistance; this can be seen on the derivative of the voltage (3.24), resulting in Eq. (4.1).

$$\frac{dV}{dI} = -\left(\frac{V_t}{I_{sc}-I} + R_s\right) \tag{4.1}$$

It is worth pointing out that, due to model limitations, the series resistance calculated from the equations in (3.19) ***is not identical to the panel's effective series resistance***, and it should be treated as a fitting parameter, which can have somewhat arbitrary values, depending on the properties of the module, e.g. short-circuit current, open-circuit voltage, fill-factor, etc. It has been shown [58,88] that this parameter can even become negative when fitting the single-diode model to experimental data. According to experimental measurements during this project, these occur especially at low irradiation conditions.

The panel equivalent series resistance is estimated here as the slope of the $I-V$ curve in the vicinity of the open-circuit voltage (Eq. (3.24)).

$$R_{se} = -\left.\frac{dV}{dI}\right|_{V=V_{oc}} \tag{4.2}$$

where R_{se} is the panel equivalent estimated series resistance.

In Publication 9 results considering series resistance estimation of a PV panel at high solar irradiation are presented. The results in this publication show that at high irradiation intensities the slope of the $I-V$ curve at open-circuit conditions very closely approximates the change in the effective series resistance of the module.

Irradiance effects

Among the many works dealing with series resistance estimation of PV modules, little attention is paid to examining the measurements during low irradiation intensities. One example that counters this is the analysis made in [70, 93], where measurements have been taken over a wide range of irradiations, from 10% of STC value and higher.

Equation (4.1) also predicts that R_{se} (4.2) is strongly dependent on the panel short-circuit current. As I_{sc} decreases, the first term in (4.1) becomes more dominant. As has been discussed in the previous section, in conditions of high irradiation the slope of the I-V curve at open-circuit offers good performance in estimating the panel's (increased) series resistance. However, at lower irradiations, according to Eq. (4.1), it is expected to increasingly overestimate the panel's series resistance. Therefore, in these conditions, the effect of low irradiations should be compensated for. In Fig. 4.1(a) the estimated series resistance, based on the slope of the experimental I-V curve at open-circuit versus irradiation, is plotted.

As can be seen in Fig. 4.1, the slope of the I-V curve at open-circuit is approximately a linear function of the reciprocal of irradiation (Fig. 4.1(b)), and, therefore, as the irradiation decreases, its value strongly increases. This is in good accordance with the results presented in [93] and [70] . A linear fitting of the last four data values from Fig. 4.1(b) predicts a series resistance of $\approx 0.9\Omega$ for the BPMSX120 [2] panel used. Using the datasheet values for this PV panel and solving Eq. (4.3) R_{se}, gives a value of $\approx 1.08\Omega$.

A method based on the simple model, which compensates for environmental effects, is proposed in the next section.

Proposed normalisation method for R_{se} to STC

Using the derivative of the voltage with current (4.1) and applying it to the open-circuit conditions, results in Eq. (4.3).

$$\left.\frac{dV}{dI}\right|_{OC} = -\left(\frac{V_t}{I_{sc}} + R_s\right) \tag{4.3}$$

According to this, the equivalent measured series resistance of the panel in two different environmental conditions can be written as Equations (4.4) and (4.5). R_{sm} stands for the model's series resistance, as in (3.24).

$$R_{seAct} = \frac{V_{tAct}}{I_{scAct}} + R_{sm} \tag{4.4}$$

$$R_{seSTC} = \frac{V_{tSTC}}{I_{scSTC}} + R_{sm} \tag{4.5}$$

$$\begin{cases} V_{tSTC} = V_{tAct}\frac{T_{Act}}{T_{STC}} \\ I_{scSTC} = I_{scSTC}\frac{G_{STC}}{G_{Act}} \end{cases} \tag{4.6}$$

where

- R_{seAct} - estimated series resistance based on the slope of the $I-V$ curve at open-circuit in actual environmental conditions
- R_{seSTC} - estimated series resistance based on the slope of the $I-V$ curve at open-circuit in STC

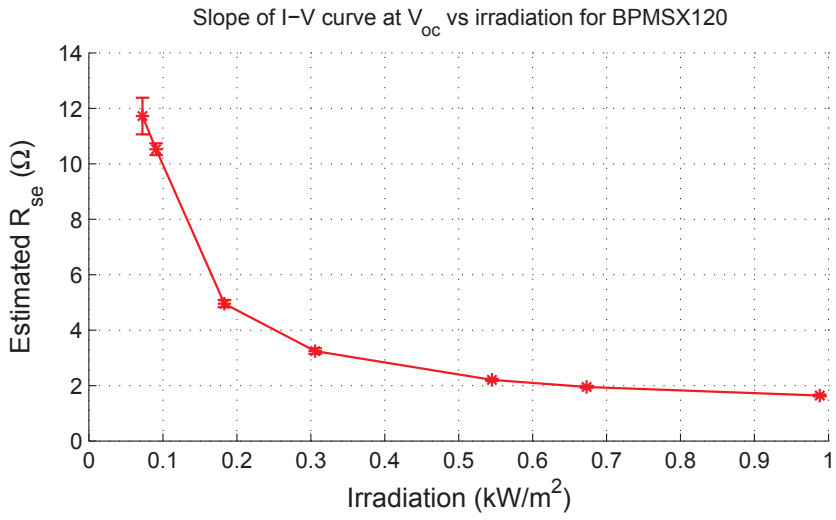

(a)

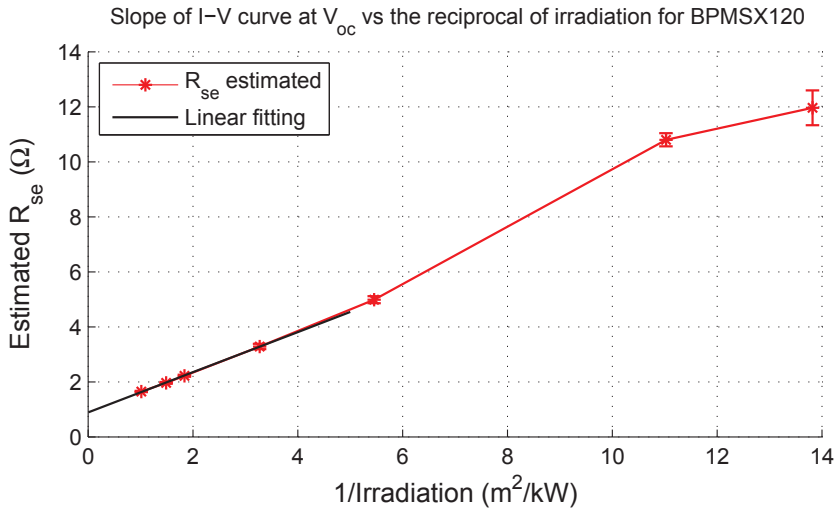

(b)

Figure 4.1: *Slope of the I-V curve at open-circuit versus irradiance (a) and the reciprocal of irradiation (b). The data points represent the mean of the results, based on 15 consecutive measurements repeated every 12 seconds under the same conditions, while the vertical bars denote the standard deviations of the results over the respective set of measurements.*

- V_{tAct} - thermal voltage calculated based on measurement taken in the actual environmental conditions
- V_{tSTC} - thermal voltage calculated based on measurement taken in STC
- T_{Act} - Actual temperature
- T_{STC} - STC temperature

Using the translation equations for V_t and I_{sc} from (4.6), and inserting them into (4.5), the estimation of the equivalent series resistance corresponding to STC can be found as in Eq. (4.7).

$$R_{seSTC} = R_{seAct} - \frac{V_{tSTC}}{I_{scSTC}} \left(\frac{T_{Act}}{T_{STC}} \frac{G_{STC}}{G_{Act}} - 1 \right) \tag{4.7}$$

It can be observed in Fig. 4.2 that normalising the R_{se} estimations to STC provides good results down to irradiations of below $200W/m^2$, giving usable estimates of the increased series resistance.

In Fig. 4.2, R_{seB} represents the base value for calculating dependency of series resistance estimation on various irradiation conditions. It is a result of an estimation at irradiation conditions close to $1kW/m^2$ with temperature compensation to STC.

As the slope of the I-V curve at open-circuit is mainly determined by the instantaneous irradiation intensity and is not strongly affected by temperature, the compensation for temperature to STC have little effect on the outcome. This is confirmed in Fig. 4.3, where the effect of temperature compensation on the output of R_{se} estimation is shown; the temperature effect is minor, even at its high values.

Figure 4.4 shows the estimations of different resistances connected in series with three different PV panels. Although the method slightly underestimates the added resistor value (with an error of $\approx 0.15\Omega$ in the worst case, for the SE50SPH panel [4]), the error remains relatively small and the method is suitable for detecting even relatively small changes in the series resistance of the modules.

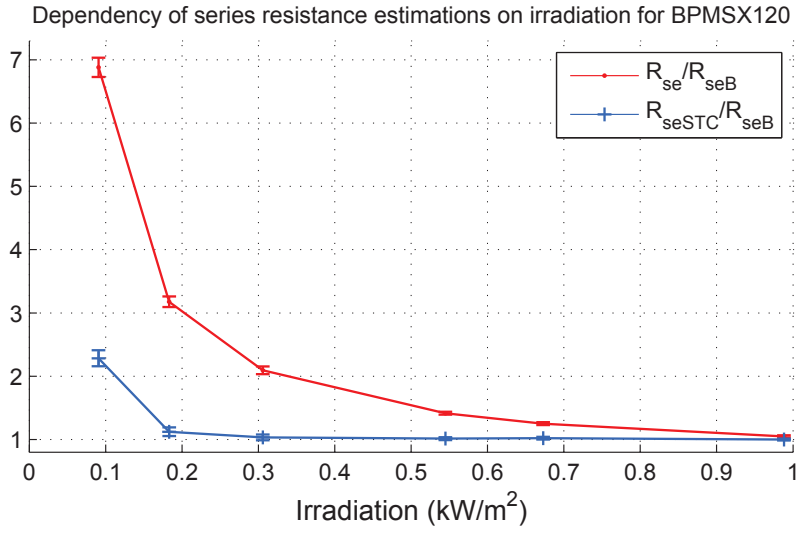

(a)

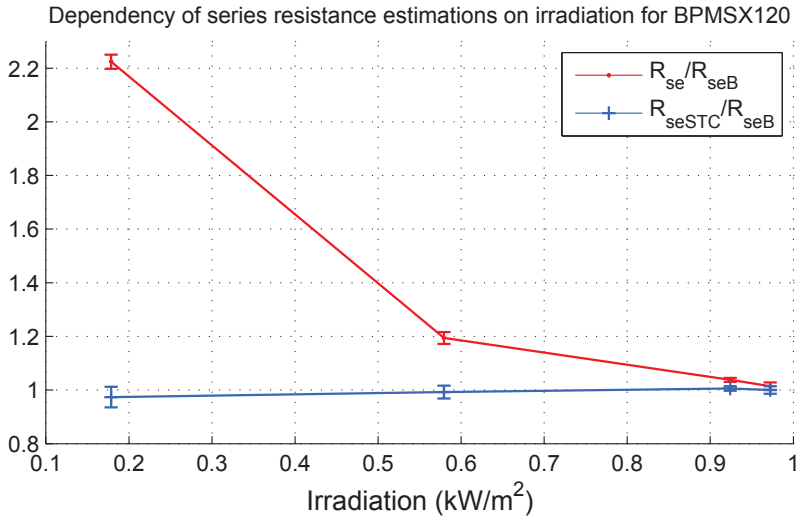

(b)

Figure 4.2: *Effect of irradiation on the series resistance estimation for the BPMSX120 PV panel. Using the slope translation method, the irradiance dependency is greatly reduced - at irradiations above 20% of STC, the estimation result is quasi-independent of irradiation. With an additional series resistance of* 1.2Ω *(b), the change in series resistance is detected with a relatively good precision throughout all the considered irradiation levels. . The data points represent the mean of the results based on 15 consecutive measurements repeated every 12 seconds under the same conditions, and the vertical bars denote the standard deviations of the results over the respective set of measurements.*

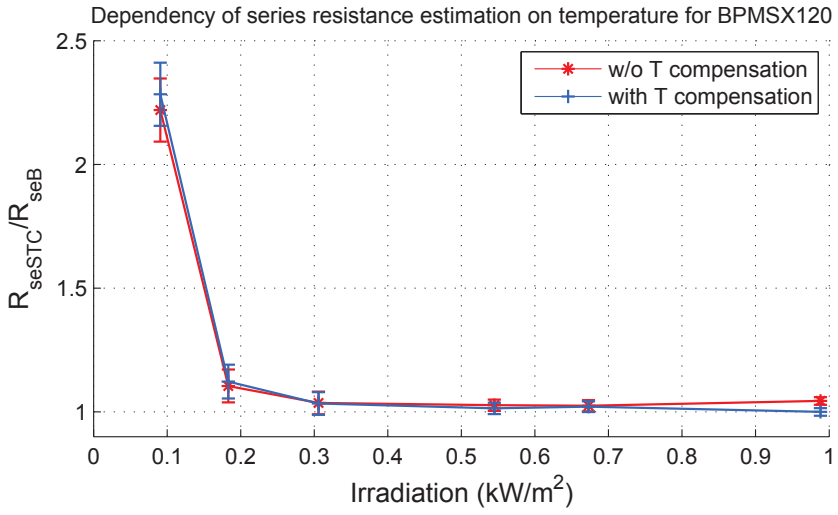

(a)

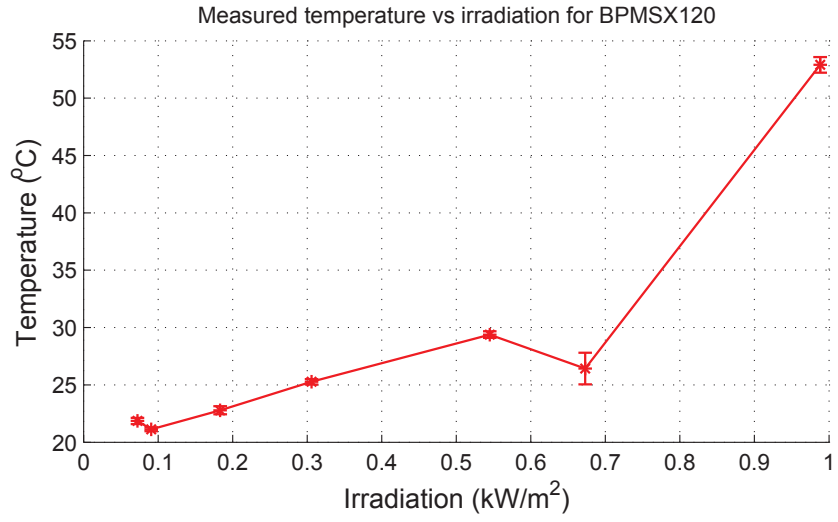

(b)

Figure 4.3: *Temperature effect on the series resistance estimation for the BPMSX120 module. On (a) the average estimation results for various irradiation intensities with and without normalising the temperature to STC are plotted, while on (b) the corresponding average temperature values are shown. The data points represent the mean of the results based on 15 consecutive measurements repeated every 12 seconds under the same conditions, and the vertical bars denote the standard deviations of the results over the respective set of measurements.*

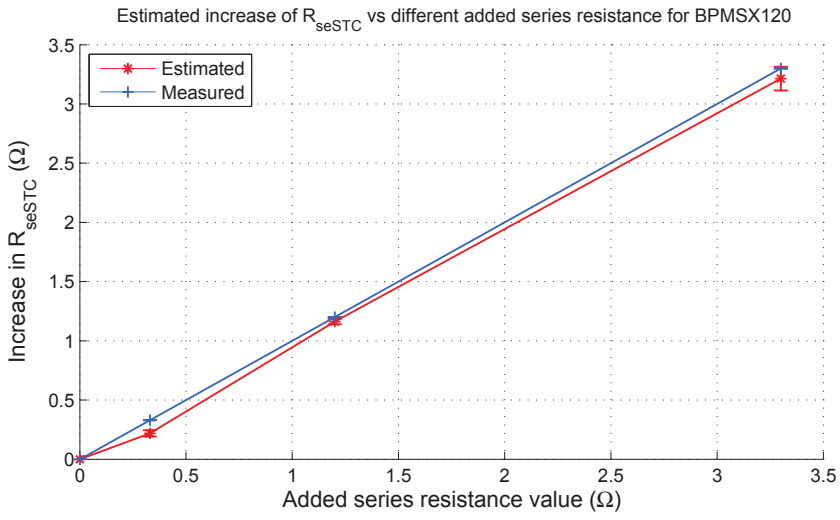

(a)

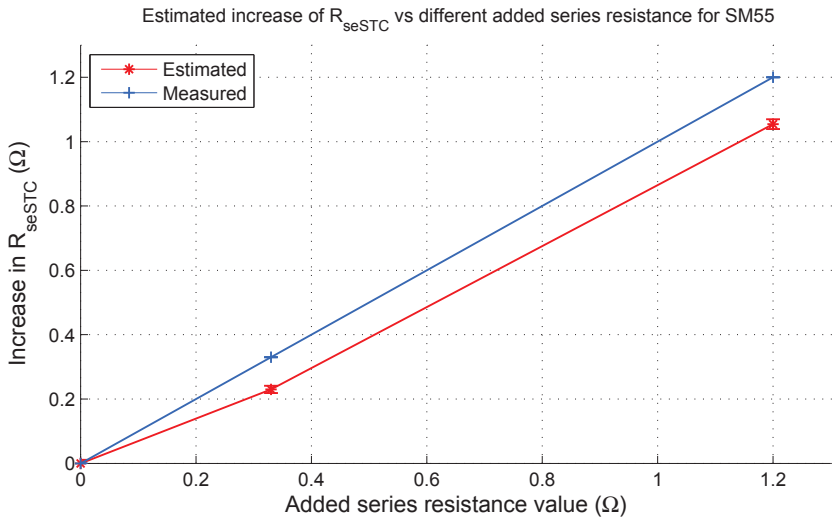

(b)

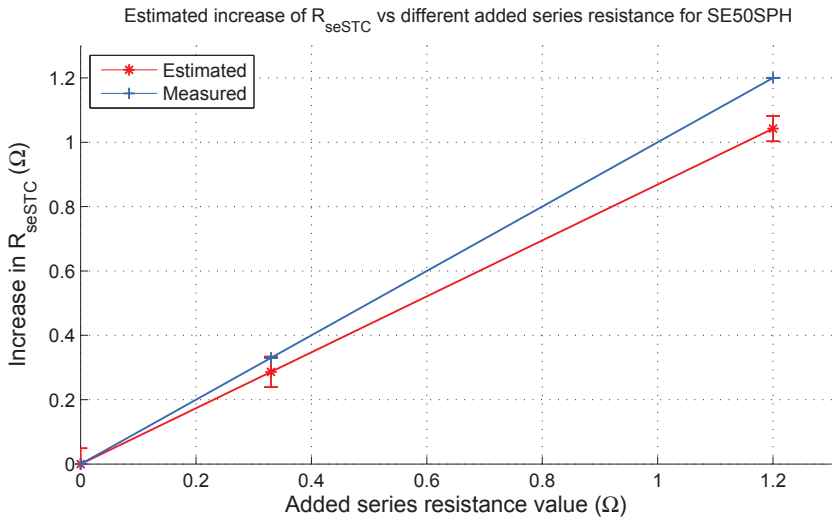

(c)

Figure 4.4: *Series resistance estimations for the three crystalline silicone panels versus various added series resistances. The data points represent the mean of the results based on 15 consecutive measurements repeated every 12 seconds under the same conditions, and the vertical bars denote the standard deviations of the results over the respective set of measurements.*

4.3 Partial shadowing detection

It is well-known that partial shadowing of photovoltaic arrays can overproportionally reduce the system's output power. It has been identified as a major reason for reducing the energy yield of grid connected photovoltaic systems [98].

The problem of partial shading has been extensively treated in the literature, on one hand as a cause of hot-spot formation and cell damage, and, on the other hand, with the utilisation of bypass diodes, as a cause of power loss due to average irradiation reduction and mismatch losses [63, 69, 71, 84, 87, 99–101]

As presented in [98], in the German 1000-Roofs-PV-Programme that was started in 1990, partial shadowing of PV arrays turned out to be one of the main reasons for the reduction in energy yield [90, 102].

From a diagnostic point of view, it is of particular interest to detect such events, first of all because a failure of one or more cells generally means reduced or no power production of those cells, and therefore the entire submodule. A partial shadow has a very similar effect on the module output, and therefore its continuous detection may indicate a failure, e.g. a discoloration of the covering plastic sheet (see Table 4.1).

Secondly, if a single cell from a block of bypass-diode protected series connected cells is covered, it will become reverse biased, and act as a load, burning most of the energy produced by the rest of the cells. Although the number of cells per bypass diode is generally selected such that the cells will be protected from reverse breakdown, a cell continuously exposed to these conditions will age and eventually fail faster.

From the point of view of the MPPT, partial shadows can create multiple peaks on the $P-V$ curve, thus making it difficult to identify the optimum operating point.

Partial shadowing detection based on thermal voltage monitoring

Shadowing part of a PV panel creates a deviation of its $I-V$ curve from the normal characteristic. Depending on the area, intensity, and position of the shadow in respect to the bypass diodes, it creates different shapes of the $I-V$ curve (Fig. 4.6).

The simplified form of the thermal voltage expression (Eq. (3.23)) suggests that changes in the module MPP current (I_{mp}) relative to its short-circuit current, as well as changes in V_{mp} have direct impact on the value of V_t. The experimental measurements (Fig. 4.7) indicates that V_t shows substantial sensitivity, even to a relatively small partial shadow, e.g. the ones presented on Fig. 4.6(a).

During high irradiation conditions, the simple four-parameter model exhibits good fitting with experimental measurements and therefore the partial shadowing condition can be detected solely based on the value of the calculated V_t. Comparing Fig. 4.7 with Fig. 4.6, it can be observed that partial shadows corresponding to 4.6(a) produce an increased V_t, while partial shadows corresponding to 4.6(b) will strongly decrease the value of V_t. This property can be

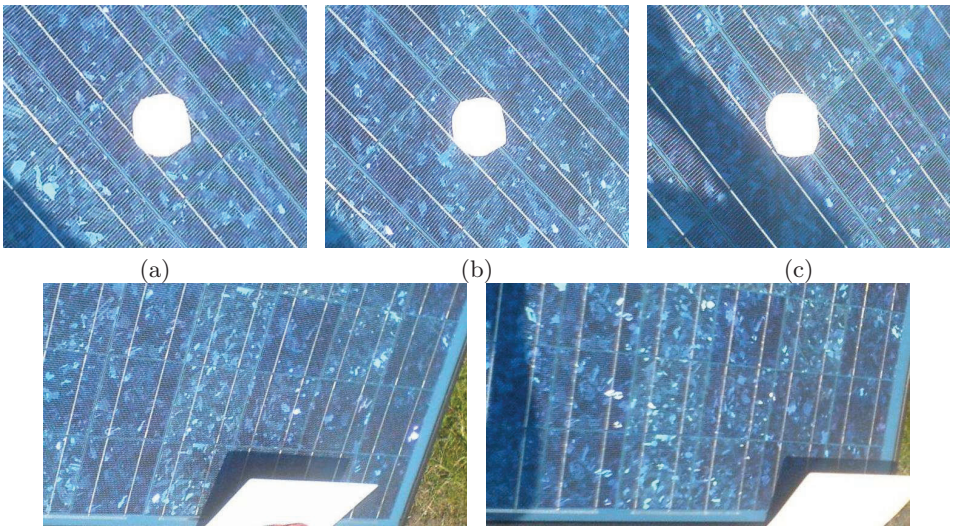

Figure 4.5: *Partial shadows on the BPMSX120 panel for experimental measurements used to create the characteristics on Fig. 4.6. The photo on (a) shows 'Dirt 1', which is a round white spot of* $\approx 10cm^2$ *in the middle of a cell, on (b) the same spot is between two adjacent cells, covering parts from both of them ('Dirt 2'), while on (c) the spot is at the meeting points of four cells, corresponding to 'Dirt 3'. The photo on Fig. 4.5(d) shows the shadowing of two cells, which belong to two different bypass diode protected submodule,('PS 1 Cell 2 Blocks') while (e) shows the shadowing of two cells within the same submodule ('PS 2 Cells 1 Block').*

explained by the change of the MPP relative to the ideal coordinates (V_{mp} and I_{mp}), which is reflected by V_t, and it provides additional information about the type of the shadow. This method of partial shadow detection shows robustness against changes in series resistance (see Fig. 4.8).

However, during low irradiation conditions, the sensitivity of the method decreases due to the restrictions of the model used to calculate V_t. As it is shown on Fig. 4.9, the thermal voltage exhibits a dependency on the irradiation, showing an increasing value as the irradiance falls. Therefore, at irradiations below 40-50% of STC, the increased value of V_t can trigger a false positive for partial shadows like 'Dirt 2' and 'Dirt 3' on Fig. 4.6(a). Nevertheless, partial shadowing, such as the ones presented in Fig. 4.6(b) produce a strong decrease of V_t, together with a decrease of fill factor, thereby their presence can be detected also at low irradiation conditions using the above method.

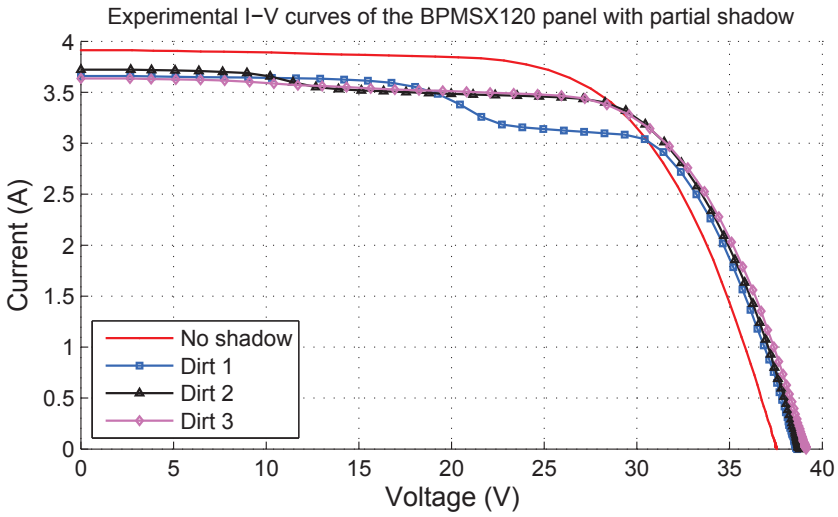

(a)

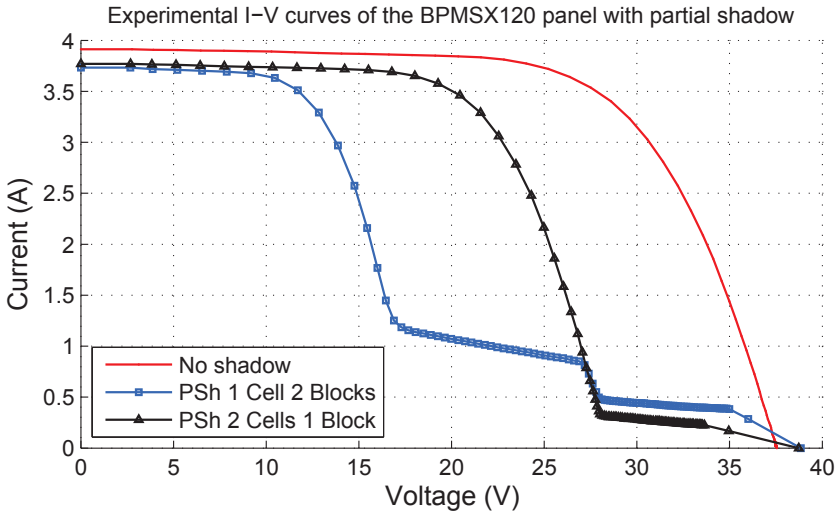

(b)

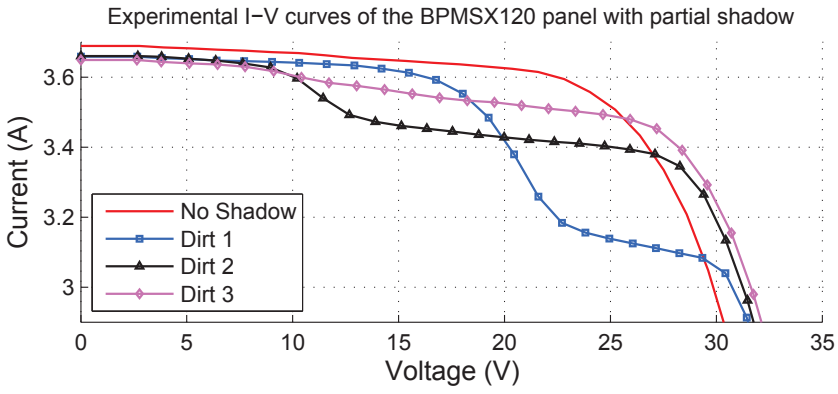

(c)

Figure 4.6: *Measured I-V curves of a BPMSX120 module under different shadowing conditions, normalised to the same irradiation. For the sake of clarity, 4.6(a) has been repeated on 4.6(c) showing the curves in the vicinity of short-circuit current.*

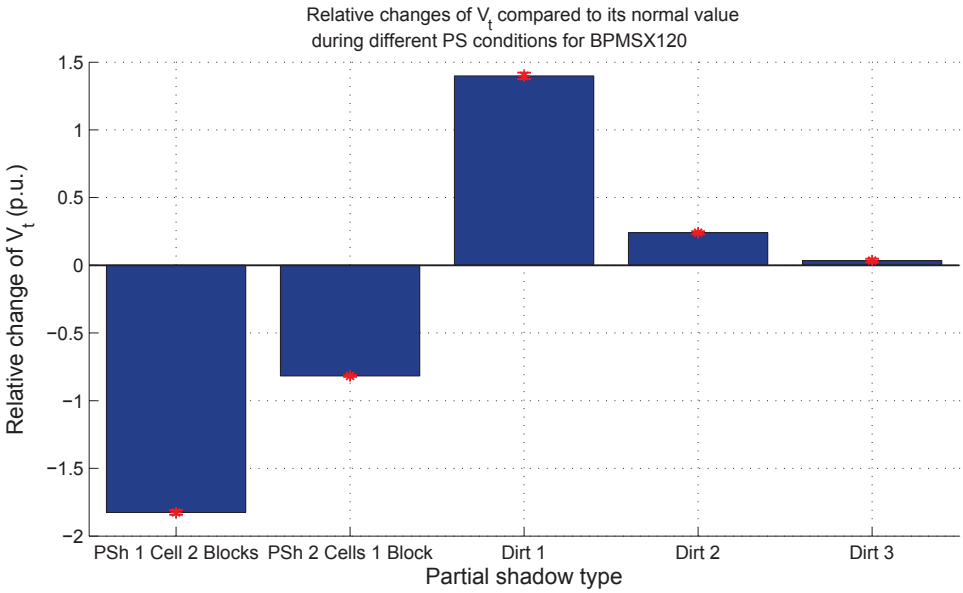

Figure 4.7: *Bar plot of the calculated thermal voltages for the BPMSX120 in different partial shadowing conditions. The data values represent the mean of the results based on 15 consecutive measurements repeated every 12 seconds under the same conditions, and the vertical bars denote their standard deviations over the respective set of measurements.*

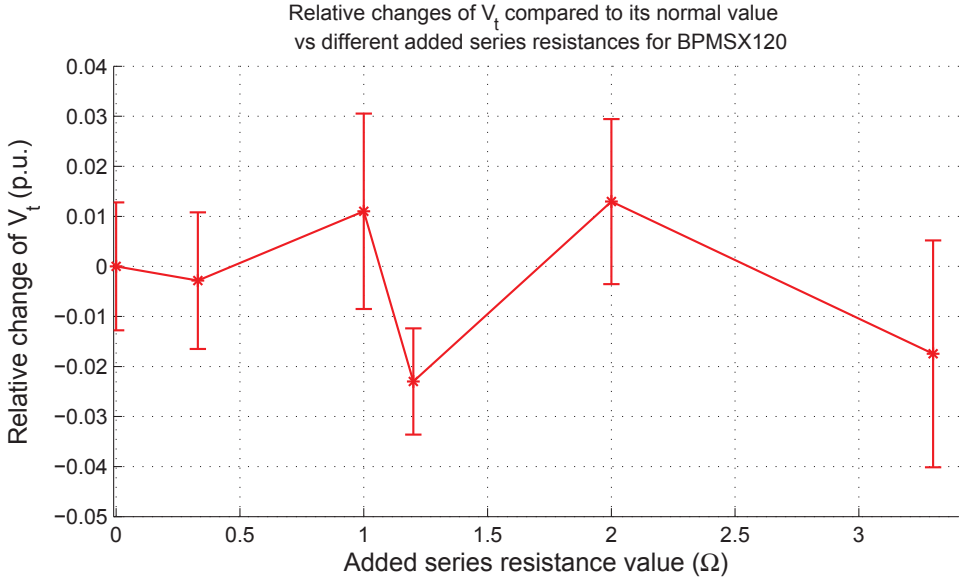

Figure 4.8: *Calculated thermal voltages versus various series resistance values added to the panel. The data points represent the mean of the results based on 15 consecutive measurements repeated every 12 seconds under the same conditions, and the vertical bars denote the standard deviations of the results over the respective set of measurements.*

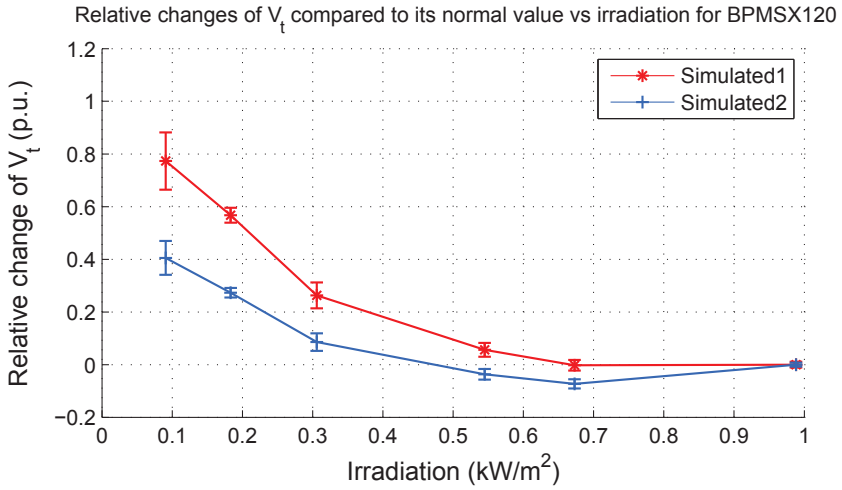

(a)

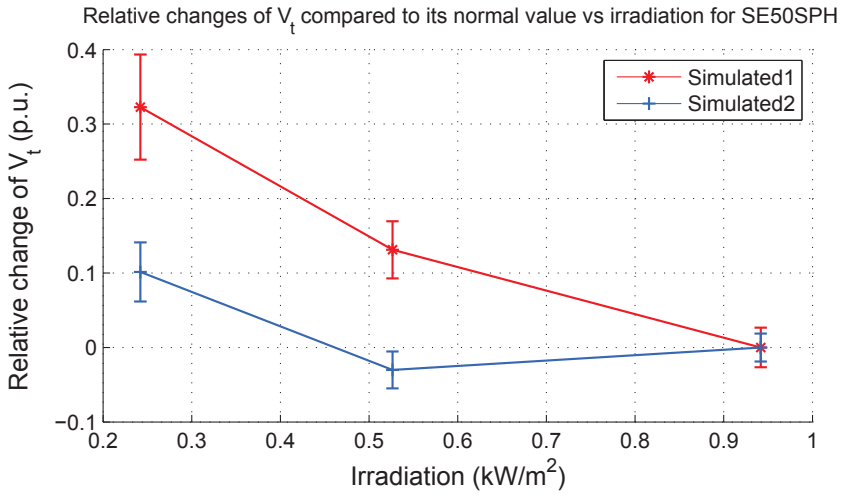

(b)

Figure 4.9: *Deviation of the thermal voltage from its normal value versus irradiance, normalised to the value calculated from the measurement at the highest irradiation.* 'Simulated 1' *represents* V_t *calculated based on* (3.20)*, while* 'Simulated 2' *denotes the thermal voltage according to* (3.23) *The data points are the results of 15 consecutive measurement in the same conditions, and the vertical bars denote the standard deviations of the results over the set of measurements.*

4.4 Temperature estimation

Increases in the temperature of PV modules can indicate bad ventilation and explain reduced power production. The temperature can have large variations over the array, especially in case of facade installations [92], and therefore it is difficult to measure the array's actual temperature. A method to estimate the array's effective temperature, in accordance with the IEC 60904-5 standard [103] is presented in the following. The parameter of the PV panel most affected by temperature, is generally the open-circuit voltage, which is easily accessible to measure. Thereby this value will be used to estimate the effective temperature of the panel.

In STC, the open-circuit voltage can be written as:

$$V_{ocSTC} = V_{tSTC} \ln\left(\frac{I_{scSTC}}{I_0}\right) \tag{4.8}$$

The value of V_{oc} in STC is known from datasheet value or found by reference measurements. If one considers that V_t is independent of irradiation, from the above equation it follows that the open-circuit voltage depends logarithmically on the irradiation:

$$V_{oc}(G) = V_{ocSTC} + V_{tSTC} \ln\left(\frac{G}{G_{STC}}\right) \tag{4.9}$$

However, as has been shown in §4.3, V_t calculated from the measured $I-V$ curve increases at low irradiations, due to the limitations of the simple model. In order to compensate for this drawback of the four-parameter model at low irradiation conditions, a correction factor is added to Eq.(4.9), which aims to improve the estimation accuracy at low irradiation levels:

$$V_{oc}(G) = V_{ocSTC} + \left(V_{tSTC} + \frac{(V_{tSTC} - V_t)}{V_{tSTC}}\right) \ln\left(\frac{G}{G_{STC}}\right) \tag{4.10}$$

Adding the temperature dependence to (4.10), results the expression of the open-circuit voltage as a function of the actual environmental conditions, based on STC values.

$$V_{oc}(G,T) = V_{oc}(G) + k_v (T - T_{STC}) \tag{4.11}$$

According to the above, the panel's actual temperature can be calculated, based on measurement of the open-circuit voltage and irradiance, and knowledge of the datasheet parameters such as the open-circuit voltage and its temperature coefficient.

$$T = \frac{V_{oc}(G,T) - V_{oc}(G) + k_v T_{STC}}{k_v} \tag{4.12}$$

Fig. 4.10 displays the results of the temperature estimation based on Eq. 4.12 over a wide range of irradiation for three crystalline silicone PV panels. The results show a maximum deviation of $\approx 4^oC$ for the BPMSX120, $\approx 5^oC$ for the SE50SPH photovoltaic panel, and $\approx 1^oC$ for the SM55 [3]. It should be noted that for the latter panel all the measurements were taken at medium-high irradiation levels. In the case of the SE50SPH panel the temperature coefficient of

the open-circuit voltage was not available, and therefore a standard value of $k_v = V_{oc} \cdot 44 \cdot 10^{-4}$ (for silicone panels) [92, 104] was used.

It is worth pointing out that this method relies on the panel's open-circuit voltage in STC, taken from the datasheet. This might introduce errors into the estimation if, due to ageing, the panel actual V_{oc} in STC has changed. Nevertheless, in the case of crystalline silicone panels, according to field data presented in [94], and [89], the open-circuit voltage change due to ageing is very small, which is in good accordance with results presented here.

4.5 Nominal power estimation

Measuring the maximum power in STC for a PV panel allows the comparison of the measured values to datasheet ones and an estimation of the overall efficiency degradation of the panel due to ageing, increased series resistances, or other reasons. It is often used as a verification tool of the datasheet values, as part of quality-inspection [104, 105] or as a method to predict the generated energy during natural sunlight conditions [106,107]. Although, in order to obtain high precision and reliable results, expensive equipment and controlled environmental conditions are generally needed [108,109], the authors of [104,105,107] have shown that satisfactory results can be achieved using algebraic methods for predicting the generator's performances under natural sunlight conditions, based on knowledge of the panel's parameters in STC conditions.

In the present work, keeping in mind the diagnostics purposes, the nominal power estimation of the panel is used to quantify the overall power loss due to all degradation effects, e.g. slacking of contacts, discoloration of the encapsulating material, soiling, ageing, or partial shadowing. Therefore, adopting similar approach to that used in the previous sections, the accent is on determining changes (decreases) of the peak power, compared to a reference measurement or datasheet values and quantify the power reduction. Once again, the four-parameter simplified model is used, as described by Eq.(3.9), and a method which combines algebraic and numerical solutions based on measured parameters, is proposed. Using the measured $I - V$ curve and environmental data, some parameters whose dependence on environmental conditions is known, are determined and, based on these parameters the maximum power point in STC is estimated. From the measured characteristic, the thermal voltage V_t is calculated, considered to be independent of irradiation and to be a linear function of temperature.

The other basic parameter determined from the actual measurement and rendered to STC is the model's series resistance R_{sm}. Using the method described in §4.2 the panel's effective series resistance R_{se} is determined and translated to STC by applying Eq. (4.7). In the next step the *model* series resistance in STC conditions can be calculated using Eq. (4.5).

Considering the above, the equations used to estimate the panel peak power (Publication 9) are the following:

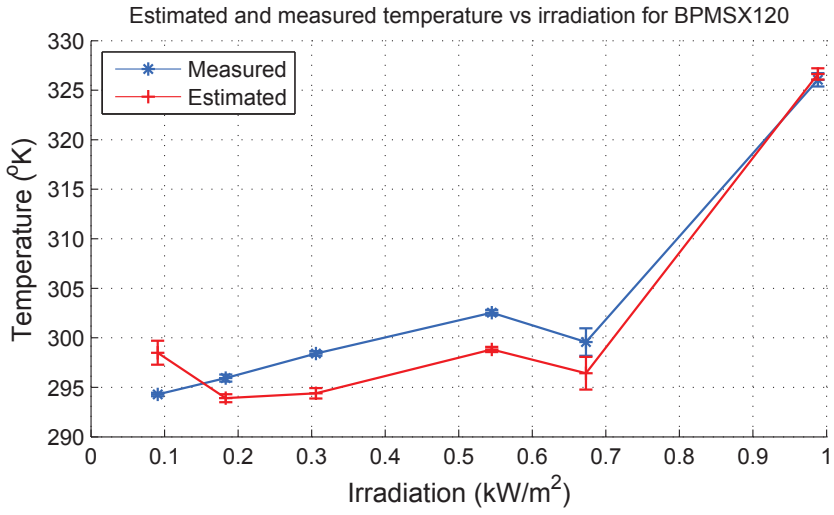

(a)

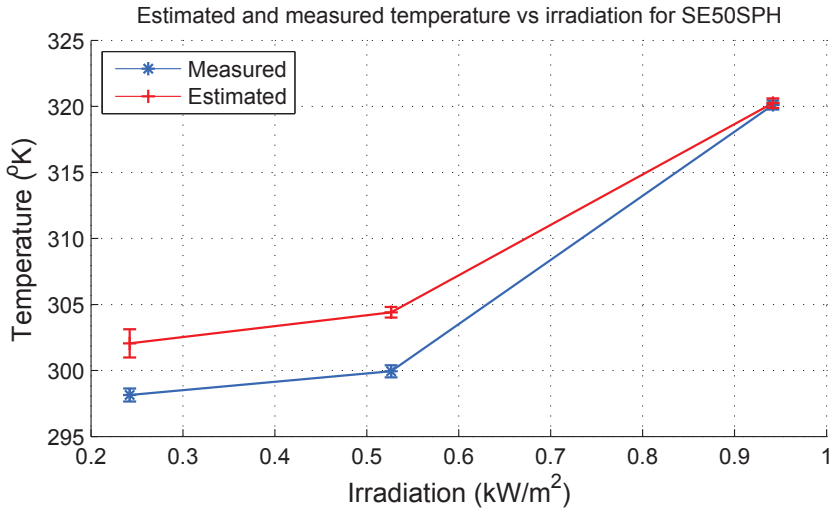

(b)

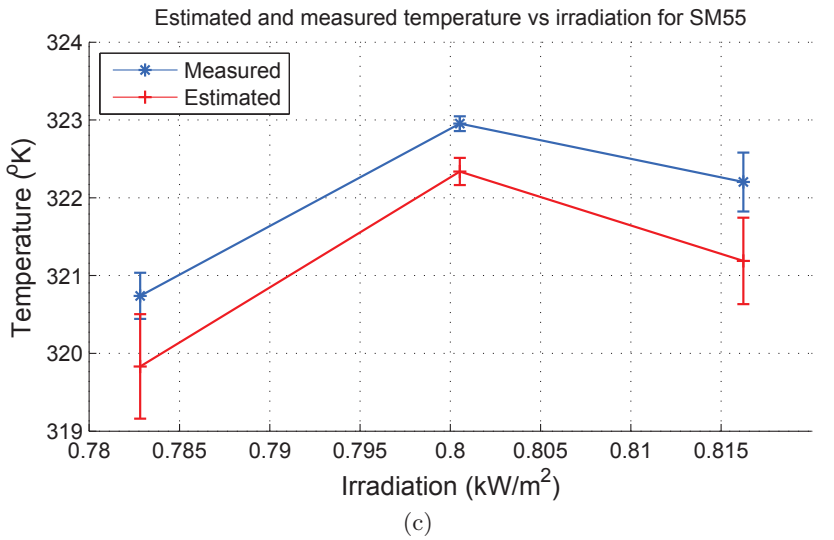

(c)

Figure 4.10: *Measured and estimated temperature versus irradiation for three crystalline PV panels. The data points represent the mean of the results based on 15 consecutive measurements repeated every 12 seconds under the same conditions, and the vertical bars denote the standard deviations of the results over the respective set of measurements.*

$$V_{mpSTC} = V_{ocSTC} + V_{tSTC} \ln\left(\frac{V_{tSTC}}{V_{mpSTC} + V_{tSTC}}\right) - \frac{I_{scSTC}\, V_{mpSTC}\, R_{sSTC}}{V_{mpSTC} + V_{tSTC}} \tag{4.13}$$

$$I_{mpSTC} = \frac{I_{scSTC}\, V_{mpSTC}}{V_{mpSTC} + V_{tSTC}} \tag{4.14}$$

As can be seen on Eq. (4.13), the expression of the MPP voltage in STC (V_{mpSTC}) is transcendental, therefore a numerical method is needed to solve it. Using a simple Newton-Raphson algorithm, (with initial condition parameters taken from the datasheet) the solution can be found within a few iterations.

The above rated power estimation method uses the assumption that the thermal voltage changes linearly with the temperature and it is independent of irradiation. Although, from modelling point of view, these assumptions are commonly used, and have been adopted previously in the literature [105], due to model limitations, V_t being considered independent on irradiation introduces estimation errors at low irradiation levels (Fig. 4.9). Therefore, in order to minimise this error, for the purpose of rated power estimation, the simplified expression (3.23) has been used to calculate V_t, which shows less sensitivity to low irradiation levels.

Thorough assessment of the accuracy of the estimation method is difficult in the absence of high precision laboratory equipment, where Standard Test Conditions can be reproduced. As this equipment was unavailable, the results of the estimation method have been compared to those of a commercial photovoltaic $I - V$ curve tracer, which has an estimation accuracy of $\pm$ 5%, according to the product datasheet.

The results of peak power estimations based on measurements in various conditions are showed on Figures 4.12, 4.13, and 4.14. As can be seen in 4.12, the result of the estimation show good robustness against irradiations, down to approximately $300W/m^2$. When using the method to quantify power losses due to increased series resistance it shows an approximately linear response to the added series resistance. In the case of various partial shadowing, it shows relatively good sensitivity even to small shadows (like 'Dirt 1' and 'Dirt 2' on Fig. 4.14), but the effect of 'Dirt 3' is not reflected in this method of peak power estimation. In case of severe distortion of the I-V curve by e.g. a shadow as described by Fig 4.5(e), the fitting of the curve fails, and the estimation has no result. For the conditions where peak power estimation was not possible, the results are shown on the figures as zero.

4.6 Summary

This chapter discussed the detection of failures and power reducing effects on photovoltaic arrays. The main causes of possible power production losses are connected to failures involving increased series resistance. Other main factors which reduce the power output are the reduced

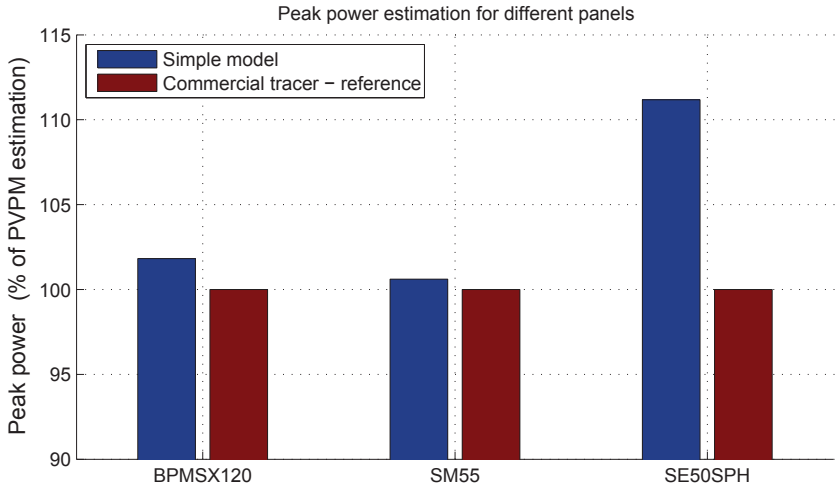

Figure 4.11: *Estimated STC power calculated from measurements taken at natural ambient conditions (high irradiation) for three crystalline silicone panels. The data points represent the mean of the results based on 15 consecutive measurements repeated every 12 seconds under the same conditions, and the vertical bars denote the standard deviations of the results over the respective set of measurements.*

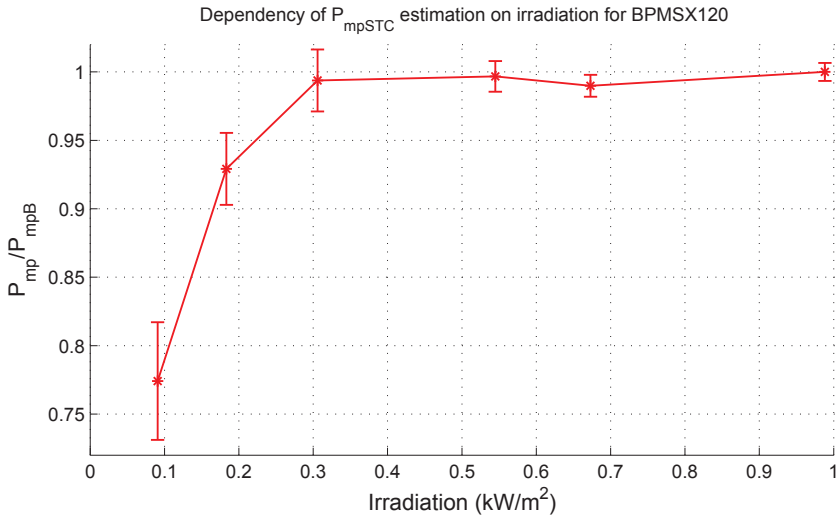

Figure 4.12: *Evaluation of the estimated STC power versus irradiation for the BPMSX120 panel. The data points represent the mean of the results based on 15 consecutive measurements repeated every 12 seconds under the same conditions, and the vertical bars denote the standard deviations of the results over the respective set of measurements.P_{mpB} is the result of an estimation at irradiation conditions close to $1kW/m^2$ with temperature compensation to STC.*

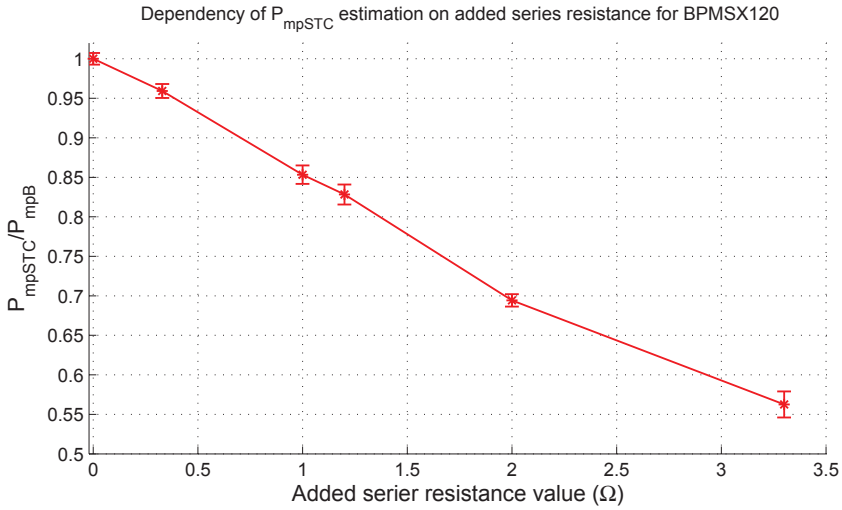

Figure 4.13: *Estimated STC power in conditions of increased series resistance. The data points represent the mean of the results based on 15 consecutive measurements repeated every 12 seconds under the same conditions, and the vertical bars denote the standard deviations of the results over the respective set of measurements.*P_{mpB} *is the result of an estimation at irradiation conditions close to* $1kW/m^2$ *with temperature compensation to STC.*

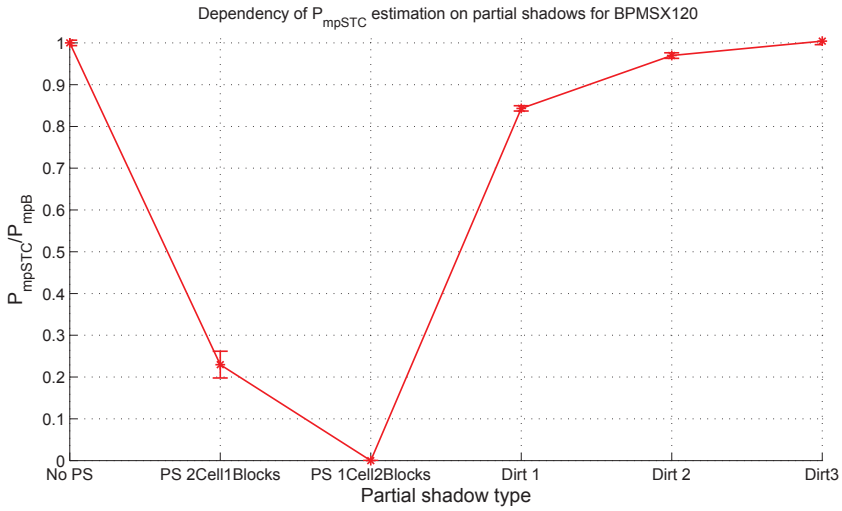

Figure 4.14: *Estimated STC power in conditions of different partial shadows. The data points represent the mean of the results based on 15 consecutive measurements repeated every 12 seconds in the same conditions, and the vertical bars denote the standard deviations of the results over the respective set of measurements.*P_{mpB} *is the result of an estimation at irradiation conditions close to* $1kW/m^2$ *with temperature compensation to STC.*

transparency of the cell covering layers, including soiling, dust, stains, discoloration of the plastic cover, etc.

The equivalent series resistance of the panel has been identified using the slope of the $I - V$ curve in open-circuit conditions, and a simple scheme to reduce the sensitivity of the measurement to environmental conditions has been proposed. The sensitivity of the method to environmental conditions has been investigated.

Partial shadow effects creating distortions of the $I - V$ curve has been discussed. It has been proposed the monitoring of the thermal voltage V_t for detecting partial shadows, due to its simplicity and robustness against other failures, such as series resistance increases. However, in the case of small area spots (Fig. 4.5(c)) distributed over several cells on the panels, their presence is difficult to detect. Another limitation of the proposed method is that at low irradiation conditions it can trigger false positives of small area shadows due to the increase of the V_t at low irradiations. Nevertheless, partial shadows which create a decrease of V_{mp} can be detected throughout all irradiation ranges.

In order to quantify power losses caused by a number of factors, such as increased series resistance, partial shadowing or other reasons, the STC peak power estimation is used. A mixed analytical-numerical method is proposed, employing the already-determined parameters.

Chapter 5

Conclusions

This chapter intends to summarise the work which has been carried out throughout this thesis, emphasising those elements, which contribute to Maximum Power Point Tracking and diagnostics for PV arrays. The chapter ends with an outlook to further research which have been enabled by the work presented in this thesis.

5.1 Summary

The present report has two main subjects: *Maximum Power Point Tracking*, which is described in Chapter 2, and *Diagnostics of PV panels*, described in Chapter 4. Additionally, several models have been developed and built in Chapter 3 for: a.) simulating the behaviour of PV arrays in different environmental conditions and thus used to test MPPT algorithms, and b.) for determining key parameters, whose changes would provide information about the state of the PV panels /array, and thus used for diagnostic purposes.

In the beginning of Chapter 2 an overview of the main MPPT algorithms is given, and the their difficulty of tracking in variable conditions has been pointed out. Both of the most popular MPP trackers, the $P\&O$ and the INC share the shortcoming of possible misdirectional tracking during rapidly changing conditions due to their inability to distinguish the result of their own perturbations from the environmental changes. A simple and effective technique, which can be used for both the $P\&O$ and INC, has been proposed to overcome this drawback.The method separates the MPPT effects from environmental changes and provides correct information to the tracker, which therefore is not affected by the environmental changes. The method has been implemented based on the $P\&O$, and the experimental results demonstrate that it preserves the advantages of the existing trackers in offering high efficiency during stable conditions, while adding the benefit of virtually unchanged efficiency during fast changing conditions. Furthermore, the algorithm has been implemented on a commercial PV inverter, the REFUSOL 11K [56], currently on the market.

In order to the test the performance of the MPP trackers, both in simulations and experimentally, a PV simulator, which is able to take into account the environmental changes regarding e.g. irradiation and temperature, is needed. Furthermore, in order to assess the effects of dif-

ferent partial shadows on the PV output power, the cells' reverse characteristics also need to be modelled. This comes with the price of the necessity of having to include the shunt resistance into the model, making parameter determination more difficult. In Chapter 3 an overview of the existing models used to describe the behaviour of PV panels is provided, followed by the parameter determination for the five-parameter single-exponential model based on datasheet values, which has been used for the implementation of a PV simulator taking into account the shape of partial shadows.

One important conclusion from the PV simulator implementation in Chapter 3 is that the five-parameter model which takes into account the shunt resistance, is not suitable for diagnostic purposes due to the fact that it does not allow the determination of analytic formulae for the model's parameters, which makes its use difficult in real-time calculations. Furthermore, as iterative methods have to be used for parameter determination, the initial values for the parameters have to be chosen with care to ensure that the iteration converges. Therefore a simplified three-parameter model has been used throughout Chapter 4, dedicated to diagnostic functions of PV panels, based on simple analytic expressions for the model parameters, derived in Chapter 3.

Combining the model calculations with measurements, a method to determine changes in the panel's series resistance, based on the slope of the $I-V$ curve at open-circuit conditions has been proposed. The benefits of the proposed method include: robustness to irradiance changes and applicability over a wide range of irradiations, the fact that it does not need the entire $I-V$ curve unlike other methods described in the literature ([88,97]), and its robustness against other failures which would distort the $I-V$ curve of the panel, e.g. partial shadows.

As mentioned in Chapter 4, partial shadowing is a major reason for the energy yield reduction of photovoltaic systems. Its early detection is important, not only due to the immediate power reduction of the PV array, but also to protect the shadowed cells from long-term exposure to increased temperature (see §4.3 on page 49). In order to detect such events, a method based on thermal voltage monitoring has been proposed. The main advantages of this method are the simple expression for the thermal voltage, high sensitivity to even a relatively small area of partial shadow and very good robustness against changes in series resistance.

As it has been described in Chapter 4 the array temperature directly affects its power output, and high temperatures can seriously reduce the energy yield. While high temperature does not necessarily mean a malfunction of the array, it can explain reduced power production and its detection enables measures to be taken. Considering that the temperature can have large variations over the area of the array (see §4.4), in some cases it can be difficult to measure [92] the array's average temperature. Consequently, a simple temperature estimation method based on the IEC 60904-5 standard, using the measurement of the open-circuit voltage with compensation for low irradiation, has been presented. At high irradiation conditions the method shows good accuracy, while the worst case accuracy is $\approx 5K$ at low irradiation.

In order to quantify power losses due to different failures, e.g. partial shadows or increased series resistance, a model based approach, which includes the series resistance, thermal voltage and temperature (as determined in Chapter 4) has been proposed to estimate the panel rated power (in STC). Although it is known that the single-exponential model is not precise at low irradiation conditions, using the previously determined parameters it was possible to achieve relatively good accuracy. The main advantage of the method is that it relies on already determined parameters (R_s, V_t, I_0) based on measurement, and therefore reduces the errors introduced by the limitation of the single-exponential model in low irradiation conditions.

5.2 Future work

The attempts made in this thesis to contribute to the improvement of MPPT techniques and diagnostics of photovoltaic arrays have far from finished the task in these subjects. There is a lot of room for improvement, especially in diagnostics, which is a relatively new area.

Regarding MPPT control, would be interesting to investigate the possibility of tracking during partially shaded conditions. The existing methods, as presented in [52,53,110] are based on periodically sweeping the entire $I - V$ characteristic of the array. The optimisation of this process using the information provided by the diagnostic function could be an interesting research topic.

The shunt resistance, although it is generally not considered to be one of the parameters with a major influence on the PV output power [18,104] (as series resistance increase, or partial shadowing are), however, monitoring its change would offer a more complete characterisation of the solar array. For example, according to experimental results, certain types of partial shadows could not be detected using the thermal voltage monitoring method (see Fig. 4.7), which could be detected by the change in the apparent shunt resistance.

Although the PV panels used for experimental tests of the diagnostic methods presented here contain up to 72 cells and 4 bypass diodes (in the case of BPMSX120 panel [2]), which can be considered as a small-scale representation of a photovoltaic array, a full-scale residential PV system should be also considered for field testing.

As has been previously mentioned, the models and diagnostic functions used in this work consider crystalline silicone PV cells. It would be an interesting topic to test their validity on amorphous silicone cells.

Bibliography

[1] IEA-PVPS, "Trends in Photovoltaic Applications. Survey report of selected IEA countries between 1992 and 2007," International Energy Agency - Photovoltaic Power Systems Programme, Tech. Rep. IEA PVPS T1-17:2008, August 2008.

[2] B. Petrol, *BP MSX 120 Data Sheet*, BP Solar, 2001.

[3] Siemens, *Siemens Solar Module SM 55 Data Sheet*, Siemens Solar GmbH, Postfach 46 07 05, D-80915 München, Germany, 1998.

[4] Solel, *Solel SE50SPH Data Sheet*, Solel.

[5] B. Bletterie, R. Bruendlinger, and S. Spielauer, "Quantifying dynamic MPPT performance under realistic conditions First test results Ű the way forward," in *21st European Photovoltaic Solar Energy Conference and Exhibition*, September 2006.

[6] UNEP, "Global Trends in Sustainable Energy Investment 2008," United Nations Environment Programme, Tech. Rep., 2008, executive summary.

[7] IEA-PVPS, "Trends in Photovoltaic Applications. Survey report of selected IEA countries between 1992 and 2003," International Energy Agency IEA, Report T1-13, 2004. [Online]. Available: http://www.iea-pvps.org/products/rep1_13.htm

[8] ——, "Trends in photovoltaic applications. Survey report of selected IEA countries between 1992 and 2005," International Energy Agency - Photovoltaic Power Systems Programme, Report IEA-PVPS Task 1 T1-15:2006, 2006. [Online]. Available: http://www.iea-pvps.org/products/download/rep1_15.pdf

[9] U. DOE, "Solar energy technologies program. multi-year program plan 2007-2011," U.S. Department of Energy, Tech. Rep., 2007.

[10] EWEA, "Delivering energy and climate solutions. EWEA 2007 annual report." European Wind Energy Association, Tech. Rep., 2007.

[11] E. P. T. Platform, "A Strategic Research Agenda for Photovoltaic Solar Energy Technology," European Photovoltaic Technology Platform, Tech. Rep., 2007.

[12] W. C. Sinke, C. Ballif, A. Bett, B. Dimmler, D. Dimova-Malinovska, P. Fath, F. Ferrazza, H. Gabler, M. Hall, A. Martí, N. Mason, E. Mellikov, A. Milner, P. Mogensen, C. Panhuber, N. Pearsall, J. Poortmans, C. Protogeropoulos, G. Sarre, D. Sarti, P. StrauSS, M. Topic, R. van Zolingen, and T. Zdanowicz, "A strategic research agenda for photovoltaic solar energy technology," in *Proc. of the 22nd European Photovoltaic Solar Energy Conference and Exhibition*, September 2007.

[13] PV-TRAC, "A Vision for Photovoltaic Technology," European Comission - Photovoltaic Technology Research Advisory Council, Tech. Rep., 2005.

[14] J. Y. Ahn, J. H. Park, and B. Cho, "Dual-module based maximum power point tracking control of PV system," in *Applied Power Electronics Conference and Exposition, 2004. APEC '04. Nineteenth Annual IEEE*, vol. 3, 2004, pp. 1509–1514 Vol.3.

[15] L. Egiziano, N. Femia, D. Granozio, G. Petrone, G. Spagnuolo, and M. Vitelli, "Photovoltaic inverters with Perturb & Observe MPPT technique and one-cycle control," in *Circuits and Systems Proceedings IEEE International Symposium on*, 2006, pp. 4 pp.–.

[16] EPIA, "EPIA roadmap," EPIA, Report, June 2004. [Online]. Available: http://www.epia.org/04events/docs/EPIAroadmap.PDF

[17] U. DOE. The History of Solar. U.S. Department of Energy - Energy Efficiency and Renewable Energy. [Online]. Available: www1.eere.energy.gov/solar/pdfs/solar_timeline.pdf

[18] V. Benda, "Solar cell and module fabrication technology," November 2008, course presented at the Institute of Energy Technology.

[19] D. Pachon, I. Anton, and G. Sala, "Rating and modelling of concentrator systems," in *Photovoltaic Specialists Conference, 2002. Conference Record of the Twenty-Ninth IEEE*, 2002, pp. 1600–1603.

[20] M. Shahidehpour and F. Schwarts, "Don't let the sun go down on pv [photovoltaic systems]," *Power and Energy Magazine, IEEE*, vol. 2, no. 3, pp. 40–48, 2004.

[21] *PHOTON International. The Photovoltaic Magazine*, no. 9, September 2008, page 92.

[22] *MATLAB Getting Started Guide*, The Mathworks, Inc, 3 Apple Hill Drive Natick, MA 01760-2098, 2008. [Online]. Available: www.mathworks.com

[23] *PLECS Piece-Wise Linear Electrical Circuit Simulator User Manual*, 2nd ed., PLEXIM GmbH, Technoparkstrasse 1 8005 Zurich Switzerland, 2008. [Online]. Available: http://www.plexim.com

[24] *dSPACE 1103 Controller Board*, dSPACE GmbH, 2008. [Online]. Available: http://www.dspace.com

[25] *Delta Elektronika SM1500 Datasheet*, Delta Elektronika BV, 4300 AA Zierzikzee, Netherlands, 2007. [Online]. Available: http://www.delta-elektronika.nl

[26] *Delta Elektronika SM3000 Datasheet*, Delta Elektronika BV, 4300 AA Zierzikzee, Netherlands, 2007. [Online]. Available: http://www.delta-elektronika.nl

[27] *Danfoss VLT 5000 Data Sheet*, Danfoss A/S, Nordborgvej 81, 6430 Nordborg, Denmark, 2006.

[28] D. Hohm and M. Ropp, "Comparative study of maximum power point tracking algorithms using an experimental, programmable, maximum power point tracking test," in *Photovoltaic Specialists Conference, 2000. Conference Record of the Twenty-Eighth IEEE*, 2000, pp. 1699–1702.

[29] W. Xiao and W. Dunford, "A modified adaptive hill climbing MPPT method for photovoltaic power systems," in *Power Electronics Specialists Conference, 2004. PESC 04. 2004 IEEE 35th Annual*, vol. 3, 2004, pp. 1957–1963 Vol.3.

[30] C. W. Tan, T. Green, and C. Hernandez-Aramburo, "An improved maximum power point tracking algorithm with current-mode control for photovoltaic applications," in *Power Electronics and Drives Systems, 2005. PEDS 2005. International Conference on*, vol. 1, 2005, pp.

[31] T. Shimizu, O. Hashimoto, and G. Kimura, "A novel high-performance utility-interactive photovoltaic inverter system," *Power Electronics, IEEE Transactions on*, vol. 18, no. 2, pp. 704–711, 2003.

[32] J.-H. Park, J.-Y. Ahn, B.-H. Cho, and G.-J. Yu, "Dual-module-based maximum power point tracking control of photovoltaic systems," *Industrial Electronics, IEEE Transactions on*, vol. 53, no. 4, pp. 1036–1047, 2006.

[33] J.-M. Kwon, K.-H. Nam, and B.-H. Kwon, "Photovoltaic power conditioning system with line connection," *Industrial Electronics, IEEE Transactions on*, vol. 53, no. 4, pp. 1048–1054, 2006.

[34] W. Xiao, W. G. Dunford, P. R. Palmer, and A. Capel, "Application of Centered Differentiation and Steepest Descent to maximum power point tracking," *Industrial Electronics, IEEE Transactions on*, vol. 54, no. 5, pp. 2539–2549, 2007.

[35] I.-S. Kim, M.-B. Kim, and M.-J. Youn, "New maximum power point tracker using sliding-mode observer for estimation of solar array current in the grid-connected photovoltaic

system," *Industrial Electronics, IEEE Transactions on*, vol. 53, no. 4, pp. 1027–1035, August 2006.

[36] N. Femia, D. Granozio, G. Petrone, G. Spagnuolo, and M. Vitelli, "Predictive & adaptive MPPT Perturb and Observe method," *Aerospace and Electronic Systems, IEEE Transactions on*, vol. 43, no. 3, pp. 934–950, 2007.

[37] H. Haeberlin, L. Borgna, M. Kaempfer, and U. Zwahlen, "Measurement of dynamic mpp-tracking efficiency at grid-connected pv inverters," in *21st Photovoltaic Solar Energy Conference, Dresden, Germany*, 2006.

[38] H. Haeberlin, "Optimum DC operating voltage for grid-connected PV plants," in *20th European Photovoltaic Solar Energy Conference*, 2005.

[39] H. Haeberlin, L. Borgna, M. Kaempfer, and U. Zwahlen, "New tests at grid-connected pv inverters:overview over test results and measured values of total effiencies η_{tot}," in *21st European Solar Energy Conference, Dresden, Germany*, 2006.

[40] E. Roman, R. Alonso, P. Ibanez, S. Elorduizapatarietxe, and D. Goitia, "Intelligent PV module for grid-connected PV systems," *Industrial Electronics, IEEE Transactions on*, vol. 53, no. 4, pp. 1066–1073, June 2006.

[41] C. Hua, J. Lin, and C. Shen, "Implementation of a dsp-controlled photovoltaic system with peak power tracking," *Industrial Electronics, IEEE Transactions on*, vol. 45, no. 1, pp. 99–107, 1998.

[42] T. Esram and P. Chapman, "Comparison of photovoltaic array maximum power point tracking techniques," *Energy Conversion, IEEE Transaction on*, vol. 22, no. 2, pp. 439–449, 2007.

[43] N. Femia, G. Petrone, G. Spagnuolo, and M. Vitelli, "Optimizing sampling rate of P&O MPPT technique," in *Power Electronics Specialists Conference, 2004. PESC 04. 2004 IEEE 35th Annual*, vol. 3, 2004, pp. 1945–1949 Vol.3.

[44] G. A. R. F. Brambilla A., Gambarara M., "New approach to photovoltaic arrays maximum power point tracking," in *Proceedings of Power Electronics Specialists Conference*, 2004.

[45] C. Dorofte, U. Borup, and F. Blaabjerg, "A combined two-method mppt control scheme for grid-connected photovoltaic systems," in *Power Electronics and Applications, 2005 European Conference on*, 2005, pp. 10 pp.–.

[46] N. Femia, G. Petrone, G. Spagnuolo, and M. Vitelli, "Optimization of Perturb and Observe maximum power point tracking method," *Power Electronics, IEEE Transactions on*, vol. 20, no. 4, pp. 963–973, 2005.

[47] ——, "Perturb and Observe MPPT technique robustness improved," in *Industrial Electronics, 2004 IEEE International Symposium on*, vol. 2, 2004, pp. 845–850 vol. 2.

[48] K. Hussein, I. Muta, T. Hoshino, and M. Osakada, "Maximum photovoltaic power tracking: an algorithm for rapidly changing atmospheric conditions," *Generation, Transmission and Distribution, IEE Proceedings-*, vol. 142, no. 1, pp. 59–64, 1995.

[49] C. Hua and C. Shen, "Comparative study of peak power tracking techniques for solar storage system," in *Applied Power Electronics Conference and Exposition, 1998. APEC '98. Conference Proceedings 1998., Thirteenth Annual*, vol. 2, 1998, pp. 679–685 vol.2.

[50] W. Swiegers and J. Enslin, "An integrated maximum power point tracker for photovoltaic panels," in *Industrial Electronics, 1998. Proceedings. ISIE '98. IEEE International Symposium on*, vol. 1, 1998, pp. 40–44 vol.1.

[51] J. Schoeman and J. D. van Wyk, "A simplified maximal power controller for terrestrial photovoltaic panel arrays," in *PESC '82; Annual Power Electronics Specialists Conference, 13th, Cambridge, MA, June 14-17, 1982, Record (A84-18376 06-33). New York, Institute of Electrical and Electronics Engineers, 1982, p. 361-367.*, 1982, pp. 361–367.

[52] T. Noguchi, S. Togashi, and R. Nakamoto, "Short-current pulse-based adaptive maximum-power-point tracking for a photovoltaic power generation system," *Electrical Engineering in Japan*, vol. 139, no. 1, pp. 65–72, 2002. [Online]. Available: http://dx.doi.org/10.1002/eej.1147

[53] ——, "Short-current pulse-based maximum-power-point tracking method for multiple photovoltaic-and-converter module system," *Industrial Electronics, IEEE Transactions on*, vol. 49, no. 1, pp. 217–223, 2002.

[54] G. J. Yu, Y. S. Jung, J. Y. Choi, and G. S. Kim, "A novel two-mode mppt control algorithm based on comparative study of existing algorithms," *Solar Energy*, vol. 76, no. 4, pp. 455–463, Apr. 2004. [Online]. Available: http://www.sciencedirect.com/science/article/B6V50-49VC541-3/2/e2167001ada4349bd20d7efbdbaaf045

[55] H. Haeberlin and L. Borgna, "A new approach for semi-automated measurement of pv inverters, especially MPP tracking efficiency, using a linear pv array simulator with high stability," in *Proc. of the 19th European Photovoltaic Solar Energy Conference*, June 2004, pp. 2332–2336.

[56] *REFU Power Quality REFUSOL - Solar Inverter*, REFU Elektronik GmbH, Uracher Strasse 91, D-72555 Metzingen, Germany, 2008. [Online]. Available: http://www.refu-elektronik.de

[57] W. Shockley, "The theory of p-n junctions in semiconductors and p-n junction transistors," *Bell System Technical Journal*, vol. 28, pp. 435–89, 1949.

[58] D. Chan and J. Phang, "Analytical methods for the extraction of solar-cell single- and double-diode model parameters from I-V characteristics," *Electron Devices, IEEE Transactions on*, vol. 34, no. 2, pp. 286–293, 1987.

[59] E. Q. B. Macabebe and E. E. van Dyk, "Extraction of device parameters from dark current-voltage characteristics of PV devices," *Physica Status Solidi (c)*, vol. 5, no. 2, pp. 616–619, 2008. [Online]. Available: http://dx.doi.org/10.1002/pssc.200776834

[60] H. J. Hovel, in *Proc. 10th IEEE Photovoltaic Specialists' Conf*, 1973, p. 34.

[61] J. P. Charles, G. Bordure, A. Khoury, and P. Mialhe, "Consistency of the double exponential model with physical mechanisms of conduction for a solar cell under illumination," *Journal of Physics D: Applied Physics*, vol. 18, no. 11, pp. 2261–2268, 1985. [Online]. Available: http://stacks.iop.org/0022-3727/18/2261

[62] J. Beier and B. Voss, "Humps in dark I-V-curves - analysis and explanation," in *Photovoltaic Specialists Conference, 1993., Conference Record of the Twenty Third IEEE*, 1993, pp. 321–326.

[63] D. King, J. Dudley, and W. Boyson, "PVSIM: a simulation program for photovoltaic cells, modules, and arrays," in *Photovoltaic Specialists Conference, 1996., Conference Record of the Twenty Fifth IEEE*, 1996, pp. 1295–1297.

[64] D. King, B. Hansen, J. Kratochvil, and M. Quintana, "Dark current-voltage measurements on photovoltaic modules as a diagnostic or manufacturing tool," in *Photovoltaic Specialists Conference, 1997., Conference Record of the Twenty-Sixth IEEE*, 1997, pp. 1125–1128.

[65] E. Meyer and E. van Dyk, "Assessing the reliability and degradation of photovoltaic module performance parameters," *Reliability, IEEE Transactions on*, vol. 53, no. 1, pp. 83–92, March 2004.

[66] J. A. Jervase, H. Bourdoucen, and A. Al-Lawati, "Solar cell parameter extraction using genetic algorithms," *Measurement Science and Technology*, vol. 12, no. 11, pp. 1922–1925, 2001. [Online]. Available: http://stacks.iop.org/0957-0233/12/1922

[67] A. Kaminski, J. Marchand, A. Fave, and A. Laugier, "New method of parameters extraction from dark I-V curve," *Photovoltaic Specialists Conference, 1997., Conference Record of the Twenty-Sixth IEEE*, pp. 203–206, 29 Sep-3 Oct 1997.

[68] M. Wolf, G. Noel, and R. Stirn, "Investigation of the double exponential in the current-voltage characteristics of silicon solar cells," *Electron Devices, IEEE Transactions on*, vol. 24, no. 4, pp. 419–428, 1977.

[69] V. Quaschning and R. Hanitsch, "Numerical simulation of photovoltaic generators with shaded cells," in *Universities Power Engineering Conference*, vol. 30th, 1995, pp. 583–586.

[70] J. A. d. Cueto, "Method for analyzing series resistance and diode quality factors from field data Part II: Applications to crystalline silicon," *Solar energy materials and solar cells*, vol. 59, pp. 393–, 1999.

[71] J. Bishop, "Computer simulation of the effect of electrical mismatches in photovoltaic cell interconnection circuits." *Solar cells*, vol. 25, pp. 73–89, 1988.

[72] G. Araujo and E. Sanchez, "A new method for experimental determination of the series resistance of a solar cell," *Electron Devices, IEEE Transactions on*, vol. 29, no. 10, pp. 1511–1513, 1982, nG.

[73] M. Chegaar, Z. Ouennoughi, and A. Hoffmann, "A new method for evaluating illuminated solar cell parameters," *Solid-state electronics*, vol. 45, pp. 293–, 2001, oK.

[74] G. Walker, "Evaluating MPPT converter topologies using a Matlab PV model," *Journal of Electrical and Electronics Engineering, Australia*, vol. 21, pp. 49–55, 2001.

[75] W. Xiao, W. Dunford, and A. Capel, "A novel modeling method for photovoltaic cells," in *Power Electronics Specialists Conference, 2004. PESC 04. 2004 IEEE 35th Annual*, vol. 3, 2004, pp. 1950–1956 Vol.3.

[76] T. El Shatter and M. Elhagry, "Sensitivity analysis of the photovoltaic model parameters," in *Circuits and Systems, 1999. 42nd Midwest Symposium on*, vol. 2, 1999, pp. 914–917 vol. 2.

[77] IEC, *Datasheet and nameplate information for photovoltaic modules*, Danish Standard Organization Std. DS/EN 50 380, 2003.

[78] J.-P. Charles, I. Mekkaoui-Alaoui, G. Bordure, and P. Mialhe, "A critical study of the effectiveness of the single and double exponential models for i-v characterization of solar cells," *Solid-State Electronics*, vol. 28, no. 8, pp. 807–820, Aug. 1985. [Online]. Available: http://www.sciencedirect.com/science/article/B6TY5-46VDPCH-CW/2/6de574183cbbd6fff5a8b933de1ff3bb

[79] D. Chan, J. Phang, J. Phillips, and M. Loong, "A comparison of extracted solar cell parameters from single and double lumped circuit models," in *Tech. Digest of 1st International Photovoltaic Science and Engineering Conference*, Nov 1984, pp. 151–153.

[80] G. Petrone, G. Spagnuolo, and M. Vitelli, "Analytical model of mismatched photovoltaic fields by means of Lambert W-function," *Solar Energy Materials and Solar Cells*, vol. 91, no. 18, pp. 1652–1657, Nov. 2007. [Online]. Available: http://www.sciencedirect.com/science/article/B6V51-4P3TYF4-2/2/ef791af197e34a15b62cfa95e5e1a9e3

[81] M. Alonso-Garcia and J. Ruiz, "Analysis and modelling the reverse characteristic of photovoltaic cells," *Solar Energy Materials and Solar Cells*, vol. 90, no. 7-8, pp. 1105–1120, May 2006.

[82] M. Danner and K. Bucher, "Reverse characteristics of commercial silicon solar cells-impact on hot spot temperatures and module integrity," in *Photovoltaic Specialists Conference, 1997., Conference Record of the Twenty-Sixth IEEE*, 1997, pp. 1137–1140.

[83] L. Castaner and S. Silvestre, *Modelling photovoltaic systems using PSpice.* John Wiley and Sons, LTD, 2002.

[84] H. Rauschenbach, "Electrical output of shadowed solar arrays," *Electron Devices, IEEE Transactions on*, vol. 18, no. 8, pp. 483–490, 1971.

[85] J. Gow and C. Manning, "Development of a photovoltaic array model for use in power-electronics simulation studies," *Electric Power Applications, IEE Proceedings-*, vol. 146, no. 2, pp. 193–200, 1999.

[86] G. Vachtsevanos and K. Kalaitzakis, "Hybrid photovoltaic simulator for utility interactive studies," *IEEE Transactions on Power Electronics*, vol. EC-2:2, pp. 227–231, 1987.

[87] N. Kaushika and N. Gautam, "Energy yield simulations of interconnected solar PV arrays," *Energy Conversion, IEEE Transactions on*, vol. 18, no. 1, pp. 127–134, 2003.

[88] G. Kuntz and A. Wagner, "Internal series resistance determinated of only one IV-curve under illumination," in *19th Photovoltaic Solar Energy Conference Paris*, 2004.

[89] A. Reis, N. Coleman, M. Marshall, P. Lehman, and C. Chamberlin, "Comparison of PV module performance before and after 11-years of field exposure," in *Photovoltaic Specialists Conference, 2002. Conference Record of the Twenty-Ninth IEEE*, 2002, pp. 1432–1435.

[90] B. Decker and U. Jahn, "Performance of 170 grid connected PV plants in Northern Germany–Analysis of yields and optimization potentials," *Solar Energy*, vol. 59, no. 4-6, pp. 127–133, 1997. [Online]. Available: http://www.sciencedirect.com/science/article/B6V50-3SP7889-8/2/95e00e68fdfc23fe57766e062647f5e3

[91] H. Lukamp, "Reliability study of grid connected PV systems," IEA-PVPS, Report IEA-PVPS Task7 IEA T7-08: 2002, March 2002. [Online]. Available: http://www.iea-pvps.org/products/download/rep7_08.pdf

[92] V. Benda, "Solar cell physics and construction," November 2008.

[93] J. A. d. Cueto, "Method for analyzing series resistance and diode quality factors from field data of photovoltaic modules," *Solar energy materials and solar cells*, vol. 55, pp. 291–, 1998.

[94] K. Machida, T. Yamazaki, and T. Hirasawa, "Secular degradation of crystalline photovoltaic modules," *Solar Energy Materials and Solar Cells*, vol. 47, no. 1-4, pp. 149–153, Oct. 1997. [Online]. Available: http://www.sciencedirect.com/science/article/B6V51-3SN13XC-47/2/7a5670bbf1327b821078e5c3f844caba

[95] L. D. Bernardez and R. H. Buitrago, "Dark I-V curve measurement of single cells in a photovoltaic module," *Progress in Photovoltaics: Research and Applications*, vol. 14, no. 4, pp. 321–327, 2006. [Online]. Available: http://dx.doi.org/10.1002/pip.665

[96] A. Kaminski, J. J. Marchand, and A. Laugier, "Non ideal dark I-V curves behavior of silicon solar cells," *Solar Energy Materials and Solar Cells*, vol. 51, no. 3-4, pp. 221–231, Feb. 1998. [Online]. Available: http://www.sciencedirect.com/science/article/B6V51-3VHSGC8-1/2/7443fcbccc5258be7ea3df950a2d8224

[97] IEC, *Procedures for temperature and irradiance corrections to measured I-V characteristics of crystalline silicon photovoltaic devices*, International Electrotechnical Commission Std. 60 891, 2001.

[98] A. Woyte, J. Nijsa, and R. Belmansa, "Partial shadowing of photovoltaic arrays with different system configurations-literature review and field test results," *Solar energy*, vol. 74, pp. 217–, 2003.

[99] A. Kovach and J. Schmid, "Determination of energy output losses due to shading of building-integrated photovoltaic arrays using a raytracing technique," *Solar Energy*, vol. 57, no. 2, pp. 117–124, Aug. 1996. [Online]. Available: http://www.sciencedirect.com/science/article/B6V50-3WFND58-4/2/af38140e02135366cdf5bb007ad29570

[100] H. Nagayoshi and M. Atesh, "Partial shading effect emulation using multi small scale module simulator units," in *Photovoltaic Specialists Conference, 2005. Conference Record of the Thirty-first IEEE*, 2005, pp. 1710–1713.

[101] R. Pinkerton, "Solar array string characteristics in strange places," in *Energy Conversion Engineering Conference and Exhibit, 2000. (IECEC) 35th Intersociety*, vol. 1, 2000, pp. 681–691 vol.1.

[102] T. Erge, V. Hoffmann, K. Kiefer, E. Rossler, U. Rindelhardt, G. Teichmann, B. Decker, J. Grochowski, G. Heilscher, M. Schneider, G. Blasser, H. Ossenbrink, H. Becker, W. Vaassen, B. Genennig, H. Riess, and P. Sprau, "The german 1000-roofs-pv-programme - a resume of the 5 years pioneer project for small grid-connected pv systems." in *Proceedings of the 2nd World Conference on PVSEC, Vienna*, 1998, p. 2648Ű2651.

[103] IEC, *Photovoltaic devices - Part 5 Determination of the equivalent cell temperature (ECT) of photovoltaic (PV) devices by the open-circuit voltage method*, International Electrotechnical Commission Std. IEC 60 904-5, June 1995.

[104] C. Bendel and A. Wagner, "Photovoltaic measurement relevant to the energy yield," in *WCPEC-3 World Conference on Photovoltaic Energy Conversion, Osaka, Japan*, 2003.

[105] A. Wagner, "Peak-power and internal series resistance measurement under natural ambient conditions," in *Eurosun 2000, Copenhagen*, 2000.

[106] G. Nofuentes, J. Aguilera, R. L. Santiago, J. de la Casa, and L. Hontoria, "A reference-module-based procedure for outdoor estimation of crystalline silicon pv module peak power," *Progress in Photovoltaics: Research and Applications*, vol. 14, no. 1, pp. 77–87, 2006. [Online]. Available: http://dx.doi.org/10.1002/pip.636

[107] M. Fuentes, G. Nofuentes, J. Aguilera, D. Talavera, and M. Castro, "Application and validation of algebraic methods to predict the behaviour of crystalline silicon pv modules in mediterranean climates," *Solar Energy*, vol. 81, no. 11, pp. 1396–1408, Nov. 2007. [Online]. Available: http://www.sciencedirect.com/science/article/B6V50-4N3PY20-3/2/65e6c09fcced5739b8714a81907a5e6c

[108] C. Osterwald, S. Anevsky, A. Barua, P. Chaudhuri, J. Dubard, K. Emery, B. Hansen, D. King, J. Metzdorf, F. Nagamine, R. Shimokawa, Y. Wang, T. Wittchen, W. Zaaiman, A. Zastrow, and J. Zhang, "The world photovoltaic scale: an international reference cell calibration program," in *Photovoltaic Specialists Conference, 1997., Conference Record of the Twenty-Sixth IEEE*, 1997, pp. 1209–1212.

[109] K. Bucher, "Pv module and cell calibration procedures, accuracy and problems introduced by recent technological cell and module improvements," in *Proceeding of the 16th European Photovoltaic Solar Energy Conference*, 2000, pp. 603–606.

[110] S. B. Kjær, "Design and Control of an Inverter for Photovoltaic Applications," Ph.D. dissertation, Aalborg University - Institute of Energy Technology, January 2005.

Part II

Publications

Publication 1

Improved MPPT method for rapidly changing environmental conditions

by D. Sera, R. Teodorescu, T. Kerekes and F. Blaabjerg

Improved MPPT method for rapidly changing environmental conditions

D. Sera*, T. Kerekes*, R. Teodorescu*, and F. Blaabjerg*
* Aalborg University/Institute of Energy Technology, Aalborg, Denmark
des@iet.aau.dk, tak@iet.aau.dk, ret@iet.aau.dk, and fbl@iet.aau.dk

Abstract — A well-known limitation of the Perturb and Observe (P&O) MPPT method is that it can get confused and track in wrong direction during rapidly changing irradiation. The present work offers a simple and effective solution to this problem, by using an additional measurement of the solar array's power in the middle of the MPPT sampling period. The method has been experimentally tested and compared with the traditional P&O method.

I. INTRODUCTION

The power delivered by the photovoltaic (PV) module depends on the irradiance, temperature, and shadowing conditions. The PV panel has a nonlinear characteristic, and the power has a Maximum Power Point (MPP) at a certain working point, with coordinates V_{MPP} voltage and I_{MPP} current. Since the MPP depends on solar irradiation and cell temperature, it is never constant over time; thereby Maximum Power Point Tracking (MPPT) should be used to track its changes.

The penetration of PV systems as distributed power generation systems has been increased dramatically in the last years. In parallel with this, Maximum Power Point Tracking (MPPT) is becoming more and more important as the amount of energy produced by PV systems is increasing.

One of the most frequently used MPPT methods is the Perturb and Observe (P&O) algorithm, due to its simplicity and the low computational power it needs.

A well-known shortcoming of the P&O is that it can get confused and track in wrong direction during rapidly changing irradiation. This can happen when the change in insolation between two MPPT sampling instances causes larger power change than the one caused by the voltage increment of the MPPT. In this case the algorithm is unable to decide whether the change in power is caused by its own voltage increment or by the change in irradiation. The present work offers a simple solution to this problem, by separating the two power changes coming from the different sources, and providing the MPPT algorithm with the power change caused exclusively by its own previous command. This is done with the help of an additional measurement of the solar array's power at the middle of the MPPT sampling period, when no voltage perturbation from the MPPT is present.

The experimental results show that the proposed algorithm, called dP-P&O, is able to prevent the P&O MPPT from tracking in wrong way during rapidly changing irradiation, and it considerably increases its tracking efficiency, thus leading to more power production.

II. THE P&O MAXIMUM POWER POINT TRACKING ALGORITHM

The P&O is one of the so called 'hill-climbing' methods, which are based on the fact that in case of the V-P characteristic, on the left of the MPP the variation of the power against voltage $dP/dV > 0$, while at the right, $dP/dV < 0$. (see Fig. 1) [4]

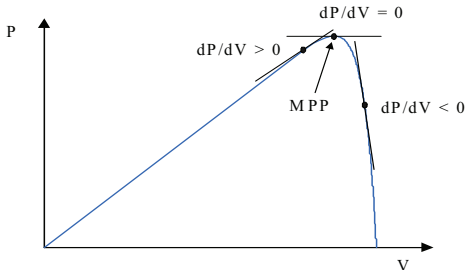

Fig. 1 Sign of the dP/dV at different positions on the power characteristic

In Fig. 1, if the operating voltage of the PV array is perturbed in a given direction and $dP/dV > 0$, it is known that the perturbation moved the array's operating point toward the MPP. The P&O algorithm would then continue to perturb the PV array voltage in the same direction. If $dP/dV < 0$, then the change in operating point moved the PV array away from the MPP, and the P&O algorithm reverses the direction of the perturbation. [1]

The main advantage of the P&O method is that it is easy to implement, and its low computational demand. However, it has some limitations, like oscillations around the MPP in steady state operation, slow response speed, and tracking in wrong way under rapidly changing atmospheric conditions. [1][2][3].

In many cases the solar array is connected to an AC load, for example the grid, in case of distributed power generation. In this case the power drawn from the array has a ripple with double the grid frequency. Thereby the sampled voltage and current should be averaged over one period of the power ripple, in order to decouple the ripple component of the drawn power.

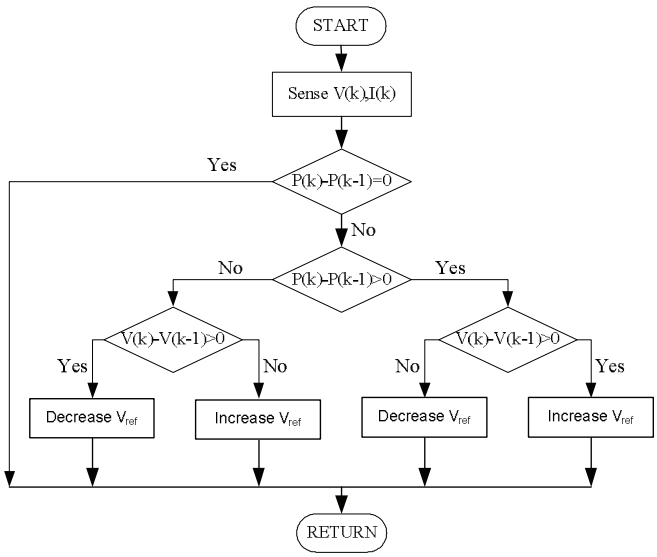

Fig. 2 The flowchart of the P&O MPPT method

The P&O method in rapidly changing irradiance

As mentioned before, the P&O method can be confused in rapidly changing insolation conditions. If the change in the insolation intensity causes bigger change in power than the one caused by the increment in the voltage, the MPPT can get confused, as it will interpret the change in the power as an effect of its own action. This is illustrated in the figures below:

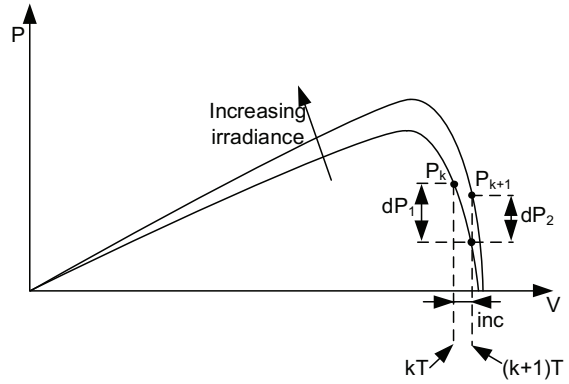

Fig. 3 In case of slow irradiation changes, the P&O method is able to determine the right tracking direction

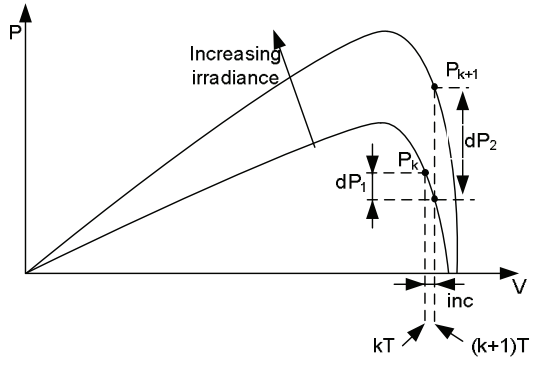

Fig. 4 In case of rapidly changing irradiation, the P&O method is unable to determine the right tracking direction

On Fig. 3 and Fig. 4:

T – the sampling period of the MPPT,

P_k, P_{k+1} – the powers measured at the k and the k+1 sampling instances

dP_1 – the change in power caused by the perturbation of the MPPT

dP_2 – the change in power caused by the increase in irradiation

inc – the voltage increment of the MPPT

If dP1 > dP2 the MPPT is able to interpret correctly the change in the power between two sampling instances. (Fig. 3), as the overall change in power will reflect the effect of the perturbation. On the other hand, if dP2 > dP1, the MPPT is unable to determine the right direction of tracking as for example $P_{k+1}–P_k$ in Fig. 4 is positive regardless of the perturbation direction of the MPPT. In the case, depicted on Fig. 3, the P&O would continue to increase the voltage reference until the irradiation change is stopped, dP1 becomes larger than dP1.

III. THE PROPOSED METHOD

The proposed method performs an additional measurement of power in the middle of the MPPT sampling period without any perturbation, as illustrated in the figure below.

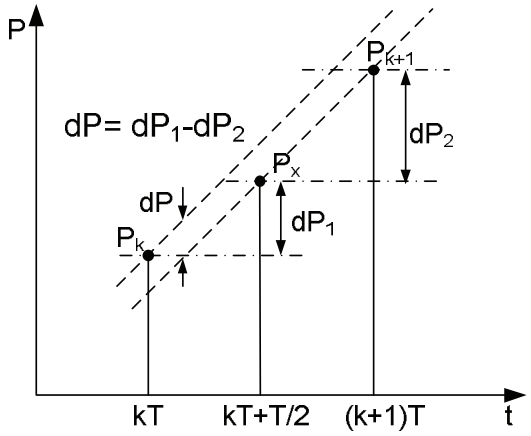

Fig. 5 Measurement of the power between two MPPT sampling instances

As it can be seen on the figure, the change in power between P_x and P_{k+1} reflects only the change in power due to the environmental changes, as no action has been made by the MPPT. The difference between P_x and P_k contains the change in power caused by the perturbation of the MPPT plus the irradiation change. Thereby, assuming that the rate of change in the irradiation is constant over one sampling period of the MPPT, the dP *caused purely by the MPPT command* can be calculated as:

$$dP = dP_1 - dP_2 = (P_x - P_k) - (P_{k+1} - P_x) = \\ = 2P_x - P_{k+1} - P_k \quad (1)$$

The resulting dP reflects the changes due to the perturbation of the MPPT method.

It should be noticed that the above calculation is based on assuming that the rate of power change is constant over one MPPT sampling period – which is fairly true in most of the practical cases.

However, when the power does not change linearly, the calculation of dP contains an error. On Fig. 5, if the slope of the power increase (without the effect of the MPPT command) changes between the time instants kT and (k+1)T, equation (1) will become:

$$dP = dP_1 - dP_2 = (P_x - P_k) - (P_{k+1} + dP_{error} - P_x) = \\ = 2P_x - P_{k+1} - P_k - dP_{error} \quad (2)$$

In the above equation, $P_{k+1} + dP_{error}$ is the power measured at time instance (k+1)T in case when the slope of the power increase has changed during the MPPT sampling period. P_{k+1} is the power at (k+1)T in case when the slope does not change.

According to (2), if the slope of the power due to irradiation changes during the sampling period, the calculation of dP will contain an error dP_{error}.

However, as the MPPT looks only at the sign of the dP, this error can cause problems only when it becomes larger than the power change caused by the MPPT command.

If we note the dP calculated in (1) as dP_{ideal}, when the power curve was linear and the dP has been calculated without errors:

$$dP_{ideal} = 2P_x - P_{k+1} - P_k \quad (3)$$

Than the calculated dP becomes:

$$dP = dP_{ideal} - dP_{error} \quad (4)$$

The condition for the sign of dP to be correct is the absolute value of dP_{error} to be smaller than the absolute value of dP_{ideal}, $|dP_{ideal}| > |dP_{error}|$. The value of dP_{ideal} can be adjusted by the voltage increment and/or the sampling frequency of the MPPT.

The dP-P&O MPPT (patent pending)

The flowchart of the modified method, containing the additional block to calculate the dP is shown on Fig. 6:

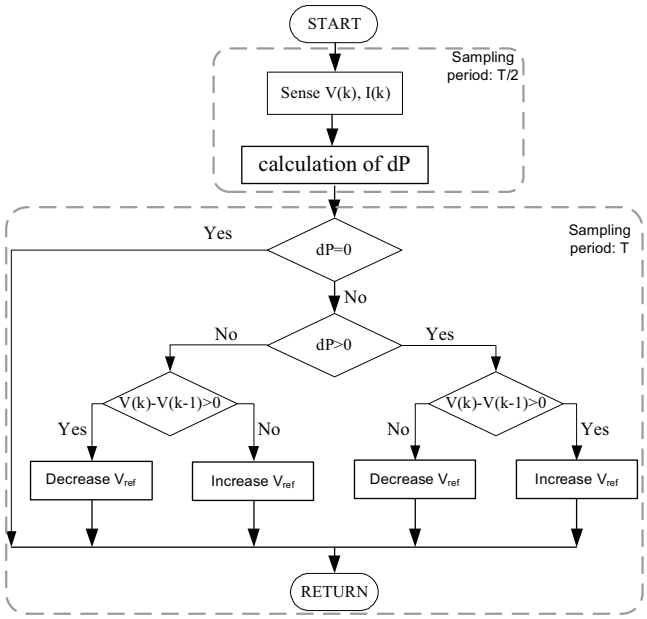

Fig. 6 The flowchart of the dp-P&O method

In the dp-P&O the P_k-P_{k-1} (see Fig. 2) is replaced by the dP calculated in (1) and thereby can be avoided the confusion of the MPPT due to the rapidly changing irradiation.

IV. EXPERIMENTAL TESTS

Both the traditional and improved methods were implemented on a laboratory setup, using a control system as visualized on Fig. 8. The setup consists of the following main components, as it can be seen in the picture below:

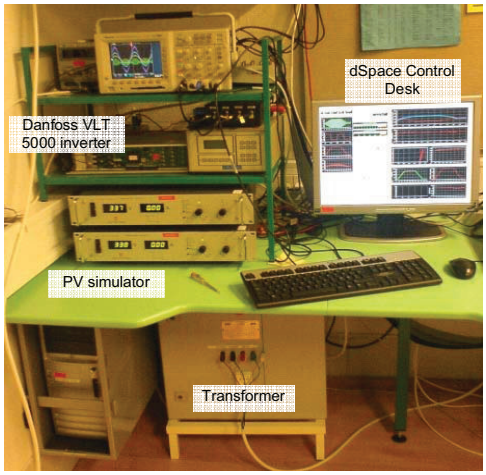

Fig. 7 The experimental setup.

A **PV simulator**, made of two programmable series connected Delta Elektronika SM300-10 DC power supplies, having V_{max}=300V, I_{max}=10A. Their output voltages were controlled in real time according to a photovoltaic model of a PV array. The model is based on a series connected array of 15 BPMSX120 PV panels. The panels have the following main characteristics: maximum delivered power P_M = 120W, shortcircuit current I_{SC} = 3.87A, open circuit voltage V_{OC} = 42.1V. The model is using the following equations:

$$v = n_{ps}V_{OC} + n_{ps} \cdot n_s \cdot V_T \ln\left(1 - \frac{i}{I_{SC,1000} \cdot \frac{G}{1000}}\right) \quad (5)$$

$$V_{OC} = n_s V_T \ln\left(\frac{1 + I_{SC,1000} \cdot \frac{G}{1000}}{I_0}\right)$$

Where:

n_{ps} – the number of panels connected in series,

n_s – the number of cells in one panel

V_T – thermal voltage (V)

$I_{SC,\,1000}$ – shortcircuit current at standard conditions (at 1000 W/m^2 irradiation) (A)

G – irradiation (W/m^2)

- A Danfoss VLT 5000 5KW 3 phase **inverter**. The inverter is used in single-phase mode, with unipolar PWM, having an effective switching frequency of 20 kHz. The inverter is connected to an LC filter, with the parameters L = 1.4mH, C = 2 µF. The setup is connected to the grid through a **transformer**, having a shortcircuit inductance of 2mH.
- The control system together with the solar array model has been implemented on a DS1103 **dSpace system**, as also shown on Fig. 8.The control system has been implemented in Simulink, in discrete time, and using the real time workshop, and dSpace RTI toolbox, has been generated a real time code for the dSpace system.

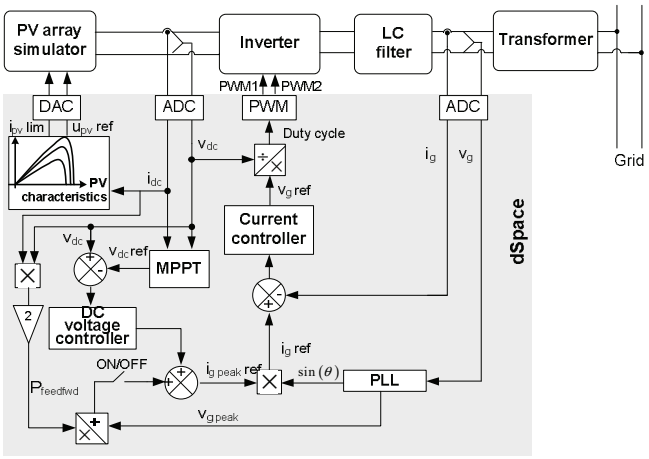

Fig. 8 Experimental laboratory setup

The tests have been made in the following conditions:

- The control system sampling frequency is 10 kHz, same as the PWM outputs frequency.
- The DC voltage controller is a proportional one, with a gain of 0.1.
- The MPPT algorithm sampling frequency is 2Hz, and the voltage increment is set to 2V.
- The current controller is a Proportional-Resonant one. The Phase Lock Loop (PLL) has a settling time of 0.02s. As the current loop has a much faster response than the MPPT, it can be considered ideal from its point of view.
- In order to verify the effect of rapidly changing irradiation conditions, an irradiation ramp change was used. This irradiation change starts from 125 W/m^2, stops at 800 W/m^2, waits at this level for 40s, and decreases again back to 125 W/m^2 with a constant slope. A 25s period for the increasing and decreasing ramp was selected. This corresponds to approximately 60 W/s slope of the output power change. The limit of 800W/m^2 irradiation is due to the output current limitation of the used inverter.
- As the behavior of the MPPT is significantly affected by the presence or absence of a power feed-forward, the P&O and the dP-P&O have been compared in two different cases: first, when no power feed-forward was used, and second, when the power feed-forward was switched on, as shown on Fig. 8.

In the following the results of the experimental tests of the proposed dP-P&O method will be presented and compared to the results of the traditional P&O method.

Power feed-forward switched off

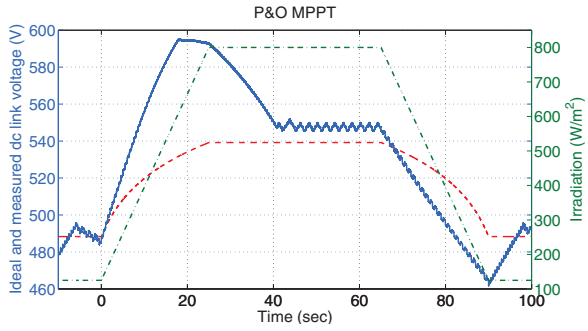

Fig. 9 Ideal and measured DC link voltage during the irradiation change. The DC link voltage (continuous line) increases far beyond the optimal value (dashed line). The actual irradiation (dash-dotted line) is represented on the right axis.

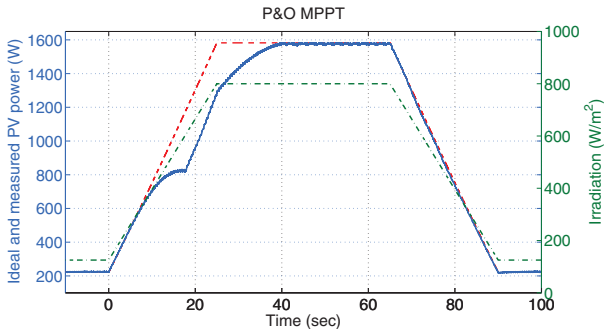

Fig. 10 Ideal and measured PV power during the irradiation change. The power drawn by the P&O MPPT (continuous line) cannot follow the maximum available (dashed line) from the PV array during rapidly increasing irradiation (dash-dotted line)

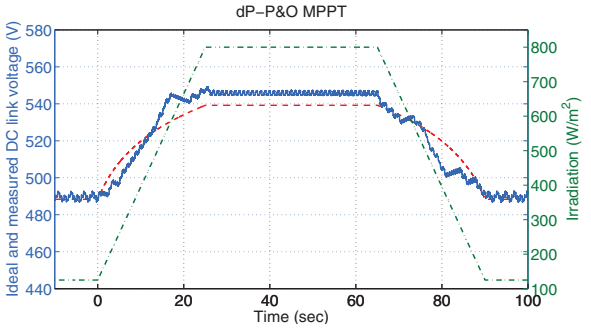

Fig. 11 In case of the dP-P&O, the DC link voltage (continuous line) tracks the optimal value (dashed line) with a fairly good precision also during irradiation change (dash-dotted line).

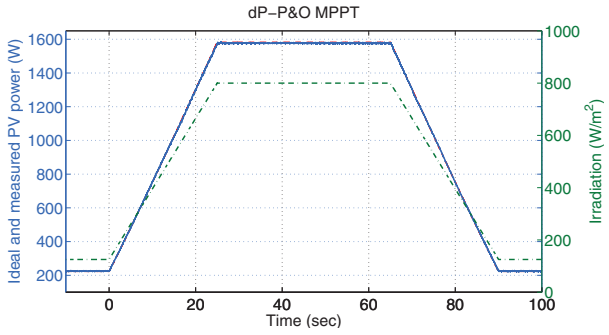

Fig. 12 The power drawn by the dP-P&O (continuous line) follows with a good precision the maximum available power (dashed line) even under rapidly changing irradiance (dash-dotted line)

On the above graphs, the curves for the ideal power and the optimal DC link voltage are calculated based on the same model used to control the DC power sources.

Based on the measured and ideal (calculated) power at the actual irradiation, the instantaneous efficiency is calculated based on the following formula:

$$\eta_{inst} = \frac{P_{PV\_meas}}{P_{MPP\_ideal}} \cdot 100 \qquad (6)$$

In order to evaluate the dynamic efficiency for the entire test interval, the following formula was used:

$$\eta_{dynamic} = \frac{P_{PV\_meas\_mean}}{P_{MPP\_ideal\_mean}} \cdot 100 \qquad (7)$$

Where: $P_{PV\_meas\_mean}$ – is the mean value of the measured power over the entire test time, and
$P_{PV\_ideal\_mean}$ – is the mean value of the maximum available power over the test time, based on the PV model.
On the next plot one can see the instantaneous efficiencies of P&O and dP-P&O, according to (6).

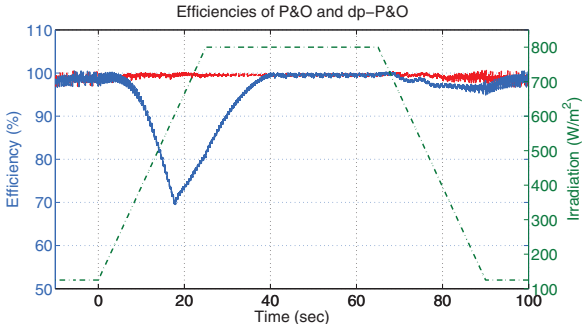

Fig. 13 The efficiency of the traditional P&O method decreases to as low as 70% during rapidly increasing irradiation, while the efficiency of dP-P&O is not affected.

As it can be seen on Fig. 13, in steady-state operation, when the irradiation is constant, the P&O and the dP-P&O are performing similarly, which was expected. On the other hand, when the irradiation increases, the traditional P&O get confused, as it cannot interpret correctly the change in power caused by the irradiation and the one caused by its own command. During the irradiation change, the instantaneous efficiency of the traditional P&O can fall about 30% (depending on the speed and duration of the irradiation change), while the dP-P&O tracks the MPP with same efficiency as in steady-state operation.

For the entire period represented on Fig. 13, the calculated dynamic efficiencies of the two methods according to (7), are 99.6% for the dP-P&O, and 94.5% for the classical P&O. This means an efficiency improvement of about 5% for the dP-P&O method.

Power feed-forward switched on

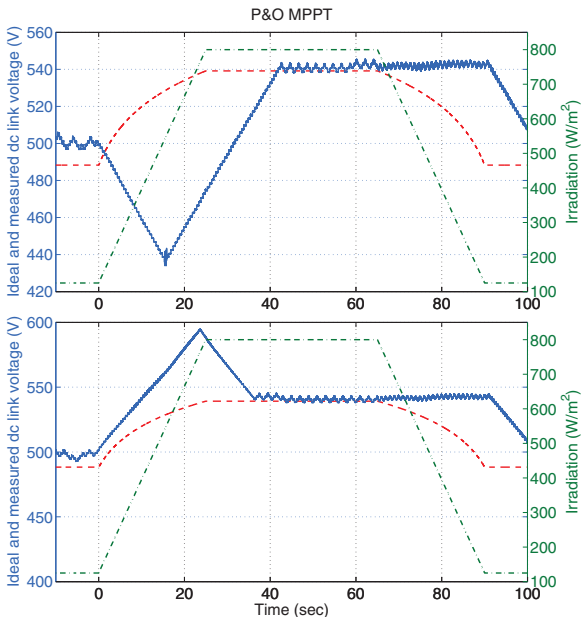

Fig. 14 Ideal (dashed line) and measured (continuous line) DC link voltage during the irradiation change, in two different cases. On the upper figure the P&O decreases the DC voltage, while on the lower figure it increases. In both cases it continues to perturb in the direction it had at the moment when the irradiance started to increase, according to Fig. 4.

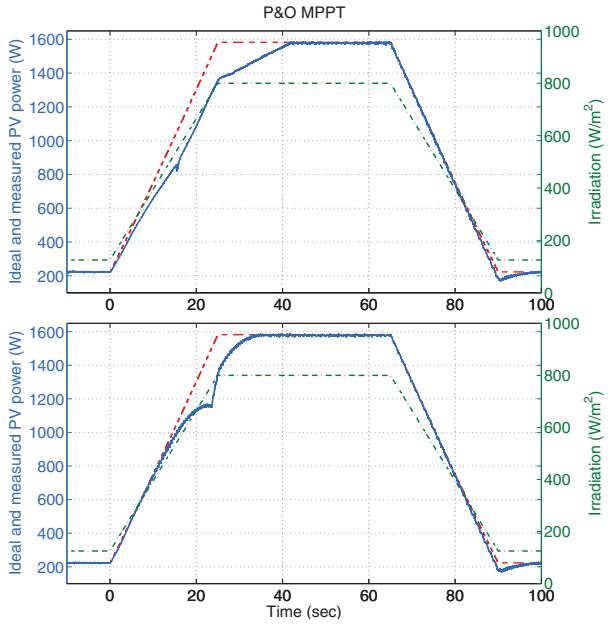

Fig. 15 Ideal and measured PV power during the irradiation change, for the two cases on Fig. 14. Due to the wrong tracking, the power drawn by the P&O MPPT (continuous line) is well below the maximum available (dashed line).The irradiance is represented on the right axis (dash-dotted)

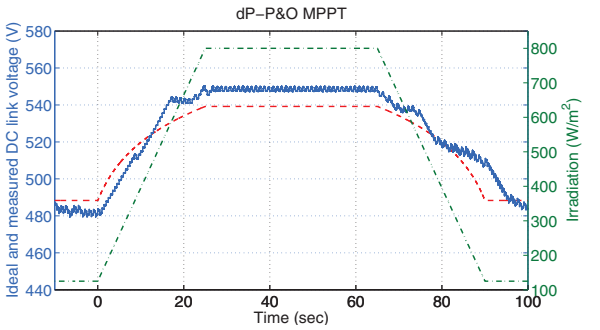

Fig. 16 In case of the dP-P&O, the DC link voltage (continuous line) tracks the optimal value (dashed line) with a fairly good precision also during irradiation change (dash-dotted line). The presence of the power feed-forward does not have a noticeable effect on the behavior of the dP-P&O.

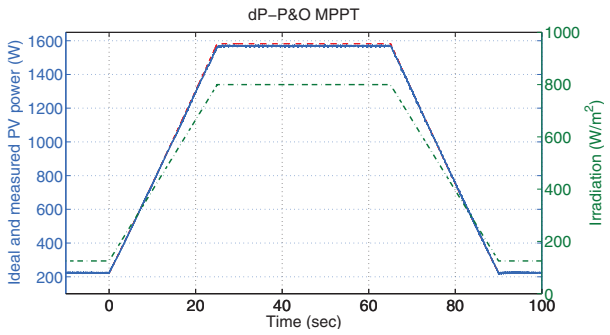

Fig. 17. As in the case when no power feed-forward was used, the power drawn by the dP-P&O (continuous line) follows with a good precision the maximum available power (dashed line) even under rapidly changing irradiance (dash-dotted line)

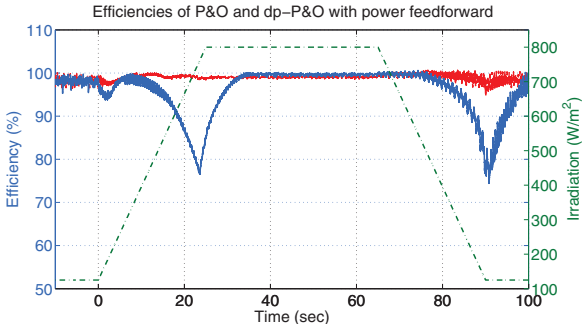

Fig. 18 The instantaneous efficiency of the traditional P&O method (considered the case on upper plot at Fig. 14) can decrease to below 80% during rapidly increasing and decreasing irradiation, while the efficiency of dP-P&O is not affected.

The instantaneous efficiencies plotted on Fig. 18 are calculated in the same way as those on Fig. 13 based on (6). In case when power feed-forward is used, the instantaneous efficiency of the P&O during increase and decrease of irradiance can fall more than 20% of its steady state efficiency. The dP-P&O behaves similar to the case when no power feed-forward was used, and it is not affected significantly by the irradiance change.

In this case the calculated dynamic efficiency for the total test time, based on (7), are 99.2% for dP-P&O method, and 96.8% for the P&O.

V. CONCLUSIONS

In this paper an improved P&O algorithm has been presented, which is able to avoid wrong tracking during rapidly changing irradiation. It has been experimentally tested and compared with the classical P&O algorithm.

Two different cases were considered, with and without power feed-forward, for a given irradiation profile. The experimental results demonstrated that in both cases the dP-P&O method performs superior to the traditional P&O during rapidly changing irradiance, resulting in higher dynamic efficiency.

In case when the power feed-forward is switched on, the dynamic efficiency improvement from the P&O to the dP-P&O is about 2.4%, while in the case when no power feed-forward is used, the improvement is more than 5%.

REFERENCES

[1] Hohm D.P., Ropp M.E.: “Comparative Study of Maximum Power Point Tracking Algorithms Using an Experimental, Programmable, Maximum Power Point Tracking Test Bed”. Photovoltaic Specialists Conference, 2000. Conference Record of the Twenty-Eighth IEEE 15-22 Sept. 2000 Pages:1699 – 1702

[2] Femia N., Petrone G., Spagnuolo G., Vitelli M.: “Optimizing sampling rate of P&O MPPT technique” Power Electronics Specialists Conference, 2004. PESC04. 2004 IEEE 35th Annual Volume 3, 20-25 June 2004 Pages: 1945 - 1949 Vol.3

[3] Brambilla A., Gambarara M., Garutti A., Ronchi F.: “New approach to photovoltaic arrays maximum power point tracking”. Power Electronics Specialists Conference, 1999. PESC 99. 30th Annual IEEE Volume 2, 27 June-1 July 1999 Pages: 632 - 637 vol.2

[4] Weidong Xiao, Dunford W.G.: “A modified adaptive hill climbing MPPT method for photovoltaic power systems” *Power Electronics Specialists Cnference, 2004. PESC 04. 2004* IEEE 35th Annual Volume 3, 20-25 June 2004 Pages: 1957 - 1963 Vol.3

,

Publication 2

Optimised Maximum Power Point Tracker for Fast Changing Environmental Conditions

by D. Sera, R. Teodorescu, J. Hantschel, and M. Knoll

Optimized Maximum Power Point Tracker for Fast-Changing Environmental Conditions

Dezso Sera, *Student Member, IEEE*, Remus Teodorescu, *Senior Member, IEEE*, Jochen Hantschel, and Michael Knoll

***Abstract*—This paper presents a high-performance maximum power point tracker (MPPT) optimized for fast cloudy conditions, e.g., rapidly changing irradiation on the photovoltaic panels. The rapidly changing conditions are tracked by an optimized hill–climbing MPPT method called dP-P&O. This algorithm separates the effects of the irradiation change from the effect of the tracker's perturbation and uses this information to optimize the tracking according to the irradiation change. The knowledge of the direction of the irradiation change enables the MPPT to use different optimized tracking schemes for the different cases of increasing, decreasing, or steady irradiance. When the irradiance is changing rapidly this strategy leads to faster and better tracking, while in steady-state conditions it leads to lower oscillations around the MPP. The simulations and experimental results show that the proposed dP-P&O MPPT provides a quick and accurate tracking even in very fast changing environmental conditions.**

***Index Terms*—Fast-changing irradiation, maximum power point tracking, photovoltaic, solar.**

I. INTRODUCTION

THE worldwide-installed photovoltaic (PV) power capacity today shows a nearly exponential increase, which is mostly dominated by grid-connected applications [1]. In these applications, the typical goal is to extract the maximum possible power from the PV plant during the entire time of operation; thereby, these systems need a maximum power point tracker (MPPT), which sets the system working point to the optimum, following the weather (i.e., solar irradiance and temperature) conditions. There are many MPPT strategies that are available [2]–[10] for different converter topologies, which provide high performance tracking during "nice" weather conditions, i.e., at strong and stable solar irradiation and no partial shadowing. These trackers are satisfactory if the PV system is installed at a place where the possibility of clouds and partial shading is very low. However, in many cases, when the PV system is installed in an urban area, partial shadowing by the neighboring buildings is sometimes inevitable [11]. Similarly, on places where the moving clouds are very often present on the sky, for example, Northern Europe, the irradiation can show fast changes even though the average value is fairly high. In these cases, if the MPPT is not able to detect the partial shadowing and if is not able to react quickly to the fast irradiation changes, the PV system capacity will not be optimally used.

Manuscript received October 31, 2007; revised March 27, 2008.

D. Sera is with the Institute of Energy Technology, Aalborg University, 9220 Aalborg East, Denmark (e-mail: des@iet.aau.dk).

R. Teodorescu is with the Power Electronics Section, Green Power Laboratory, Institute of Energy Technology, Aalborg University, 9220 Aalborg East, Denmark (e-mail: ret@iet.aau.dk).

J. Hantschel is with the REFU-Elektronik GmbH, 72555 Metzingen, Germany (e-mail: jochen.hantschel@refu-elektronik.de).

M. Knoll was with the REFU-Elektonik GmbH, 72555 Metzingen, Germany. He is now with Daimler AG, 70546 Stuttgart, Germany (e-mail: ferchau.knoll@daimler.com).

Color versions of one or more of the figures in this paper are available online at http://ieeexplore.ieee.org.

Digital Object Identifier 10.1109/TIE.2008.924036

II. MPPTs IN RAPIDLY CHANGING CONDITIONS

As it was mentioned in Section I, an MPPT algorithm that provides high-performance tracking in steady-state conditions can easily be found. A very popular hill-climbing method is the perturb and observe (P&O) [2], [12], [13] tracker, which has some important advantages as simplicity, applicability to almost any PV system configuration, and good performance in steady-state operation. However, as with most of the hill-climbing methods, there is a tradeoff between the accuracy and speed of the tracking.

A. dP-P&O Method

The dP-P&O MPPT method [14] is an improvement of the classical P&O in the sense that it can prevent itself from tracking in the wrong direction during rapidly changing irradiance, which is a well-known drawback of the classical P&O algorithm.

The dP-P&O determines the correct tracking direction by performing an additional measurement in the middle of the MPPT sampling period, as shown in Fig. 2. As it can be seen in the figure, the change in power between P_x and P_{k+1} only reflects the change in power due to the environmental changes, as no action has been made by the MPPT. The difference between P_x and P_k contains the change in power caused by the perturbation of the MPPT plus the irradiation change. Thereby, assuming that the rate of change in the irradiation is constant over one sampling period of the MPPT, the dP that is purely caused by the MPPT command can be calculated as follows:

$$\begin{aligned} dP &= dP_1 - dP_2 = (P_x - P_k) - (P_{k+1} - P_x) \\ &= 2P_x - P_{k+1} - P_k. \end{aligned} \tag{1}$$

The resulting dP reflects the changes due to the perturbation of the MPPT method. The flowchart of the dP-P&O can be seen in Fig. 1. Equation (1) represents a small extra computational load compared to the classical P&O method, where, in order to determine the next perturbation direction, a difference between two consecutive measurements of power is used (Fig. 2). In case of dP-P&O, an extra measurement needs to be taken;

0278-0046/$25.00 © 2008 IEEE

Authorized licensed use limited to: IEEE Xplore. Downloaded on January 23, 2009 at 11:28 from IEEE Xplore. Restrictions apply.

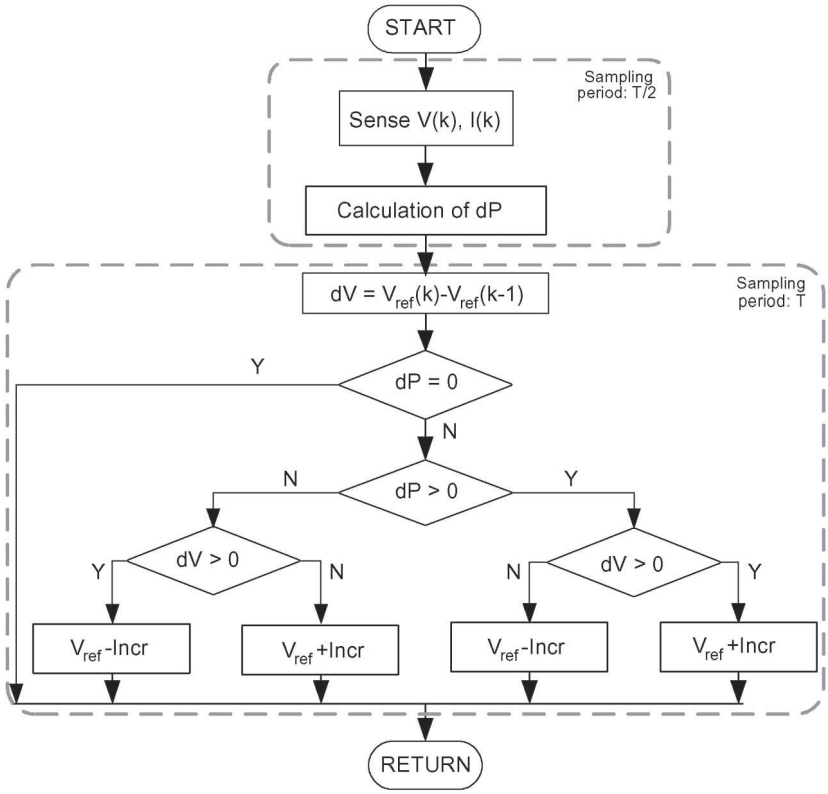

Fig. 1. Flowchart of the dP-P&O algorithm.

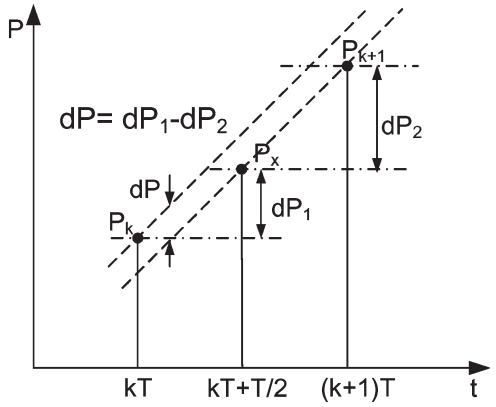

Fig. 2. Measurement of the power between two MPPT sampling instances.

however, this does not require a new sampling of the measured PV voltage and current, as they are sampled with high frequency for the dc voltage controller and power feedforward (see Fig. 4).

Determining the dP allows tracking in the correct direction during irradiation changes. However, in order to track very fast changes of irradiation, the voltage perturbation step has to be increased. This would lead to oscillations around the MPP in steady-state conditions, degrading the overall performance. To overcome this drawback, the information regarding the change of output power due to external conditions dP_2 is used. From the value of dP_2, it can be determined if the irradiation is stable, increasing, or decreasing. This information allows the use of an optimized tracking strategy for the different cases. The flowchart of this method is shown in Fig. 3.

In Fig. 3, the symbols have the following meanings:

1) ThN—negative threshold for dP;
2) ThP—positive threshold for dP.

In Fig. 3, if the change in power due to irradiation $(|dP_2|)$ is smaller than the change of power due to the MPPT perturbation $(|dP|)$, it is considered to be a slowly changing condition and the system will use the basic dP-P&O algorithm with small increment values to reduce oscillations around the MPP.

B. Optimized dP-P&O During Rapidly Changing Irradiation

The inverter control system considered when examining the optimized dP-P&O MPPT is shown in Fig. 4.

In Fig. 4, the MPPT gives the voltage reference to the dc voltage controller, whose output will serve as the reference for the grid current peak value. The dc voltage controller is a proportional integrator, whereas the grid current controller is considered ideal as well as the inverter.

If a fast rise of irradiation was detected by dP_2 in Fig. 3, it means that the MPPT should increase the PV array reference voltage in order to follow the irradiation change. Thereby, in this situation, the MPPT switching strategy is in favor of increasing the voltage reference. $V_{\rm dc}$ref in Fig. 4 is decreased only when the voltage was increased in the previous MPPT sampling instance, and it caused a reduction of power $dP <$ ThN. A negative threshold value ThN has been applied in order to avoid unnecessary switching around the MPP. If—due to the action of the MPPT in the last sampling period—dP becomes negative, the MPPT holds the voltage reference at the same level for one sampling period instead of decreasing it, unless

Authorized licensed use limited to: IEEE Xplore. Downloaded on January 23, 2009 at 11:28 from IEEE Xplore. Restrictions apply.

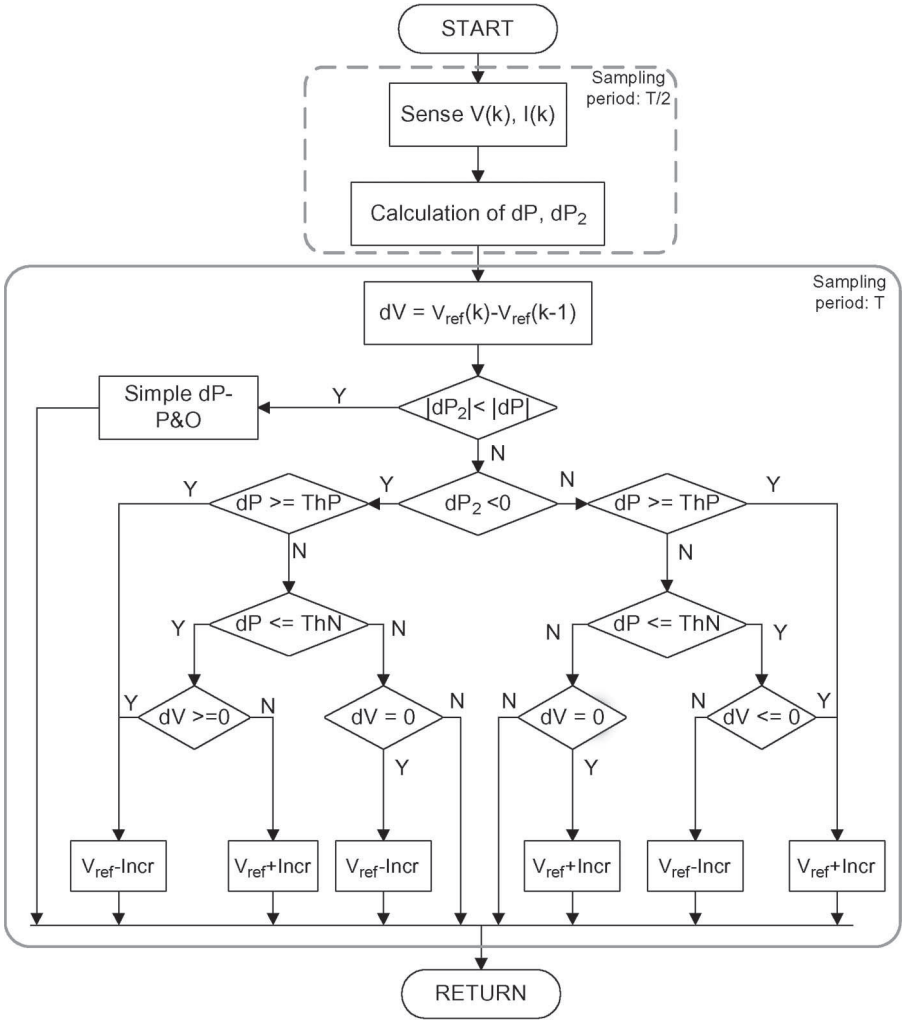

Fig. 3. Flowchart of the dP-P&O method with optimized tracking.

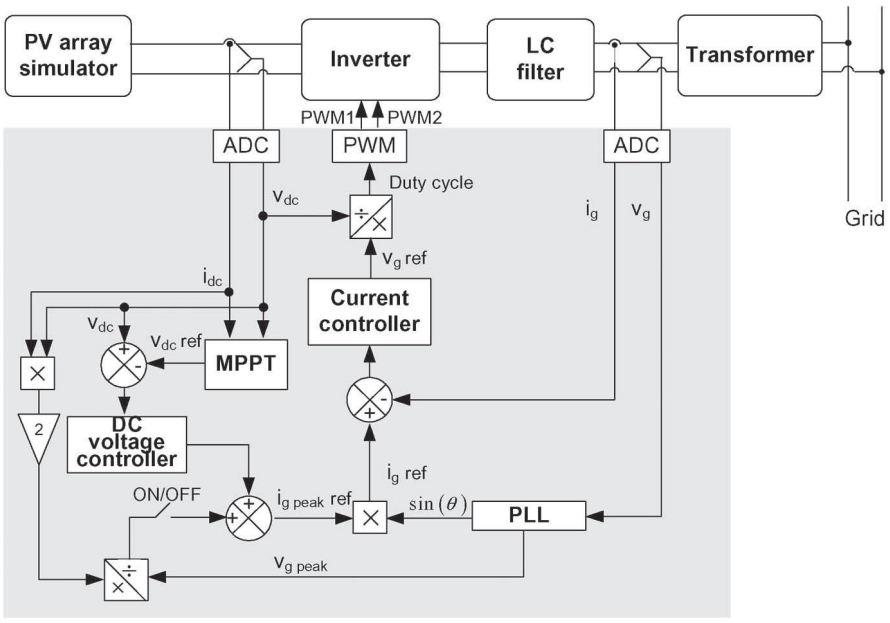

Fig. 4. Single phase MPPT and current control structure for green power inverter.

Authorized licensed use limited to: IEEE Xplore. Downloaded on January 23, 2009 at 11:28 from IEEE Xplore. Restrictions apply.

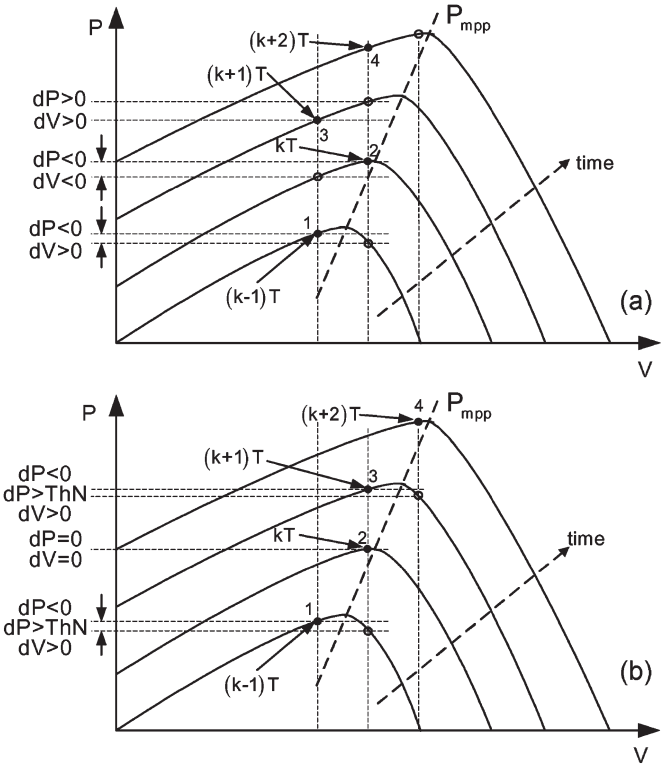

Fig. 5. Movement of the operating point of the PV system on the P–V characteristic (a) with the basic dP-P&O tracking method and (b) with the optimized tracking.

the caused decrease of power became larger than the threshold ($|dP| > |\text{ThN}|$). The flowchart in Fig. 3 assumes that the MPP voltage increases with irradiance, which is valid in most of the cases. However, in some cases, due to the panel series resistance at high irradiation levels, the MPP voltage could decrease with irradiation [15].

C. Determination of the Threshold Values

A theoretical analysis regarding the optimal choice of the main parameters (sampling frequency and perturbation size) of the P&O method, which is also valid for the dP-P&O, can be found in [16].

The threshold ThP has been chosen to be zero. This is because if the last perturbation had a positive effect on the output power, regardless of the size of the change, the MPPT should continue the perturbation in the same direction. A nonzero ThP would introduce a stationary error in the tracking by stopping the perturbation when the working point is approaching the MPP. On the other hand, when choosing the negative threshold ThN, the goal is to avoid unnecessary switching when the MPPT is closely following the changing MPP in varying irradiation, as it is shown in Fig. 5. If |ThN| is chosen to be too large, it would allow the working point to move away too far from the MPP, decreasing the MPPT efficiency. On the other hand, if |ThN| is too small, it will result in unnecessary switching around the MPP, also causing additional losses. In order to obtain the value of ThN, the change of power ΔP_I due to one voltage increment in the vicinity of MPP should be determined first, which requires a model of the used PV system. For the present purpose, a simple model is sufficient.

The current–voltage relationship of a PV panel using an ideal single-diode model can be described as follows:

$$I = I_{\text{sc}} - I_0 \left(e^{\frac{V}{n_s V_t}} - 1 \right) \tag{2}$$

where I_{sc} is the panel short-circuit current, I_0 is the dark saturation current, and V_t is the cell's thermal voltage. I_{sc} is given in the panel data sheet, whereas I_0 and V_t can be calculated by using the data sheet values and the panel basic equations or by measurements [17]–[19].

From (2), the panel voltage as a function of current can be expressed as follows:

$$V = n_s V_t \ln \left(\frac{I_{\text{sc}} - I}{I_0} \right). \tag{3}$$

If the PV system current is perturbed by a small dI, from (3)

$$V' = n_s V_t \ln \left(\frac{I_{\text{sc}} - I - dI}{I_0} \right). \tag{4}$$

From (3) and (4), the change of voltage caused by the small current perturbation can be calculated as follows:

$$\begin{aligned} dV_I &= V' - V \\ &= n_s V_t \left(\ln \left(\frac{I_{\text{sc}} - I - dI}{I_0} \right) - \ln \left(\frac{I_{\text{sc}} - I}{I_0} \right) \right) \end{aligned} \tag{5}$$

$$dV_I = n_s V_t \ln \left(\frac{I_{\text{sc}} - I - dI}{I_{\text{sc}} - I} \right). \tag{6}$$

By solving (6) for dI, the effect of a small voltage perturbation on the array current can be obtained as follows:

$$dI_V = (I_{\text{sc}} - I) \left(1 - e^{\frac{dV}{n_s V_t}} \right). \tag{7}$$

The general expression of the power change due to a small voltage perturbation has the form

$$dP_V = dV I + dI_V V + dI_V dV. \tag{8}$$

By inserting (7) into (8), the PV power change due to a small voltage perturbation at an arbitrary point of the V–I characteristic can be estimated.

If one replaces the term dV in the aforementioned equation with Incr, it will result in the variation of power due to one perturbation of the MPPT.

Obviously, (8) depends on the actual irradiation conditions and the instantaneous working point of the system on the V–I characteristic. It is well known that, at a given irradiation intensity

$$\left. \frac{\partial P}{\partial V} \right|_{\text{MPP}} = 0. \tag{9}$$

Authorized licensed use limited to: IEEE Xplore. Downloaded on January 23, 2009 at 11:28 from IEEE Xplore. Restrictions apply.

From (9), the change of power due to a small ΔV is the minimum in the vicinity of the MPP

$$\left|\frac{\Delta P}{\Delta V}\right|_{\mathrm{MPP}} \leq \left|\frac{\Delta P}{\Delta V}\right|_{\substack{V\neq V_{\mathrm{MPP}}\\ I\neq I_{\mathrm{MPP}}}}. \tag{10}$$

The calculation of the threshold values are based on (8), where the actual working point on the I–V characteristic is considered to be $V = V_{\mathrm{MPP}} \pm \mathrm{Incr}$, with a perturbation that moves the working point away from MPP.

III. Simulation Results

The inverter-control structure shown in Fig. 4 has been implemented in Simulink in order to verify and compare the behavior of the optimized dP-P&O to the basic dP-P&O. The considered system parameters are described in the following. The PV array consists of three parallel strings, each containing 16 series-connected BPMSX120 PV panels with the following data sheet parameters:

1) $I_{\mathrm{sc}} = 3.87$ A—short-circuit current in STC[1];
2) $V_{\mathrm{OC}} = 42.1$ V—open-circuit voltage in STC;
3) $V_{\mathrm{MPP}} = 33.7$ V—voltage at the MPP in STC;
4) $I_{\mathrm{MPP}} = 3.56$ A—current at the MPP in STC;
5) $P_{\mathrm{MPP}} = 120$ W—power at the MPP in STC.

Considering that each string contains 16 panels with the aforementioned parameters, the rated MPP voltage of the system results as $V_{\mathrm{rated}} = 16 \times 33.7 = 539$ V. The maximum power of the entire plant results as $P_{\mathrm{rated}} = 3 \times 16 \times 120 = 5760$ W. The rated current of the system is $I_{\mathrm{rated}} = 3 \times 3.56 = 10.68$ A. The model of the PV plant is using the detailed single-diode model, considering the full characteristic of the cells, where the reverse characteristic equations were implemented according to [20]. The inverter and the grid current controller are considered ideal; they are modeled by an ideal current source and a two-sample delay, respectively. The LC filter and grid impedance have been modeled by using the PLECS toolbox, with values of $L_f = 1.7$ mH and $C_f = 4.3$ μF for the LC filter and $L_g = 50$ μH and $R_g = 0.2$ Ω for the grid impedance. The minimum system voltage allowed is $V_{\mathrm{sys\,min}} = 150$ V.

In order to visualize and compare the behavior of the initial and optimized dP-P&O algorithms, they have been simulated in the following two different MPPT configurations: 1) when the MPPT provides the dc current reference (Figs. 6 and 7) and 2) when the MPPT provides the dc voltage reference (Figs. 8 and 9). In the following, the simulation results for these two cases will be presented.

A. Comparison of the MPPT Algorithms With Current Reference as Output

In order to facilitate the comparison of the basic and optimized dP-P&O, the same current increment values were used

[1]Standard test conditions—The testing conditions to measure photovoltaic cell or module nominal output power. Irradiance level is 1000 W/m^2, with the reference air mass of 1.5 solar spectral irradiance distribution and cell or module junction temperature of 25 °C.

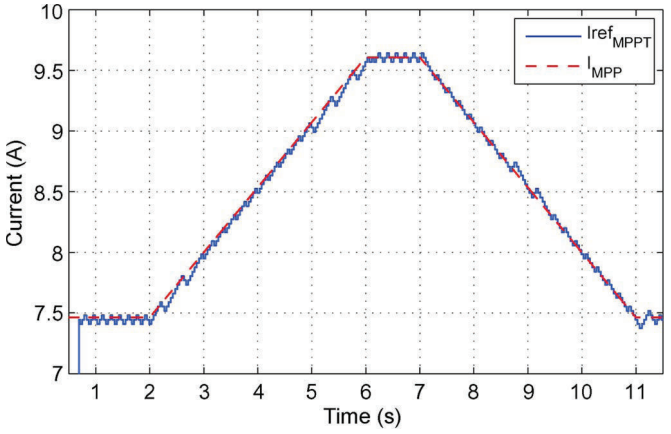

Fig. 6. Current references of the basic dP-P&O algorithm and the ideal MPP current during rapidly changing irradiation. It can be seen that the tracker "turns back" when it crosses the MPP current. The trapezoidal irradiation profile starts at 2 s on the time axis, reaches the maximum at 6 s, and returns to the initial level at 11 s.

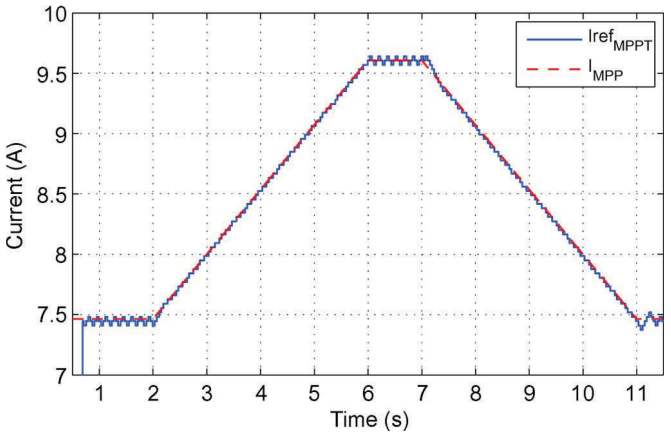

Fig. 7. Current references of the optimized dP-P&O algorithm and the ideal MPP current during rapidly changing irradiation. The tracker does not decrease the current reference when it reaches the MPPT current but waits for one MPPT period without perturbation instead.

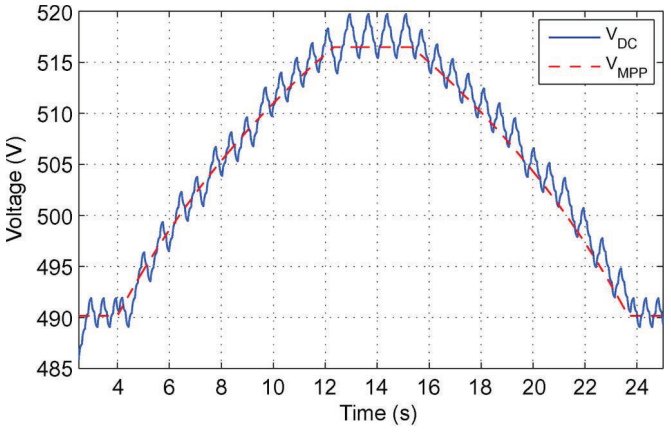

Fig. 8. PV system voltage and ideal MPP voltage during a trapezoidal irradiation profile. It can be seen that the dc voltage oscillates around the optimum value during the irradiation slope. The ramp starts at 4 s on the time axis from 250 W/m^2, reaches its maximum (500 W/m^2) at 12.5 s, and arrives back at its initial value at 24 s.

Authorized licensed use limited to: IEEE Xplore. Downloaded on January 23, 2009 at 11:28 from IEEE Xplore. Restrictions apply.

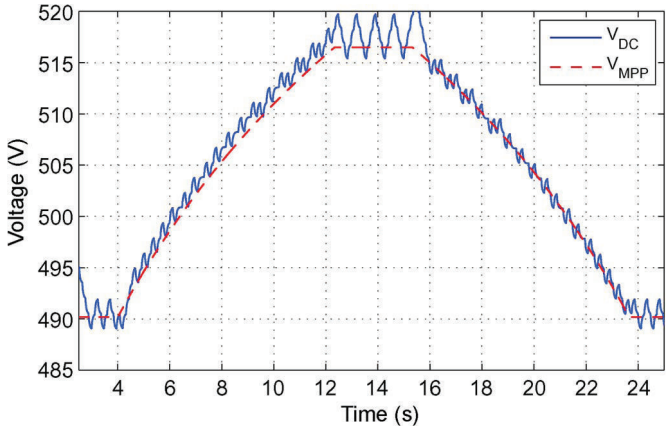

Fig. 9. PV system voltage and ideal MPP voltage during a trapezoidal irradiation profile. It can be seen that the dc voltage ripple is considerably decreased during the ramp.

for both strategies: $\text{Incr}_{\min} = 12$ mA for steady-state conditions and $\text{Incr} = 3 \times 12$ mA for rapidly changing conditions. The MPPT sampling frequency is, in both cases, $f_{\text{MPPT}} = 25$ Hz.

In order to verify the effect of rapidly changing irradiation conditions, an irradiation ramp change was used. This irradiation change starts from 700 W/m^2, stops at 900 W/m^2, waits at this level for 1 s, and decreases again back to 700 W/m^2 with a constant slope. A 4-s period for the increasing and decreasing ramps was selected. The aforementioned values were selected in order to shorten the simulation time; the focus was put on the visualization of the different tracking behaviors of the initial and optimized dP-P&O algorithms. One should note that, in case the MPPT provides the dc current reference instead of the dc voltage, it needs higher dynamics in order to be able to follow the increasing irradiance, which is due to the linear dependence of MPP current with irradiance, as opposed to the case with the MPP voltage logarithmic dependence.

B. Comparison of the MPPT Algorithms With Voltage Reference as Output

In the present section, the behaviors of the basic and optimized dP-P&O trackers with dc voltage reference (identical to the block scheme in Fig. 4) are simulated and compared. As this configuration has been implemented on the experimental setup, the simulation settings follow the practical case. Accordingly, a voltage increment of $\text{Incr} = 1$ V and an MPPT sampling rate of $f_{\text{MPPT}} = 8.33$ Hz (every sixth grid voltage period) are used, both in rapidly changing irradiation and steady-state conditions. An irradiation ramp starts from 250 W/m^2, stops at 500 W/m^2, waits at this level for 5 s, and again decreases back to 250 W/m^2 with a constant slope. The slope of the irradiation was chosen to be 30 W/m^2/s, which corresponds to 8.3 s as the duration of the increasing and decreasing ramps. The aforementioned values were selected in order to shorten the simulation time; the focus was put on the visualization of the different tracking behavior of the initial and optimized dP-P&O algorithms. The relatively low irradiation values were chosen in order to accentuate the effect of irradiation change on the PV system MPP voltage.

IV. Experimental Tests and Results

Both the traditional and improved methods were implemented and experimentally tested on an industrial PV inverter, which was manufactured by REFU Elektronik GmbH, Germany. The laboratory setup, using a control system as shown in Fig. 4, consists of the following main components.

A PV simulator, which is built of two programmable series-connected Delta Elektronika SM300-10 dc power supplies having Vmax $= 300$ V and Imax $= 10$ A, was used. Their output voltages were controlled in real time by a DS1103 dSpace system according to a PV model of a PV array. The model is based on a number of series-/parallel-connected BP-MSX120 PV panels where the input parameters are the maximum power in STC (P_{MP}), the voltage at the $P_{\text{MP}}(V_{\text{MP}})$, and the solar irradiation intensity.

The equations on which the model is based are shown as follows:

$$V = n_{\text{ps}} V_{\text{OC}} + n_{\text{ps}} \cdot n_s \cdot V_t \ln\left(1 - \frac{I}{I_{\text{sc,STC}} \cdot \frac{G}{1000}}\right)$$
$$V_{\text{OC}} = n_s V_t \ln\left(\frac{1 + I_{\text{sc,STC}} \cdot \frac{G}{1000}}{I_0}\right) \quad (11)$$

where

n_{ps}	number of panels connected in series;
n_s	number of cells in one panel;
V_t	thermal voltage (V);
$I_{\text{sc,STC}}$	short-circuit current at STC (A);
G	irradiation (W/m^2).

The output of the PV simulator is connected to the solar inverter manufactured by REFU Elektronik GmbH, Germany. The rated power of the PV inverter is 15 kW with a 50-Hz 400-V three-phase output and dc input voltage range of 150–800 V.

As the used solar inverter is a newly developed product by REFU Electronik, not all the technical parameters are available, only the ones relevant for MPPT operation. Thereby, the current control loop has been considered ideal from the MPPT point of view. The inverter has a dc link capacitor value of $C_{\text{dc}} = 4$ mF, and the system sampling frequency, which is identical to the switching frequency, is $f_{\text{sw}} = 16$ kHz. The sampling of the measured signals has a resolution of 12 b. The PV inverter real-time control is running on a Motorola PowerPC 400-MHz processor.

Due to the three-phase configuration and the large value of the dc link capacitor, the effects of power oscillations at double grid frequency on the dc link voltage have been neglected.

The MPPT structure of the solar converter corresponds to the one shown in Fig. 4. The MPPT dc voltage increment and perturbation frequency has been chosen identical for all three considered tests: the classic P&O (Fig. 10), the dP-P&O, as well as for the improved dP-P&O; these settings correspond to those described in Section III-B: $\text{Incr} = 1$ V and MPPT sampling rate $f_{\text{MPPT}} = 8.33$ Hz.

In order to test the MPP tracker behaviors in dynamic conditions, a linear irradiation ramp was used. The ramp starts

Authorized licensed use limited to: IEEE Xplore. Downloaded on January 23, 2009 at 11:28 from IEEE Xplore. Restrictions apply.

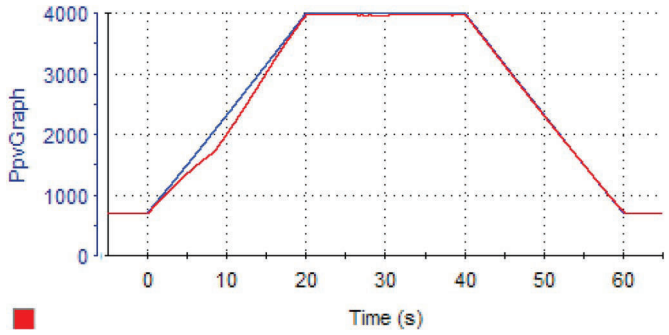

Fig. 10. Experimental measurement of the (red signal) PV array power during a trapezoidal irradiation profile, using the classical P&O MPPT method, compared to the (blue signal) ideal MPP power.

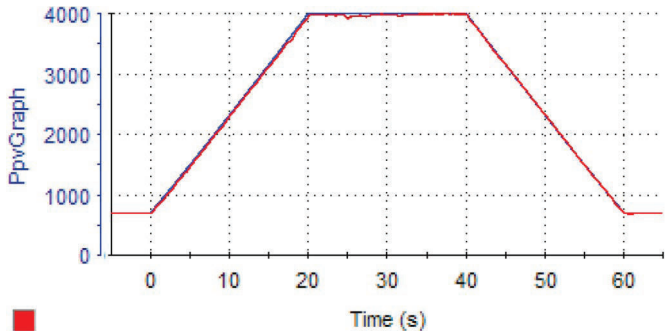

Fig. 11. Experimental measurement of the (red signal) PV array power (W) during a trapezoidal irradiation profile, using the dP-P&O MPPT method, compared to the (blue signal) ideal MPP power.

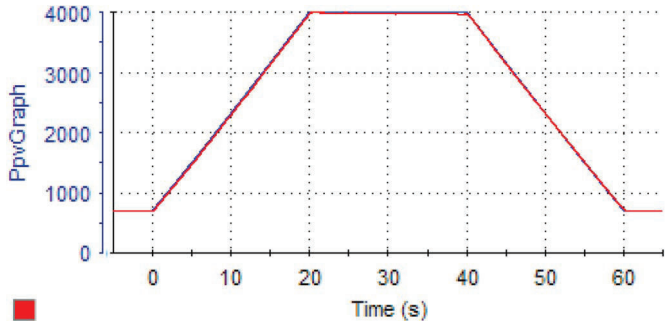

Fig. 12. Experimental measurement of the (red signal) PV array power (W) during a trapezoidal irradiation profile, using the optimized dP-P&O MPPT method, compared to the (blue signal) ideal MPP power.

at 5 s on the time axis from 200 W/m^2, reaches its maximum (1000 W/m^2) at 20 s, and arrives back to its initial value at 60 s.

In the following, the experimental results using the previously described setup will be presented.

It can be seen in Figs. 11 and 12 as well as in Figs. 13 and 14 that the optimized dP-P&O algorithm performs slightly better than the initial one. The relatively small difference in their performance is due to two main factors: 1) the noisy measurement environment, which is present in most applications and 2) the characteristic of the controlled dc voltage sources used as PV simulators. The sources have output capacitors for the reduction of voltage ripples, which inherently reduces

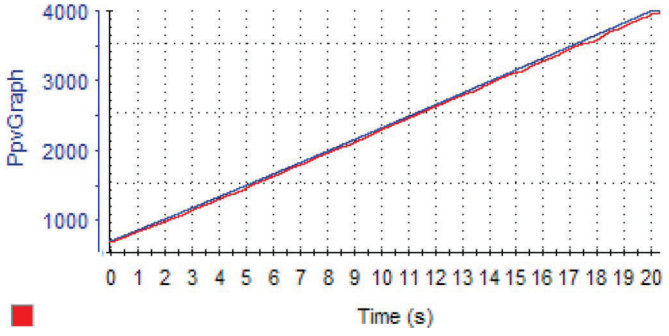

Fig. 13. Experimental measurement of the (red signal) PV array power (W) during a trapezoidal irradiation profile, using the dP-P&O MPPT method, compared to the (blue signal) ideal MPP power, which is zoomed on the increasing ramp.

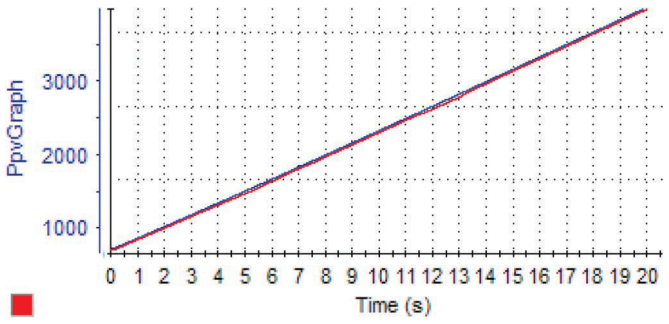

Fig. 14. Experimental measurement of the (red signal) PV array power (W) during a trapezoidal irradiation profile, using the optimized dP-P&O MPPT method, compared to the (blue signal) ideal MPP power, which is zoomed on the increasing ramp.

their control bandwidth. Thereby, the PV simulator cannot be considered identical to a real PV system in terms of voltage controllability and response time. This means that, around MPP, where a voltage perturbation creates a relatively small change of power [see (10)], the simulator has difficulties in adjusting the voltage accordingly. This results in larger voltage oscillations of the MPP tracker around the MPP than in the case of a real PV system, without decreasing the output power.

However, the considered MPPT algorithms are tracking the power and not the voltage; therefore, they are able to keep the output power close to the optimum (maximum) value in both cases. Nevertheless, an increase of efficiency in favor of the optimized dP-P&O can be seen when looking at the zoom of the increasing ramp of the power in Figs. 13 and 14. This can also be seen in the efficiency plots in Figs. 16 and 17.

Due to the facts considered previously and in order to show the real power tracking capabilities of the algorithms, they have been assessed based on comparing the inverter input power to the ideal MPP given by the model.

The instantaneous efficiencies corresponding to the traditional dP-P&O method can be seen in Fig. 15, whereas the basic and optimized dP-P&O algorithms are shown in Figs. 16 and 17, respectively. It can be seen that the average efficiency of the optimized dP-P&O during the entire test period is approximately 99.4%, which is about approximately 0.4% higher compared to the basic dP-P&O. It can also be noted that the efficiency in Fig. 17 shows less variation when compared to the basic dP-P&O efficiency plot.

Authorized licensed use limited to: IEEE Xplore. Downloaded on January 23, 2009 at 11:28 from IEEE Xplore. Restrictions apply.

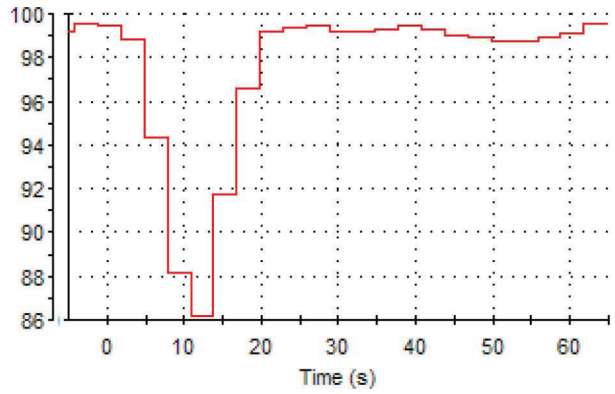

Fig. 15. Experimental measurement of the instantaneous MPPT efficiency (in percentage and averaged over 3 s) of the classical P&O algorithm.

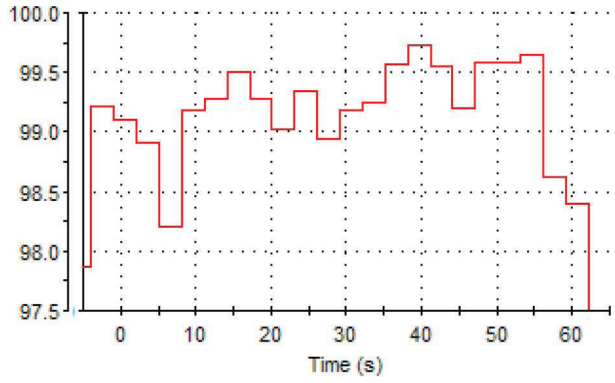

Fig. 16. Experimental measurement of the instantaneous MPPT efficiency (in percentage and averaged over 3 s) of the basic dP-P&O algorithm during the trapezoidal irradiation profile.

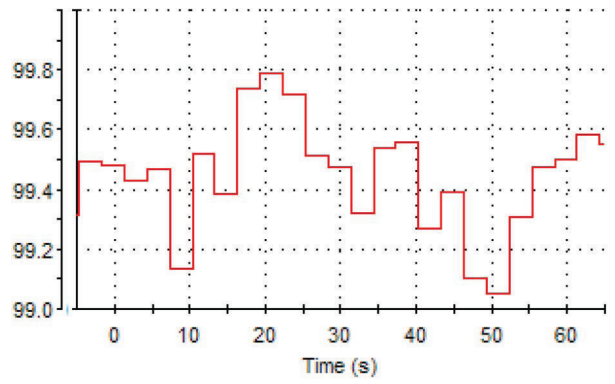

Fig. 17. Experimental measurement of the instantaneous MPPT efficiency (averaged over 3 s) of the optimized dP-P&O algorithm.

V. Conclusion

In this paper, a fast MPPT algorithm for rapid irradiation changes has been presented. The method is using an additional measurement of power inside the MPPT algorithm without perturbation and uses this information to separate the effects of the environment from the tracker's perturbations. Furthermore, by identifying the environmental changes, it allows the use of optimized tracking for different operational states: stable, increasing, or decreasing irradiation. By optimizing the perturbation scheme for the different cases, it can achieve faster tracking during irradiation change and more accuracy at steady state. The proposed optimized dP-P&O method has been implemented and compared to the basic dP-P&O and the classical P&O algorithm. The experimental results show that both algorithms perform clearly better than the classical P&O algorithm, providing accurate tracking even in very fast changing irradiation conditions.

References

[1] [s.n], "Trends in photovoltaic applications. Survey report of selected IEA countries between 1992 and 2005," Int. Energy Agency, Paris, France, Rep. IEA-PVPS Task 1 T1-15:2006, 2006. [Online]. Available: http://www.iea-pvps.org/products/download/rep1_15.pdf

[2] D. Hohm and M. Ropp, "Comparative study of maximum power point tracking algorithms using an experimental, programmable, maximum power point tracking test," in *Proc. 28th IEEE Conf. Rec. Photovoltaic Spec.*, 2000, pp. 1699–1702.

[3] W. Xiao and W. Dunford, "A modified adaptive hill climbing MPPT method for photovoltaic power systems," in *Proc. 35th IEEE Annu. PESC*, 2004, vol. 3, pp. 1957–1963.

[4] C. W. Tan, T. Green, and C. Hernandez-Aramburo, "An improved maximum power point tracking algorithm with current-mode control for photovoltaic applications," in *Proc. Int. Conf. PEDS*, 2006, vol. 1, pp. 489–494.

[5] L. Egiziano, N. Femia, D. Granozio, G. Petrone, G. Spagnuolo, and M. Vitelli, "Photovoltaic inverters with Perturb & Observe MPPT technique and one-cycle control," in *Proc. IEEE Int. Symp. Circuits Syst.*, 2006, pp. 3718–3721.

[6] T. Shimizu, O. Hashimoto, and G. Kimura, "A novel high-performance utility-interactive photovoltaic inverter system," *IEEE Trans. Power Electron.*, vol. 18, no. 2, pp. 704–711, Mar. 2003.

[7] J.-H. Park, J.-Y. Ahn, B.-H. Cho, and G.-J. Yu, "Dual-module-based maximum power point tracking control of photovoltaic systems," *IEEE Trans. Ind. Electron.*, vol. 53, no. 4, pp. 1036–1047, Jun. 2006.

[8] J.-M. Kwon, K.-H. Nam, and B.-H. Kwon, "Photovoltaic power conditioning system with line connection," *IEEE Trans. Ind. Electron.*, vol. 53, no. 4, pp. 1048–1054, Jun. 2006.

[9] W. Xiao, W. G. Dunford, P. R. Palmer, and A. Capel, "Application of centered differentiation and steepest descent to maximum power point tracking," *IEEE Trans. Ind. Electron.*, vol. 54, no. 5, pp. 2539–2549, Oct. 2007.

[10] I.-S. Kim, M.-B. Kim, and M.-J. Youn, "New maximum power point tracker using sliding-mode observer for estimation of solar array current in the grid-connected photovoltaic system," *IEEE Trans. Ind. Electron.*, vol. 53, no. 4, pp. 1027–1035, Jun. 2006.

[11] E. Roman, R. Alonso, P. Ibanez, S. Elorduizapatarietxe, and D. Goitia, "Intelligent PV module for grid-connected PV systems," *IEEE Trans. Ind. Electron.*, vol. 53, no. 4, pp. 1066–1073, Jun. 2006.

[12] C. Hua and C. Shen, "Comparative study of peak power tracking techniques for solar storage system," in *Proc. 13th Annu. APEC*, 1998, vol. 2, pp. 679–685.

[13] N. Femia, G. Petrone, G. Spagnuolo, and M. Vitelli, "Perturb and Observe MPPT technique robustness improved," in *Proc. IEEE Int. Symp. Ind. Electron.*, 2004, vol. 2, pp. 845–850.

[14] D. Sera, T. Kerekes, R. Teodorescu, and F. Blaabjerg, "Improved MPPT method for rapidly changing environmental conditions," in *Proc. IEEE Int. Symp. Ind. Electron.*, 2006, vol. 2, pp. 1420–1425.

[15] V. V. R. Scarpa, G. Spiazzi, S. Buso, "Low complexity MPPT technique exploiting the effect of the PV cell series resistance," in *Proc. 23rd Annu. IEEE APEC Expo.*, Feb. 24–28, 2008, pp. 1958–1964. [Online]. Available: http://ieeexplore.ieee.org/iel5/4510696/4522647/04522996.pdf

[16] N. Femia, G. Petrone, G. Spagnuolo, and M. Vitelli, "Optimization of Perturb and Observe maximum power point tracking method," *IEEE Trans. Power Electron.*, vol. 20, no. 4, pp. 963–973, Jul. 2005.

[17] W. Xiao, W. Dunford, and A. Capel, "A novel modeling method for photovoltaic cells," in *Proc. 35th IEEE Annu. PESC*, 2004, vol. 3, pp. 1950–1956.

[18] G. Walker, "Evaluating MPPT converter topologies using a Matlab PV model," *J. Electr. Electron. Eng. Aust.*, vol. 21, no. 1, pp. 49–55, 2001.

[19] A. Wagner, "Peak-power and internal series resistance measurement under natural ambient conditions," in *Proc. EuroSun*, Copenhagen, Denmark, 2000.

[20] J. Bishop, "Computer simulation of the effect of electrical mismatches in photovoltaic cell interconnection circuits," *Sol. Cells*, vol. 25, pp. 73–89, 1988.

Authorized licensed use limited to: IEEE Xplore. Downloaded on January 23, 2009 at 11:28 from IEEE Xplore. Restrictions apply.

Dezso Sera (S'05) received the B.S. degree in electrical engineering and the M.S. degree in drives automation with energetic performances from the Technical University of Cluj-Napoca, Cluj-Napoca, Romania, in 2001 and 2002, respectively. In 2005, he received the M.Sc. degree in power electronics and drives from Aalborg University, Aalborg East, Denmark, where he is currently working toward the Ph.D. degree in the Institute of Energy Technology.

His interests include modeling, diagnostics, maximum power point tracking, and control of grid-connected photovoltaic systems.

Remus Teodorescu (S'94–M'99–SM'02) received the Dipl.Ing. degree in electrical engineering from the Polytechnical University of Bucharest, Bucharest, Romania, in 1989 and the Ph.D. degree in power electronics from the University of Galati, Galati, Romania, in 1994.

Since 1998, he has been with the Power Electronics Section, Institute of Energy Technology, Aalborg University, Aalborg East, Denmark, where he is currently a Full Professor. He has more than 120 papers published, one book, and three patents (pending). His areas of interest are design and control of power converters used in renewable energy systems, distributed generation of mainly wind power and photovoltaics, computer simulations, and digital control implementation. He is the Founder and Coordinator of the Green Power Laboratory, Aalborg University, where he is focusing on the development and test of grid converters for renewable energy systems. He is also the Coordinator of the Vestas Power Program.

Dr. Teodorescu is the corecipient of the Technical Committee Prize Paper Awards at the IEEE Industry Applications Society (IAS) Annual Meeting 1998 and the Third-ABB Prize Paper Award at the IEEE Optim 2002. He is an Associate Editor for the IEEE POWER ELECTRONICS LETTERS and the Chair of the IEEE Danish Joint Industrial Electronics Society/Power Electronics Society/IAS Chapter.

Jochen Hantschel, photograph and biography not available at the time of publication.

Michael Knoll was born in 1981 in Friedrichshafen, Germany. He received the Dipl. Engineer degree in electrical engineering from the University of Ulm, Ulm, Germany, in 2007. In his diploma thesis, he designed, assembled, and tested a new topology for a high-efficiency grid converter for photovoltaic applications.

After his studies, he was with the Software Department, REFU-Elektronik, where he worked on the implementation of the maximum power point tracker in a grid-converter. Currently, he is with the Development Department, Daimler AG, Stuttgart, Germany.

Authorized licensed use limited to: IEEE Xplore. Downloaded on January 23, 2009 at 11:28 from IEEE Xplore. Restrictions apply.

Publication 3

Power Electronics and Control of Renewable Energy Systems

by F. Iov, M. Ciobotaru, D. Sera, R. Teodorescu and F. Blaabjerg

Power Electronics and Control of Renewable Energy Systems

F. Iov, M. Ciobotaru, D. Sera, R. Teodorescu, F. Blaabjerg
Aalborg University, Institute of Energy Technology
Pontoppidanstraede 101, DK-9220 Aalborg East, Denmark
fi@iet.aau.dk, mpc@iet.aau.dk, des@iet.aau.dk, ret@iet.aau.dk, fbl@iet.aau.dk

***Abstract* – The global electrical energy consumption is still rising and there is a demand to double the power capacity within 20 years. The production, distribution and use of energy should be as technological efficient as possible and incentives to save energy at the end-user should also be set up. Deregulation of energy has in the past lowered the investment in larger power plants, which means the need for new electrical power sources may be very high in the near future. Two major technologies will play important roles to solve the future problems. One is to change the electrical power production sources from the conventional, fossil (and short term) based energy sources to renewable energy resources. Another is to use high efficient power electronics in power generation, power transmission/distribution and end-user application. This paper discuss some of the most emerging renewable energy sources, wind energy and photovoltaics, which by means of power electronics are changing from being minor energy sources to be acting as important power sources in the energy system.**

I. Introduction

In classical power systems, large power generation plants located at adequate geographical places produce most of the power, which is then transferred towards large consumption centers over long distance transmission lines. The system control centers monitor and regulate the power system continuously to ensure the quality of the power, namely frequency and voltage. However, now the overall power system is changing, a large number of dispersed generation (DG) units, including both renewable and non-renewable sources such as wind turbines, wave generators, photovoltaic (PV) generators, small hydro, fuel cells and gas/steam powered Combined Heat and Power (CHP) stations, are being developed [1], [2] and installed. A wide-spread use of renewable energy sources in distribution networks and a high penetration level will be seen in the near future many places. E.g. Denmark has a high power capacity penetration (> 20%) of wind energy in major areas of the country and today 18% of the whole electrical energy consumption is covered by wind energy. The main advantages of using renewable energy sources are the elimination of harmful emissions and inexhaustible resources of the primary energy. However, the main disadvantage, apart from the higher costs, e.g. photovoltaic, is the uncontrollability. The availability of renewable energy sources has strong daily and seasonal patterns and the power demand by the consumers could have a very different characteristic. Therefore, it is difficult to operate a power system installed with only renewable generation units due to the characteristic differences and the high uncertainty in the availability of the renewable energy sources. This is further strengthened as no real large energy storage systems exist.

The wind turbine technology is one of the most emerging renewable energy technologies. It started in the 1980'es with a few tens of kW production power to today with multi-MW size wind turbines that are being installed. It also means that wind power production in the beginning did not have any impact on the power system control but now due to their size they have to play an active part in the grid. The technology used in wind turbines was in the beginning based on a squirrel-cage induction generator connected directly to the grid. By that power pulsations in the wind are almost directly transferred to the electrical grid. Furthermore there is no control of the active and reactive power, which typically are important control parameters to regulate the frequency and the voltage. As the power range of the turbines increases those control parameters become more important and it is necessary to introduce power electronics [3] as an interface between the wind turbine and the grid. The power electronics is changing the basic characteristic of the wind turbine from being an energy source to be an active power source. The electrical technology used in wind turbine is not new. It has been discussed for several years [6]-[50] but now the price pr. produced kWh is so low, that solutions with power electronics are very attractive.

This paper will first discuss the basic development in power electronics and power electronic conversion. Then different wind turbine configurations will be explained both aerodynamically and electrically. Also different control methods will be shown for a wind turbine. They are now also installed in remote areas with good wind conditions (off-shore, on-shore) and different possible configurations are shown and compared. Next the PV-technology is discussed including the necessary basic power electronic conversion. Power converters are given and more advanced control features described. Finally, a general technology status of the wind power and the PV technology is presented demonstrating still more efficient and attractive power sources for the future.

1-4244-0645-5/07/$20.00©2007 IEEE

II. MODERN POWER ELECTRONICS

Power electronics has changed rapidly during the last thirty years and the number of applications has been increasing, mainly due to the developments of the semiconductor devices and the microprocessor technology. For both cases higher performance is steadily given for the same area of silicon, and at the same time they are continuously reducing in price. A typical power electronic system, consisting of a power converter, a load/source and a control unit, is shown in Fig. 1.

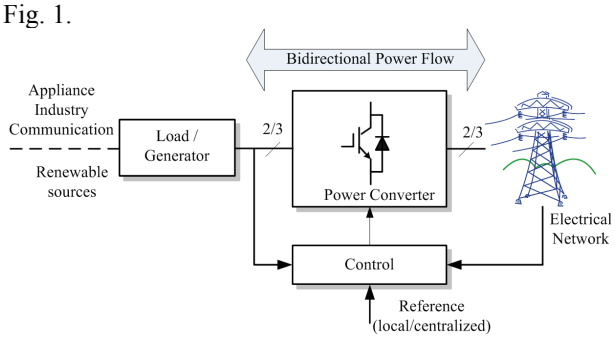

Fig. 1. Power electronic system with the grid, load/source, power converter and control.

The power converter is the interface between the load/generator and the grid. The power may flow in both directions, of course, dependent on topology and applications.

Three important issues are of concern using such a system. The first one is reliability; the second is efficiency and the third one is cost. For the moment the cost of power semiconductor devices is decreasing 1÷5 % every year for the same output performance and the price pr. kW for a power electronic system is also decreasing. An example of a mass-produced and high competitive power electronic system is an adjustable speed drive (ASD). The trend of weight, size, number of components and functions in a standard Danfoss Drives A/S frequency converter can be seen in Fig. 2. It clearly shows that power electronic conversion is shrinking in volume and weight. It also shows that more integration is an important key to be competitive as well as more functions become available in such a product.

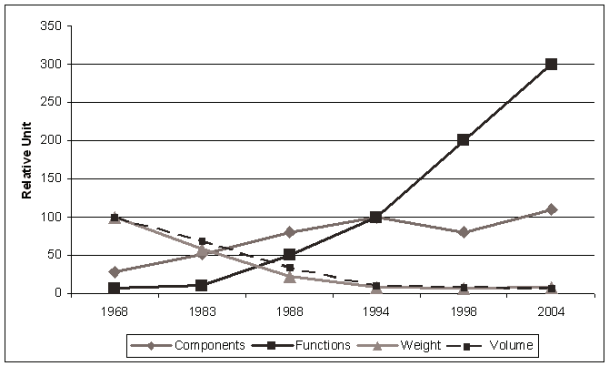

Fig. 2. Development of standard adjustable speed drives for the last four decades.

The key driver of this development is that the power electronic device technology is still undergoing important progress.

Fig. 3 shows different power devices and the areas where the development is still going on.

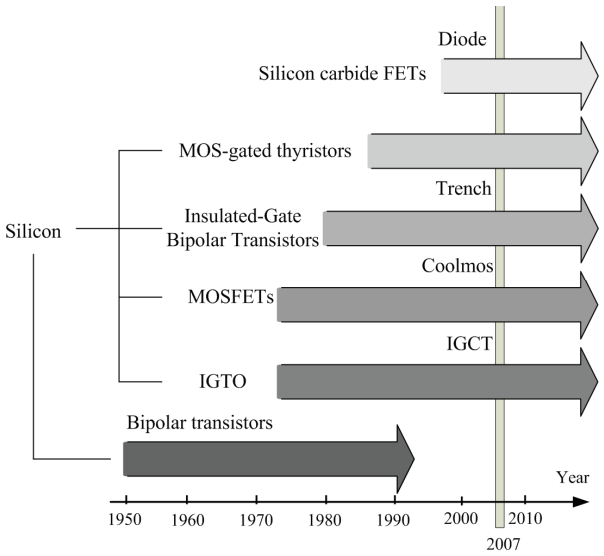

Fig. 3. Development of power semiconductor devices in the past and in the future [36].

The only power device which is not under development any more is the silicon-based power bipolar transistor because MOS-gated devices are preferable in the sense of easy control. The breakdown voltage and/or current carrying capability of the components are also continuously increasing. Important research is going on to change the material from silicon to silicon carbide, which may dramatically increase the power density of power converters.

III. WIND ENERGY CONVERSION

Wind turbines capture power from the wind by means of aerodynamically designed blades and convert it to rotating mechanical power. The number of blades is normally three. As the blade tip-speed should be lower than half the speed of sound the rotational speed will decrease as the radius of the blade increases. For multi-MW wind turbines the rotational speed will be 10-15 rpm. The most weight efficient way to convert the low-speed, high-torque power to electrical power is to use a gear-box and a standard fixed speed generator as illustrated in Fig. 4.

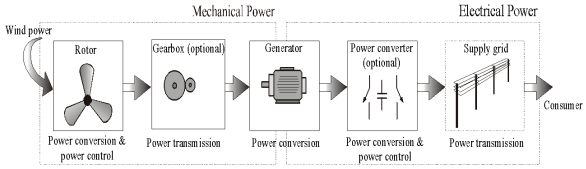

Fig. 4. Converting wind power to electrical power in a wind turbine [19].

The gear-box is optional as multi-pole generator systems are possible solutions. Between the grid and the generator a power converter can be inserted.

The possible technical solutions are many and a technological roadmap starting with wind energy/power and converting the mechanical power into electrical power is shown in Fig. 5. The electrical output can either be ac or dc. In the last case a power converter will be used as interface to the grid.

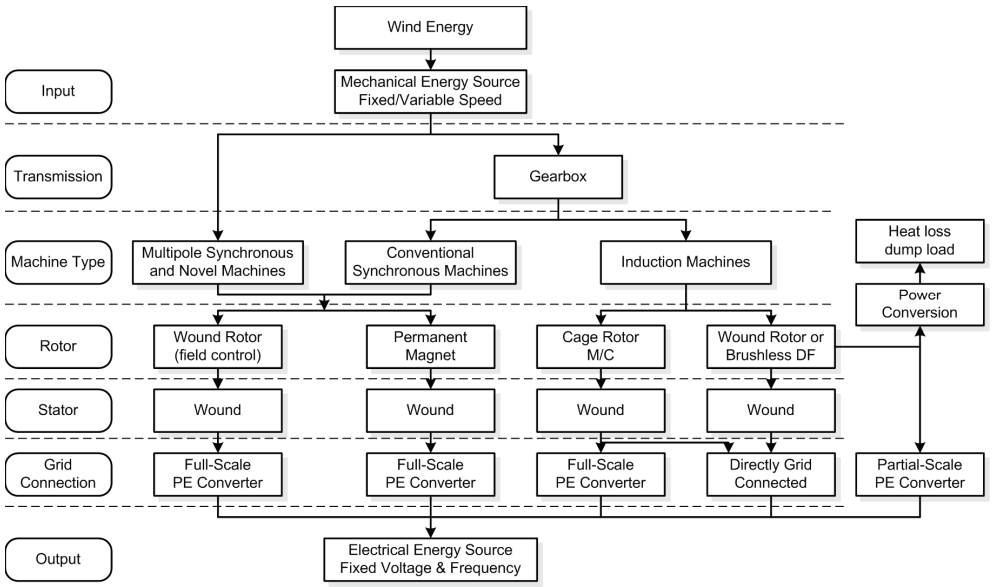

Fig. 5. Technological roadmap for wind turbine's technology [3].

A. Control methods for wind turbines

The development in wind turbine systems has been steady for the last 25 years and four to five generations of wind turbines exist and it is now proven technology. It is important to be able to control and limit the converted mechanical power at higher wind speed, as the power in the wind is a cube of the wind speed. The power limitation may be done either by stall control (the blade position is fixed but stall of the wind appears along the blade at higher wind speed), active stall (the blade angle is adjusted in order to create stall along the blades) or pitch control (the blades are turned out of the wind at higher wind speed) [6], [7]. The basic output characteristics of these three methods of controlling the power are summarized in Fig. 6.

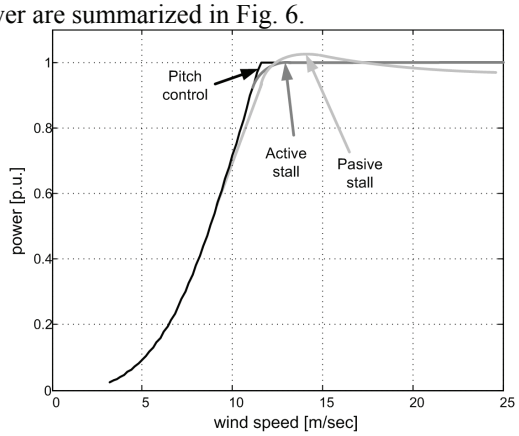

Fig. 6. Power characteristics of different fixed speed wind turbine systems.

Another control variable in wind turbine system is the speed. Based on this criterion the wind turbines are classified into two main categories [6], [7]; namely fixed speed and variable speed wind turbines respectively.

A fixed speed wind turbine has the advantages of being simple, robust, reliable, well proven and with low cost of the electrical parts. Its direct drawbacks are the uncontrollable reactive power consumption, mechanical stress and limited power quality control. Due to its fixed speed operation, wind speed fluctuations are converted to mechanical torque fluctuations, beneficially reduced slightly by small changes in generator slip, and transmitted as fluctuations into electrical power to the grid. The power fluctuations can also yield large voltage fluctuations in the case of a weak grid and thus, significant line losses [6], [7].

The variable speed wind turbines are designed to achieve maximum aerodynamic efficiency over a wide range of wind speed. By introducing the variable speed operation, it is possible to continuously adapt (accelerate or decelerate) the rotational speed of the wind turbine to the wind speed v, in such a way that tip speed ratio is kept constant to a predefined value corresponding to the maximum power coefficient. Contrary to a fixed speed system, a variable speed system keeps the generator torque nearly constant, the variations in wind being absorbed by the generator speed changes.

Seen from the wind turbine point of view, the most important advantages of the variable speed operation compared to the conventional fixed speed operation are: reduced mechanical stress on the mechanical components such as shaft and gearbox, increased power capture and reduced acoustical.

Additionally, the presence of power converters in wind turbines also provides high potential control capabilities for both large modern wind turbines and wind farms to fulfill the high technical demands imposed by the grid operators [6], [7], [8] and [23], such as: controllable active and reactive power (frequency and voltage control); quick response under transient and dynamic power system situations, influence on network stability and improved power quality.

B. Wind Turbine Concepts

The most commonly applied wind turbine designs can be categorized into four wind turbine concepts. The main differences between these concepts concern the generating system and the way in which the aerodynamic efficiency of the rotor is limited during above the rated value in order to prevent overloading. These concepts are presented in detail in the following paragraphs.

1) Fixed Speed Wind Turbines (WT Type A)

This configuration corresponds to the so called Danish concept that was very popular in 80's. This wind turbine is fixed speed controlled machine, with asynchronous squirrel cage induction generator (SCIG) directly connected to the grid via a transformer as shown in Fig. 7.

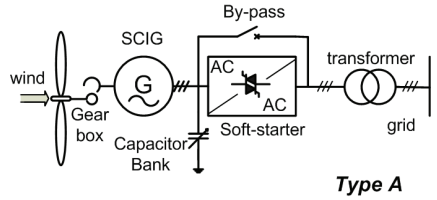

Fig. 7. Fixed speed wind turbine with directly grid connected squirrel-cage induction generator.

This concept needs a reactive power compensator to reduce (almost eliminate) the reactive power demand from the turbine generators to the grid. It is usually done by continuously switching capacitor banks following the production variation (5-25 steps) Smoother grid connection occurs by incorporating a soft-starter. Regardless the power control principle in a fixed speed wind turbine, the wind fluctuations are converted into mechanical fluctuations and further into electrical power fluctuations. These can yield to voltage fluctuations at the point of connection in the case of a weak grid. Because of these voltage fluctuations, the fixed speed wind turbine draws varying amounts of reactive power from the utility grid (in the case of no capacitor bank), which increases both the voltage fluctuations and the line losses.

Thus, the main drawbacks of this concept are: does not support any speed control, requires a stiff grid and its mechanical construction must be able to support high mechanical stress caused by wind gusts.

2) Partial Variable Speed Wind Turbine with Variable Rotor Resistance (WT Type B)

This configuration corresponds to the limited variable speed controlled wind turbine with variable rotor resistance, known as OptiSlip (Vestas^{TM}) as presented in Fig. 8.

It uses a wound rotor induction generator (WRIG) and it has been used by the Danish manufacturer Vestas Wind Systems since the mid 1990's.

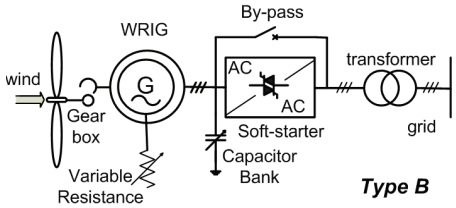

Fig. 8. Partial variable speed wind turbine with variable rotor resistance.

The generator is directly connected to the grid. The rotor winding of the generator is connected in series with a controlled resistance, whose size defines the range of the variable speed (typically 0-10% above synchronous speed). A capacitor bank performs the reactive power compensation and smooth grid connection occurs by means of a soft-starter. An extra resistance is added in the rotor circuit, which can be controlled by power electronics Thus, the total rotor resistance is controllable and the slip and thus the power output in the system are controlled. The dynamic speed control range depends on the size of the variable rotor resistance. Typically the speed range is 0-10% above synchronous speed. The energy coming from the external power conversion unit is dumped as heat loss. In [24] an alternative concept using passive component instead of a power electronic converter is described. This concept achieves 10% slip, but it does not support controllable slip.

3) Variable Speed WT with partial-scale frequency converter (WT Type C)

This configuration, known as the doubly-fed induction generator (DFIG) concept, corresponds to the variable speed controlled wind turbine with a wound rotor induction generator (WRIG) and partial-scale frequency converter (rated to approx. 30% of nominal generator power) on the rotor circuit as shown in Fig. 9.

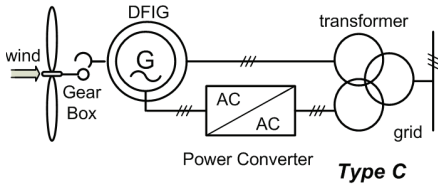

Fig. 9. Variable speed wind turbine with partial scale power converter.

The stator is directly connected to the grid, while a partial-scale power converter controls the rotor frequency and thus the rotor speed. The power rating of this partial-scale frequency converter defines the speed range (typically ±30% around synchronous speed). Moreover, this converter performs the reactive power compensation and a smooth grid connection. The control range of the rotor speed is wide compared to that of OptiSlip. Moreover, it captures the energy, which in the OptiSlip concept is burned off in the controllable rotor resistance. The smaller frequency converter makes this concept attractive from an economical point of view. Moreover, the power electronics is enabling the wind turbine to act as a more dynamic power source to the grid. However, its main drawbacks are the use of slip-rings and the protection schemes in the case of grid faults.

4) Variable Speed Wind Turbine with Full-scale Power Converter (WT Type D)

This configuration corresponds to the full variable speed controlled wind turbine, with the generator connected to the grid through a full-scale frequency converter as shown in Fig. 10.

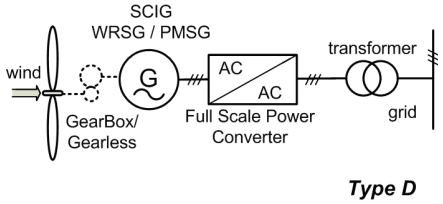

Fig. 10. Variable speed wind turbine with full-scale power converter.

The frequency converter performs the reactive power compensation and a smooth grid connection for the entire speed range. The generator can be electrically excited (wound rotor synchronous generator WRSG) or

permanent magnet excited type (permanent magnet synchronous generator PMSG). The stator windings are connected to the grid through a full-scale power converter.

Some variable speed wind turbines systems are gearless – see dotted gearbox in Fig. 10. In these cases, a bulky direct driven multi-pole generator is used. The wind turbine companies Enercon, Siemens Wind Power, Made and Lagerwey are examples of manufacturers using this configuration.

C. System comparison of wind turbines.

Comparing the different wind turbine topologies in respect to their performances will reveal a contradiction between cost and performance to the grid [5], [7]. A technical comparison of the main wind turbine concepts, where issues on grid control, cost, maintenance, internal turbine performance is given in Table 1.

Table 1. System comparison of wind turbine configurations.

System	Type A	Type B	Type C	Type D
Variable speed	No	No	Yes	Yes
Control active power	Limited	Limited	Yes	Yes
Control reactive power	No	No	Yes	Yes
Short circuit (fault-active)	No	No	No/Yes	Yes
Short circuit power	contribute	contribute	contribute	limit
Control bandwidth	1-10 s	100 ms	1 ms	0.5-1 ms
Standby function	No	No	Yes +	Yes ++
Flicker (sensitive)	Yes	Yes	No	No
Softstarter needed	Yes	Yes	No	No
Rolling capacity on grid	Yes, partly	Yes, partly	Yes	Yes
Reactive compensator (C)	Yes	Yes	No	No
Island operation	No	No	Yes/No	Yes
Investment	++	++	+	0
Maintenance	++	++	0	+

D. Control of Wind Turbines

Controlling a wind turbine involves both fast and slow control dynamics. Overall the power has to be controlled by means of the aerodynamic system and has to react based on a set-point given by a dispatched center or locally with the goal to maximize the power production based on the available wind power. The power controller should also be able to limit the power. An example of an overall control scheme of a wind turbine with a doubly-fed generator system is shown in Fig. 11 [5], [37].

Below maximum power production the wind turbine will typically vary the speed proportional with the wind speed and keep the pitch angle θ fixed. At very low wind the speed of the turbine will be fixed at the maximum allowable slip in order not to have over voltage. A pitch angle controller limits the power when the turbine reaches nominal power. The generated electrical power is done by controlling the doubly-fed generator through the rotor-side converter. The control of the grid-side converter is simply just keeping the dc-link voltage fixed. Internal current loops in both converters are used which typically are linear PI-controllers, as it is illustrated in Fig. 11. The power converters to the grid-side and the rotor-side are voltage source converters.

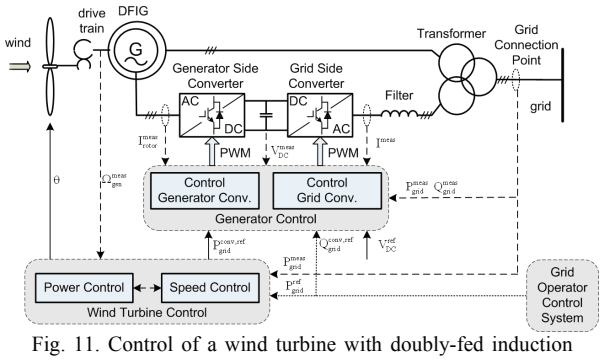

Fig. 11. Control of a wind turbine with doubly-fed induction generator (WT Type C).

Another solution for the electrical power control is to use the multi-pole synchronous generator. A passive rectifier and a boost converter are used in order to boost the voltage at low speed. The system is industrially used today and it is shown in Fig. 12.

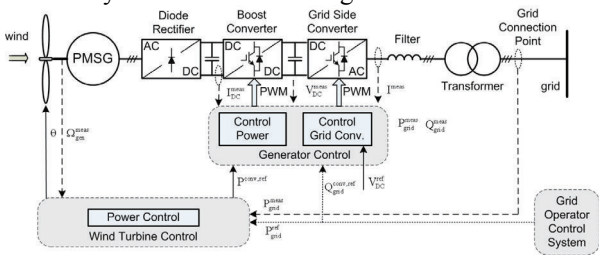

Fig. 12. Control of active and reactive power in a wind turbine with multi-pole synchronous generator (WT Type D).

A grid-side inverter is interfacing the dc-link to the grid. Common for both systems are they are able to control active and reactive power to the grid with high dynamics

E. Wind Farm Configurations

In many countries energy planning is going on with a high penetration of wind energy, which will be covered by large offshore wind farms. These wind farms may in the future present a significant power contribution to the national grid, and therefore, play an important role on the power quality and the control of complex power systems. Consequently, very high technical demands are expected to be met by these generation units, such as to perform frequency and voltage control, regulation of active and reactive power, quick responses under power system transient and dynamic situations, for example, to reduce the power from the nominal power to 20 % power within 2 seconds. The power electronic technology is again an important part in both the system configurations and the control of the offshore wind farms in order to fulfill the future demands.

One off-shore wind farm equipped with power electronic converters can perform both active and reactive power control and also operate the wind turbines in variable speed to maximize the energy captured and reduce the mechanical stress and acoustical noise. This solution is shown in Fig. 13 and it is in operation in Denmark as a 160 MW off-shore wind power station.

The active stall wind farms based on wind turbine Type A (see Fig. 7) are directly connected to the grid. A reactive power compensation unit is used in the connection point as shown in Fig. 14.

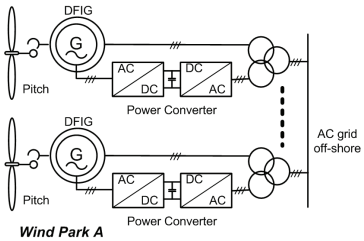

Fig. 13. DFIG based wind farm with an AC grid connection.

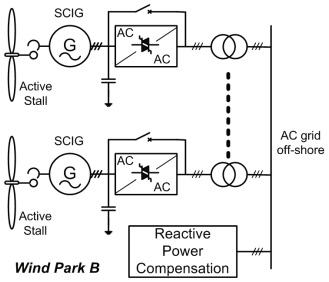

Fig. 14. Active stall wind farm with an AC grid connection.

For long distance power transmission from off-shore wind farm, HVDC may be an interesting option. In an HVDC transmission system, the low or medium AC voltage at the wind farm is converted into a high dc voltage on the transmission side and the dc power is transferred to the on-shore system where the DC voltage is converted back into AC voltage as shown in Fig. 15. The topology may even be able to vary the speed on the wind turbines in the complete wind farm [47], [48].

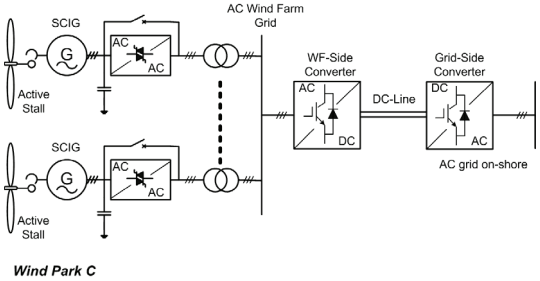

Fig. 15. Active stall wind farm with a DC-link grid connection.

Another possible DC transmission system configuration is shown in Fig. 16, where each wind turbine has its own power electronic converter, so it is possible to operate each wind turbine at an individual optimal speed. A common DC grid is present on the wind farm while a full scale power converter is used for the on-shore grid connection.

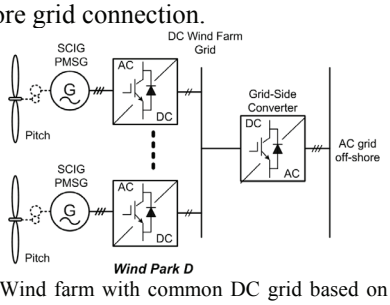

Fig. 16. Wind farm with common DC grid based on variable speed wind turbines with full scale power converter.

A comparison of these possible wind farm topologies is given in Table 2.

As it can be seen the wind farms have interesting features in order to act as a power source to the grid. Some have better abilities than others. Bottom-line will always be a total cost scenario including production, investment, maintenance and reliability. This may be different depending on the planned site.

Table 2. Comparison of wind farm topologies.

	Wind Park A	Wind Park B	Wind Park C	Wind Park D
Individual speed control	Yes	No	Yes	No
Control active power electronically	Yes	No	Yes	Yes
Control reactive power	Yes	Centralized	Yes	Yes
Short circuit (active)	Partly	Partly	Yes	Yes
Short circuit power	Contribute	Contribute	No	No
Control bandwidth	10-100 ms	200ms - 2s	10 -100 ms	10 ms – 10 s
Stand by-function	Yes	No	Yes	Yes
Soft-starter needed	No	Yes	No	No
Rolling capacity on grid	Yes	Partly	Yes	Yes
Redundancy	Yes	Yes	No	No
Investment	+	++	+	+
Maintenance	+	++	+	+

F. Grid connection requirements

Some European countries have at this moment dedicated grid codes for wind power. These requirements reflect, in most of the cases, the penetration of wind power into the electrical network or a future development is prepared.

The requirements for wind power cover a wide range of voltage levels from medium voltage to very high voltage. The grid codes for wind power address issues that make the wind farms to act as a conventional power plant into the electrical network. These requirements have focus on power controllability, power quality, fault ride-through capability and grid support during network disturbances. According to several references [6] and [8] in some of the cases these requirements are very stringent.

1) Active power control

According to this demand the wind turbines must be able to control the active in the Point-of-Common-Coupling (PCC) in a given power range. The active power is typically controlled based on the system frequency e.g. Denmark, Ireland, Germany [51]-[57] so that the power delivered to the grid is decreased when the grid frequency rise above 50 Hz. A typical characteristic for the frequency control in the Danish grid code is shown in Fig. 17.

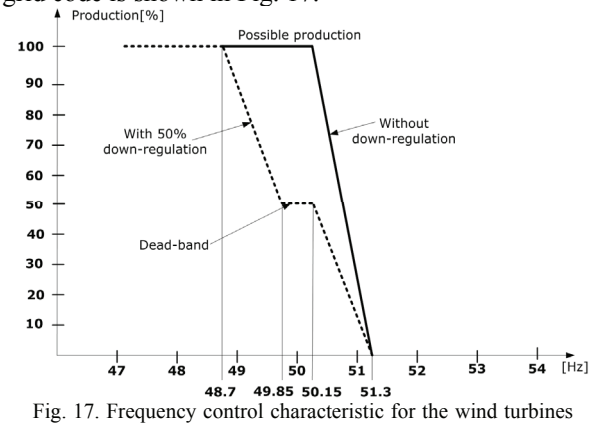

Fig. 17. Frequency control characteristic for the wind turbines connected to the Danish grid [52].

On the contrary other grid codes, e.g. Great Britain [58] specifies that the active power output must be kept constant for the frequency range 49.5 to 50.5 Hz, and a drop of maximum 5% in the delivered power is allowed when frequency drops to 47 Hz.

Curtailment of produced power based on system operator demands is required in Denmark, Ireland, Germany and Great Britain.

Currently, Denmark has the most demanding requirements regarding the controllability of the produced power. Wind farms connected at the transmission level shall act as a conventional power plant providing a wide range of controlling the output power based on Transmission System Operator's (TSO) demands and also participation in primary and secondary control [52]. Seven regulation functions are required in the wind farm control. Among these control functions, each one prioritized, the following must be mentioned: delta control, balance control, absolute production and system protection as shown in Fig. 18.

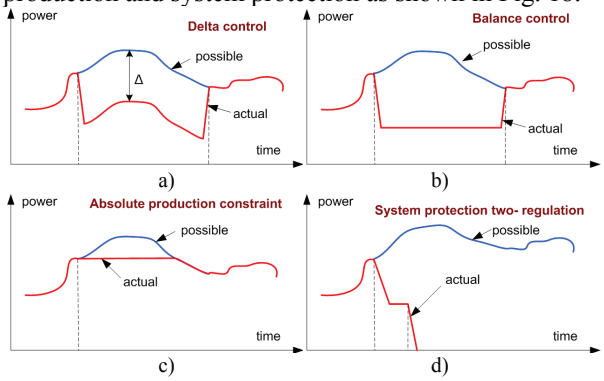

Fig. 18. Regulation function for active power implemented in wind farm controller required by the Danish grid codes: a) delta control, b) balance control, c) absolute production constraint and d) system protection.

2) Reactive power control and voltage stability

Reactive power is typically controlled in a given range. The grid codes specify in different ways this control capability. The Danish grid code gives a band for controlling the reactive power based on the active power output as shown in Fig. 19.

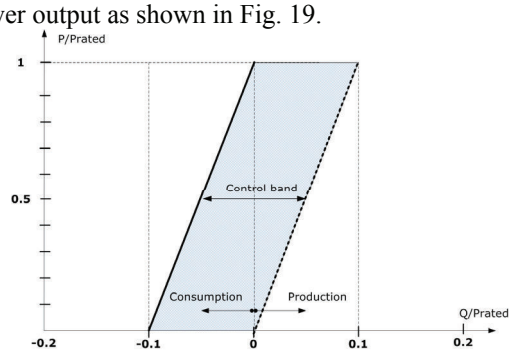

Fig. 19. Danish grid code demands for the reactive power exchange in the PCC [51], [52].

The Irish grid code specifies e.g. the reactive power capability in terms of power factor as shown in Fig. 20.

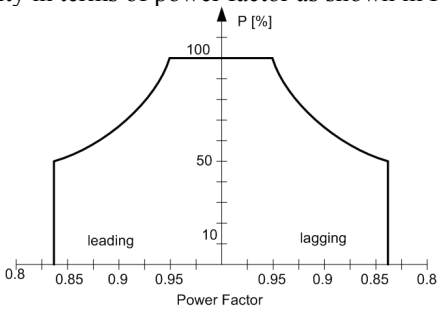

Fig. 20. Requirements for reactive power control in the Irish grid code for wind turbines [54].

The German transmission grid code for wind power specifies that the wind power units must provide a reactive power provision in the connection point without limiting the active power output as shown in Fig. 21.

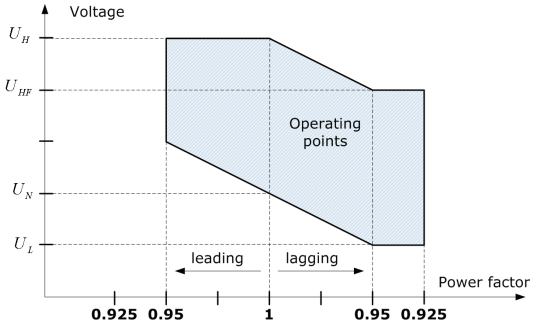

Fig. 21. Requirements for reactive power provision of generating units without limiting the active power output in the German transmission grid code [55], [56].

3) Power Quality

Power quality issues are addressed especially for wind turbines connected to the medium voltage networks. However, some grid codes, e.g. in Denmark and Ireland have also requirements at the transmission level.

Mainly two standards are used for defining the power quality parameters namely: IEC 61000-x-x and EN 50160. Specific values are given for fast variations in voltage, short term flicker severity, long term flicker severity and the total harmonic distortion. A schedule of individual harmonics distortion limits for voltage are also given based on standards or in some cases e.g. Denmark custom harmonic compatibility levels are defined. Interharmonics may also be considered [51].

4) Ride through capability

All considered grid codes requires fault ride-through capabilities for wind turbines. Voltage profiles are given specifying the depth of the voltage dip and the clearance time as well. One of the problems is that the calculation of the voltage during all types of unsymmetrical faults is not very well defined in some grid codes. The voltage profile for ride-through capability can be summarized as shown in Fig. 22.

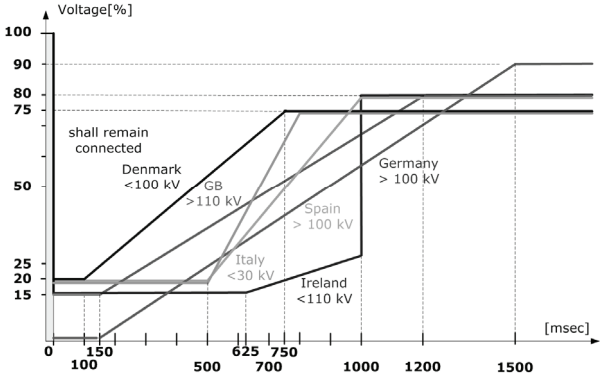

Fig. 22. Voltage profile for fault ride-through capability in European grid codes for wind power [7].

Ireland's grid code is very demanding in respect with the fault duration while Denmark has the lowest short circuit time duration with only 100 msec. However, Denmark's grid code requires that the wind turbine shall remain connected to the electrical network during successive faults which is a technical challenge.

On the other hand Germany and Spain requires grid support during faults by reactive current injection up to 100% from the rated current [55], [56] and [59] as shown in Fig. 23.

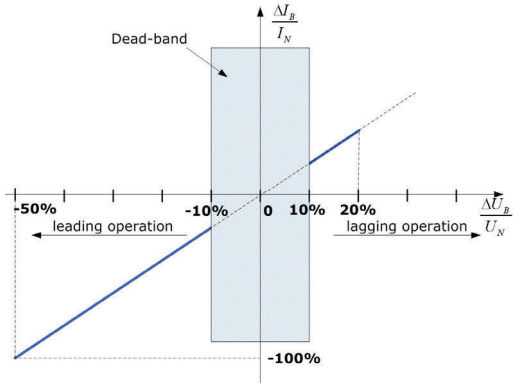

Fig. 23. Reactive current support during faults as specified in the German grid code [55].

This demand is relative difficult to meet by some of the wind turbine concepts e.g. active stall wind turbine with directly grid connected squirrel cage induction generator (WT Type A).

A summary regarding the interconnection requirements for wind power in Europe is given in detail in Appendix I.

IV. SOLAR ENERGY POWER CONVERSION

Photovoltaic (PV) power supplied to the utility grid is gaining more and more visibility due to many national incentives [65]. With a continuous reduction in system cost (PV modules, DC/AC inverters, cables, fittings and man-power), the PV technology has the potential to become one of the main renewable energy sources for the future electricity supply.

The PV cell is an all-electrical device, which produces electrical power when exposed to sunlight and connected to a suitable load. Without any moving parts inside the PV module, the tear-and-wear is very low. Thus, lifetimes of more than 25 years for modules are easily reached. However, the power generation capability may be reduced to 75% ~ 80% of nominal value due to ageing. A typical PV module is made up of around 36 or 72 cells connected in series, encapsulated in a structure made of e.g. aluminum and tedlar. An electrical model of PV cell is shown in Fig. 24.

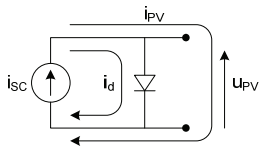

Fig. 24. Electrical model and characteristics of a PV cell.

Several types of proven PV technologies exist, where the crystalline (PV module light-to-electricity efficiency: η = 10% - 15%) and multi-crystalline (η = 9% - 12%) silicon cells are based on standard microelectronic manufacturing processes.

Other types are: thin-film amorphous silicon (η = 10%), thin-film copper indium diselenide (η = 12%), and thin-film cadmium telluride (η = 9%). Novel technologies such as the thin-layer silicon (η = 8%) and the dye-sensitised nano-structured materials (η = 9%) are in their early development. The reason to maintain a high level of research and development within these technologies is to decrease the cost of the PV-cells, perhaps on the expense of a somewhat lower efficiency. This is mainly due to the fact that cells based on today's microelectronic processes are rather costly, when compared to other renewable energy sources.

The series connection of the cells benefit from a high voltage (around 25 V ~ 45 V) across the terminals, but the weakest cell determines the current seen at the terminals.

This causes reduction in the available power, which to some extent can be mitigated by the use of bypass diodes, in parallel with the cells. The parallel connection of the cells solves the 'weakest-link' problem, but the voltage seen at the terminals is rather low.

Typical curves of a PV cell current-voltage and power-voltage characteristics are plotted in Fig. 25a and Fig. 25b respectively, with insolation and cell temperature as parameters.

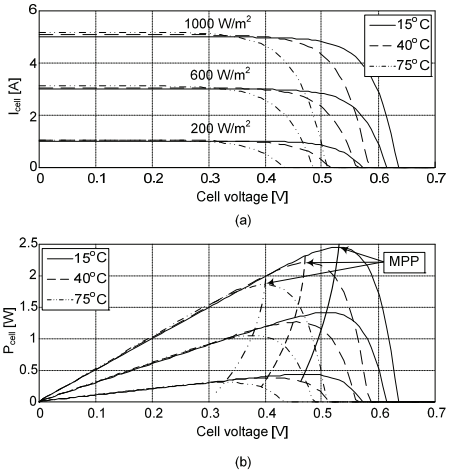

Fig. 25. Characteristics of a PV cell. Model based on the British Petroleum BP5170 crystalline silicon PV module. Power at standard test condition (1000 W/m2 irradiation, and a cell temperature of 25°C): 170 W @ 36.0 V [4].

The graph reveals that the captured power is determined by the loading conditions (terminal voltage and current). This leads to a few basic requirements for the power electronics used to interface the PV module(s) to the utility grid.

An overview of the power converter topologies for PV systems including their control techniques is given in the following sections. Next grid monitoring methods including grid voltage monitoring, grid impedance estimation and islanding detection are presented.

A. Structures for PV systems

The general block diagram of a grid connected photovoltaic system is similar with the one shown in Fig. 1. It consists of a PV array, a power converter with a filter, a controller and the grid utility.

The PV array can be a single panel, a string of PV panels or a multitude of parallel strings of PV panels. Centralized or decentralized PV systems can be used as depicted in Fig. 26.

1) Central inverters

In this topology the PV plant (typical > 10 kW) is arranged in many parallel strings that are connected to a single central inverter on the DC-side (Fig. 26a). These

inverters are characterized by high efficiency and low cost pr. kW. However, the energy yield of the PV plant decreases due to module mismatching and potential partial shading conditions. Also, the reliability of the plant may be limited due to the dependence of power generation on a single component: a failure of the central inverter results in that the whole PV plant is out of operation.

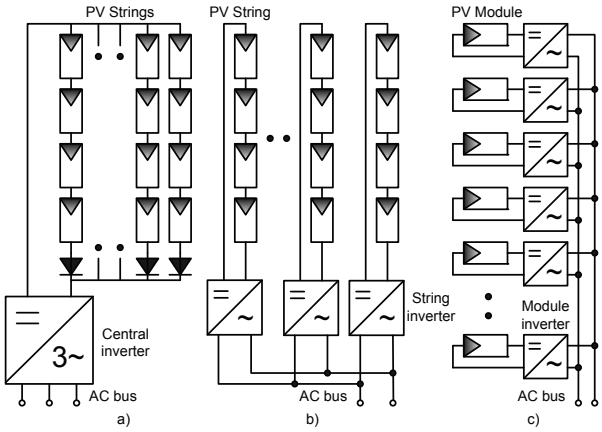

Fig. 26 Structures for PV systems: a) Central inverter, b) String inverter and c) Module integrated inverter [71].

2) String inverters

Similar to the central inverter, the PV plant is divided into several parallel strings. Each of the PV strings is assigned to a designated inverter, the so-called "string inverter" (see Fig. 26b). String inverters have the capability of separate Maximum Power Point (MPP) tracking of each PV string. This increases the energy yield by the reduction of mismatching and partial shading losses. These superior technical characteristics increase the energy yield and enhance the supply reliability. String inverters have evolved as a standard in PV system technology for grid connected PV plants.

An evolution of the string technology applicable for higher power levels is the multi-string inverter. It allows the connection of several strings with separate MPP tracking systems (via DC-DC converter) to a common DC-AC inverter. Accordingly, a compact and cost-effective solution, which combines the advantages of central and string technologies, is achieved. This multi-string topology allows the integration of PV strings of different technologies and of various orientations (south, north, west and east). These characteristics allow time-shifted solar power, which optimizes the operation efficiencies of each string separately. The application area of the multi-string inverter covers PV plants of 3-10 kW.

3) Module integrated inverter

This system uses one inverter for each module (Fig. 26c). This topology optimizes the adaptability of the inverter to the PV characteristics, since each module has its own Maximum Power Point (MPP) tracker. Although the module-integrated inverter optimizes the energy yield, it has a lower efficiency than the string inverter. Module integrated inverters are characterized by a more extended AC-side cabling, since each module of the PV plant has to be connected to the available AC grid (e.g. 230 V/ 50 Hz). Also, the maintenance processes are quite complicated, especially for facade-integrated PV systems. This concept can be implemented for PV plants of about 50- 400 W peak.

B. Topologies for PV inverters

The PV inverter technology has evolved quite a lot during the last years towards maturity [66]. Still there are different power configurations possible as shown in Fig. 27.

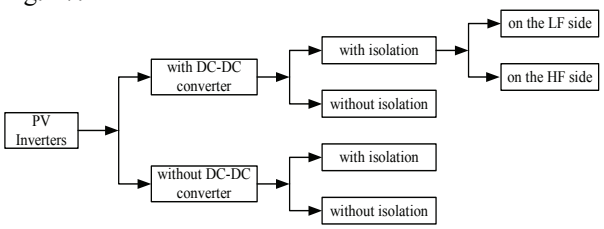

Fig. 27. Power configurations for PV inverters.

The question of having a dc-dc converter or not is first of all related to the PV string configuration. Having more panels in series and lower grid voltage, like in US and Japan, it is possible to avoid the boost function with a dc-dc converter. Thus a single stage PV inverter can be used leading to higher efficiencies.

The issue of isolation is mainly related to safety standards and is for the moment only required in US. The drawback of having so many panels in series is that MPPT is harder to achieve especially during partial shading, as demonstrated in [67]. In the following, the different PV inverter power configurations are described in more details.

1) PV inverters with DC-DC converter and isolation

The isolation is typically acquired using a transformer that can be placed on either the grid frequency side (LF) as shown in Fig. 28a or on the high-frequency (HF) side in the dc-dc converter as shown in Fig. 28b. The HF transformer leads to more compact solutions but high care should be taken in the transformer design in order to keep the losses low.

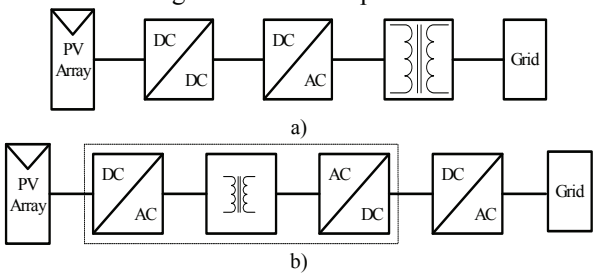

Fig. 28. PV inverter system with DC-DC converter and isolation transformer: a) on the Low Frequency (LF) side and b) on the High Frequency (HF) side.

In Fig. 29 a PV inverter with an HF transformer using an isolated push-pull boost converter is presented [68].

In this solution the dc-ac inverter is a low cost inverter switched at the line frequency. The new solutions on the market are using PWM dc-ac inverters with IGBT's switched typically at 10-20 kHz leading to a better power quality performance.

Other solutions for high frequency dc-dc converters with isolation include: full-bridge isolated converter, Single-Inductor push-pull Converter (SIC) and Double-Inductor Converter (DIC) [69].

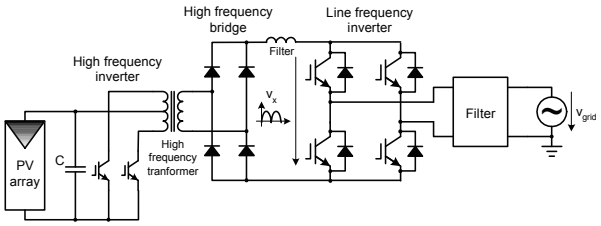

Fig. 29. PV inverter with a high frequency transformer in the dc-dc converter.

In order to keep the magnetic components small high switching frequencies in the range of 20 – 100 kHz are typically employed. The full-bridge converter is usually utilized at power levels above 750 W. The advantages of this topology are: good transformer utilization – bipolar magnetization of the core, good performance with current programmed control – reduced DC magnetization of transformer. The main disadvantages in comparison with push-pull topology are the higher active part count and the higher transformer ratio needed for boosting the dc voltage to the grid level.

The single inductor push-pull converter can provide boosting function on both the boosting inductor and transformer, reducing the transformer ratio. Thus higher efficiency can be achieved together with smoother input current. On the negative side higher blocking voltage switches are required and the transformer with tap point puts some construction and reliability problems.

Those shortcomings can be alleviated using the double inductor push-pull converter (DIC) where the boost inductor has been split into two. Actually this topology is equivalent with two inter-leaved boost converters leading to lower ripple in the input current. The transformer construction is simpler not requiring a tap point. The single disadvantage of this topology remains the need for an extra inductor.

2) PV inverters with DC-DC converter without isolation

In some countries as the grid-isolation is not mandatory, more simplified PV inverter design can be used, like shown in Fig. 30a.

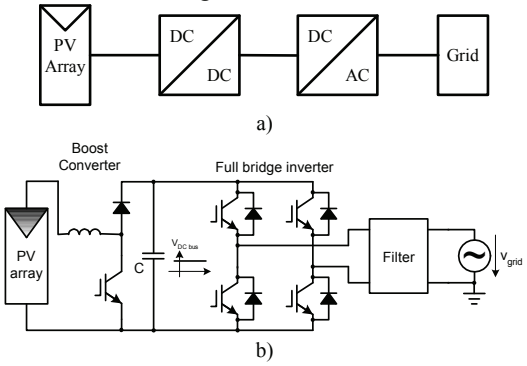

Fig. 30. PV inverter system with DC-DC converter without isolation transformer a) General diagram and b) Practical example with boost converter and full-bridge inverter.

In Fig. 30b a practical example [70] using a simple boost converter is shown.

3) PV inverters without DC-DC converter and with isolation

The block diagram of this topology is shown in Fig. 31.

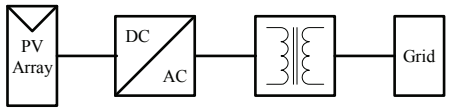

Fig. 31. General diagram of a PV system without DC-DC converter and with isolation transformer.

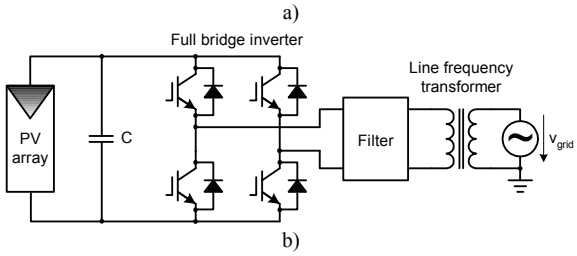

Fig. 32. Practical example of a PV system without DC-DC converter and with a full-bridge converter and isolation grid side transformer.

A PV inverter topology is presented in Fig. 32, in which a line frequency transformer is used. For higher power levels, self-commutated inverters using thyristors may be used [70].

4) PV inverters without DC-DC converter and without isolation

This topology is shown in Fig. 33a.

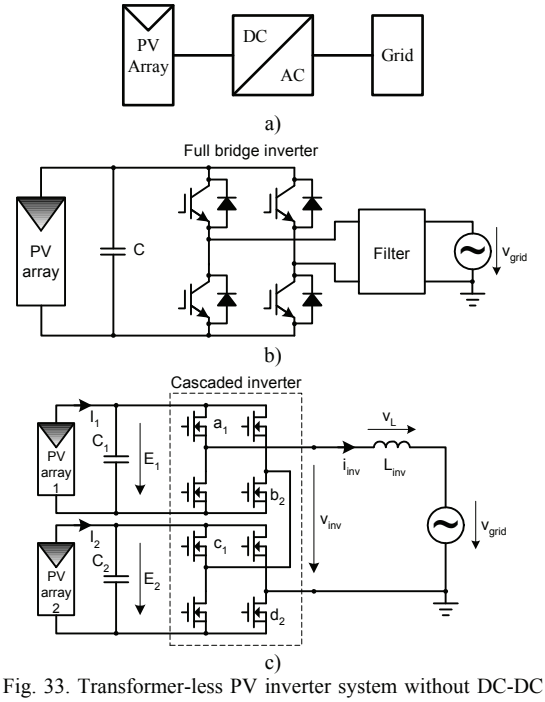

Fig. 33. Transformer-less PV inverter system without DC-DC converter: a) general diagram, b) typical example with full-bridge inverter and c) multilevel inverter.

In Fig. 33b, a typical transformer-less topology is shown using PWM IGBT inverters. This topology can be used when a large number of PV panels are available connected in series producing in excess of the grid voltage peak at all times.

Another interesting PV inverter topology without boost and isolation can be achieved using a multilevel concept. Grid connected photovoltaic systems with a five level cascaded inverter is presented in Fig. 33c [68]. The redundant inverter states of the five level cascaded inverter allow for a cyclic switching scheme which minimizes the switching frequency, equalizes stress evenly on all switches and minimizes the voltage ripple on the DC capacitors.

C. Control of PV inverters

Based on the above presented power converter topologies it can be concluded that two main structures are used in PV applications namely the double-stage conversion (DC to DC plus DC to AC) and the single stage conversion (DC to AC only). Therefore, the next sections present the control techniques used for these topologies.

1) Control of DC-DC boost converter

In order to control the output dc-voltage to a desired value, a control system is needed which automatically can adjust the duty cycle, regardless of the load current or input changes. There are at least two types of control for the dc-dc converters: the direct duty-cycle control and the current control [71].

Direct duty cycle - The output voltage is measured and then compared to the reference. The error signal is used as input in the compensator, which will calculate it from the duty-cycle reference for the pulse-width modulator as shown in Fig. 34a.

Current control - The converter output is controlled by the choice of the transistor peak current. The control signal is a current and a simple control network switches on and off the transistor such its peak current follows the control input. The current control (Fig. 34b), in the case of an isolated boost push-pull converter has some advantages against the duty-cycle control e.g. simpler dynamics (removes one pole from the control to output transfer function). Also as it uses a current sensor it can provide a better protection of the switch by limiting the current to acceptable levels.

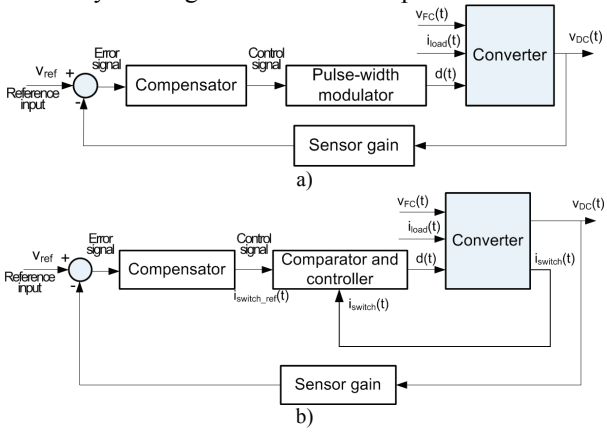

Fig. 34. Control strategies for switched dc-dc converters a) direct duty-cycle control and b) current control.

Among the drawbacks of the current control it can be mentioned that it requires an extra current sensor and it has a susceptibility to noise and thus light filtering of the feedback signals is required.

2) Control of DC-AC converter

For the grid-connected PV inverters in the range of 1-5 kW, the most common control structure for the DC-AC grid converter is using a current-controlled H-bridge PWM inverter which has a low-pass output filter. Typically L-filters are used but the new trend is to use LCL filters that have a higher order filter (3rd) which leads to a more compact design. The drawback is that due to its own resonance frequency it can produce stability problems and special control design is required [72]. A typical single-stage PV grid-connected converter with an LCL filter is shown in Fig. 35.

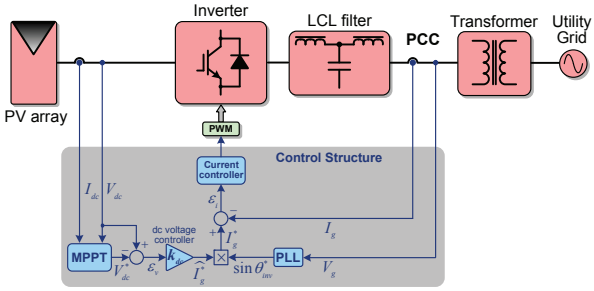

Fig. 35. Single-stage PV grid-connected system.

The main elements of the control structure are the synchronization algorithm based on PLL, the MPPT, the input power control, the grid current controller including the PWM generator.

The harmonics level in the grid current is still a controversial issue for PV inverters. The IEEE 929 standard from year 2000 allows a limit of 5% for the current Total Harmonic Distortion (THD) factor with individual limits of 4% for each odd harmonic from 3rd to 9th and 2% for 11th to 15th while a recent draft of European IEC61727 suggests something similar. These levels are far more stringent than other domestic appliances such as IEC61000-3-2 as PV systems are viewed as generation sources and so they are subject to higher standards than load systems.

Classical PI control with grid voltage feed-forward (v_{ff}) [13], as depicted in Fig. 36a, is commonly used for current-controlled PV inverters, but this solution exhibits two well known drawbacks: inability of the PI controller to track a sinusoidal reference without steady-state error and poor disturbance rejection capability. This is due to the poor performance of the integral action.

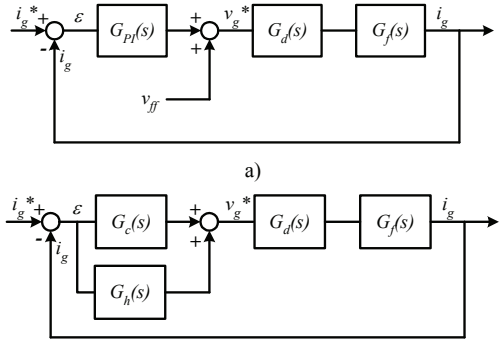

Fig. 36. The current loop of a PV inverter: a) with PI controller and b) with P+Resonant (PR) controller.

In order to get a good dynamic response, a grid voltage feed-forward (v_{ff}) is used, as depicted in Fig. 26a. This leads in turn to stability problems related to the delay introduced in the system by the voltage feedback filter.

In order to alleviate these problems, a second order generalized integrator (GI) as reported in [72], [73] and [74] can be used. The GI is a double integrator that achieves an infinite gain at a certain frequency, also called resonance frequency, and almost no gain exists outside this frequency. Thus, it can be used as a notch filter in order to compensate the harmonics in a very selective way. This technique has been primarily used

in three-phase active filter applications as reported in [73]. Another approach reported in [72] where a new type of stationary-frame regulators called P+Resonant (PR) is introduced and applied to three-phase PWM inverter control. In this approach the PI dc-compensator is transformed into an equivalent ac-compensator, so that it has the same frequency response characteristics in the bandwidth of concern. The current loop of the PV inverter with PR controller is depicted in Fig. 36b.

The harmonic compensator (HC) $G_h(s)$ as defined in [75] is designed to compensate the selected harmonics 3rd, 5th and 7th as they are the most prominent harmonics in the current spectrum. A processing delay typical equal to sampling time for the PWM inverters is introduced in [72].

Thus it is demonstrated the superiority of the PR controller in respect to the PI controller in terms of harmonic current rejection.

The issue of stability when several PV inverters run in parallel on the same grid becomes more and more important, especially when LCL filters are used. Thus, special attention is required when designing the current control.

3) Maximum Power Point Tracking (MPPT)

In order to capture the maximum power available from the PV array, a Maximum Power Point Tracker (MPPT) is required. The maximum power point of PV panels is a function of solar irradiance and temperature as depicted in Fig. 25. This function can be implemented either in the dc-dc converter or in the DC-AC converter. Several algorithms can be used in order to implement the MPPT like:

a) Perturb and Observe method

The most commonly used MPPT algorithm is the Perturb and Observe (P&O), due to its ease of implementation in its basic form. Fig. 25 shows the characteristic of a PV array, which has a global maximum at the MPP. Thus, if the operating voltage of the PV array is perturbed in a given direction and dP/dV > 0, it is known that the perturbation is moving the operating point towards the MPP. The P&O algorithm would then continue to perturb the PV array voltage in the same direction. If dP/dV < 0, then the change in operating point moved the PV array away from the MPP, and the P&O algorithm reverses the direction of the perturbation. [76] A problem with P&O is that it oscillates around the MPP in steady state operation. It can also track into the wrong direction, away from the MPP, under rapidly increasing or decreasing irradiance levels [77]-[79]. There are several variations of the basic P&O that have been proposed to minimize these drawbacks. These include using an average of several samples of the array power and dynamically adjusting the magnitude of the perturbation of the PV operating point.

b) Improved P&O method for rapidly changing irradiance

The method performs an additional measurement of power in the middle of the MPPT sampling period without any perturbation, and based on these measurements, it calculates the change of power due to the varying irradiation, [80] according to Fig. 37.

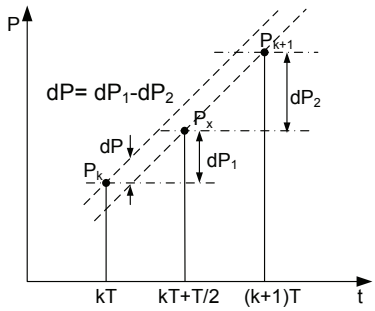

Fig. 37. Measurement of the power between two MPPT sampling instances.

Assuming that the rate of change in the irradiation is constant over one sampling period of the MPPT, the dP caused purely by the MPPT command can be calculated as:

$$dP = dP_1 - dP_2 = (P_x - P_k) - (P_{k+1} - P_x) = 2P_x - P_{k+1} - P_k \quad (1)$$

The resulting 'dP' reflects the changes due to the perturbation of the MPPT method.

Using the above calculation in the flowchart of the dp-P&O method, (see Fig. 38) can be avoided the confusion of the MPPT due to the rapidly changing irradiation.

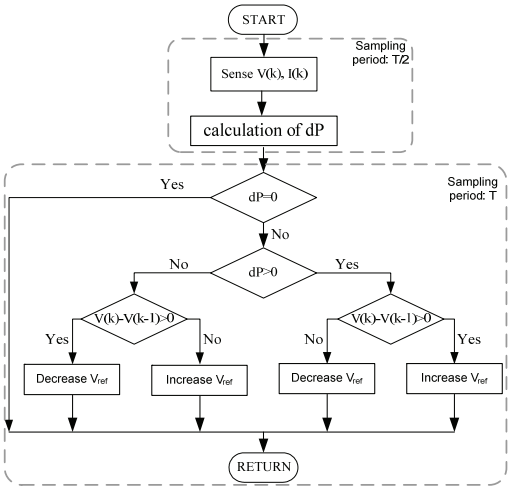

Fig. 38. The flowchart of the dp-P&O method.

The experimental results show that the dP-P&O method performs superior to the traditional P&O during rapidly changing irradiance, resulting in higher dynamic efficiency, see Fig. 39.

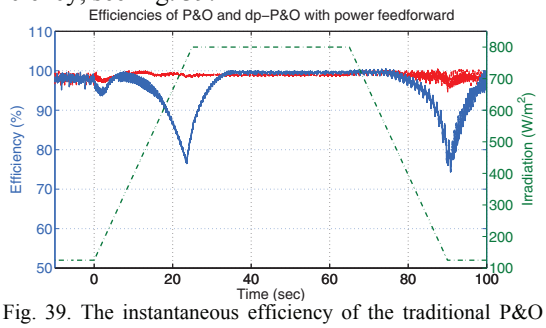

Fig. 39. The instantaneous efficiency of the traditional P&O method can decrease to below 80% during rapidly increasing and decreasing irradiation, while the efficiency of dP-P&O is not affected.

c) Incremental conductance method

The incremental conductance algorithm seeks to overcome the limitations of the P&O algorithm by using the PV array's incremental conductance to compute the sign of dP/dV without a perturbation. It does this using an expression derived from the

condition that, at the MPP, dP/dV = 0. Beginning with this condition, it is possible to show that, at the MPP dI/dV = -I/V [76] and [81]. Thus, incremental conductance can determine that the MPPT has reached the MPP and stop perturbing the operating point. If this condition is not met, the direction in which the MPPT operating point must be perturbed can be calculated using the relationship between dI/dV and -I/V. This relationship is derived from the fact that dP/dV is negative when the MPPT is to the right of the MPP and positive when it is to the left of the MPP. This algorithm has advantages over perturb and observe in that it can determine when the MPPT has reached the MPP, where perturb and observe oscillates around the MPP. Also, incremental conductance can track rapidly increasing and decreasing irradiance conditions with higher accuracy than perturb and observe [76]. However, because of noise and errors due to measurement and quantization, this method can also produce oscillations around the MPP; and it can also be confused in rapidly changing atmospheric conditions [77]. One disadvantage of this algorithm is the increased complexity when compared to perturb and observe. This increases real-time computational time, and slows down the sampling frequency of the array voltage and current.

d) Parasitic capacitance method

The parasitic capacitance method is a refinement of the incremental conductance method that takes into account the parasitic capacitances of the solar cells in the PV array. Parasitic capacitance uses the switching ripple of the MPPT to perturb the array. To account for the parasitic capacitance, the average ripple in the array power and voltage, generated by the switching frequency, are measured using a series of filters and multipliers and then used to calculate the array conductance. The incremental conductance algorithm is then used to determine the direction to move the operating point of the MPPT. One disadvantage of this algorithm is that the parasitic capacitance in each module is very small, and will only come into play in large PV arrays where several module strings are connected in parallel. Also, the DC-DC converter has a sizable input capacitor used to filter out the small ripple in the array power. This capacitor may mask the overall effects of the parasitic capacitance of the PV array.

e) Constant voltage method

This algorithm makes use of the fact that the MPP voltage changes only slightly with varying irradiances, as depicted in Fig. 25. The ratio of VMP/VOC depends on the solar cell parameters, but a commonly used value is 76% [76] and [82]. In this algorithm, the MPPT momentarily sets the PV array current to zero to allow a measurement of the array's open circuit voltage. The array's operating voltage is then set to 76% of this measured value. This operating point is maintained for a set amount of time, and then the cycle is repeated. A problem with this algorithm is that the available energy is wasted when the load is disconnected from the PV array; also the MPP is not always located at 76% of the array's open circuit voltage [76].

4) Input power control for PV applications

For PV applications, the input power control can be realized through the use of either DC-DC converter or DC-AC converters. The control strategies of the input power in the case of a power configuration of PV system without DC-DC converter (single-stage PV converter) are presented in the following. The implementation of the MPPT could be realized in two different ways in this case:

– the output of the MPPT is the AC current amplitude reference;

– the output of the MPPT is the DC voltage reference.

In the first case the MPPT block has I_{pv} and V_{pv} as inputs and the output variable is the AC current amplitude reference ($\hat{I}_{ref}$) as depicted in Fig. 40a [83].

In the second case the MPPT block has the same inputs (I_{pv} and V_{pv}) but the output variable of the algorithm is the dc voltage reference (V^*_{pv}). The dc voltage controller (P or PI controller) is used to control the DC voltage loop to produce the AC current amplitude reference ($\hat{I}_{ref}$). Then the AC current amplitude reference is multiplied by *sin(θ)*, which is captured from a phase-looked-loop (PLL) circuit to produce the output current reference command I_{ref} of the inverter. This topology is described in Fig. 40b [84] and [85].

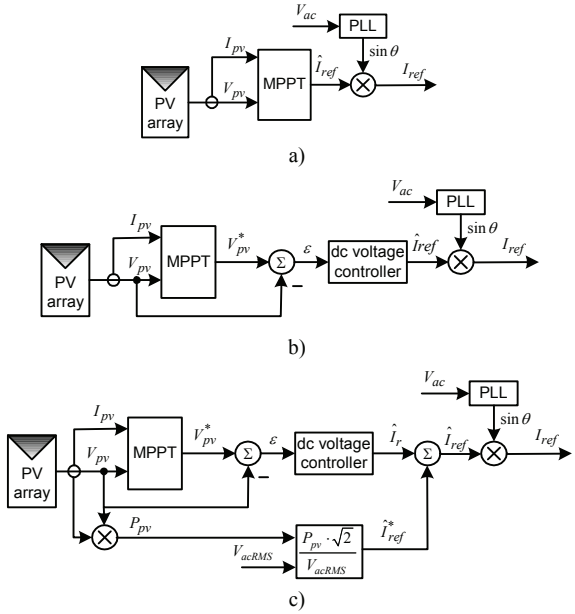

Fig. 40. Control structures of the input power. a) the output of MPPT is the ac current amplitude reference ($\hat{I}_{ref}$), b) the output of the MPPT is the dc voltage reference (V^*_{pv}) and a dc voltage controller is used, c) new control structure where a feed-forward of the input power is used.

In Fig. 40c a new control strategy of input power is proposed. The new element introduced is a power feed-forward. The computed value of the current amplitude reference using the PV power (P_{pv}) and the RMS value of the ac voltage (V_{acRMS}) is added to the output value of the dc voltage controller ($\hat{I}_r$) resulting in an ac-current amplitude reference ($\hat{I}_{ref}$). Using the input power feed-forward the dynamic of the PV system is improved being known the fact that the MPPT is rather slow.

D. PV systems - Grid monitoring

1) Grid voltage monitoring

The increased penetration of DPGS connected to the electrical grid based on sources such as PV necessitates better grid condition detection in order to meet standard specifications in terms of power quality and safety.

Grid-connected converter systems rely on accurate and fast detection of the phase angle, amplitude and frequency of the utility voltage to guarantee the correct generation of the reference signals. This is also required by the relevant grid codes which are country specific and can vary also in respect to the generation system (e.g. PV systems, wind turbines, fuel cell, etc). The grid codes may refer to different standards for distributed generation systems. These standards impose the operation conditions of the grid-connected converter systems in terms of grid voltage amplitude and frequency. Considering grid voltage monitoring requirements for interconnection of PV systems to the grid, the standard IEC61727 [86] and IEEE 929 [87] are given as examples. These standards apply to utility-interconnected PV power systems operating in parallel with the utility and utilizing static (solid-state) non-islanding inverters for the conversation of DC to AC.

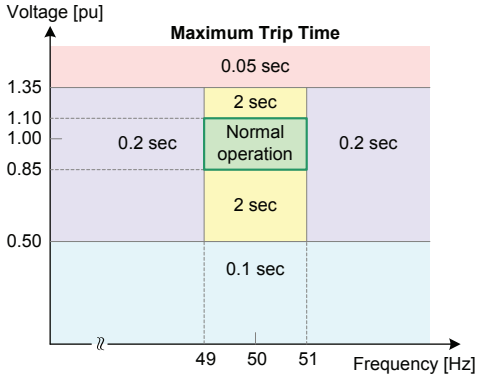

Fig. 41. Maximum trip times for both voltage amplitude and frequency according to the standard IEC61727 [86].

Fig. 41 shows the boundaries of operation in respect to grid voltage amplitude and frequency. A continuous operation area between 0.85 and 1.10 pu and ± 1 Hz around the nominal frequency is defined. Abnormal conditions can arise on the utility system that requires a response from the grid-connected PV system. This response is to ensure the safety of utility maintenance personnel and the general public, as well as to avoid damage to connected equipment, including the PV system. The abnormal utility conditions of concern are the grid voltage amplitude and frequency excursions above or below the values stated in Fig. 41. If the voltage amplitude or frequency exceeds the predefined limits, the grid-connected PV system has to cease to energize the utility line within the specified time interval. As it can be noticed from Fig. 41, the most restrictive requirement is when the maximum trip time is 0.05 seconds for a grid voltage amplitude excursion above 1.35 pu. An accurate and fast grid voltage monitoring algorithm is required in order to comply with these requirements.

Fig. 42 presents the principle of the grid voltage monitoring which consists in obtaining the parameters of the grid voltage as presented in (2).

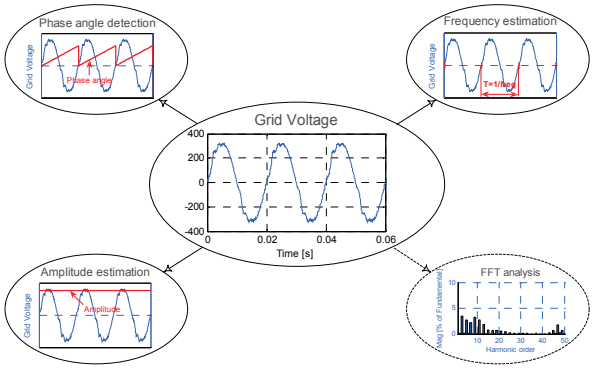

Fig. 42. Grid voltage monitoring principles.

$$v(t) = \underbrace{\hat{V} \cdot \sin(\omega \cdot t)}_{Fundamental} + \underbrace{\sum \hat{V}_h \cdot \sin(\omega_h \cdot t + \theta_h)}_{Harmonics} \quad (2)$$

The voltage equation is divided in two main parts: the fundamental and the harmonics. The grid phase angle ($\omega \cdot t$) is mostly used for synchronization. Moreover, the detection of the grid phase angle can also be used for anti-islanding detection algorithms [88]. The frequency of the grid voltage (ω) is used for over/under frequency detection algorithms but also to provide information to the control system (such as resonant controllers or filters which need to adjust the resonance frequency). The amplitude of the grid voltage ($\hat{V}$) is required for over/under voltage and to provide information to the control system (such as power feed forward loop). Additional information such as harmonic content of the grid voltage can be required for some algorithms (e.g. harmonics monitoring for the passive anti-islanding methods [88] or active power filters applications.

a) Grid voltage monitoring techniques – Overview

Different algorithms are used in order to monitor the grid voltage. In the technical literature numerous methods using different techniques are presented. These methods can be organized in three main categories:

- methods based on Zero-Crossing Detection (ZCD),
- methods based on Phase-Locked Loop (PLL)
- methods based on arctangent function ($\tan^{-1}$).

A simple method of obtaining the phase and frequency information is to detect the zero-crossing point of the grid voltage [89]-[91]. This method has two major drawbacks as described in the following.

Since the zero crossing point can be detected only at every half cycle of the utility frequency, the phase tracking action is impossible between the detecting points and thus the fast dynamic performance can not be obtained [92]. Some work has been done in order to alleviate this problem using multiple level crossing detection as presented in [93].

Significant line voltage distortion due to notches caused by power device switching and/or low frequency harmonic content can easily corrupt the output of a conventional zero-crossing detector [94]. Therefore, the zero-crossing detection of the grid voltage needs to obtain its fundamental component at the line frequency. This task is usually made by a digital filter. In order to avoid the delay introduced by this filter numerous techniques are used in the technical literature. Methods based on advanced filtering techniques are presented in

[94]-[98]. Other methods use Neural Networks for detection of the true zero-crossing of the grid voltage waveform [99]-[101]. An improved accuracy in the integrity of the zero-crossing can also be obtained by reconstructing a voltage representing the grid voltage [102]-[105].

However, starting from its simplicity, when the two major drawbacks are alleviated by using advanced techniques, the zero-crossing method proves to be rather complex and unsuitable for applications which require accurate and fast tracking of the grid voltage.

The arctangent function technique is another solution for detecting the phase angle and frequency of the grid voltage. An orthogonal voltage system is required in order to implement this technique. This method is used in adjustable speed drives applications in order to transform the feedback signals to a reference frame suitable for control purposes [19]. However, this method has the drawback that requires additional filtering in order to obtain an accurate detection of the phase angle and frequency in the case of a distorted grid voltage. Therefore, this technique is not suitable for grid-connected converter applications.

Recently, there has been an increasing interest in PLL techniques for grid-connected converter systems [106]. Usually, the PLL technique is mainly applied in communication technologies. Though, it has been proven that its application in the grid-connected converter systems was a success [91], [92], [106]-[126]. Used for such systems, the PLL is a grid voltage phase detection algorithm. The main task of the PLL algorithm is to provide a unitary power factor operation of a grid-connected converter system. This task involves synchronization of the converter output current with the grid voltage, and to provide a clean sinusoidal current reference to the current controller. Moreover, using the PLL, the grid voltage parameters such as amplitude and frequency, can be easily monitored.

Like in the case of the arctangent function technique, an orthogonal voltage system is required for the PLL algorithm. In a three-phase system, the grid voltage information can easily be obtained through the Clarke Transformation. However, for a single-phase system, the grid voltage is much more difficult to acquire [91]. Therefore, more attention should be paid for the generation of the orthogonal voltage system.

The general structures of a single-phase and three-phase PLL including the grid voltage monitoring are presented in Fig. 43a and Fig. 43b respectively. Usually, the main difference among different single-phase PLL methods is the orthogonal voltage system generation structure.

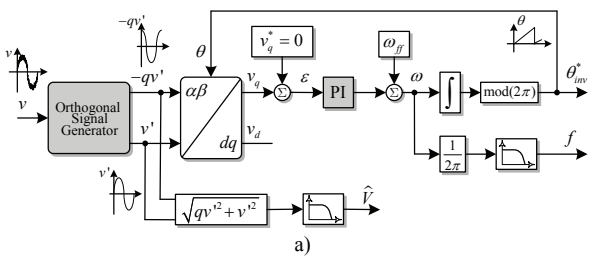

a)

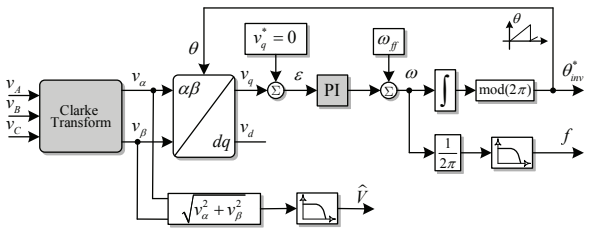

b)

Fig. 43. General structure of a: a) single-phase PLL and b) three-phase PLL.

Next paragraph discusses about techniques used for generating the orthogonal voltage systems. The structure responsible for generating the orthogonal voltage system is called orthogonal signal generator.

b) Orthogonal signal generators

In the technical literature, some techniques for generating the orthogonal voltage components from a single-phase input signal are described, some of which are compared in [106] and [127]. An easy technique of generating the orthogonal voltage system in a single-phase system incorporates a transport delay function, which is responsible for introducing a phase shift of 90 degrees with respect to the fundamental frequency of the input signal [115]. A related method, but more complex of creating a phase shift of 90 degrees, uses the Hilbert Transformation [106] and [110]. Other methods of generating the orthogonal voltage system are based on inverse Park Transformation [106], [115], [122] and [126], using resonant structures such as Second Order Generalized Integrator (SOGI) [117] or Kalman estimator-based filter [112].

2) Grid impedance estimation

In order to comply with certain stringent standard requirements for islanding detection such as the German standard VDE 0126-1-1 [128] for grid-connected PV systems, it is important to estimate the impedance of the distribution line (grid). The standard requirement is to isolate the supply within 5 s after an impedance change of 1 ohm. Therefore, the PV inverters should make use of an online estimation technique in order to meet these regulation requirements. Moreover, the estimation of the grid impedance can also be used in order to increase the stability of the current controller by adjusting its parameters online (see Fig. 46). If the variation is mainly resistive then the damping of the line filter is significant and makes the PV inverter control more stable. As it can be noticed from Fig. 45, if the variation is mainly inductive, then the bandwidth of the controller decreases [129]. Also, in this case, due to the additional inductance of the grid, the tuning order of the line filter becomes lower and the filter will not fulfill the initial design purpose. In order to alleviate this problem, the gain scheduling method can be used for adjusting online the current controller parameters, as presented in Fig. 46. Therefore, besides the standard requirements the knowledge about the grid impedance value is an added feature for the PV inverter [130].

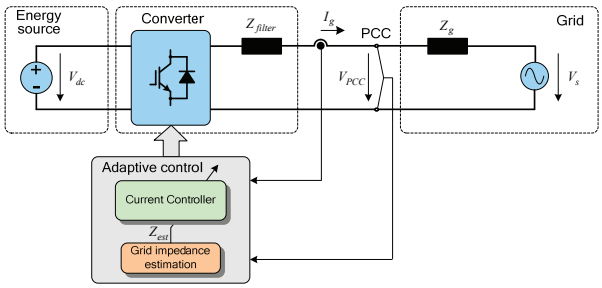

Fig. 44. Adaptive control of the grid-connected inverter [138].

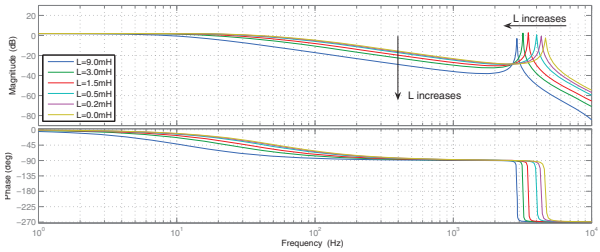

Fig. 45. Bode plot of plant for different values of the grid inductance L in case of using an LCL filter.

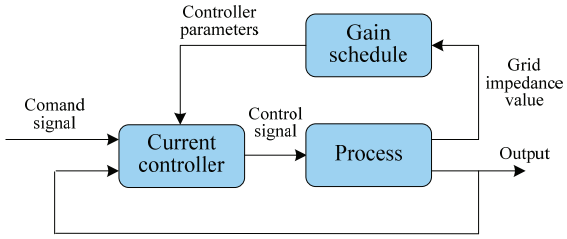

Fig. 46.Gain scheduling method [138].

According to [130] different techniques, as presented in [131]-[136] can be used for line impedance measurements. It is noticeable that, usually, these methods use special hardware devices. Once the inputs are acquired by voltage and current measurement, the processing part follows, typically involving large mathematical calculations in order to obtain the impedance value.

The state of the art divides the measuring solutions into two major categories: the passive and the active methods.

The passive method uses the non characteristic signals (line voltages and currents) that are already present in the system. This method depends on the existing background distortion of the voltage [137] and, in numerous cases, the distortion has neither the amplitude nor the repetition rate to be properly measured. This will not be interesting for implementing it in a PV inverter.

Active methods make use of deliberately "disturbing" the power supply network followed by acquisition and signal processing [131], [132], [133] and [135]. The way of "disturbing" the network can vary, therefore, active methods are also divided into two major categories: transient methods and steady-state methods.

Other two new active methods for estimating the grid impedance are presented in [138] and [139]. The method presented in [138] is based on producing a small perturbation on the output of the power converter that is in the form of periodical variations of active and reactive power (PQ variations). The control diagram for the implementation of this technique is shown in Fig. 47.

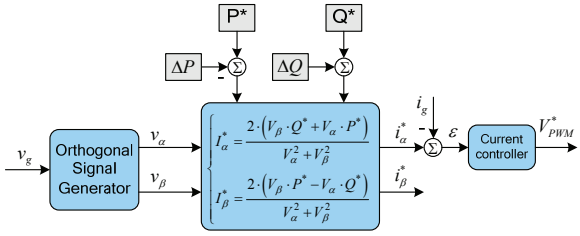

Fig. 47. Control diagram of the PQ control technique [138].

The main idea is to make the power converter working in two operation points (see Fig. 48) in order to solve the equation of the equivalent grid impedance.

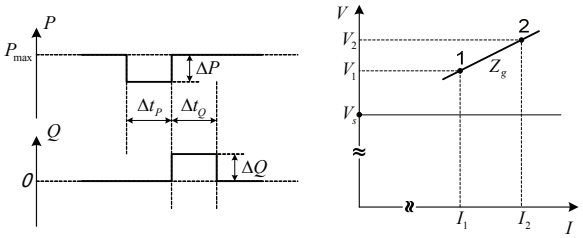

Fig. 48. a) Principle for the variation of active (P) and reactive (Q) power; b) Power converter working in two operation points [138].

During the perturbation, measurements of voltage and current are performed and signal processing algorithms are used in order to estimate the value of the grid impedance.

The method proposed in [139] is based on producing a perturbation on the output of the power converter that is in the form of periodical injection of one or two voltage harmonic signals (see Fig. 49). The single harmonic injection uses a 600 Hz signal and the double harmonic injection uses a 400 Hz and 600 Hz signals, respectively. During the perturbation, the current response(s) at the same frequency as the injected signal(s) is/are measured. The value of the grid impedance is estimated using two different signal processing algorithms. The DFT technique is used for the single harmonic injection and the statistic technique is used for the double harmonic injection (see Fig. 50).

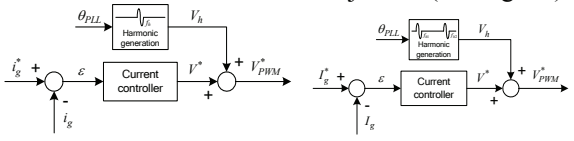

Fig. 49. Harmonic injection methods [139]: a) single harmonic injection; b) double harmonic injection.

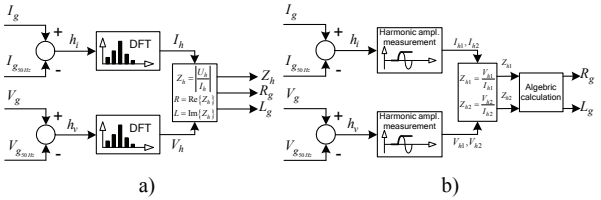

Fig. 50. Grid impedance estimation algorithms [139]: a) single harmonic injection; b) double harmonic injection.

3) Islanding detection

A grid-connected PV system shall cease to energize the utility line from a de-energized distribution line irrespective of connected loads or other generators

within specified time limits. This is to prevent back-feeding to the line, also called islanding, which could create hazardous situation for utility maintenance personnel and the general public. Although the probability of islanding occurrence is extremely low [158], standards dealing with the interconnection of inverter based photovoltaic system with the grid require that an effective anti-islanding method is incorporated into the operation of the inverter [87], [140], [141].

The German standard VDE 0126-1-1 [128] for grid-connected PV systems requires isolating the supply within 5 s after an impedance change of 1 ohm. The test setup proposed by this standard is shown in Fig. 51.

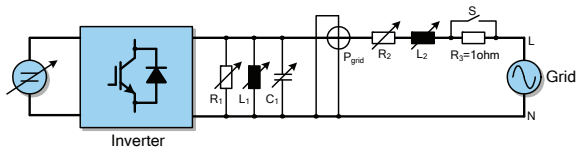

Fig. 51. Test setup for the German standard VDE 0126-1-1 [128].

According to IEEE 929-2000 standard, a PV inverter shall cease to energize the utility line in ten cycles or less when subjected to a typical islanded load in which either of the following is true:

• There is at least a 50% mismatch in real power load to inverter output (that is, real power load is <50% or >150% of inverter power output).

• The islanded-load power factor is <0.95 (lead or lag).

If the real-power-generation-to-load match is within 50% and the islanded-load power factor is >0.95, then a PV inverter will cease to energize the utility line within 2 seconds whenever the connected line has a quality factor of 2.5 or less.

The test setup for the IEEE 929-2000 is depicted in Fig. 52.

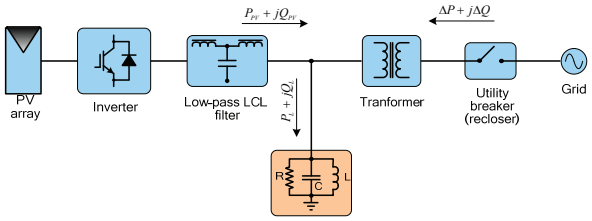

Fig. 52. Islanding operation test setup for IEEE 929-2000 standard [87].

There are numerous islanding detection methods for grid-connected PV systems reported in the technical literature [142]-[157] and their development has been summarized in a number of recent technical papers [147] and reports [142], [143]. They can be classified into two broad categories, namely, passive and active which can be inverter built or utility supported. The passive methods are based on the detection of the following:

• Over-voltage/under-voltage protection (OVP/UVP) [142], [144].

• Over-frequency/under-frequency protection (OFP /UFP) [142], [144].

• Voltage phase jump [142], [144], [147].

• Voltage harmonic monitoring [144], [147].

• Current harmonic monitoring.

However, passive methods have a number of weaknesses and inability to detect islanding. The use of non-detection zones (NDZs) is used as a measure of performance for both these techniques as well as the active ones in a number of papers [152], [154]. An evaluation of different but most widely-used passive anti-islanding methods is offered for passive methods in [136] and an excellent overview report for both passive and active methods is available in [142].

Active methods have been developed in order to overcome the limitations of the passive methods. In simple terms, active methods introduce perturbations in the inverter output power for a number of parameters as follows:

• Output power variation either real or reactive [144], [155].

• Active frequency drift or frequency shift up/down [142], [147]-[151].

• Sliding mode or slip-mode frequency shift [142], [147], [151].

• Sandia frequency shift or accelerated frequency drift or active frequency drift with positive feedback [147], [150].

• Impedance estimation [138], [139].

• Detection of impedance at a specific frequency or monitoring of harmonic distortion [142], [157].

• Sandia voltage shift [142].

• Frequency jump [142].

In a recent paper, it has been shown that although the effectiveness of passive methods can be established by non-detection zones [146] as represented by the power mismatch space (ΔP vs. ΔQ), in active frequency drifting methods their performance can be evaluated by using load parameter space based on the values of the quality factor and resonant frequency of the local load [154].

Although most of the papers have been concentrated on PV inverters, islanding detection is also needed for all other inverter based systems using different sources such as fuel cells [140], [155]. The algorithm proposed in [155] is an active method and continuously perturbs the reactive power supplied by the inverter by as much as ±5% while monitoring the utility voltage and frequency simultaneously. When islanding occurs, the deviation of the frequency taking place results in a real power reduced to 80%. A drop in voltage positively confirms islanding which in turn results in the inverter being successfully disconnected.

Many papers have concentrated on single-phase inverters and others also address three-phase technology [143], using DQ implementation [156]. Recently, the power mismatch for the 3rd and 5th harmonics and the implementation of an active anti-islanding method using resonant controllers was reported in [157].

Although numerous techniques exist and their implementation varies as it has been discussed so far, it is important to note that a recommendation for robust software based algorithms would simplify matters for the easier adoption of the most robust and simplest technique of all, and this should be kept as a guide for the further development of the anti-islanding technology [158].

V. Status and Trends

A. Wind power

The wind turbine market was dominated in the last years by ten major companies [6], [48] and [50]. At the end of 2005 the wind turbine market share by manufacturer was as shown in Fig. 53.

The Danish company VESTAS Wind Systems A/S was still on the top position among the largest manufacturers of wind turbines in the world, followed by GE Wind, as the second largest in the world. German manufacturers ENERCON, Gamesa and Suzlon are in third, fourth and fifth positions, respectively. Notice that, the first four largest suppliers (Vestas, Gamesa, Enercon, GE Wind) had much larger markets with the first leading positions, compared to the others.

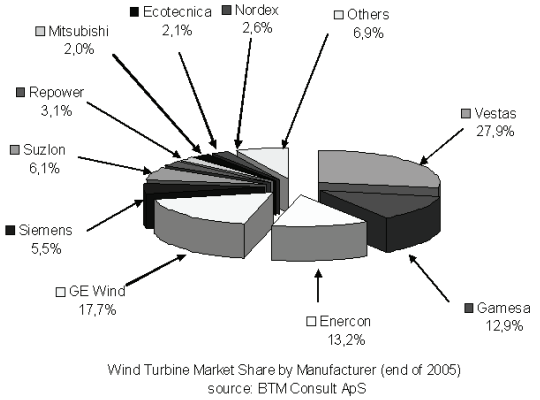

Fig. 53. Wind turbine market share by manufacturer (end of 2005).

Nowadays, the most attractive concept seemed to be the variable speed wind turbine with pitch control. Out of the Top Five-suppliers, only Siemens Wind Power (ex Bonus) used the 'traditional' active stall fixed speed concept, while the other manufacturers had at least one of their two largest wind turbines with the variable speed concept.

However, recently Siemens Wind Power has released the multi-megawatt class variable speed full-scale power converter wind turbine based on the squirrel-cage induction generator. The most used generator type was the induction generator (WRIG and SCIG). Only ENERCON and GE wind used the synchronous generator (WRSG). Only one manufacturer, ENERCON, offered a gearless variable speed wind turbine. All wind turbines manufacturers used a step-up transformer for connection of the generator to the grid.

A trend towards the configuration using a doubly-fed induction generator concept (Type C) with variable speed and variable pitch control, can be identified. In order to illustrate this trend, a dedicated investigation of the market penetration for the different wind turbine concepts is presented in [6]. The analysis cover approximately 75% of the accumulated world power installed at the end of 2004 as shown in Fig. 54.

Full-scale power converter based wind turbines have a relative constant market share over the years, while the interest for the variable-rotor resistance wind turbines (Type B) have fall down in the considered period.

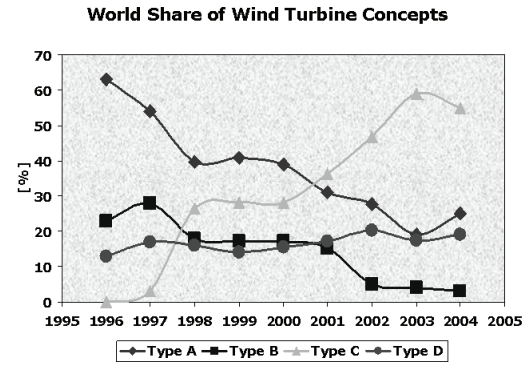

Fig. 54. Wind World share of yearly installed power for the considered wind turbine concepts (see Fig. 7 to Fig. 10).

B. Solar power

PV solar electricity is also a booming industry; since 1980, when terrestrial applications began, annual installation of photovoltaic power has increased to above 750 MWp, the cumulative installed PV power in 2004 reaching approximately 2.6 GWp [159] and [160].

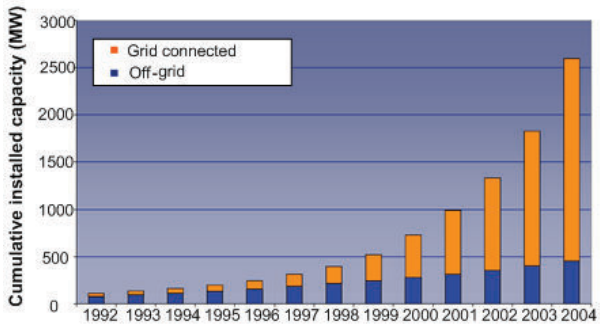

Fig. 55. Cumulative installed capacity from 1992 to 2004 in the IEA-PVPS reporting countries (source: IEA-PVPS, http://www.iea-pvps.org).

The annual rate of growth has varied between 20% in 1994 to over 40% in 2000, but the growth between 2002 and 2003 of 36% has been similar to the latest three years. As in the previous years the vast majority of new capacity was installed in Japan, Germany, and USA, with these three countries accounting for about 88% of the total installed in the year [160].

Historically the main market segments for PV were the remote industrial and developing country applications where PV power over long term is often more cost-effective than alternative power options such as diesel generator or mains grid extension. According to the IEA-PVPS, since 1997, the proportion of new grid-connected PV installed in the reporting countries rose from 42% to more than 93% in 2004 [160] (see Fig. 55).

According to [161], the prices for PV modules are around €5.7/Wp in Europe, with the lowest prices of: €3.10/Wp for monocrystalline modules, €3.02/Wp for polycrystalline modules and €2.96/Wp for thin film modules.

The prices for PV modules in the recent years are shown in Fig. 56.

In addition to the PV module cost, the cost and reliability of PV inverters are basic issues if market competitive PV supply systems are the aim. The inverter cost share represents about 10-15% of the total investment cost of a grid connected system.

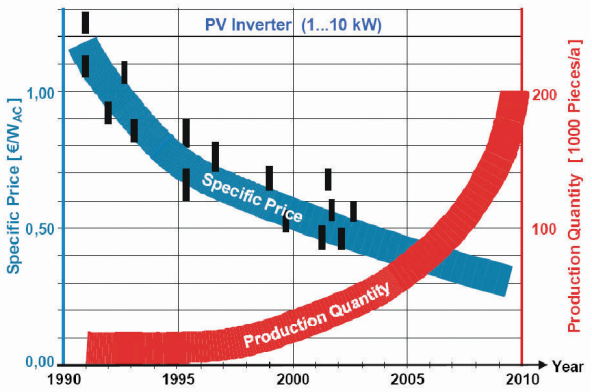

Fig. 56. Development and prognoses of specific cost and production quantity for the PV inverter of nominal powers between 1 and 10 kW during two decades (¦ indicates specific prices of products on the market [162].

The development of PV inverter specific cost (€/WAC) in small to medium power range (1-10 kW) is illustrated in Fig. 56. It can be seen that the inverter cost of this power class has decreased by more than 50% during the last decade. The main reasons for this reduction are the increase of the production quantities and the implementation of new system technologies (e.g. string-inverters). A further 50 % reduction of the specific cost is anticipated during the coming decade. The corresponding specific cost is expected to achieve about 0.3 €/WAC by the year 2010, which requires the implementation of specific measures for the development and the manufacturing processes [162].

VI. Conclusion

The paper discusses the applications of power electronic for both wind turbine and photovoltaic technologies. The development of modern power electronics has been briefly reviewed. The applications of power electronics in various kinds of wind turbine generation systems and offshore wind farms are also illustrated, showing that the wind turbine behavior/performance is significantly improved by using power electronics. They are able to act as a contributor to the frequency and voltage control by means of active and reactive power control.

Furthermore, PV systems are discussed including technology, inverters and their control methods.

Finally, a status of the wind turbine and PV market is given and some future trends are highlighted. Both wind and PV will be important power sources for the future energy system.

VII. References

[1] S. Heier, "Grid integration of wind energy conversion systems", translated by Rachel Waddington, John Wiley, 1998. ISBN-10: 0-47-197143X.

[2] E. Bossanyi, "Wind Energy Handbook", John Wiley, 2000.

[3] L.H. Hansen, L. Helle, F. Blaabjerg, E. Ritchie, S. Munk-Nielsen, H. Bindner, P. Sørensen and B. Bak-Jensen, "Conceptual survey of Generators and Power Electronics for Wind Turbines", Risø-R-1205(EN), 2001.

[4] F. Blaabjerg, and Z. Chen, "Power electronics as an enabling technology for renewable energy integration", Journal of Power Electronics, vol. 3, no.2, 2003, pp. 81-89.

[5] F. Blaabjerg, F. Iov, R. Teodorescu, Z. Chen, "Power Electronics in Renewable Energy Systems", keynote paper presented at EPE-PEMC Conference, 2006, Portoroz, Slovenia, pp. 1-17.

[6] A.D. Hansen, F. Iov, F. Blaabjerg, L.H. Hansen, "Review of contemporary wind turbine concepts and their market penetration", Journal of Wind Engineering, 28(3), 2004, pp. 247-263.

[7] F. Iov, F. Blaabjerg, "UNIFLEX-PM. Advanced power converters for universal and flexible power management in future electricity network – Converter applications in future European electricity network". Deliverable D2.1, EC Contract no. 019794(SES6), February 2007, p. 171, (available on line www.eee.nott.ac.uk/uniflex/Deliverables.htm).

[8] D. Milborrow, "Going mainstream at the grid face. Examining grid codes for wind", *Windpower Monthly*, September 2005, ISSN 109-7318.

[9] F. Iov, A.D. Hansen, P. Sørensen, N.A. Cutululis, "Mapping of grid faults and grid codes". Risø-R-1617(EN) (2007) 41 p. (available online at www.risoe.dk).

[10] Z. Chen, E. Spooner, "Grid Power Quality with Variable-Speed Wind Turbines", IEEE Trans. on Energy Conversion, Vol. 16, No.2, June 2001, pp. 148-154.

[11] F. Iov, Z. Chen, F. Blaabjerg, A. Hansen, P. Sorensen, "A New Simulation Platform to Model, Optimize and Design Wind Turbine", Proc. of IECON, 2002, Vol. 1, pp. 561-566.

[12] S. Bolik, "Grid Requirements Challenges for Wind Turbines", Proc. of Fourth International Workshop on Large-Scale Integration of Wind Power and Transmission Networks for Offshore Windfarms, 2003.

[13] E. Bogalecka, "Power control of a doubly fed induction generator without speed or position sensor", Proc. of EPE, 1993, Vol.8, pp. 224-228.

[14] O. Carlson, J. Hylander, K. Thorborg, "Survey of variable speed operation of wind turbines", Proc. of European Union Wind Energy Conference, Sweden, 1996, pp. 406-409.

[15] M. Dahlgren, H. Frank, M. Leijon, F. Owman, L. Walfridsson, "Wind power goes large scale", ABB Review, 2000, Vol.3, pp. 31-37.

[16] M.R. Dubois, H. Polinder, J.A. Ferreira, "Comparison of Generator Topologies for Direct-Drive Wind Turbines", IEEE Nordic Workshop on Power and Industrial Electronics (Norpie 2000), Aalborg-Denmark, pp. 22-26.

[17] L.H. Hansen, P.H. Madsen, F. Blaabjerg, H.C. Christensen, U. Lindhard, K. Eskildsen, "Generators and power electronics technology for wind turbines", Proc. of IECON '01, Vol. 3, 2001, pp. 2000-2005.

[18] Z. Chen, E. Spooner, "Wind turbine power converters: a comparative study", Proc. of PEVD, 1998, pp. 471-476.

[19] M.P. Kazmierkowski, R. Krishnan, F. Blaabjerg,"Control in Power Electronics-Selected problems", Academic Press, 2002. ISBN 0-12-402772-5.

[20] Å. Larsson, "The Power quality of Wind Turbines", Ph.D. report, Chalmers University of Technology, Göteborg, Sweden, 2000.

[21] R. Pena, J.C. Clare, G.M. Asher, "Doubly fed induction generator using back-to-back PWM converters and its application to variable speed wind-energy generation". IEE proceedings on Electronic Power application, 1996, pp. 231-241.

[22] J. Rodriguez, L. Moran, A. Gonzalez, C. Silva, "High voltage multilevel converter with regeneration capability", Proc. of PESC, 1999, Vol.2, pp.1077-1082.

[23] P. Sørensen, B. Bak-Jensen, J. Kristian, A.D. Hansen, L. Janosi, J. Bech, " Power Plant Characteristics of Wind Farms", Proc. of the Int. Conf. in Wind Power for the 21st Century, 2000.

[24] K. Wallace, J.A. Oliver, "Variable-Speed Generation Controlled by Passive Elements", Proc. of ICEM, 1998, pp. 1554-1559.

[25] S. Bhowmik, R. Spee, J.H.R. Enslin, "Performance optimization for doubly fed wind power generation systems", IEEE Trans. on Industry Applications, Vol. 35, No. 4 , July-Aug. 1999, pp. 949-958.

[26] Z. Saad-Saoud, N. Jenkins, "The application of advanced static VAr compensators to wind farms", IEE Colloquium on Power Electronics for Renewable Energy, 1997, pp. 6/1 - 6/5.

[27] J.B. Ekanayake, L. Holdsworth, W. XueGuang, N. Jenkins, "Dynamic modelling of doubly fed induction generator wind turbines", IEEE Trans. on Power Systems, Vol. 18 , No. 2 , May 2003 , pp.803-809.

[28] D. Arsudis, "Doppeltgespeister Drehstromgenerator mit Spannungszwischenkreis Umrichter in Rotorkreis für Wind Kraftanlagen, Ph.D. Thesis, 1998, T.U. Braunschweig, Germany.

[29] D. Arsudis, “Sensorlose Regelung einer doppelt-gespeisten Asynchronmaschine mit geringen Netzrückwirkungen“, Archiv für Elektrotechnik, Vol. 74, 1990, pp. 89-97.
[30] T. Matsuzaka, K. Trusliga, S. Yamada, H. Kitahara, “A variable speed wind generating system and its test results”. Proc. of EWEC ’89, Part Two, 1989, pp. 608-612.
[31] R.S. Barton, T.J. Horp, G.P. Schanzenback, “Control System Design for the MOD-5A 7.3 MW wind turbine generator”. Proc. of DOE/NASA workshop on Horizontal-Axis Wind Turbine Technology Workshop, 1984, pp. 157-174.
[32] O. Warneke, “Einsatz einer doppeltgespeisten Asynchronmaschine in der Großen Windenergie-anlage Growian”, Siemens-Energietechnik 5, Heft 6, 1983, pp. 364-367.
[33] L. Gertmar, “Power Electronics and Wind Power”, Proc. of EPE 2003, paper 1205.
[34] F. Blaabjerg, Z. Chen, S.B. Kjær, “Power Electronics as Efficient Interface in Dispersed Power Generation Systems”, IEEE Trans. on PE, Vol. 19, No. 4, 2004, pp. 1184-1194.
[35] E.N. Hinrichsen, “Controls for variable pitch wind turbine generators”, IEEE Trans. on Power Apparatus and Systems, Vol. 103, No. 4, 1984, pp. 886-892.
[36] B.J. Baliga, “Power IC’s in the saddle”, IEEE Spectrum, July 1995, pp. 34-49.
[37] A.D. Hansen, C. Jauch, P. Soerensen, F. Iov, F. Blaabjerg. “Dynamic Wind Turbine Models in Power System Simulation Tool DigSilent”, Report Risoe-R-1400 (EN), Dec. 2003, ISBN 87-550-3198-6 (80 pages).
[38] T. A. Lipo, “Variable Speed Generator Technology Options for Wind Turbine Generators”, NASA Workshop on HAWTT Technology, May 1984, pp. 214-220.
[39] K. Thorborg, “Asynchronous Machine with Variable Speed”, Appendix G, Power Electronics, 1988, ISBN 0-13-686593-3, pp. G1.
[40] D. Arsudis, W. Vollstedt, “Sensorless Power control of a Double-Fed AC-Machine with nearly Sinusoidal Line Currents”, Proc. of EPE, 1989, pp. 899-904.
[41] M. Yamamoto, O. Motoyoshi, “Active and Reactive Power control for Doubly-Fed Wound Rotor Induction Generator”, Proc. of PESC, 1990, Vol. 1, pp. 455-460.
[42] O. Carlson, J. Hylander, S. Tsiolis, ”Variable Speed AC-Generators Applied in WECS”, European Wind Energy Association Conference and Exhibition, October 1986, pp. 685-690.
[43] J.D. van Wyk, J.H.R. Enslin, “A Study of Wind Power Converter with Microcomputer Based Maximal Power Control Utilising an Oversynchronous Electronic Schertives Cascade”, Proc. of IPEC, 1983, Vol. I, pp. 766-777.
[44] T. Sun, Z. Chen, F. Blaabjerg, ”Flicker Study on Variable Speed Wind Turbines With Doubly Fed Induction Generators”. IEEE Trans. on Energy Conversion, Vol. 20, No. 4, 2005, pp. 896-905.
[45] T. Sun, Z. Chen, F. Blaabjerg, “Transient Stability of DFIG Wind Turbines at an External Short-circuit-Fault”. Wind Energy, 2005, Vol. 8, pp. 345-360.
[46] L. Mihet-Popa, F. Blaabjerg, I. Boldea, “Wind Turbine Generator Modeling and Simulation Where Rotational Speed is the Controlled Variable”. IEEE Transactions on Industry Applications, 2004, Vol. 40, No. 1. pp. 3-10.
[47] F. Iov, P. Soerensen, A. Hansen, F. Blaabjerg, “Modelling, Analysis and Control of DC-connected Wind Farms to Grid”, International Review of Electrical Engineering, Praise Worthy Prize, February 2006, pp.10, ISSN 1827-6600.
[48] F. Iov, P. Soerensen, A. Hansen, F. Blaabjerg, “Modelling and Control of VSC based DC Connection for Active Stall Wind Farms to Grid”, IEE Japan Trans. on Industry Applications, April 2006, Vol. 126-D, No. 5.
[49] A. Cameron, E. de Vries, “Top of the list”, Renewable Energy World, James & James, January-February 2006, Vol. 9, No. 1, pp. 56-66, ISSN 1462-6381.
[50] A. Cameron, “Changing winds”, BTM’s world market update, Renewable Energy World, Pennwell Co., July-August 2006, Vol. 9, No. 4, pp. 28-41, ISSN 1462-6381.
[51] EnergiNet – Grid connection of wind turbines to networks with voltages below 100 kV, Regulation TF 3.2.6, May 2004, p. 29.
[52] Energinet - Grid connection of wind turbines to networks with voltages above 100 kV, Regulation TF 3.2.5, December 2004, p. 25.
[53] ESB Networks – Distribution Code, version 1.4, February 2005.
[54] CER – Wind Farm Transmission Grid Code Provisions, July 2004.
[55] E.ON-Netz – Grid Code. High and extra high voltage, April 2006.
[56] VDN – Transmission Code 2003. Network and System Rules of the German Transmission System Operators, August 2003.
[57] VDN – Distribution Code 2003. Rules on access to distribution networks, August 2003.
[58] National Grid Electricity Transmission plc – The grid code, Issue 3, Revision 17, September 2006.
[59] Gambica Technical Guide - Managing Harmonics. A guide to ENA Engineering Recommendation G5/4-1, 4th Edition, 2006, The Energy Networks Association.
[60] REE – Requisitos de respuesta frente a huecos de tension de las instalaciones de produccion de regimen especial, PO 12.3, November 2005.
[61] ENEL – DK 5400 - Criteri di allacciamento di clienti alla rete AT della distribuzione, October 2004.
[62] ENEL - – DK 5740 - Criteri di allacciamento di impianti di produzione alla rete MT di ENEL distribuzione, February 2005.
[63] TERNA - Codice di trasmissione, dispacciamento, sviluppo e sicurezza della rete, 2006.
[64] CEI 11/32, Appendice N.6 – Normativa impianti di produzione eolica, February 2006 (draft).
[65] IEA International Energy Agency: Trends in Photovoltaic Applications. Survey report of selected IEA countries between 1992 and 2003. Source: http://www.oja-services.nl/iea-pvps/products/download/rep1_13.pdf.
[66] H. Haeberlin, “Evolution of Inverters for Grid connected PV systems from 1989 to 2000“, Proc. of Photovoltaic Solar Energy Conference, 2001.
[67] T. Shimizu, M. Hirakata, T. Kamezawa, H. Watanabe, “Generation Control Circuit for Photovoltaic Modules“, IEEE Trans. On Power Electronics, Vol. 16, No. 3, May, 2001, pp. 293-300.
[68] M. Calais, V.G. Agelidis, L.J. Borle, M.S. Dymond, “A transformerless five level cascaded inverter based single phase photovoltaic system”, Proc. of PESC, 2000, Vol. 3, pp. 1173-1178.
[69] R.W. Erickson, D. Maksimovic, “Fundamentals of Power Electronics”, Kluwer Academic Pub; March 1, 1997, ISBN: 0-412-08541-0, 773 pages.
[70] M. Calais, J. Myrzik, T. Spooner, V.G. Agelidis, “Inverters for single-phase grid connected photovoltaic systems - An overview”, Proc. of PESC ’02, 2002, Vol. 4, pp. 1995 – 2000.
[71] F. Blaabjerg, R. Teodorescu, Z. Chen, M. Liserre, “Power Converters and Control of Renewable Energy Systems”, Proc. of ICPE, 2004, pp. 1-19.
[72] R. Teodorescu, F. Blaabjerg, M. Liserre, U. Borup, ” A New Control Structure for Grid-Connected PV Inverters with Zero Steady-State Error and Selective Harmonic Compensation”, Proc. of APEC, 2004, Vol. 1, pp. 580-586.
[73] S. Fukuda and T. Yoda, “A novel current-tracking method for active filters based on a sinusoidal internal mode”, IEEE Trans. on Ind. App., 2001, Vol.37, No. 3, pp. 888-895.
[74] X. Yuan, W. Merk, H. Stemmler and J. Allmeling, “Stationary-Frame Generalized Integrators for Current Control of Active Power Filters with Zero Steady-State Error for Current Harmonics of Concern Under Unbalanced and Distorted Operating Conditions”, IEEE Trans. on Ind. App., Vol. 38, No. 2, 2002, pp. 523-532.
[75] M. Ciobotaru, R. Teodorescu, F. Blaabjerg, “Control of single-stage single-phase PV inverter”, Proc. of EPE’05, 10 pages, ISBN : 90-75815-08-5.
[76] D.P. Hohm, M.E. Ropp, “Comparative Study of Maximum Power Point Tracking Algorithms Using an Experimental, Programmable, Maximum Power Point Tracking Test Bed”. IEEE Proc. of Photovoltaic Specialists Conference, 2000, Pages:1699-1702.
[77] N. Femia, G. Petrone, G. Spagnuolo, M. Vitelli, “Optimizing sampling rate of P&O MPPT technique”, Proc. of PESC, 2004, Vol. 3, pp. 1945-1949.
[78] A. Brambilla, M. Gambarara, A. Garutti, F. Ronchi, “New approach to photovoltaic arrays maximum power point tracking”, Proc. of PESC, 1999, Vol. 2, pp. 632-637.
[79] X. Liu, L.A.C. Lopes, “An improved perturbation and observation maximum power point tracking algorithm for PV arrays”, Proc. of PESC, 2004, Vol. 3, Pages: 2005 - 2010.

[80] D. Sera, T. Kerekes, R. Teodorescu, and F. Blaabjerg, “Improved MPPT method for rapidly changing environmental conditions,” in Industrial Electronics, 2006 IEEE International Symposium on, Vol. 2, 2006, pp.1420-1425.
[81] K.H. Hussein, I. Muta, T. Hoshino, M. Osakada, “Maximum photovoltaic power tracking: an algorithm for rapidly changing atmospheric conditions”. IEE Trans. on Generation, Transmission and Distribution, Jan. 1995, Vol. 142, No. 1, pp. 59-64.
[82] W. Swiegers, Enslin J.H.R.: “An integrated maximum power point tracker for photovoltaic panels”, Proc. of ISIE, 1998, Vol. 1, pp. 40-44.
[83] T.J. Liang, Y.C. Kuo and J.F. Chen, “Single-stage photovoltaic energy conversion system”, IEE Proceedings Electric Power Applications, 2001, Vol. 148, No. 4, pp. 339-344.
[84] Y.C. Kuo and T.J. Liang, “Novel Maximum-Power-Point-Tracking Controller for Photovoltaic Energy Conversion System”, IEEE Trans. on Industrial Electronics, 2001, Vol. 48, No. 3, pp. 594-601.
[85] M. Nikraz, H. Dehbonei, C.V.N. Curtin, “Digital control of a voltage source inverter in photovoltaic applications”, Proc. of PESC, 2004, Vol. 5, 2004, pp. 3266-3271.
[86] "Characteristics of the utility interface for photovoltaic (PV) systems," IEC 61727-2002, 2002.
[87] IEEE Standard 929-2000: IEEE Recommended practice for utility interface of photovoltaic (PV) systems.
[88] M. Francesco De, L. Marco, D.A. Antonio, and P. Alberto, "Overview of Anti-Islanding Algorithms for PV Systems. Part I: Passive Methods," Proc. of EPE-PEMC, 2006, pp. 1878-1883.
[89] F. M. Gardner, "Phaselock Techniques", Publisher: Wiley-Interscience, 1979, Vol. 2nd edition, ISBN-10: 0471042943, 304 pages.
[90] F. Mur, V. Cardenas, J. Vaquero, and S. Martinez, "Phase synchronization and measurement digital systems of AC mains for power converters", Proc. of CIEP, 1998, pp. 188-194.
[91] J. W. Choi, Y.K. Kim, and H.G. Kim, "Digital PLL control for single-phase photovoltaic system", IEE Trans. on Electric Power Applications, 2006, Vol. 153, pp. 40-46.
[92] S.K. Chung, "A phase tracking system for three phase utility interface inverters", IEEE Trans. on Power Electronics, 2000, Vol. 15, pp. 431-438.
[93] C. T. Nguyen and K. Srinivasan, "A New Technique for Rapid Tracking of Frequency Deviations Based on Level Crossings," IEEE Trans. on Power Apparatus and Systems, 1984, Vol. PAS-103, pp. 2230-2236.
[94] B.P. McGrath, D.G. Holmes, J.J.H. Galloway, "Power converter line synchronization using a discrete Fourier transform (DFT) based on a variable sample rate", IEEE Trans. on Power Electronics, 2005, Vol. 20, pp. 877-884.
[95] O. Vainio, S. J. Ovaska, and M. Polla, "Adaptive filtering using multiplicative general parameters for zero-crossing detection", IEEE Trans. on Industrial Electronics, 2003, vol. 50, pp. 1340-1342.
[96] S. Valiviita, S. J. Ovaska, and J. Kyyra, "Adaptive signal processing system for accurate zero-crossing detection of cycloconverter phase currents", Proc. of PCC, 1997, Vol.1, pp. 467-472
[97] O. Vainio and S. J. Ovaska, "Noise reduction in zero crossing detection by predictive digital filtering," IEEE Trans. on Industrial Electronics, 1995, vol. 42, pp. 58-62.
[98] R.W. Wall, "Simple methods for detecting zero crossing", Proc. of IECON, 2003, Vol.3, pp. 2477-2481.
[99] S. Valiviita, "Neural network for zero-crossing detection of distorted line voltages in weak AC-systems", Proc. of IMTC, 1998, Vol.1, pp. 280-285.
[100] S. Das, P. Syam, G. Bandyopadhyay, and A.K. Chattopadhyay, "Wavelet transform application for zero-crossing detection of distorted line voltages in weak AC-systems", Proc. of INDICON, 2004, pp. 464-467.
[101] S. Valiviita, "Zero-crossing detection of distorted line voltages using 1-b measurements", IEEE Trans. on Industrial Electronics, 1999, Vol. 46, pp. 917-922.
[102] R. Weidenbrug, F. P. Dawson, and R. Bonert, "New synchronization method for thyristor power converters to weak", IEEE Trans. on Industrial Electronics, 1993, Vol. 40, pp. 505-511.
[103] D.M. Baker and V.G. Agelidis, "Phase-locked loop for microprocessor with reduced complexity voltage controlled oscillator suitable for inverters," Proc. of PEDES, 1998, pp. 464-469 Vol.1.
[104] D. Nedeljkovic, J. Nastran, D. Voncina, and V. Ambrozic, "Synchronization of active power filter current reference to the network", IEEE Trans. on Industrial Electronics, 1999, vol. 46, pp. 333-339.
[105] D. Nedeljkovic, V. Ambrozic, J. Nastran, and D. Hudnik, "Synchronization to the network without voltage zero-cross detection", Proc. of MELECON, 1998, Vol. 2, pp. 1228-1232.
[106] S. M. Silva, B. M. Lopes, B. J. C. Filho, R. P. Campana, and W. C. Bosventura, "Performance evaluation of PLL algorithms for single-phase grid-connected systems," Proc. of IAS, 2004, Vol.4, pp. 2259-2263.
[107] W. Tsai-Fu, S. Chih-Lung, N. Hung-Shou, and L. Guang-Feng, "A 1phi-3W inverter with grid connection and active power filtering based on nonlinear programming and fast-zero-phase detection algorithm", IEEE Trans. on Power Electronics, 2005, Vol. 20, pp. 218-226.
[108] P. Rodriguez, A. Luna, M. Ciobotaru, R. Teodorescu, F. Blaabjerg, "Advanced Grid Synchronization System for Power Converters under Unbalanced and Distorted Operating Conditions", Proc. of IECON, 2006, pp. 5173-5178.
[109] L. R. Limongi, R. Bojoi, C. Pica, F. Profumo, and A. Tenconi, "Analysis and Comparison of Phase Locked Loop Techniques for Grid Utility Applications", Proc. of PCC, 2007, pp. 674-681.
[110] M. Saitou, N. Matsui, and T. Shimizu, "A control strategy of single-phase active filter using a novel d-q transformation", Proc. of IAS, 2003, Vol. 2, pp. 1222-1227.
[111] P. Rodriguez, J. Pou, J. Bergas, J. I. Candela, R. P. Burgos, and D. Boroyevich, "Decoupled Double Synchronous Reference Frame PLL for Power Converters Control", IEEE Trans. on Power Electronics, 2007, vol. 22, pp. 584-592.
[112] K. De Brabandere, T. Loix, K. Engelen, B. Bolsens, J. Van den Keybus, J. Driesen, and R. Belmans, "Design and Operation of a Phase-Locked Loop with Kalman Estimator-Based Filter for Single-Phase Applications", Proc. of IECON, 2006, pp. 525-530.
[113] P. Rodriguez, J. Pou, J. Bergas, I. Candela, R. Burgos, and D. Boroyevic, "Double Synchronous Reference Frame PLL for Power Converters Control", Proc. of PESC, 2005, pp. 1415-1421.
[114] T. Ostrem, W. Sulkowski, L. E. Norum, and C. Wang, "Grid Connected Photovoltaic (PV) Inverter with Robust Phase-Locked Loop (PLL)", Proc. of TDC, 2006, pp. 1-7.
[115] M. Ciobotaru, R. Teodorescu, and F. Blaabjerg, "Improved PLL structures for single-phase grid inverters", Proc. of PELINCEC, 2005, pp. 1-6.
[116] S. Shinnaka, "A New Frequency-Adaptive Phase-Estimation Method Based on a New PLL Structure for Single-Phase Signals", Proc. of PCC, 2007, pp. 191-198.
[117] M. Ciobotaru, R. Teodorescu, and F. Blaabjerg, "A New Single-Phase PLL Structure Based on Second Order Generalized Integrator", Proc. of PESC, 2006, pp. 1-6.
[118] V. Kaura and V. Blasko, "Operation of a phase locked loop system under distorted utility conditions", Proc. of APEC, 1996, Vol.2, pp. 703-708.
[119] S. K. Chung, "Phase-locked loop for grid-connected three-phase power conversion systems", IEE Trans. on Electric Power Applications, 2000, vol. 147, pp. 213-219.
[120] A. W. Krieger and J. C. Salmon, "Phase-locked loop synchronization with gated control," Proc. of CCECE, 2005, pp. 523-526.
[121] A. V. Timbus, R. Teodorescu, F. Blaabjerg, M. Liserre, and P. Rodriguez, "PLL Algorithm for Power Generation Systems Robust to Grid Voltage Faults", Proc. of PESC, 2006. pp. 1-7.
[122] L. N. Arruda, S. M. Silva, and B. J. C. Filho, "PLL structures for utility connected systems", Proc. of IAS, 2001, Vol. 4, pp. 2655-2660.
[123] E. S. Sreeraj and K. Chatterjee, "Power Factor Improvement in One Cycle Controlled Converter", Proc. of ISIE, 2006, pp. 1454-1460.
[124] S. K. Chung, H. B. Shin, and H. W. Lee, "Precision control of single-phase PWM inverter using PLL compensation", IEE Trans. on Electric Power Applications, 2005, Vol. 152, pp. 429-436.
[125] A. Timbus, M. Liserre, R. Teodorescu, and F. Blaabjerg, "Synchronization Methods for Three Phase Distributed Power Generation Systems. An Overview and Evaluation", Proc. of PESC, 2005, pp. 2474-2481.

[126] L. N. Arruda, B. J. Cardoso Filho, S. M. Silva, S. R. Silva, and A. S. A. C. Diniz, "Wide bandwidth single and three-phase PLL structures for grid-tied", Proc. of Photovoltaic Specialists Conference, 2000, pp. 1660-1663.
[127] J. Salaet, S. Alepuz, A. Gilabert, and J. Bordonau, "Comparison between two methods of DQ transformation for single phase converters control. Application to a 3-level boost rectifier", Proc. of PESC, 2004, Vol.1, pp. 214-220.
[128] DIN VDE 0126-1-1, "Automatic disconnection device between a generator and the public low-voltage grid", June 2005.
[129] M. Liserre, R. Teodorescu, and F. Blaabjerg, "Stability of grid-connected PV inverters with large grid impedance variation", in Proc. of PESC, 2004, pp. 4773–4779.
[130] L. Asiminoaei, R. Teodorescu, F. Blaabjerg, U. Borup, "Implementation and Test of an Online Embedded Grid Impedance Estimation Technique for PV Inverters", IEEE Trans. on Industrial Electronics, 2005, vol.52, no.4, pp. 1136-1144.
[131] M. Sumner, B. Palethorpe, D. Thomas, P. Zanchetta, M.C. Di Piazza, "Estimation of power supply harmonic impedance using a controlled voltage disturbance", Proc. of PESC, 2001, vol.2, pp. 522-527.
[132] M.C. Di Piazza, P. Zanchetta, M. Sumner, D.W.P. Thomas, "Estimation of load impedance in a power system", Proc. of Harmonics and Quality of Power Conference, 2000, vol.2, pp. 520-525.
[133] M. Sumner, B. Palethorpe, D.W.P. Thomas, P. Zanchetta, M.C. Di Piazza, "A technique for power supply harmonic impedance estimation using a controlled voltage disturbance", IEEE Trans. on Power Electronics, 2002, vol.17, no.2, pp. 207-215.
[134] J.P. Rhode, A.W. Kelley, M.E. Baran, "Line impedance measurement: a nondisruptive wideband technique", Proc. of IAS, 1995, vol.3, pp. 2233-2240.
[135] N. Ishigure, K. Matsui, F. Ueda, "Development of an on-line impedance meter to measure the impedance of a distribution line", Proc. of ISIE, 2001, vol.1, pp. 549-554.
[136] Tsukamoto, M.; Ogawa, S.; Natsuda, Y.; Minowa, Y.; Nishimura, S., "Advanced technology to identify harmonics characteristics and results of measuring," Harmonics and Quality of Power, 2000. Proceedings. Ninth International Conference on, vol.1, pp., 341-346.
[137] K.O.H. Pedersen, A.H. Nielsen, and N.K. Poulsen, "Short-circuit impedance measurement," IEE Trans. on Generation, Transmission and Distribution, 2003, vol. 150, no. 2, pp. 169–174.
[138] M. Ciobotaru, R. Teodorescu, P. Rodriguez, A. Timbus and F. Blaabjerg, "Online grid impedance estimation for single-phase grid-connected systems using PQ variations", Proc. of PESC, 2007, pp. 2306-2312.
[139] M. Ciobotaru, R. Teodorescu and F. Blaabjerg, "On-line grid impedance estimation based on harmonic injection for grid-connected PV inverter", Proc. of ISIE, 2007, pp. 2437-2442.
[140] IEEE Standard 1547-2003: IEEE Standard for interconnecting distributed resources with electric power systems.
[141] A. Woyte, K. De Brabandere, D.V. Dommelen, R. Belmans, and J. Nijs, "International harmonization of grid connection guidelines: adequate requirements for the prevention of unintentional islanding", Progress in Photovoltaics: Research and Applications, 2003, Vol. 11, pp. 407-424.
[142] W. Bower and M Ropp, "Evaluation of islanding detection methods for photovoltaic utility-interactive power systems", IEA Task V Report IEA-PVPS T5-09, March 2002.
[143] Z. Ye, R. Walling, L. Garces, R. Zhou, L. Li and T. Wang, "Study and development of anti-islanding control for grid-connected inverters", National Renewable Energy Laboratory, NREL/SR-560-36243, May 2004.
[144] H. Kobayashi, K. Takigawa and E. Hashimoto, "Method for preventing islanding phenomenon on utility grid with a number of small scale PV systems", Proc. of. Photovoltaic Specialists Conference, 1991, pp. 695-700.
[145] A. Kitamura, M. Okamoto, F. Yamamoto, K. Nakaji, H. Matsuda, K. Hotta, "Islanding phenomenon elimination study at Rokko test center", Proc. of Photovoltaic Specialists Conference, 1994, Vol. 1, p. 759-762.
[146] Z. Ye, A. Kolwalkar, Y. Zhang, P. Du and R. Walling, "Evaluation of anti-islanding schemes based on non-detection zone concept", IEEE Trans. on Power Electronics, 2004, Vol. 19, No. 5, pp. 1171-1176.
[147] M.E. Ropp, M. Begovic and A. Rohatgi, "Prevention of islanding in grid-connected photovoltaic systems", Progress in Photovoltaics: Research and Applications, 1999, Vol. 7, pp. 39-59.
[148] M.E. Ropp, M. Begovic and A. Rohatgi, "Analysis and performance assessment of the active frequency drift method of islanding prevention", IEEE Trans. on Energy Conversion, 1999, Vol. 14, No. 3, pp. 810-816.
[149] S. Yuyama, T. Ichinose, K. Kimoto, T. Itami, T. Ambo, C. Okado, K. Nakajima. S. Hojo, H. Shinohara, S. Ioka and M. Kuniyoshi, "A high-speed frequency shift method as a protection for islanding phenomena of utility interactive PV systems", Solar Energy Materials and Solar Cells, 1994, Vol. 35, pp. 477-486.
[150] P. Sanchis, L. Marroyo and J. Coloma, "Design methodology for the frequency shift method of islanding prevention and analysis of its detection capability", Progress in Photovoltaics: Research and Applications, 2005, Vol. 13, pp. 409-428.
[151] G.A. Smith, P.A. Onions and D.G. Infield, "Predicting islanding operation of grid connected PV inverters", IEE Trans. Electrical Power Applications, 2000, Vol. 147, No 1, pp. 1-5.
[152] M.E. Ropp, M. Begovic, A. Rohatgi, G.A. Kern, H. Bonn and S. Gonzalez, "Determining the relative effectiveness of islanding detection methods using phase criteria and non-detection zones", IEEE Trans. on Energy Conversion, 2000, Vol. 15, No. 3, pp. 290-296.
[153] G.K. Hung, C.C. Chang and C.L. Chen, "Automatic phase-shift method for islanding detection of grid-connected photovoltaic inverters", IEEE Trans. on Energy Conversion, 2003, Vol. 18, No. 1, pp. 169-173.
[154] V. John, Z. Ye and A. Kolwalkar, "Investigation of anti-islanding protection of power converter based distributed generators using frequency domain analysis", IEEE Trans. on Power Electronics, 2004, Vol. 19, No. 5, pp. 1177-1183.
[155] L.A.C. Lopes and H. Sun, "Performance assessment of active frequency drifting islanding detection methods", IEEE Trans. on Energy Conversion, 2006, Vol. 21, No. 1, pp. 171-180.
[156] C. Jeraputra and P.N. Enjeti, "Development of a robust anti-islanding algorithm for utility interconnection of distributed fuel cell powered generation", IEEE Trans. on Power Electronics, 2004, Vol. 19, No. 5, pp. 1163-1170.
[157] Z. Ye, L. Li, L. Garces, C. Wang, R. Zhang, M. Dame, R. Walling and N. Miller, "A new family of active anti-islanding schemes based on DQ implementation for grid-connected inverters", Proc. of PESC, 2004, pp. 235-241.
[158] N. Cullen, J. Thornycroft and A. Collinson, "Risk analysis of islanding of photovoltaic power systems within low voltage distribution networks", IEA Report PVPS T5-08, March 2002.
[159] European Photovoltaic Industry Association: EPIA Roadmap. Source: http://www.epia.org/04events/docs/EPIAroadmap.pdf.
[160] IEA International Energy Agency: Trends in Photovoltaic Applications. Survey report of selected IEA countries between 1992 and 2003. Source: http://www.oja-services.nl/iea-pvps/products/download/rep1_13.pdf.
[161] G. Cramer , M. Ibrahim and W. Kleinkauf, "PV System Technologies: State-of-the-art and Trends in Decentralized Electrification." Science Direct-Refocus, Vol. 5, pp. 38-42. source: www.sciencedirect.com, www.re-focus.net.
[162] Mohammad Shahidehpour, Fred Schwartz, "Don't Let the Sun Go Down on PV". IEEE Power and Energy Magazine, 2004, Vol. 2, No. 3, pp. 40-48.

Appendix I. Review of connection requirements for wind power in European grid codes [7].

		Denmark		Ireland	Germany	Great Britain	Spain	Italy (draft)
Voltage Level		DS	TS	DS(TS)	TS(DS)	TS(DS)	TS	> 35 kV
Power Level		all	all	≥5MW	all	all	all	> 10 MW
Tolerance over frequency range		yes	yes	yes	yes	yes	-	yes
Frequency	**Frequency control**	all	all	all	all	all	-	> 25 MW
	MW Curtailment	20-100% P_r	20-100% P_r	yes	yes	-	-	-
	Maximum Ramp Rates	10-100% P_r/min	10-100% P_r/min	1-30 MW/min	yes	-	-	<20% P_r/min
Voltage	**Voltage Control**	no	no	yes	no	no	-	no
	Reactive Power Control	yes	yes	yes	yes	yes	-	yes
Voltage quality	**Fast voltage variations**	≤ 3%	≤ 3%	-	≤ 2%	≤ 3%-	-	EN 50160
	Short Term Flicker Severity	-	≤ 0.3	≤ 0.35	-	≤0.8	-	EN 50160
	Long Term Flicker Severity	≤ 0.35	≤ 0.2	≤ 0.35	≤ 0.46	≤0.6	-	EN 50160
	Harmonic Compatibility Levels	Specific levels	-	Specific Levels[1)]	EN 50160	IEC 61000-3-2	-	EN 50160
	THD	-	≤ 1.5%	≤ 1.5%	≤ 8%	N/A	-	EN 50160
Fault ride-through	**Fault duration**	100 msec	100 msec	625 msec	150 msec	140 msec	500 msec	500 msec
	Min voltage	25%U_r	25%U_r	15%U_r	0%U_r	15%U_r	20%U_r	20% U_r
	Recovery time	1 sec	1 sec	3 sec	1.5 sec	1.2 sec	1 sec	0.3 sec
	Voltage profile	2, 3-ph	1, 2, 3- ph	1, 2, 3- ph	generic	generic	generic	generic
	Reactive current injection	no	no	no	Up to 100%	no	Up to 100%	no
Island operation		not required	not required	not required	not required	not required	not required	not required
Black start capability		not required	not required	may	if required	not required	not required	not required
Signals, Communication and Control	**Availability**	yes	yes	yes	yes	yes	-	yes
	Active power output	yes	yes	yes	yes	yes	-	yes
	Reactive power output	yes	yes	yes	yes	yes	-	yes
	MW Curtailment	yes	yes	yes	yes	yes	-	-
	Frequency control	yes	yes	yes	yes	yes	-	-
	Circuit breaker status	yes	yes	yes	yes	yes	-	yes
	Meteorological data: Wind speed, wind direction, air pressure and temperature	yes	yes	yes	-	-	-	yes

1) Harmonic compatibility levels are given in general for loads and installations. DSO shall provide a schedule of individual limits where appropriate.

Publication 4

Teaching Maximum Power Point Trackers Using a Photovoltaic Array Model with Graphical User Interface

by D. Sera, R. Teodorescu, T. Kerekes

Teaching Maximum Power Point Trackers Using a Photovoltaic Array Model with Graphical User Interface

Dezso Sera, Remus Teodorescu Tamas Kerekes
des@iet.aau.dk; ret@iet.aau.dk; tak@iet.aau.dk;
Institute of Energy Technology; Aalborg University
Pontoppidanstraede 101
DK-9220, Aalborg, Denmark

Abstract

This work intends to present a laboratory work material for teaching Maximum Power Point Tracking (MPPT) for graduate students. For good understanding of the MPPT methods, it is important to be aware of the PV arrays' characteristics in various conditions. Thereby a detailed model of the PV array has been developed, using Matlab. The model allows characterizing the PV array in different temperature, irradiance and shading conditions, using Graphical User Interface (GUI). The outputs of the model are the I(V) and P(V) characteristics, as well as the voltage, current, and power at the Maximum Power Point of the PV array. The current and voltage vectors are automatically loaded into a look-up table in a Simulink model. Two of the most popular MPPT algorithms, the Perturb & Observe (P&O) and the Incremental Conductance (INC) have been considered: first simulated in Simulink and than experimentally tested on a DSP platform. For experimental validation, a hardware setup with a grid connected inverter and a TMS320 F2812 eZdsp board was used.

Keywords: Teaching, Photovoltaic, Maximum Power Point Tracking, Graphical User Interface

1. MODELING THE PV ARRAY

The basic (and most commonly used) expression of the solar panel output voltage in function of the load current is described by the following equation:[1]

$$v = n_s \cdot V_T \ln\left(\frac{I_{SC} - i}{I_0}\right), where$$
$$V_T = \frac{K_B \cdot T \cdot n}{q} \quad (1)$$
$$I_{SC} = I_{SC,1000} \cdot \frac{G}{1000}$$

I_{SC} – Current at shortcircuit	q = 1.6 10^{-19} [C]
$I_{SC,\ 1000}$ – given in datasheet	T –temperature [K]
G – irradiation	n – diode non-ideality factor
V_{OC} – Open loop voltage	n_s – number of cells in series
K_B = 1.3806 10-23 [J/K]	Io – dark current

1.1. The Graphical User Interface (GUI)

Based on the above equations, the PV model has been implemented using Matlab. The GUI, represented in Figure 1, allows the student to plot the I(V) and P(V) characteristics of a PV. The user has access to choose the type of the PV panels (BP-MSX120 or KC125G), the irradiation intensity (in % of the Standard Test Conditions, STC), the cell temperature, as well as the number of panels in series, which form the string and the number of strings in parallel. These options offer a very high flexibility and a wide range of different PV plant configurations with different voltage and current levels can be simulated.

Furthermore, the effects of the partial shading can be visualized by choosing the shading degree and the shaded area. Modeling the partial shading effects has been made based on the assumption that every cell has its own bypass diode.

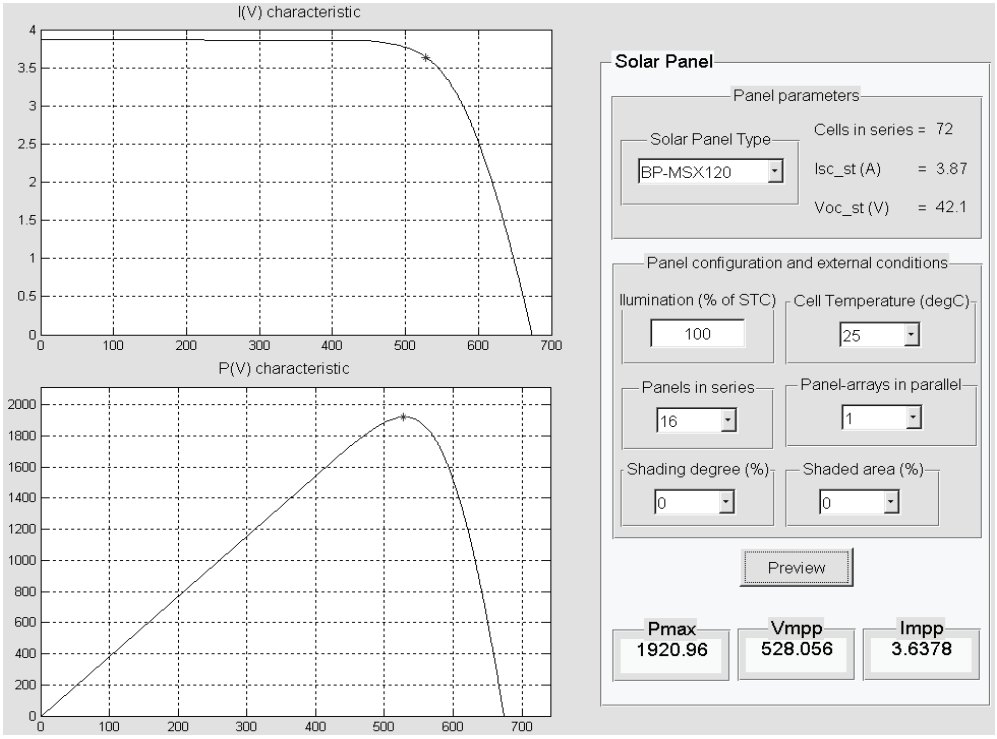

Figure 1 The Graphical User Interface for the PV model

2. SIMULATION OF THE MAXIMUM POWER POINT TRACKING METHODS

2.1 The Perturb & Observe (P&O) method

The most commonly used MPPT algorithm is the (P&O), due to its ease of implementation in its basic form. However, it has some limitations, like oscillations around the MPP in steady state operation, slow response speed, and even tracking in wrong way under rapidly changing atmospheric conditions. [2][3][4][5]

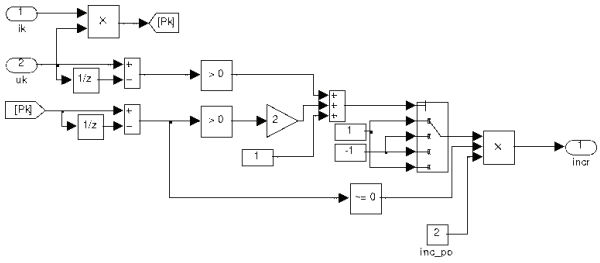

Figure 2 The Simulink implementation of the P&O algorithm

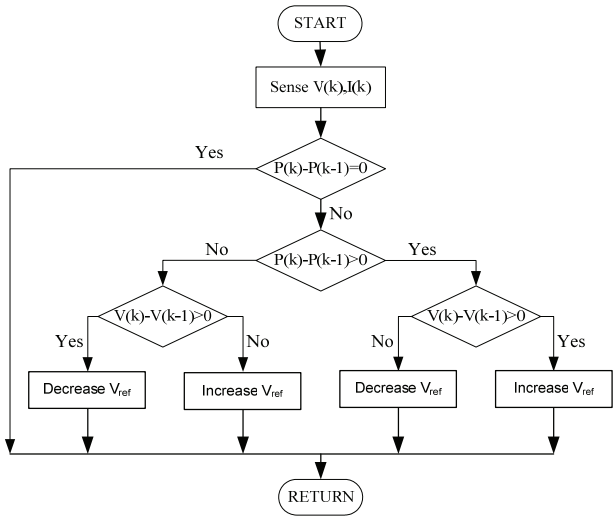

Figure 3 Flowchart of the P&O method

2.2 The Incremental Conductance (INC) method

The INC uses the PV array's incremental conductance di/dv to compute the sign of dp/dv.[1]. It does this using an expression derived from the condition that, at the MPP, dp/dv = 0. Beginning with this condition, it is possible to show that, at the MPP di/dv = -i/v [2]. Thus, INC can determine that the MPPT has reached the MPP and stop perturbing the operating point

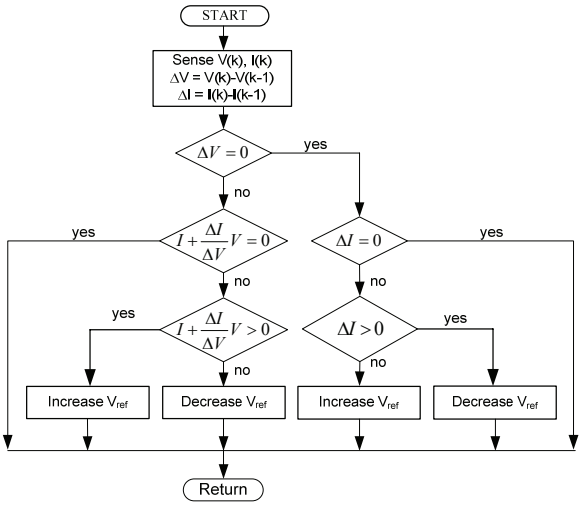

Figure 4 Flowchart of the INC method

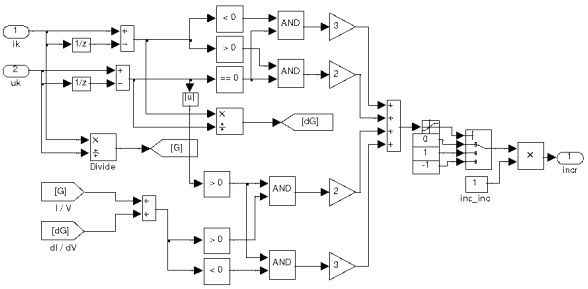

Figure 5 The Simulink implementation of the INC algorithm

The control diagram of the system for simulating the two MPPT algorithms is presented in Figure 6:

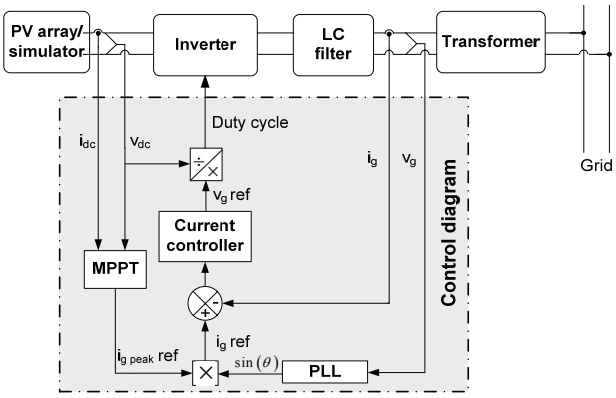

Figure 6 Block diagram of the simulation model

2.3 Laboratory tasks

The students have several tasks to complete in order to understand the effects of the MPPT sampling rate and voltage increment size, as well as the differences between the two MPPT algorithms.

a. Effect of the MPPT sampling rate and voltage increment

- Start the PV simulator. In the GUI, select the BP-MSX120 panels (16 panels in series), 50% irradiation of Standard Test Conditions (STC), and 25ºC temperature, without partial shading. (Irradiance at STC, G= 1000W/m^2)
- Experiment with a sampling frequency of 10Hz and 1Hz during an irradiance change from 30% to 100% (of STC). Measure the settling time of the PV power for both the P&O and INC.
- Tune the voltage increment to 1V and 5V at a sampling rate of 10Hz and observe its effects on the settling time of the PV power and oscillations around the MPP for both methods.

b. Efficiency of the P&O and INC algorithms

- Simulate both MPPT methods for irradiations of G= 10, 20,…120% of the STC and determine their efficiency for every value of G, by comparing the power at the DC side with the theoretical maximum power at the actual irradiation, shown in the GUI.
- Fill out Table 1
- Calculate the overall efficiency of both methods using the European efficiency formula:

$$\eta_{EU} = 0.03\cdot\eta_{5\%} + 0.06\cdot\eta_{10\%} + 0.13\cdot\eta_{20\%} + \\ + 0.1\cdot\eta_{30\%} + 0.48\cdot\eta_{50\%} + 0.2\cdot\eta_{100\%} \quad (2)$$

G[%]	G[W/m^2]	P_{MPP}[W]	P_{PV}[W] P&O	P_{PV}[W] INC	η[%] P&O	η[%] INC
5	50					
10	100					
20	200					
30	300					
50	500					
100	1000					

P_{MPP} – maximum power calculated from model
P_{PV} – maximum power drawn by the MPPT

Table 1 Comparison of the P&O and INC methods for different irradiations

3. EXPERIMENTAL VALIDATION

The hardware setup used to validate the simulation results is shown below:

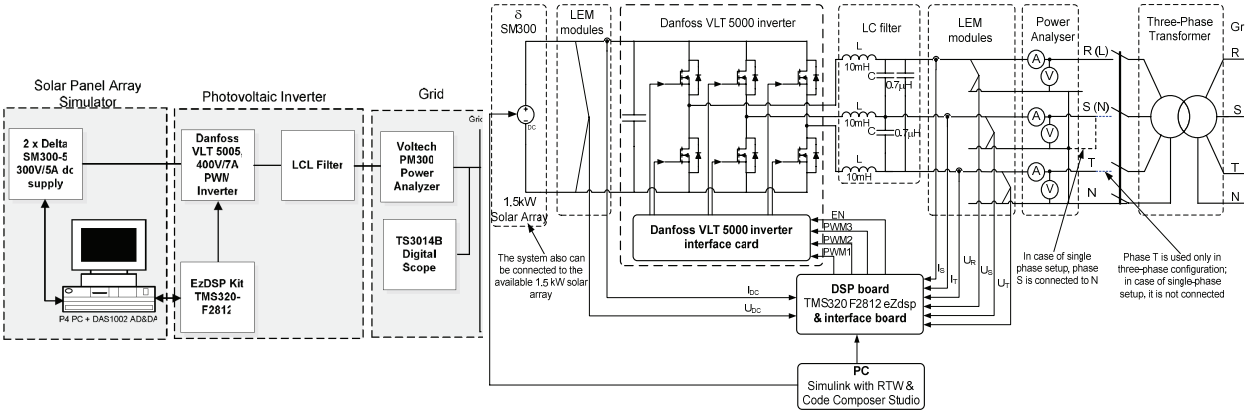

Figure 7 Block diagram and scheme of the hardware setup

For experimental testing, the control diagram from Figure 6, containing both the P&O and INC methods has been implemented in Simulink. The Real Time Workshop and Simulink together with Embedded Target for TI C2000 compile the model generating a real-time C code, which is automatically forwarded to the Code Composer Studio (CCS), a programming, debugging and monitoring environment for Texas Instruments DSPs. The DSP code is generated in CCS and is downloaded to the F2812 DSP. The CCS interface, which allows the students to tune online the control parameters, as well as to visualize the important variables, is shown in Figure 8:

The PV array is emulated by programmable DC sources, controlled from Simulink, through a Measurement Computing DAS 1002 interface card. The DC sources are controlled according to (1).

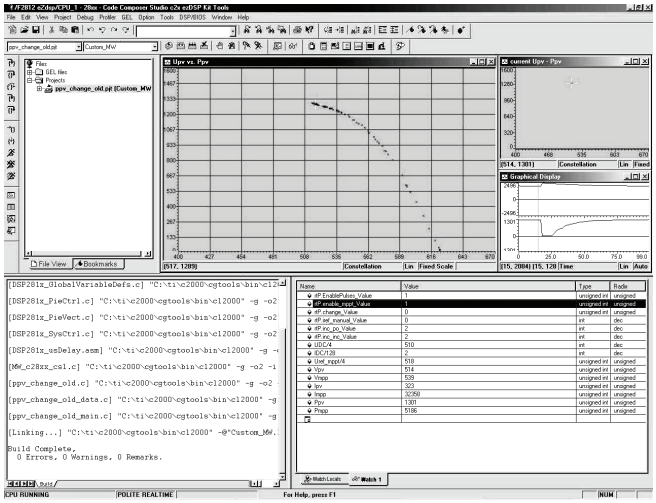

Figure 8: The CCS interface, showing the measured P(V) characteristics, as well as the control and monitoring variables

3.1. Laboratory tasks

- In order to compare the simulations with the experimental results, the same tasks are repeated as described in Section 2.3
- In addition, after filling out Table 1, the experimental measurements should be compared to the simulation results.

Conclusions

In the present paper a complete laboratory work package has been presented for testing the most popular MPPT algorithms, using a PV model with Graphical User Interface. The GUI allows the students to observe the characteristics of the PV panel in various conditions. Together with the PV model a complete Simulink control diagram for single phase PV inverter is provided, where both the P&O and INC MPPT methods are implemented. The parameters as MPPT sampling time and voltage increment size can be chosen using simulation results, and can be validated experimentally

using a Green Power Inverter setup with a TI C2000 DSP and Code Composer Studio.

The presented laboratory exercises have been used with success during a PhD course in the area of power electronics for renewable energy sources.

References

[1]. Antonio Luque and Steven Hegedus. *Handbook of Photovoltaic Science and Engineering* , John Wiley & Sons Ltd, 2003

[2]. Hohm D.P., Ropp M.E.: "Comparative Study of Maximum Power Point Tracking Algorithms Using an Experimental, Programmable, Maximum Power Point Tracking Test Bench"**.** *Photovoltaic Specialists Conference, 2000. Conference Record of the 28th IEEE 15-22 Sept. 2000 Pages:1699 - 1702*

[3]. Femia N., Petrone G., Spagnuolo G., Vitelli M.: "Optimizing sampling rate of P&O MPPT technique**"** *Power Electronics Specialists Conference, 2004. PESC 04. 2004 IEEE 35th Annual Volume 3, 20-25 June 2004*

[4]. Femia N., Petrone G., Spagnuolo G., Vitelli M.: "Optimizing duty-cycle perturbation of P&O MPPT technique" *Power Electronics Specialists Conference, 2004. PESC 04. 2004 IEEE 35th Annual Volume 3*

[5]. Liu X., Lopes L.A.C.: "An improved perturbation and observation maximum power point tracking algorithm for PV arrays**"** *Power Electronics Specialists Conference, 2004. PESC 04. 2004 IEEE 35th Annual Volume 3, 20-25 June 2004 Pages: 2005 - 2010 Vol.3*

[6]. R. Teodorescu, F. Blaabjerg, "A new control structure for grid-connected LCL PV inverters with zero steady-state error and selective harmonic compensation" *Applied Power Electronics Conference and Exposition, 2004. APEC '04.*

Publication 5

PV panel model based on datasheet values

by D. Sera, R. Teodorescu, and P. Rodriguez

PV panel model based on datasheet values

Dezso Sera, Remus Teodorescu
Aalborg University, Institute of Energy Technology,
DK-9220 Aalborg, Denmark,
Email: des@iet.aau.dk, ret@iet.aau.dk

Pedro Rodriguez
University of Catalonia, Electrical Engineering Department
Colom 1, 08222, Terrassa-Barcelona, Spain,
Email: prodriguez@ee.upc.edu

***Abstract*— This work presents the construction of a model for a PV panel using the single-diode five-parameters model, based exclusively on data-sheet parameters. The model takes into account the series and parallel (shunt) resistance of the panel. The equivalent circuit and the basic equations of the PV cell/panel in Standard Test Conditions (STC)[1] are shown, as well as the parameters extraction from the data-sheet values. The temperature dependence of the cell dark saturation current is expressed with an alternative formula, which gives better correlation with the datasheet values of the power temperature dependence . Based on these equations, a PV panel model, which is able to predict the panel behavior in different temperature and irradiance conditions, is built and tested.**

I. Introduction

Nowadays the worldwide installed Photovoltaic power capacity shows a nearly exponential increase, despite of their still relatively high cost. [1] This, along with the research for lower cost and higher efficiency devices, motivates the research also in the control of PV inverters, to achieve higher efficiency and reliability. The possibility of predicting a photovoltaic plant's behavior in various irradiance, temperature and load conditions, is very important for sizing the PV plant and converter, as well as for the design of the Maximum Power Point Tracking (MPPT) and control strategy. There are numerous methods presented in the literature, for extracting the panel parameters. The majority of the methods are based on measurements of the I-V curve or other characteristic of the panel [2] [3] [4]. In this paper a photovoltaic panel model, based only on values provided by the manufacturer's data sheet, suitable for on-line temperature and irradiance estimations and model-based MPPT, is presented.

The equivalent circuit of the single-diode model for PV cells is shown below:

The general current-voltage characteristic of a PV panel based on the single exponential model is:

$$i = I_{ph} - I_o \left(e^{\frac{v+iR_s}{n_s V_t}} - 1 \right) - \frac{v + iR_s}{R_{sh}} \tag{1}$$

In the above equation, V_t is the junction thermal voltage:

$$V_t = \frac{AkT_{stc}}{q} \tag{2}$$

[1]The testing conditions to measure photovoltaic cells or modules nominal output power. Irradiance level is $1000W/m^2$, with the reference air mass 1.5 solar spectral irradiance distribution and cell or module junction temperature of 25^oC.

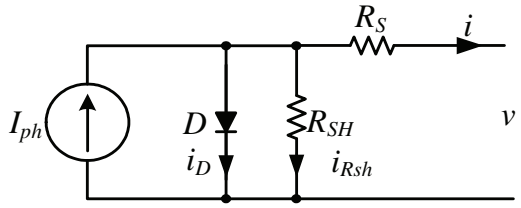

Fig. 1. Equivalent circuit of a photovoltaic cell using the single exponential model

where:

- I_{ph} - the photo-generated current in STC
- I_o - dark saturation current in STC
- R_s - panel series resistance
- R_{sh} - panel parallel (shunt)resistance
- A - diode quality (ideality) factor

are the five parameters of the model, while k is Boltzmann's constant, q is the charge of the electron, n_s is the number of cells in the panel connected in series, and $T_{stc}(^oK)$ is the temperature at STC. It is a common practice to neglect the term '-1' in (1), as in silicon devices, the dark saturation current is very small compared to the exponential term.

II. Determination of the panel model parameters from datasheet values

In order to construct a model of the PV panel, which exhibits the specifications described in the datasheet, using the above-mentioned single-diode model, there are five parameters to be determined: I_{ph}, I_o, A, R_s, and R_{sh}. The goal is to find all these parameters without any measurement, using only the data from the product data-sheet.

A. Starting equations

Equation (1) can be written for the three key-points of the V-I characteristic: the short-circuit point, the maximum power point, and the open-circuit point.

$$I_{sc} = I_{ph} - I_o\, e^{\frac{I_{sc}\,R_s}{n_s\,V_t}} - \frac{I_{sc}\,R_s}{R_{sh}} \tag{3}$$

$$I_{mpp} = I_{ph} - I_o\, e^{\frac{V_{mpp}+I_{mpp}\,R_s}{n_s\,V_t}} - \frac{V_{mpp} + I_{mpp}\,R_s}{R_{sh}} \tag{4}$$

$$I_{oc} = 0 = I_{ph} - I_o\, e^{\frac{V_{oc}}{n_s\,V_t}} - \frac{V_{oc}}{R_{sh}} \tag{5}$$

where:

- I_{sc} -short-circuit current in STC
- V_{oc} -open-circuit voltage in STC
- V_{mpp} -voltage at the Maximum Power Point (MPP) in STC
- I_{mpp} -current at the MPP in STC
- P_{mpp} -power at the MPP in STC
- k_i -temperature coefficient of the short-circuit current
- k_v -temperature coefficient of the open-circuit voltage

The above parameters are normally provided by the datasheet of the panel. An additional equation can be derived using the fact that on the P-V characteristic of the panel, at the MPP, the derivative of power with voltage is zero.

$$\left.\frac{dP}{dV}\right|_{\substack{V=V_{mpp}\\I=I_{mpp}}} = 0 \tag{6}$$

So far there are four equations available, but there are five parameters to find, therefore a fifth equation has to be found. For this purpose can be used the derivative of the current with the voltage at short-circuit conditions, which is mainly determined by the shunt resistance R_{sh} [2].

$$\left.\frac{dI}{dV}\right|_{I=I_{sc}} = -\frac{1}{R_{sh}} \tag{7}$$

B. Parameter extraction

From the expression of the current at short-circuit and open-circuit conditions, the photo-generated current I_{ph} and the dark saturation current I_o can be expressed:

$$I_{ph} = I_o\, e^{\frac{V_{oc}}{ns\ V_t}} + \frac{V_{oc}}{R_{sh}} \tag{8}$$

By inserting Eq.(8) into Eq.(3), it takes the form:

$$I_{sc} = I_o\, \left(e^{\frac{V_{oc}}{ns\ V_t}} - e^{\frac{I_{sc}\ R_s}{ns\ V_t}}\right) + \frac{V_{oc} - I_{sc}\, R_s}{R_{sh}} \tag{9}$$

The second term in the parenthesis from the above equation can be omitted, as it has insignificant size compared to the first term. Than (9) becomes:

$$I_{sc} = I_o\, e^{\frac{V_{oc}}{ns\ V_t}} + \frac{V_{oc} - I_{sc}\, R_s}{R_{sh}} \tag{10}$$

Solving the above equation for I_o, results in:

$$I_o = \left(I_{sc} - \frac{V_{oc} - I_{sc}\, R_s}{R_{sh}}\right) e^{-\frac{V_{oc}}{ns\ V_t}} \tag{11}$$

Eq.(8) and (11) can be inserted into Eq.(4), which will take the form:

$$\begin{aligned} I_{mpp} = I_{sc} &- \frac{V_{mpp} + I_{mpp}\, R_s - I_{sc}\, R_s}{R_{sh}} \\ &- \left(I_{sc} - \frac{V_{oc} - I_{sc}\, R_s}{R_{sh}}\right) e^{\frac{V_{mpp} + I_{mpp}\ R_s - V_{oc}}{ns\ V_t}} \end{aligned} \tag{12}$$

The above expression still contains three unknown parameters: R_s, R_{sh}, and A. The derivative of the power with voltage at MPP can be written as:

$$\left.\frac{dP}{dV}\right|_{\substack{V=V_{mpp}\\I=I_{mpp}}} = \frac{d\,(IV)}{dV} = I + \frac{dI}{dV}V \tag{13}$$

Thereby, to obtain the derivative of the power at MPP, the derivative of Eq.(12) with voltage should be found. However, (12) is a transcendent equation, and it needs numerical methods to express Impp. Eq.(12) can be written in the following form:

$$I = f\,(I, V) \tag{14}$$

where $f(I, V)$ is the right side of (12). By differentiating (14):

$$dI = dI\, \frac{\partial f\,(I,V)}{\partial I} + dV\, \frac{\partial f\,(I,V)}{\partial V} \tag{15}$$

the derivative of the current with voltage results in:

$$\frac{dI}{dV} = \frac{\frac{\partial}{\partial V} f\,(I,V)}{1 - \frac{\partial}{\partial I} f\,(I,V)} \tag{16}$$

From (16) and (13) results:

$$\frac{dP}{dV} = Impp + \frac{Vmpp\, \frac{\partial}{\partial V} f\,(I,V)}{1 - \frac{\partial}{\partial I} f\,(I,V)} \tag{17}$$

From the above:

$$\begin{aligned} \left.\frac{dP}{dV}\right|_{I=I_{mpp}} &= I_{mpp} \\ &+ V_{mpp} \frac{-\frac{(I_{sc}\ R_{sh} - V_{oc} + I_{sc}\ R_s)e^{\frac{V_{mpp} + I_{mpp}\ R_s - V_{oc}}{ns\ V_t}}}{ns\ V_t\ R_{sh}} - \frac{1}{R_{sh}}}{1 + \frac{(I_{sc}\ R_{sh} - V_{oc} + I_{sc}\ R_s)e^{\frac{V_{mpp} + I_{mpp}\ R_s - V_{oc}}{ns\ V_t}}}{ns\ V_t\ R_{sh}} + \frac{R_s}{R_{sh}}} \end{aligned} \tag{18}$$

There are two equations now, Eq.(12) and (18), with three unknowns. Eq.(7) can be the used as the third equation. Equations (7), (17) and (18) lead to:

$$-\frac{1}{R_{sh}}\left|_{I=I_{sc}}\right. = \frac{-\frac{(I_{sc}\ R_{sh} - V_{oc} + I_{sc}\ R_s)e^{\frac{I_{sc}\ R_s - V_{oc}}{ns\ V_t}}}{ns\ V_t\ R_{sh}} - \frac{1}{R_{sh}}}{1 + \frac{(I_{sc}\ R_{sh} - V_{oc} + I_{sc}\ R_s)e^{\frac{I_{sc}\ R_s - V_{oc}}{ns\ V_t}}}{ns\ V_t\ R_{sh}} + \frac{R_s}{R_{sh}}} \tag{19}$$

It is possible now to determine all the three unknown parameters, the R_s, A, and R_{sh} using Eq.(12), (18) and (19). As these equations does not allow to separate the unknowns and solve them analytically, they are solved using numerical methods.The flowchart for determining these variables is shown on Fig. 2

III. Construction of the PV full characteristic model

This section describes the construction of a PV panel model, following the logic of the implementation in Matlab.

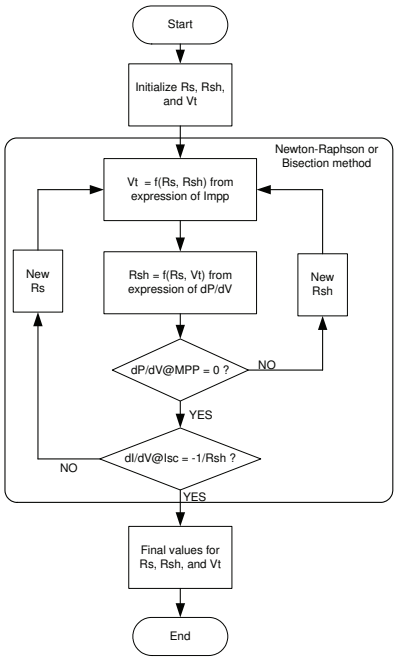

Fig. 2. Flowchart for determination of the PV panel parameters

A. Input parameters

The list of input parameters contains the values from the panel data sheet, as well as the values calculated using data sheet values. Considering the concrete case of the BP-MSX120 panels produced by British Petrol, (installed on the roof of the Green Power Laboratory at Aalborg University) the input data to the model are:

$I_{sc} = 3.87\ (A)$	$k_p = -0.5 \pm 0.05$
$I_{mpp} = 3.56\ (A)$	$n_s = 72;$
$V_{mpp} = 33.7\ (V)$	$R_s = 0.47\ (\Omega)$
$P_{mpp} = 120\ (W)$	$R_{sh} = 1365\ (\Omega)$
$k_v = -0.160 \pm 0.01$	$A = 1.397$

All the above parameters are considered in Standard Test Conditions (STC), and they are given in the product data-sheet, except the last three, R_s, R_{sh} and A, which have been calculated from the data-sheet values, as shown in the previous section.

B. Expression of photo-current I_{ph} and dark saturation current I_o

The first equations when constructing the model are the expressions of I_o from (3) and I_{ph} from (5), in STC.

$$I_o = \left(I_{sc} - \frac{V_{oc} - I_{sc}\, R_s}{R_{sh}} \right) e^{-\frac{V_{oc}}{ns\ V_t}} \tag{20}$$

$$I_{ph} = I_o\, e^{\frac{V_{oc}}{ns\ V_t}} + \frac{V_{oc}}{R_{sh}} \tag{21}$$

The above expressions are considered in STC. To include the effects of the environment, e.g. temperature and irradiance, these equations has to be completed with the corresponding terms.

C. The short-circuit current and photo-current irradiance dependence

Both of them are considered to be directly proportional to the irradiation.

$$\begin{aligned} I_{sc}(G) &= I_{sc} G \\ I_{ph}(G) &= I_{ph} G \end{aligned} \tag{22}$$

D. The open-circuit voltage irradiance and temperature dependence

In order to include the irradiance dependence in the equation of V_{oc}, the open-circuit voltage can be expressed from (5):

$$V_{oc}(G) = \ln \left(\frac{I_{ph}(G)\, R_{sh} - V_{oc}(G)}{I_o\, R_{sh}} \right) n_s\ V_t \tag{23}$$

The above equation needs to be solved numerically. Using the Newton-Raphson algorithm, the result can be found after a few iterations, using the open-circuit voltage at STC. The open-circuit voltage shows a linear dependence with the temperature:

$$V_{oc}(T) = V_{oc} + k_v (T - T_{stc}) \tag{24}$$

E. Short-circuit current temperature dependence

The short-circuit current of the PV panel depends linearly on the temperature:

$$I_{sc}(T) = I_{sc}(1 + \frac{k_i}{100}(T - T_{stc})) \tag{25}$$

F. Temperature dependence for the dark saturation current

According to Castañer and Silvestre [5], the dark saturation current does not depend on the irradiance conditions , but it shows a strong dependence with temperature. Similar approach is adopted by Rauschenbach, in [6], where the dark current is considered independent on irradiation. However, the temperature dependence is not discussed there. Castañer and Silvestre give a formula which shows a non-linear dependence with temperature:

$$J_o = B T^{XTI} e^{-\frac{E_g}{kT}} \tag{26}$$

where J_o is the dark saturation current density, B and XTI are constants independent on temperature, and E_g is the semiconductors band gap energy. Xiao et al, in [7] consider that the dark saturation current is dependent on both the irradiance and temperature, and give the following formula for I_o:

$$I_o(G,T) = \frac{I_{ph}(G,T)}{e^{\frac{V_{oc}(T)}{V_t(T)}} - 1} \tag{27}$$

Gow and Manning, in [8], and after them, Walker in [9], use a cubic dependence of I_o on temperature:

$$I_o(T) = I_o(T_1) \left(\frac{T}{T_1} \right)^{\frac{3}{A}} e^{\frac{-qV_g}{nk}(1/T1 - 1/T2)} \tag{28}$$

where $I_o(T_1)$ is the dark current calculated at a given reference (standard) temperature. V_g is the band gap energy of the semiconductor.

G. The proposed method for $I_o(T)$

This work proposes the inclusion of temperature effects in the dark current using a similar approach as in the case of the photo-current in (21) and (30), by updating the parameters of (20) with their corresponding temperature coefficients:

$$I_o(T) = \left(I_{sc}(T) - \frac{V_{oc}(T) - I_{sc}(T)\, R_s}{R_{sh}} \right) e^{-\frac{V_{oc}(T)}{n_s\, V_t}} \quad (29)$$

As the expression of I_o in (20) is valid in STC (based on the Shockley equations), it is a natural step to consider it valid also at other temperatures than the STC, as the Shockley equation includes the temperature effects. The temperature dependence of all the parameters in (20) is given in the data sheet.

H. Temperature dependence of the photo-current

The photo-current temperature dependence can be expressed by including in (21) the temperature effect:

$$I_{ph}(T) = I_o(T)\, e^{\frac{V_{oc}(T)}{n_s\, V_t}} + \frac{V_{oc}(T)}{R_{sh}} \quad (30)$$

I. Full-characteristic model

Until this point, temperature and irradiance dependence of the parameters of (1) has been expressed. The parameters in (22), (23), (24), (25), (29), (30) can be inserted in (1) to obtain the I-V relationship of the PV panel, which takes into account the the irradiance and temperature conditions. It should be noted that in order to include in one equation both the irradiation and temperature effects, the principle of superposition is applied.

If one wants to take into account also the reverse characteristics of the PV panel (the second quadrant), e.g. for modeling the effects of partial shading, (1) can be completed with the terms describing the reverse characteristic. In the literature can be found different approaches for modeling the reverse characteristic ([10], [11], [12]), but the most used method is the one described by Bishop in [10]:

$$i = I_{ph} - I_o\, e^{\frac{v + i\, R_s}{n_s\, V_t}} - \frac{(v + i\, R_s)}{R_{sh}} \left(1 + a \left(1 - \frac{v + i\, R_s}{n_s\, V_{br}} \right)^{-m} \right) \quad (31)$$

In the above equation, m is the avalanche breakdown exponent, a is the fraction of the ohmic current in the avalanche breakdown, and V_{br} is the cell junction breakdown voltage [11], [10]. It should be noted that in practice the PV panels have bypass diodes installed, in order to avoid avalanche breakdown of the cells in case of partial shading. Typically is not possible for a panel to enter to the second quadrant of the characteristics, only for individual cells, or a group of cells ($n_s = 1$ and up to several).

IV. Simulation Results

The equations from the previous section has been implemented in Matlab, in order to verify the model in different temperature and irradiance conditions. The results have been compared to the characteristics and values provided by the product data-sheet.

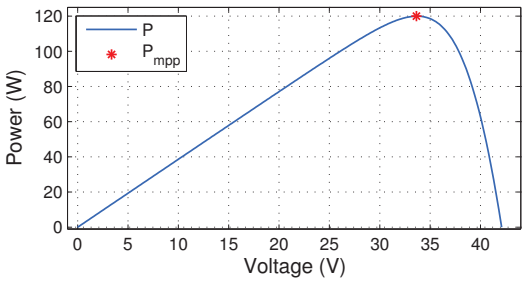

Fig. 3. V-P characteristic of the BP-MSX120 model in STC

The temperature dependencies of the model's V-I curve have been verified by plotting the characteristics for four different temperatures.

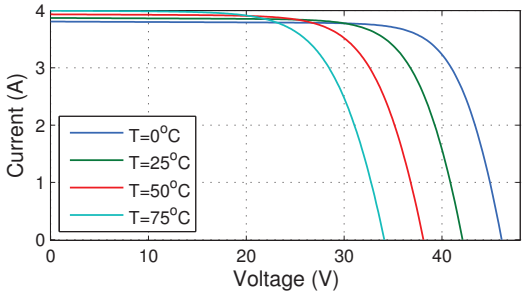

Fig. 4. Voltage-Current characteristics of the PV panel model at four different temperatures and standard irradiation

It can be seen on the above figures, that the short-circuit current, the open-circuit voltage, and the maximum power are in very good agreement with the data-sheet values. The change in the open-circuit voltage and short-circuit current are in accordance with the temperature coefficients given in the data-sheet.

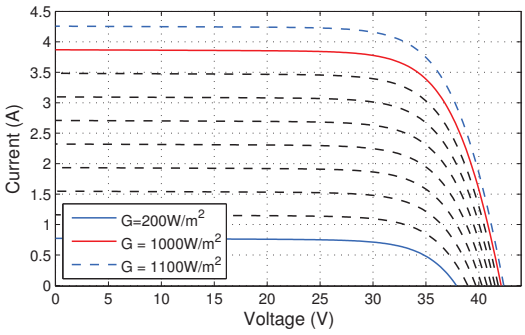

Fig. 5. V-I characteristics of the model at different irradiances and standard cell temperature

From the above figures it can be noted that, according to the theory, the short-circuit current shows a linear dependence with the irradiation, unlike the open-circuit voltage, which

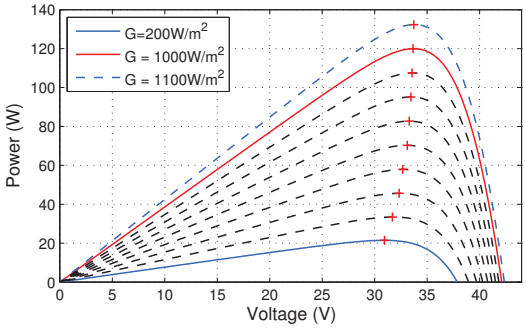

Fig. 6. V-P characteristics of the model at different irradiations and standard temperature

increases logarithmically with the irradiation.
The two-quadrant I-V characteristic of a cell can be plotted by setting the parameters a, m, and V_{br} to the desired values. More details can be found in [10], [12] and [11].

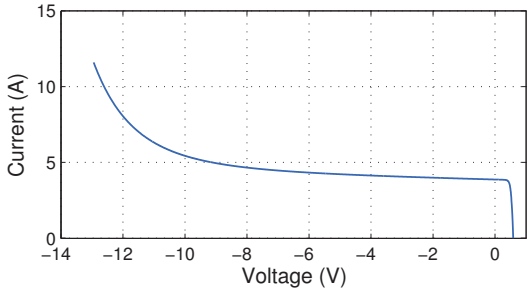

Fig. 7. Full characteristic of a PV cell using the single-diode model

Fig. 8 and 9 show that using the proposed method, the P-V characteristic of the panel is kept within the tolerance limits given in the product datasheet for both 50^oC and 75^oC . The method described in [7] performs similar to the one described here, exceeding with only a small amount the upper tolerance limit at 50^oC. The method presented in [8] predicts a lower power than the tolerance limits of the datasheet, for both considered temperatures.

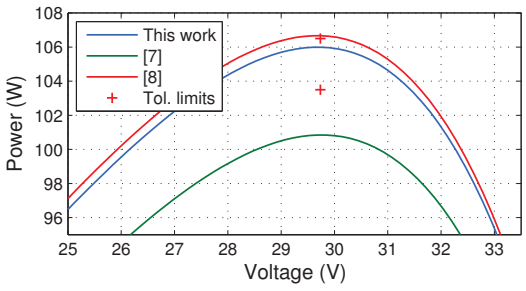

Fig. 8. Simulated P(V) characteristics in the vicinity of MPP using three different methods for temperature dependence of the dark saturation current, at 50^oC

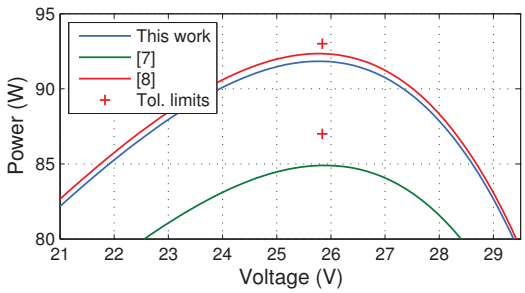

Fig. 9. Simulated P(V) characteristics in the vicinity of MPP using three different methods for temperature dependence of the dark saturation current at 75^oC

V. Conclusions

A model for photovoltaic panels, based exclusively on datasheet parameters has been developed and implemented. The method for extracting the panel parameters from datasheet values has been presented, and the obtained values have been used in the implemented model. The model exhibits a very good agreement with all the specifications given in the product datasheet. A new approach for modeling the temperature dependence of the dark saturation current has been proposed, and compared to the other presented methods. The results show that it gives better correlation with the datasheet values.

References

[1] [s.n.], "Trends in photovoltaic applications. survey report of selected iea countries between 1992 and 2005," International Energy Agency, Report IEA-PVPS Task 1 IEA PVPS T1-15:2006, 2006. [Online]. Available: http://www.iea-pvps.org/products/download/rep1_15.pdf

[2] D. Chan and J. Phang, "Analytical methods for the extraction of solar-cell single- and double-diode model parameters from i-v characteristics," *Electron Devices, IEEE Transactions on*, vol. 34, no. 2, pp. 286–293, 1987.

[3] M. Chegaar, Z. Ouennoughi, and A. Hoffmann, "A new method for evaluating illuminated solar cell parameters," *Solid-state electronics*, vol. 45, pp. 293–, 2001, oK.

[4] G. Araujo and E. Sanchez, "A new method for experimental determination of the series resistance of a solar cell," *Electron Devices, IEEE Transactions on*, vol. 29, no. 10, pp. 1511–1513, 1982, nG.

[5] L. Castaner and S. Silvestre, *Modelling photovoltaic systems using PSpice*. John Wiley and Sons, LTD, 2002.

[6] H. Rauschenbach, "Electrical output of shadowed solar arrays," *Electron Devices, IEEE Transactions on*, vol. 18, no. 8, pp. 483–490, 1971.

[7] W. Xiao, W. Dunford, and A. Capel, "A novel modeling method for photovoltaic cells," in *Power Electronics Specialists Conference, 2004. PESC 04. 2004 IEEE 35th Annual*, vol. 3, 2004, pp. 1950–1956 Vol.3.

[8] J. Gow and C. Manning, "Development of a photovoltaic array model for use in power-electronics simulation studies," *Electric Power Applications, IEE Proceedings-*, vol. 146, no. 2, pp. 193–200, 1999.

[9] G. Walker, "Evaluating mppt converter topologies using a matlab pv model," *Journal of electrical and electronics engineering, Australia*, vol. 21, pp. 49–55, 2001.

[10] J. Bishop, "Computer simulation of the effect of electrical mismatches in photovoltaic cell interconnection circuits." *Solar cells*, vol. 25, pp. 73–89, 1988.

[11] M. Alonso-Garcia and J. Ruiz, "Analysis and modelling the reverse characteristic of photovoltaic cells," *Solar Energy Materials and Solar Cells*, vol. 90, no. 7-8, pp. 1105–1120, May 2006.

[12] V. Quaschning and R. Hanitsch, "Numerical simulation of photovoltaic generators with shaded cells," in *Universities Power Engineering Conference*, vol. 30th, 1995, pp. 583–586.

Publication 6

PV inverter test setup for European efficiency, static and dynamic MPPT efficiency evaluation

by M. Valentini, A. Raducu, D. Sera, and R. Teodorescu

PV Inverter Test Setup for European Efficiency, Static and Dynamic MPPT Efficiency Evaluation

Massimo Valentini, Alin Raducu, Dezso Sera and Remus Teodorescu
Aalborg University, Institute of Energy Technology
DK-9220 Aalborg, Denmark
Email: s08masv@ponstud.aau.dk, s08alinr@ponstud.aau.dk,
des@iet.aau.dk, ret@iet.aau.dk

***Abstract*—This paper concerns the evaluation of performance of grid-connected PV inverters in terms of conversion efficiency, European efficiency, static and dynamic MPP efficiency. Semi-automated tests were performed in the PV laboratory of the Institute of Energy Technology at the Aalborg Univeersity (Danmark) on a commercial transformerless PV inverter. Thanks to the available experimental test setups, that provide the required high measuring accurancy, and the depeloped PV simulator, which is required for MPPT performance evaluation, PV inverters can be pretested before beeing tested by accreditated laboratories.**

I. Introduction

The exponential trend of the worldwide installed PV capacity experienced in the last years, shows that the PV technology has the prospective to play an important rule towards a sustainable energy system [1]. The estimation of the pay back time and the profitability of grid-connected photovoltaic (PV) systems requires information about performance of PV modules and inverters. For this reason, the attention is strongely paid on the efficiency.

This paper concerns the evaluation of the efficiency of grid-connected PV inverters. They are normally compared based on the so called European efficiency η_{EURO} which is a weighted conversion efficiency that considers several operating conditions [2]. Also the conversion efficiency is a decisive sale factor for PV inverters and therefore it strongly affects the price; the relation between conversion efficiency and price is presented in reference [2] where the analysis is based on a market survey of all PV inverter available in Germany [3].

More attention has been paid on the Maximum Power Point Tracker (MPPT) as the PV industry aims to reduce the cost associated with PV inverters by increasing the overall efficiency. The MPPT is the fundamental component for the maximization of the output power of a PV array [2] [4]. It attemps to set the system working point to the optimum, independent of weather conditions (i.e. solar irradiance and temperature). At the moment no standardized test procedures for the MPPT performance evaluation are available but several proposals exist [5] [6].

The effectiveness of the selected MPP tracking algorithm affects the overall efficiency of a grid-connected PV inverter. For this reason the so called total efficiency has been introduced to account both the conversion efficiency η and the MPPT efficiency η_{MPPT}; it is defined as the product $\eta_{tot} = \eta \cdot \eta_{MPPT}$ [7].

Both the conversion efficiency and the MPPT efficiency depend on the actual power and the dc voltage [2] [8]. In many cases only maximum values are shown to constumers; only in few cases η and η_{MPPT} are evaluated in the entire ac power range at different dc voltages (usually three levels - minimum, rated and maximum dc voltages) [7] [9].

The main goal of this paper is to show the facilities developed at the PV laboratory of the Insititute of Energy Technology (IET) at Aalborg University (Denmark) for PV inverters performance evaluation. An example of test results for a commercial grid-connected PV inverter is given. Test results regard conversion efficiency, European efficiency, static and dynamic MPPT efficiencies.

II. Conversion efficiency

For safety reasons, most grid-connecteed PV converters have a galvanic isolation which comprises a transformer that can either be placed in the dc-dc converter in the form of a high frequency transformer, or on the ac output side, in the form of a low frequency transformer [10]. In any cases, the galvanic isolation increases the cost and size of the whole system and decreases the overall efficiency of the PV converter. A higher efficiency, smaller size and weight and a lower price for the inverter can be achieved if the isolation transformer is omitted. However transformerless solutions present some safety issues caused by the solar panel parasitic capacitance to ground [10] [11].

The increased conversion efficiency of transformerless PV inverters is within $1\% - 2.5\%$ with respect to PV inverters with galvanic isolation [7].

A. Experimental test setup for conversion efficiency evaluation

A block diagram of the experimental test setup is shown in Fig.1. The setup includes a controllable dc power supply (Magna Power Electronics 1000V/45A) that feeds the PV inverter. The inverter input power P_{dc} and output power P_{ac} are measured using the precision power analyzer Yokogawa WT3000 which is characterized by a power accuracy of $\pm 0.02\%$ of reading at full scale. P_{dc} and P_{ac} are acquired using LabVIEW with a sampling period of $200ms$; it calculates the sampled conversion

Authorized licensed use limited to: Aalborg Universitetsbibliotek. Downloaded on January 25, 2009 at 12:40 from IEEE Xplore. Restrictions apply.

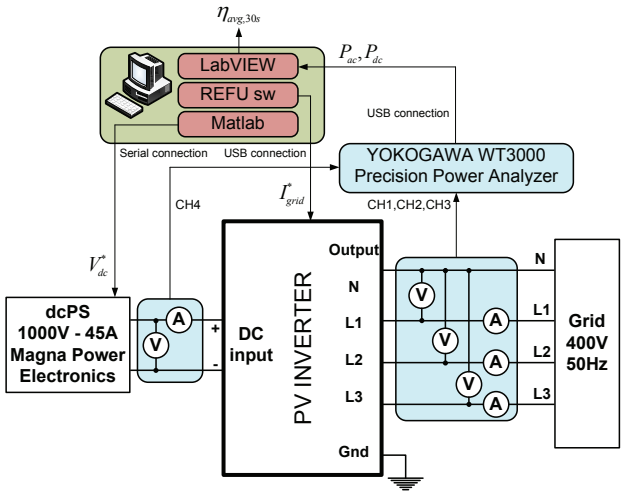

Fig. 1. Block diagram of the experimental test setup for the evaluation of the conversion efficiency. $\eta_{avg,30s}$ - conversion efficiency averaged over $30s$ time intervals; V^*_{dc} - reference dc voltage; I^*_{grid} - amplitude of the reference grid current.

efficiency $\eta(k)$ as the ratio:

$$\eta(k) = \frac{P_{ac}(k)}{P_{dc}(k)} \tag{1}$$

LabVIEW finally averages $\eta(k)$ over $30s$ time intervals. Each measure is characterized by a specific dc voltage and ac power; the dc voltage is varied by means of a Matlab script that comunicates with the dc power supply through a serial connection whereas the ac power is controlled by varing the amplitude of the reference grid current with the inverter operating in Power Supply (PS) mode.

III. European Efficiency

The most used factor for comparing grid-connected PV inverters is the so called European efficiency, which is a weighted conversion efficiency. It is a useful comparative tool for designers and consumers, as systems are installed in a wide range of solar resource regimes. It aims to approximate the integral of the conversion efficiency versus time over the entire day. The European efficiency is defined as follows [7] [12]:

$$\begin{aligned}\eta_{EURO} &= 0.03 \cdot \eta_{5\%} + 0.06 \cdot \eta_{10\%} + 0.13 \cdot \eta_{20\%} + \\ &+ 0.10 \cdot \eta_{30\%} + 0.48 \cdot \eta_{50\%} + 0.20 \cdot \eta_{100\%}\end{aligned}$$

where $\eta_{i\%}$ is the conversion efficiency at $i\%$ of the inverter ouput rated power.

IV. MPPT efficiency

In order to correctly characterize PV inverters performance, the MPP tracking must be evaluated. In fact, apart from the conversion efficiency, the MPPT efficiency also produces a reduction of the inverter output power with respect to the available power. In the last years, MPPT performance has become a sale argument for manufacturers [6]. However there are no standards which define how to evaluate MPPT performance but some proposals are presented in the literature [5] [6].

To evaluate MPPT performance, a flexible PV array simulator is required [6] [13] [14]. MPPT performance evaluation is a problematic task; in fact for most commercial PV inverters η_{MPPT} is above 99% in most of the ac power-dc voltage range [8]. It yields that a very high accurancy is a fundamental feature for the measuring system and the PV simulator (i.e. high resolution is required around the MPP on the I-V curve). Having the suitable experimental test setup, measuring static MPPT performance is rather straightforward. On the contrary, the determination of dynamic MPPT performance is a challenging task as operating conditions can be changed in many ways [12] [13] [14].

The behaviour of the MPPT can be analyzed both in static and dynamic conditions; the static MPPT efficiency describes the ability of the MPPT to find and hold the MPP under constant environmental conditions (i.e. solar irradiance and cell-temperature) whereas the dynamic MPPT efficiency describes the ability in tracking the MPP in case of variable conditions [5] [6]. The MPPT efficiency is calculated as follows:

$$\eta_{MPPT}(t) = \frac{P_{PV}(t)}{P_{MPP}(t)} \cdot 100 \tag{2}$$

where

- $P_{PV}(t)$ is the output power of the programmable dc power supply included in the PV simulator;
- $P_{MPP}(t)$ is the power at the MPP.

In case of discrete time calculations, the above variables are sampled, thus the MPPT efficency at each sample is calculated as follows:

$$\eta_{MPPT}(k) = \frac{P_{PV}(k)}{P_{MPP}(k)} \cdot 100 \tag{3}$$

In static conditions, $\eta_{MPPT}(t)$ is averaged over a specfied period when the steady state is achieved and no further variations of $\eta_{MPPT}(t)$ occur; depending on the operating conditions, the transient can take several seconds.

In dynamic conditions, when the MPP changes due to irradiance variations, the MPP tracking is usually analyzed using staircase or trapezoidal irradiance profiles [12] [15]. Knowing the values of $P_{MPP}(t)$ and $P_{PV}(t)$ during the dynamic test, the equivalent efficiency can be calculated as follows [15]:

$$\eta_{MPPT} = 100 \frac{\int_0^{T_0} P_{PV}(\tau) d\tau}{\int_0^{T_0} P_{MPP}(\tau) d\tau} \tag{4}$$

where T_0 is the test period. In case of a discrete time calculation with sampling time T_s, the MPPT efficency at each sample is calculated as follows:

$$\eta_{MPPT} = \frac{\sum_{k=1}^{N} P_{PV}(k) T_s}{\sum_{k=1}^{N} P_{MPP}(k) T_s} = \frac{\sum_{k=1}^{N} P_{PV}(k)}{\sum_{k=1}^{N} P_{MPP}(k)} \tag{5}$$

A. PV simulator

A flexible PV array simulator has been developed in the PV laboratory of the Institute of Energy Technology at Aalborg University (Denmark). It is based on the

Authorized licensed use limited to: Aalborg Universitetsbibliotek. Downloaded on January 25, 2009 at 12:40 from IEEE Xplore. Restrictions apply.

model of a PV panel which is composed by n_s series connected solar cells. Several methods for the PV module characterization are presented in the literature, mainly based on the measurement of the I-V curve. However, the developed PV simulator is based on the model of the PV panel from only the values provided by the manufacturer data sheet [16].

1) PV panel model: The equivalent circuit of the single-diode model for PV cells is shown in Fig.2 [16].

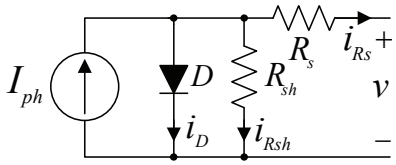

Fig. 2. Equivalent circuit of a photovoltaic cell based on the single-diode model.

The general current-voltage characteristic of a PV panel based on the single exponential model is [16]:

$$i = I_{ph} - I_o \left(e^{\frac{v+iR_s}{n_s V_t}} - 1 \right) - \frac{v + iR_s}{R_{sh}} \tag{6}$$

In the above equation, V_t is the junction thermal voltage:

$$V_t = \frac{AkT_{stc}}{q} \tag{7}$$

where:

- I_{ph} - the photo-generated current in Standard Test Conditions[1] (STC)
- I_o - dark saturation current in STC
- R_s - panel series resistance
- R_{sh} - panel parallel (shunt) resistance
- A - diode quality (ideality) factor

are the five parameters of the model, while k is Boltzmann's constant, q is the charge of the electron, n_s is the number of series cells in the PV module, and T_{stc} ($^\circ K$) is the temperature at STC. The five above parameters can be obtained from the PV model data sheet as it is explained in [16]. The model of the entire PV panel array can be obtained by considering that it is composed by N_{sp} strings in parallel, each one composed by N_{ps} panels in series.

The model takes into account irradiance and PV panel temperature dependencies. In order to get one equation with both irradiation and temperature effects, the superposition principle is applied. The irradiance dependence is taken into account by Eq.8, where it can be seen that the short circuit current I_{sc} is directly proportional to the irradiance [16]:

$$I_{sc}(G) = I_{sc,stc}\frac{G}{G_{stc}} \tag{8}$$

where $G_{stc} = 1000W/m^2$ is the irradiance is STC. The temperature dependence is taken into account by Eq.s 9 and 10 [16].

$$V_{oc}(T) = V_{oc} + k_v(T - T_{stc}) \tag{9}$$

[1]Irradiance level of $1000W/m^2$, with the reference air mass 1.5 solar spectral irradiance distribution and cell junction temperature of $25^\circ C$.

$$I_{sc}(T) = I_{sc}\left[1 + \frac{k_i}{100}(T - T_{stc})\right] \tag{10}$$

where:

- T is the PV module operating temperature in $^\circ C$;
- k_v and k_i are respectively V_{oc} and I_{sc} temperature coefficients available in the data sheet .

2) Real-time implementation: The PV simulator comprices two programmable series connected Delta Elektronika SM300-10 dc power supplies ($V_{1max} = 300V$, $V_{2max} = 330V$, $I_{max} = 10A$). The ouput voltage are controlled in real time by a DS1103 dSpace system, according to the model of the PV array. The model is based on a number of series/parallel connected BP-MSX120 PV panels.

B. Experimental test setup for MPPT evaluation

A block diagram of the experimental test setup is shown in Fig.3. The inverter input power P_{dc} is measured

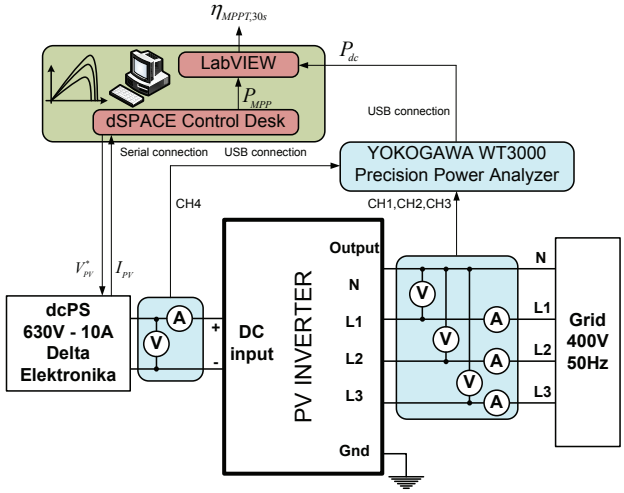

Fig. 3. Block diagram of the experimental test setup for MPPT performance evaluation. $\eta_{MPPT,30s}$ - MPPT efficiency averaged over 30s time intervals; I_{PV} - measured dc current; V^*_{PV} - reference dc voltage.

using the precision power analyzer Yokogawa WT3000 which is characterized by a power accuracy of $\pm 0.02\%$ of reading at full scale. P_{dc} is acquired using LabVIEW with a sampling period of $200ms$; it calculates the sampled MPPT efficiency $\eta_{MPPT}(k)$ according to Eq.3. In case on static MPPT evaluation, LabVIEW averages $\eta_{MPPT}(k)$ over the desired period.

V. Experimental tests and results

An example of test results on a commercial PV inverter is given; tests concer conversion efficiency, European efficiency, static and dynamic efficiency. The PV inverter under test is the transformerless Refusol 11kW from REFU Elektronik GmbH, Germany. Measurement were carried out in the PV laboratory of the Insititute of Energy Technology at Aalborg University (Denmark).

A Graphical User Interface (GUI) for real time evaluation has been developed using dSPACE ControlDesk; it is shown in Fig.4. The GUI offers the flexibility of simulating different PV panel arrays in specified environmental

Authorized licensed use limited to: Aalborg Universitetsbibliotek. Downloaded on January 25, 2009 at 12:40 from IEEE Xplore. Restrictions apply.

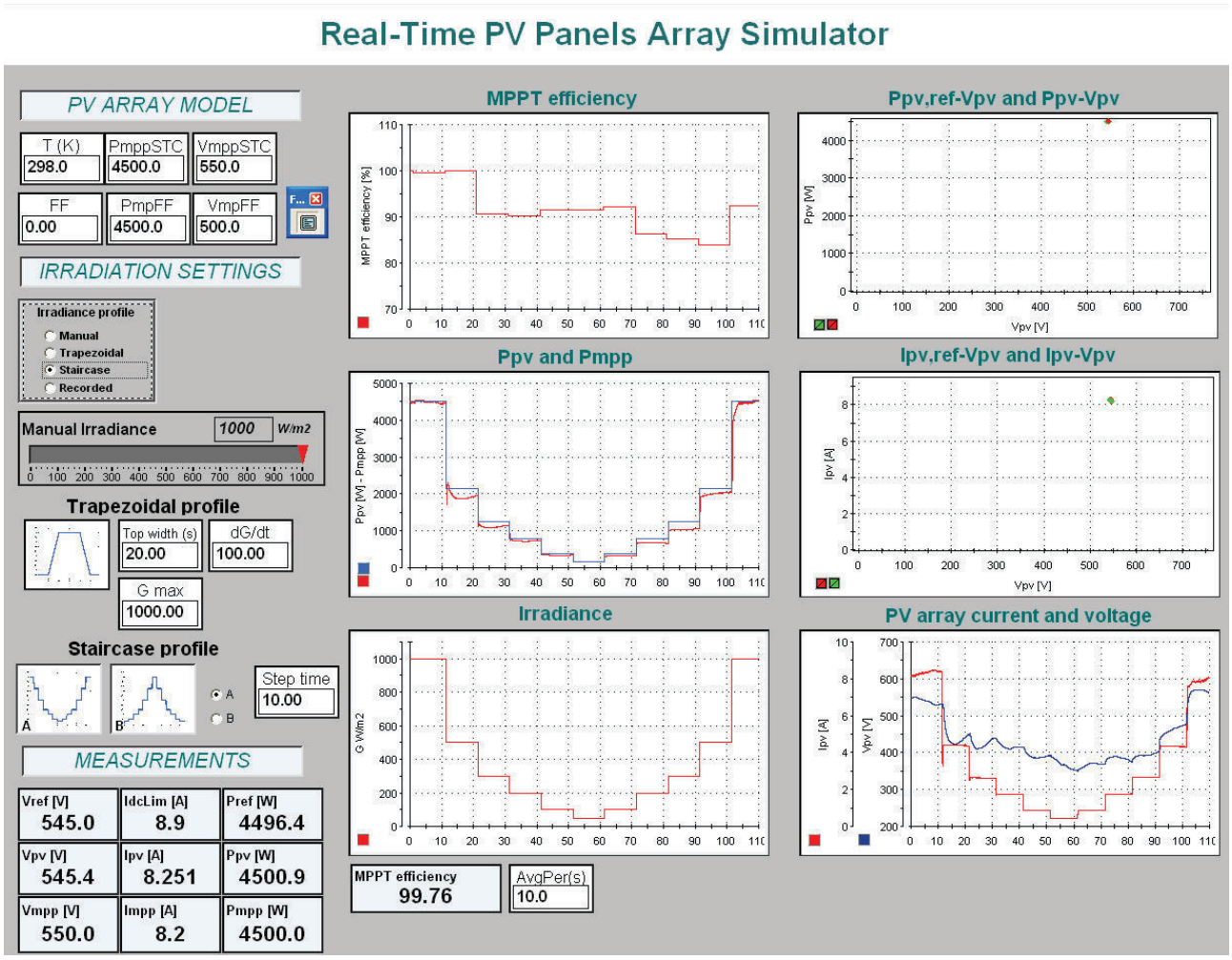

Fig. 4. Control Desk graphical user interface of the PV array simulator showing test results on a commercial PV inverter.

conditions. The PV array simulator can be used for testing the MPPT in two ways:

- simulating a specific PV panel array in specific environmental conditions. Thus, inputs are the MPP power and MPP voltage in STC and environmental conditions (PV module temperature and irradiance profile);
- specifying the MPPT at the desired operating condition. Thus, inputs are MPP power and MPP voltage and fill factor.

When the fill factor is set to zero, the first option is enabled, meaning that the PV module temperature and the irradiance have to be defined; in this case the following options for the irradiance are available:

- manual, where G is set to the desired constant value;
- trapezoidal, where G is a trapezoidal profile characterized by the desired maximum irradiance G_{max}, the top width and slope dG/dt;
- staircase, where G is a staircase profile (increasing or decreasing with respect to the first half) characterized by the desired step time;
- recorded, where G is a custom profile recorded in the PV simulator; it can be a measured irradiance profile.

Measurements were performed with fill factor of 0.7 and line-to-line grid voltage of $400V$.

A. Conversion efficiency

To demonstrate the dependence of the conversion efficiency on the dc voltage and the ac output power, the dc voltage range $[V_{min} = 200V; V_{max} = 800V]$ was devided in 21 steps of $30V$ and the ac power range in 24 steps from 5% to 120% of the output rated power. It results in a set of 504 measurements. In each measure the ac output power was regulated by controlling the amplitde of the reference grid current by means of the REFU software whereas the dc voltage was regulated by means of the serial connection between the programmable dc power supply (Magna Power Electronics 1000V/45A) and the remote computer. Experimental results are presented in Fig.5 as 3D mapping plot in the ac power versus dc voltage plane. The power is normalized according to the inverter nominal power and is stated as a percentage.

The area with the maximum efficiency is represented in brown, where the measured efficiency is above 98.0%. The maximum value is 98.1% which corresponds to $V_{dc} = 590V$ and $P_{ac\%} = 80\%$. Even below 10% of the rated power, the conversion efficiency decreases to the acceptable value of 95.0%. The white area in Fig.5

Authorized licensed use limited to: Aalborg Universitetsbibliotek. Downloaded on January 25, 2009 at 12:40 from IEEE Xplore. Restrictions apply.

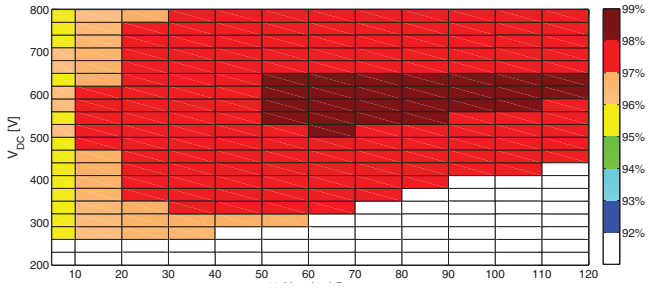

Fig. 5. Measured conversion efficiency shown as a 3D mapping plot in the ac power versus dc voltage plane.

represents the locus of forbidden operating points where the inverter is not capable to provide the required ac power at the specified dc voltage.

The conversion efficiency is also plotted in Fig.6 at four significant voltages; selected levels are:

- $V_{dc} = 440V$, which is the lowest dc voltage at which the inverter can work in the entire ac power range;
- $V_{dc} = 590V$, which is the dc voltage at which the highest conversion efficiency has been measured;
- $V_{dc} = 800V$, which is the highest dc voltage at which the inverter can work;
- $V_{dc} = 710V$, which is in the middle voltage between $V_{dc} = 590V$ and $V_{dc} = 800V$.

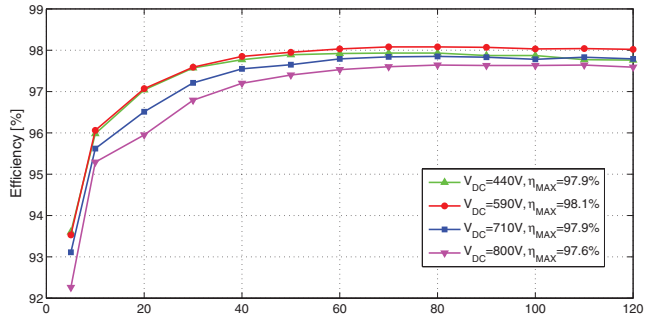

Fig. 6. Measured conversion efficiency versus the ac power at four dc voltage levels.

Fig.s 5 and 6 prove that the conversion efficiency is not only affected by the inverter output power but also by the dc voltage; in most cases, this dependence is not shown to customers in manufacturers' datasheets.

According to the IEC 61683, the worst accuracy on the conversion efficiency can be calculated as follows [17]:

$$max\ deviation = \pm 0.2 \cdot (1 - \eta) \cdot \eta[\%] \qquad (11)$$

Given $\eta_{max} = 98.1\%$, the worst accuracy is $\pm 0.38\%$; the accuracy guaranteed by the measuring system is definitely below this value thanks to the precision power analyzer Yokogawa WT3000 (an accurancy around $\pm 0.14\%$ is expected in the worst case) [2].

B. European Efficiency

Having the conversion efficiency in the entire ac power and dc voltage ranges, the European efficiency was easily calculated at different dc voltage levels (21 steps of 30V from $V_{min} = 200V$ to $V_{max} = 800V$). However only dc voltage levels at which the PV inverter is able to provide the rated power are considered. Therefore the calculation of η_{EURO} is restricted within $[410V; 800V]$. The European efficiency at different dc voltage levels is presented in Fig.7.

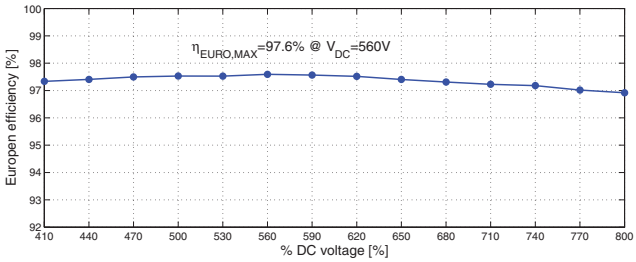

Fig. 7. European efficiency at different dc voltage levels.

The maximum European efficiency is $\eta_{EURO,max} = 97.6\%$ and is achieved at $V_{dc} = 560V$. Two considerations lead from Fig.7:

- the dependence of η_{EURO} on the dc voltage is not strong, meaning that η_{EURO} is almost constant in the entire voltage range;
- η_{EURO} is only slightly below the maximum conversion efficiency, indicating an optimal inverter topology [8].

C. Static MPPT efficiency

In static conditions, the sampled MPPT efficiency $\eta_{MPPT}(k)$ is averaged over $30s$ time intervals when no further variations occur; a stabilization time of 60s is a resonable choice.

The static MPPT efficiency was measured at different MPP voltage levels and MPP power levels (15 steps). The voltage is varied from the minimum MPP voltage $V_{min} = 200V$ to the maximum voltge of the PV simulator with $30V$ steps. This results in 90 measurements presented in Fig.8 using a three-dimentional representation.

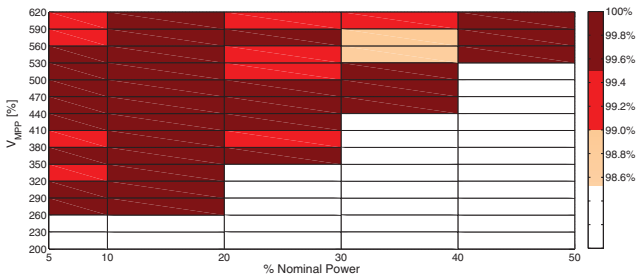

Fig. 8. Measured static MPPT efficiency shown as a 3D mapping plot in the ac power versus MPP voltage plane.

From Fig.8 it can be concluded that the inverter under test has a high static MPPT efficiency. The maximum value is 99.9% and corresponds to $V_{MPP} = 440V$ and $P_{dc\%} = 30\%$. Even below 10% of the dc nominal power, the MPPT efficiency is high. In the white area, the static MPPT effciciency can not be measured due to the limitation of the dc power supplies used in the PV simulator.

Authorized licensed use limited to: Aalborg Universitetsbibliotek. Downloaded on January 25, 2009 at 12:40 from IEEE Xplore. Restrictions apply.

D. Dynamic MPPT efficiency

In dynamic conditions the MPP tracking is usually analyzed using staircase or trapezoidal irradiance profiles [12] [15]. Here, a trapezoidal irrandiance profile is used. It is shown in Fig.9.

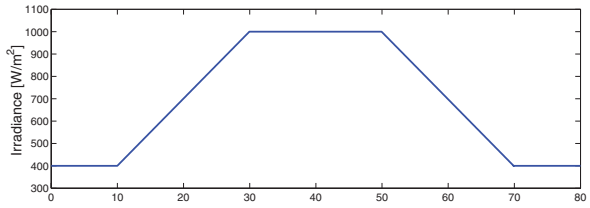

Fig. 9. Trapezoidal irrandiance profile for dynamic MPPT performance.

Fig.9 represents a fast irradiance variation at which many PV inverters can experience some troubles in the tracking (e.g. the MPP is reached slowly and thus η_{MPP} drops drastically).

The MPPT efficiency measured during the test is shown in Fig.10.

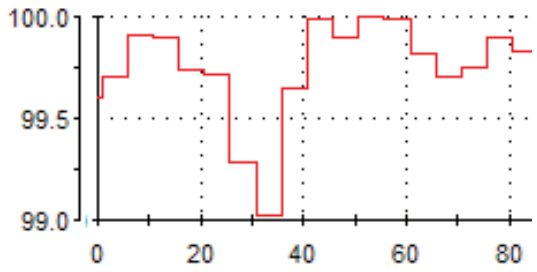

Fig. 10. Measurement MPPT efficiency (averaged over 1sec) during the trapezoidal irradiation profile (see Fig.9).

CONCLUSIONS

The main goals of this paper are (i) to show the facilities developed at the PV laboratory of the Institute of Energy Technology at the Aalborg University (Danmark) for PV inverter performance evaluation and (ii) to give an example of test results for a commercial PV inverter. Thanks to the available experimental test setups, PV inverters can be pre-tested before beeing tested by accreditated laboratory. The PV laboratory does not claim to be an accreditated laboratory but it provides good facilities to support courses dealing with the PV technology. The PV simulator included in this paper will be included in a PhD/industrial course about PV systems (visit the IET home page: www.iet.aau.dk).

ACKNOWLEDGMENT

We would like to acknowledge the suport from REFU Elektronik GmbH in providing the commercial PV inverter.

REFERENCES

[1] "Trends in photovoltaic applications. Survey report of selected IEA countries between 1992 and 2005", International Energy Agency, Report IEA-PVPS Task 1 T1-15:2006, 2006. [Online]. Available: http://www.iea-pvps.org/products/download/rep1_15.pdf

[2] F. Baumgartner, H. Schmidt, B. Burger, R. Bründlinger, H. Häberlin and M. Zehner, "Status and relevance of the dc voltage dependency of the inverter efficiency", in *22nd European Photovoltaic Solar Energy Conference and Exhibition*, no. Session 4DO.4.6, 3-7 September 2007.

[3] "Inverter market survey Germany", PHOTON, Vol. March 2007, 2007.

[4] D. Sera, R. Teodorescu and F. Blaabjerg, "New control strategies and more energy from PV systems for residential applications: State-of-art study of PV technology, modelling and MPPT algorithms", Institute of Energy Technology, Aalborg University, 2005.

[5] R. Brundlinger, B. Bletterie and J. Brand, "A new method for the assessment of the dynamic MPP tracking performance based on compressed high-resolution irradiance patters", abstract submitted for th 20th European PVSEC and Exibition, CCIB, 6-10 June 2005, Barcellona, Spain.

[6] B. Bletterie, R. Bruendlinger and S. Spielauer, "Quantifying dynamic MPPT performance under realistic conditions first test results Ű the way forward," in *21st European Photovoltaic Solar Energy Conference and Exhibition, Dresden, Deutschland*, 4-8 September 2006.

[7] H. Haeberlin, L. Borgia, M. Kaempfer and U. Zwahlen, "New tests at grid-connected PV inverters: Overview over test results and measured values of the total efficiency η_{tot}", in *21nd European Photovoltaic Solar Energy Conference, Dresden, Germany*, Sept. 2006.

[8] H. Neuenstein, "Testing SMA's SMC 8000TLI", PHOTON International, Vol. October 2007, Pag. 106-113, 2007.

[9] "Test report: Solarmax 25C from sputnik engineering AG", Berner Fachhochschule, Hochschule fur Technik und Informatik, Fachbereich Elektro-und Kommunikationsechnik, kompetensgruppe Energiesysteme Photovoltaik-Labor, CH-3400 Burgorf, Tech. Rep., 9 June 2006. Available: http://labs.hti.bfh.ch/fileadmin/user_upload/lab1/pv/wr_testberichte/Test_Report_SM25C_en_09_06_06_new_MPP_www.pdf

[10] T. Kerekes, R. Teodorescu, C. Klumpner, M. Sumner, D. Floricau and P. Rodríguez, "Evaluation of three-phase transformerless photovoltaic inverter topologies", in *2007 European Conference on Power Electronics and Applications, Pag. 1 - 10*, 2-5 Sept. 2007.

[11] T. Kerekes, R. Teodorescu and U. Borup, "Transformerless photovoltaic inverters connected to the grid", in *Applied Power Electronics Conference, APEC 2007 - Twenty Second Annual IEEE, Pag. 1733 - 1737*, Feb. 25 2007-March 1 2007.

[12] W. Bower, C. Whitaker, W. Erdman, M. Behnke and M. Fitzgerald, "Performance test protocol for evaluating inverter used in grid-connected photovoltaic systems", Sandia National Laboratory, Tech. Rep., October 2004. Available: http://www.bewengineering.com/docs/InvertrTestProto_041014.pdf

[13] D. Sera, R. Teodorescu, J. Hantschel and M. Knoll, "Optimized maximum power point tracker for fast changing environmental conditions", paper submitted to the IEEE International Symposium on Industrial Electronics Ű ISIE 2008.

[14] H. Heaberlin and L. Borgna, "A new approach for semiautomated measurement of PV inverters, especially MPP tracking efficiency, using a linear PV array simulator with high stability", in *19th European Photovoltaic Solar Energy Conference, Paris, France*, June 2004.

[15] H. Haeberlin, L. Borgna, M. Kaempfer and U. Zwahlen, "Measurement of dynamic MPP-tracking efficiency at grid-connected PV inverters", in *21st European Photovoltaic Solar Energy Conference*, 2006.

[16] D. Sera, R. Teodorescu and P. Rodrigues, "PV panel model based on datasheet values", in *IEEE International Symposium on Industrial Electronics - ISIE*, June 4-7, 2007.

[17] "IEC 61683: Photovoltaic systems - power conditioners - procedure for measuring efficiency (German version EN 61683). 1999".

Authorized licensed use limited to: Aalborg Universitetsbibliotek. Downloaded on January 25, 2009 at 12:40 from IEEE Xplore. Restrictions apply.

Publication 7

Real Time Photovoltaic Array Simulator for Testing Grid-Connected PV Inverters

by M. Valentini, A. Raducu, and D. Sera

Real Time Photovoltaic Array Simulator for Testing Grid-Connected PV Inverters

Massimo Valentini, Alin Raducu and Dezso Sera
Aalborg University, Institute of Energy Technology
DK-9220 Aalborg, Denmark
Email: s08masv@ponstud.aau.dk,
s08alinr@ponstud.aau.dk, des@iet.aau.dk

***Abstract*— In this paper a real time flexible PV array simulator is presented. It is a system that can simulate diffent PV panel arrays in specific environmental conditions. To evaluate performance of the Maximum Power Point Tracking (MPPT) of grid-connected Photovoltaic (PV) inverters only measurements undertaken with an appropriate PV array simulator provide accurate and reproducible results. Thus the PV array simulator has been developed and implemented. MPPT efficiency tests on a commercial grid-connected PV inverter have been performed to validate the PV array simulator.**

I. Introduction

Global energy consumption is rising and an increased focus on distributed power generation systems (DPGS) with renewable energy sources has been observed. The very low environmental impact of the renewable energies makes them a very attractive solution for a growing demand [1]. To increase the level of penetration of grid-connected photovoltaic systems, drawbacks must be overcome. The main disadvantages of PV systems are their low efficiency, high cost and dependence on environmental conditions, such as solar irradiance, PV module temperature and shadowing conditions. The efficiency of a PV system can be improved by implementing a control algorithm which forces the PV system to work always at the Maximum Power Point (MPP). Such a point is dependent on solar irradiance and temperature [2]; it is continuously searched by the Maximum Power Point Tracker (MPPT). Several MPPT algorithms have been developed ; they can either be implemented in the dc-dc converter or in the dc-ac converter [3] [4]. In order to correctly characterize PV inverters performance, the MPP tracking must be evaluated [5]. In fact, beyond the conversion efficiency, the MPPTs efficiency also produces a reduction of the inverter output power with respect to the maximum available power. However there are no standards which define how to evaluate MPPT performance, and manufacturers are not forced to do those kinds of tests and show the results to customers. Like the conversion efficiency, it is a good parameter for comparison with competitors'products. For MPPT performance evaluation on PV inverters, a real PV panel array is not suitable; a flexible PV array simulator is required. It is a system which can simulate different PV panel arrays in different irradiance conditions and PV module temperatures.
In this paper, a flexible PV array simulator has been developed and validated by performing MPPT efficiency tests on a commercial grid-connected PV inverter. The PV simulator is based on the model of a solar cell. Therefore such a model is introduced in the next section.

II. Modeling of PV cells

The prediction of the behavior at different irradiance, temperature and load conditions, is very important for sizing the PV plant and converter, as well as for the design of the MPPT and control strategy. Thus, several methods for PV module characterization are presented in the literature, mainly based on the measurement of the I-V curve [6] [7]. However, it is possible to develop a model of the PV panel from only the values provided by the manufacturer's data sheet [8].

The equivalent circuit of the single-diode model for PV cells is shown in Fig.1 [2] [8]. The general current-voltage

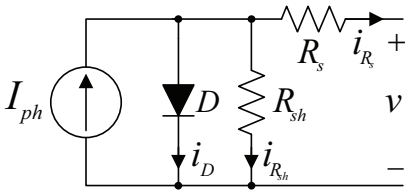

Fig. 1. Equivalent circuit of a photovoltaic cell based on the single-diode model.

characteristic of a PV panel based on the single exponential model is [2] [8]:

$$i = I_{ph} - I_o \left(e^{\frac{v+iR_s}{n_s V_t}} - 1 \right) - \frac{v + iR_s}{R_{sh}} \tag{1}$$

In the above equation, V_t is the junction thermal voltage:

$$V_t = \frac{AkT_{stc}}{q} \tag{2}$$

where:

- I_{ph} - the photo-generated current in Standard Test Conditions[1] (STC)
- I_o - dark saturation current in STC
- R_s - panel series resistance
- R_{sh} - panel parallel (shunt) resistance

[1]Irradiance level of $1000W/m^2$, with the reference air mass 1.5 solar spectral irradiance distribution and cell junction temperature of $25°C$.

978-1-4244-1666-0/08/$25.00 ©2008 IEEE

- A - diode quality (ideality) factor

are the five parameters of the model, while k is Boltzmann's constant, q is the charge of the electron, n_s is the number of series cells in the PV module, and T_{stc} ($^\circ K$) is the temperature at STC. The five above parameters can be obtained from the PV model data sheet as it is explainded in [8]. The model of the entire PV panel array can be obtained by considering that it is composed by N_{sp} strings in parallel, each one composed by N_{ps} panels in series. The model takes into account irradiance and PV panel temperature dependencies. In order to get one equation with both irradiation and temperature effects, the principle of superposition is applied.

A. Irradiance dependence

The power produced by the PV system (cell, module or array) changes when irradiance changes. It depends on the short-circuit current (I_{sc}) which is directly proportional to the irradiance through Eq.3 :

$$I_{sc}(G) = I_{sc,stc}\frac{G}{G_{stc}} \tag{3}$$

where $G_{stc} = 1000W/m^2$ is the irradiance is STC. Fig.2 shows how the power-voltage curve of a commercial PV module depends on the irradiance.

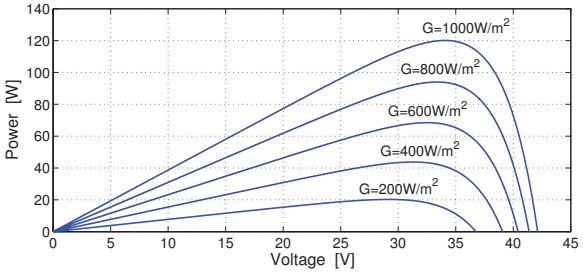

Fig. 2. Power-voltage curve of a PV module at different irradiance levels.

B. Temperature dependence

The operating temperature has a strong effect on the electrical response of a solar cell. A suitable model of temperature effects is mandatory [2]. The open-circuit voltage (V_{oc}) and the short-circuit current (I_{sc}) depend on the cell temperature as follows:

$$V_{oc}(T) = V_{oc} + k_v(T - T_{stc}) \tag{4}$$

$$I_{sc}(T) = I_{sc}\left[1 + \frac{k_i}{100}(T - T_{stc})\right] \tag{5}$$

where:

- T is the PV module operating temperature in $^\circ C$;
- k_v and k_i are respectively V_{oc} and I_{sc} temperature coefficients available in the data sheet .

Fig.3 shows how the power-voltage curve of a commercial PV module depends on the temperature.

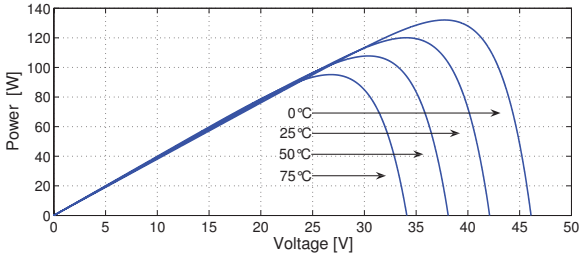

Fig. 3. Power-voltage curve of a PV module at different temperature levels.

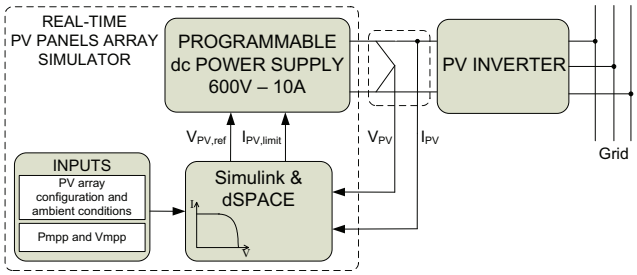

Fig. 4. PV array simulator test setup.

III. Real Time Photovoltaic Array Simulator

A block diagram of the PV array simulator test setup is represented in Fig.4. The PV simulator is composed by a programmable dc power supply, which is controlled in order to work as closely as possible with the simulated PV panels array, in the specific conditions of irradiance and PV module temperature. A wide bandwidth is required for such a control system so that the actual behavior of the desired PV panel array is closely reproduced.

The developed PV simulator is based on the voltage control of the power supply. This means that the current supplied by the programmable dc power supply is measured and used to find the operating point on the current-voltage curve of the simulated PV panels array. The correspondent voltage is used as a reference to control the power supply in the next step. The drawback of such approach is that, considering the P-V courve of the array, on the right side of the MPP, a small error in the reference voltage v_{ref} produces a big error in the current; thus current variations are experienced and can eventually lead to instability. The control system has been stabilized by filtering the measured current i_{pv}. Better results could be obtained with linear current control of the dc power supply; however such an approach would require extra hardware (an external current controller) [9].

The PV simulator has been imlemented into a dSPACE platform. A Graphical User Interface (GUI) has been developed for real time evaluation. The GUI offers the flexibility of simulating different PV panel arrays in specified environmental conditions. The PV array simulator can be used for testing the MPPT in two ways:

- simulating a specific PV panel array in specific environmental conditions. Thus, inputs are the PV panel

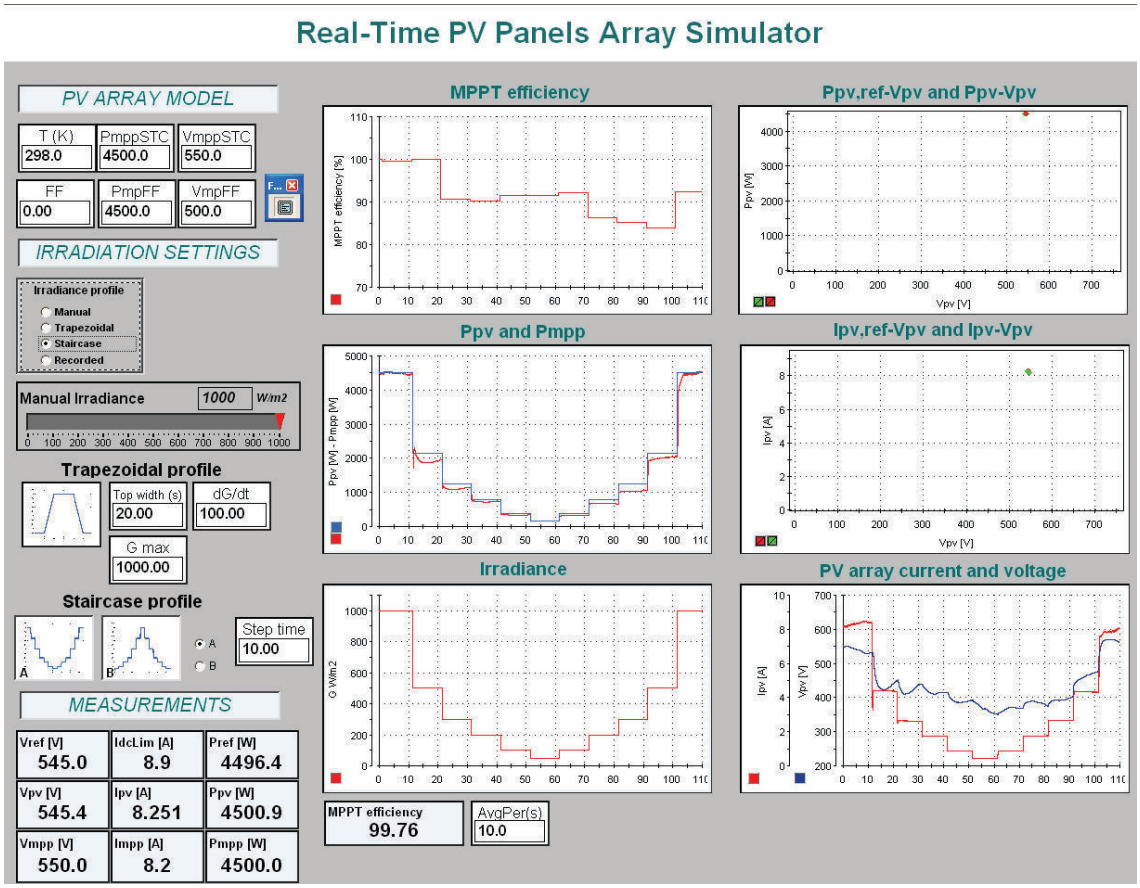

Fig. 5. Control Desk graphical user interface of the PV array simulator showing test results on a commercial PV inverter

array configuration (PV module type, N_{ps} and N_{sp}) and environmental conditions (PV module temperature and irradiance profile);

- specifying the MPPT. Thus, inputs are MPP power (P_{mpp}) and MPP voltage (V_{mpp}).

In the first case the MPP coordinates are calculated, whereas in the second case they are specified; in both cases the istanateous MPPT efficency is calculated as follows:

$$\eta_{MPPT}(t) = \frac{P_{PV}(t)}{P_{MPP}(t)} = \frac{V_{PV}(t) \cdot I_{PV}(t)}{V_{MPP}(t) \cdot I_{MPP}(t)} 100 \quad (6)$$

where

- $P_{PV}(t)$, $V_{PV}(t)$ and $I_{PV}(t)$ are respectively istantaneous output power, voltage and current of the programmable dc power supply; they define the operating point on the simulated PV panel array power-voltage and current-voltage curves;
- $P_{MPP}(t)$, $V_{MPP}(t)$ and $I_{MPP}(t)$ are respectively istantaneous power, voltage and current at the MPP.

In case of discrete time calculations, the above variables are sampled, thus the MPPT efficency at each sample is calculated as follows:

$$\eta_{MPPT}(k) = \frac{P_{PV}(k)}{P_{MPP}(k)} = \frac{V_{PV}(k) \cdot I_{PV}(k)}{V_{MPP}(k) \cdot I_{MPP}(k)} 100 \quad (7)$$

IV. MPPT EFFICIENCY TESTS

The developed PV array simultator has been used to perform MPPT efficiency tests on a commercial three-phase grid-connected PV inverter ($P_n = 15kW$, $V_n = [200V; 900V]$, $I_n = 36A$, $V_{mpp} = [200V; 850V]$).

A. MPPT efficiency in stationary conditions

In stationary conditions, $\eta_{MPPT}(t)$ is averaged over a specfied period (typically 1-10s) when the steady state is achieved and no further variation of $\eta_{MPPT}(t)$ occur; depending on the operating conditions, the transient can take several seconds. Fig.6 shows $\eta_{MPPT}(t)$ averaged over $5s$ in stationary conditions. It can be seen that the stationary MPPT efficiency of

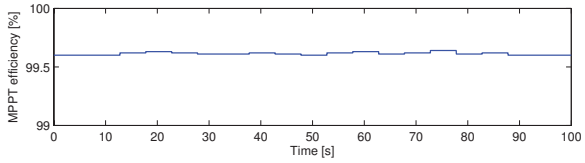

Fig. 6. MPPT efficiency in stationary conditions with $P_{mpp} = 4.5kW$ and $V_{mpp} = 550V$.

the inverter is very high ($\eta_{MPPT}(t) = 99.6\%$). This means

that the MPP tracking system has been well designed. A PV array simulator is a fundamental tool as it allows the evaluation of performance with different designs of the tracking algorithm. The stationary MPPT efficiency has been evaluated at only one operating point ($P_{mpp} = 4.5kW$,$V_{mpp} = 550V$); however in the same way it can be evaluated for different inverter output voltage and power so that the 3D graph of $\eta_{MPPT} = f(P_{inv}, V_{inv})$ can be obtained with $P_{inv} \leq P_{inv,n}$ and $V_{inv,min} \leq V_{inv} \leq V_{inv,max}$.

B. MPPT efficiency in dynamic conditions

In dynamic conditions, when the MPP changes due to irradiance variations, the MPP tracking is usually analyzed using staircase or trapezoidal irradiance profiles. If the irradiance change is fast enough, the MPPT is not able to follow the MPP operating point [5]. Knowing the values of $P_{MPP}(t)$ and $P_{PV}(t)$ during the dynamic test, the equivalent efficiency can be calculated as follows [5]:

$$\begin{aligned}\eta_{MPPT} &= 100\frac{\int_0^{T_0} P_{PV}(\tau)d\tau}{\int_0^{T_0} P_{MPP}(\tau)d\tau} \\ &= 100\frac{\int_0^{T_0} V_{PV}(\tau)\cdot I_{PV}(\tau)d\tau}{\int_0^{T_0} V_{MPP}(\tau)\cdot I_{MPP}(\tau)d\tau}\end{aligned} \tag{8}$$

where T_0 is the test period. In case of a discrete time calculation with sampling time T_s, the MPPT efficency at each sample is calculated as follows:

$$\eta_{MPPT} = \frac{\sum_{k=1}^{N} P_{PV}(k)T_s}{\sum_{k=1}^{N} P_{MPP}(k)T_s} = \frac{\sum_{k=1}^{N} P_{PV}(k)}{\sum_{k=1}^{N} P_{MPP}(k)} \tag{9}$$

1) Staircase irradiance profile: Staircase irradiance profiles are used to test the inverter MPPT efficiency at different irradiation levels, in accordance with the European Efficiency formula [10]. Fig.7 shows a staircase irradiance profile that decreases in the first half of the test so it is classified as decreasing staircase irradiance profile; it is characterized by steps of $10s$ duration. Experimental results are shown

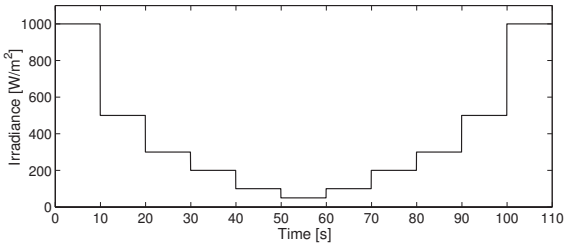

Fig. 7. Decreasing stercase irradiance profile for dynamic MPPT efficiency test ($10s$ steps; irradiation levels according to the European Efficiency test).

in Fig.8. The MPPT efficiency, calculated using Eq.9, is $\eta_{MPPT} = 96.84\%$. In Fig.8 it can be seen that the MPP tracker is not capable of follow the MPP within the step time of $10s$. This produces a reduction of the captured power with respect to the maximum available power which can be provided by the PV panel array.

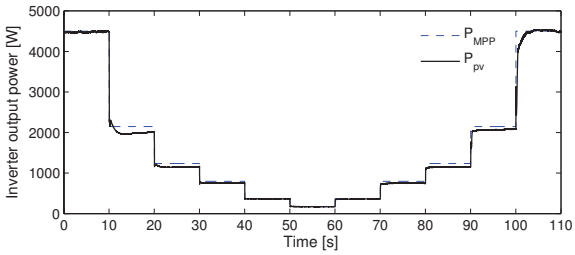

Fig. 8. Decreasing staircase irradiance profile test results.

Fig.9 shows an increasing staircase irradiance profile with $10s$ steps. Experimental results are shown in Fig.10. The MPPT

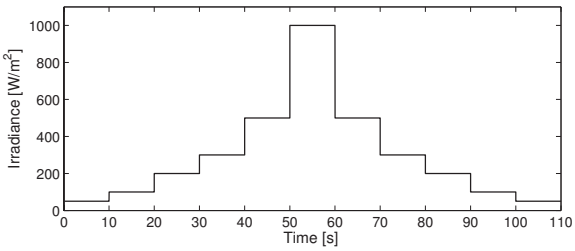

Fig. 9. Increasing staircase irradiance profile for dynamic MPPT efficiency test ($10s$ steps; irradiation levels according to the European Efficiency test).

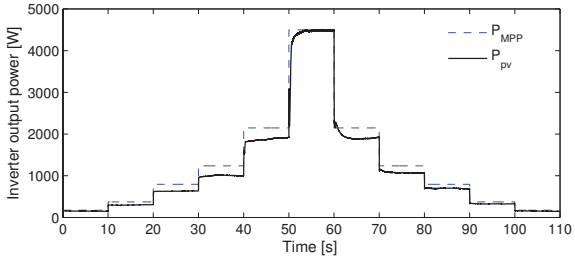

Fig. 10. Increasing staircase irradiance profile test results.

efficiency, calculated using Eq.9, is $\eta_{MPPT} = 89.72\%$. In Fig.10 it can be seen that the MPP Tracker is not capable of follow the MPP within the step time of $10s$.

2) Trapezoidal irradiance profile: Trapezoidal irradiance profiles are used to test the inverter at dynamic irradinance conditions. Fig.11 shows a trapezoidal irradiance profile. Experimental results are shown in Fig.12.The MPPT efficiency, averaged over $2s$, in represented in Fig.13.
The MPPT efficiency, calculated using Eq.9, is $\eta_{MPPT} = 97.05\%$. Fig.12 shows that in case of trapezoidal irradiance variation, which can occur when the sun is temporarely shadowed, the MPP trackng is good. This shows the good design of the tracking algorithm based on the evaluation of performance of the MPPT using a PV array simulator.

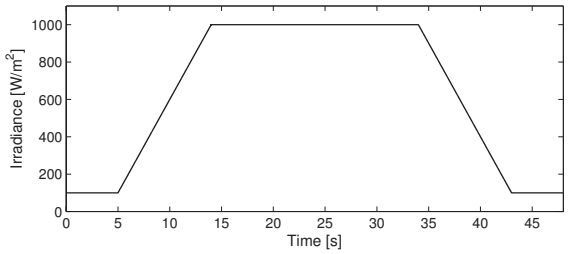

Fig. 11. Trapezoidal irradiance profile for the dynamic MPPT efficiency test.

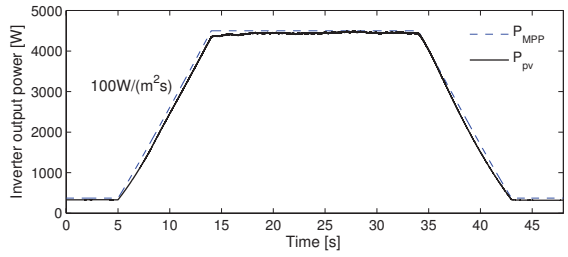

Fig. 12. Trapezoidal irradiance profile test result.

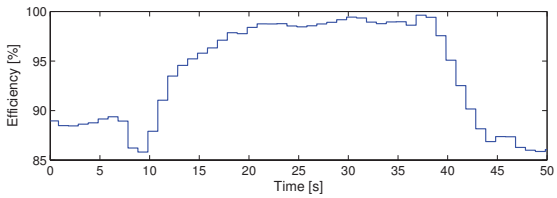

Fig. 13. MPPT efficiency during the test with trapezoidal irradiance profile.

V. Conclusions

In this paper a real time flexible PV array simulator has been developed. It is based on the model of the solar cell obtained from data sheet parameters according to [8]. It has been implemented and a Graphical User Interface using dSPACE Control Desk has been created for real time evaluation. The PV array simulator is then validated by performing MPPT efficiency tests on a commercial grid-connected PV inverter in stationary and dynamic conditions. Experimental results prove that the developed PV array simulator can be used during the design and tuning of the MPP tracking algorithm, as performance with different design criteria can be easily compared.

Acknowledgment

The authors would like to thank Professor Remus Teodorescu for providing us a very good environment for our research.

References

[1] D. Sera, F. Blaabjerg, and R. Teodorescu, "New control strategies and more energy from PV systems for residential applications: State-of-the-Art study of PV technology, modelling and MPPT algorithms," Institute of Energy Technology, Aalborg University, 2006.

[2] L. Castaner and S. Silvestre, *Modelling photovoltaic systems using PSpice*. John Wiley and Sons, LTD, September 2002, ISBN: 978-0-470-84527-1.

[3] D. Hohm and M. Ropp, "Comparative study of Maximum Power Point Tracking algorithms using an experimental, programmable, maximum power point tracking test," in *Photovoltaic Specialists Conference, 2000. Conference Record of the Twenty-Eighth IEEE*, 2000, pp. 1699-1702.

[4] D. Sera, T. Kerekes, R. Teodorescu, and F. Blaabjerg, "Improved MPPT algorithms for rapidly changing environmental conditions," in *12th International Power Electronics and Motion Control Conference*, 2006, pp. 1614-1619.

[5] H. Haeberlin, L. Borgna, M. Kaempfer, and U. Zwahlen, "Measurement of dynamic MPP-tracking efficiency at grid-connected PV inverters," in *21st European Photovoltaic Solar Energy Conference*, 2006.

[6] D. Chan and J. Phang, "Analytical methods for the extraction of solar-cell single- and double-diode model parameters from i-v characteristics," *Electron Devices, IEEE Transactions on*, vol. 34, no. 2, pp. 286-293, 1987.

[7] M. Chegaar, Z. O. , and A. Hoffmann, "A new method for evaluating illuminated solar cell parameters," *Solid-state electronics*, vol. 45, pp. 293-296, 2001.

[8] D. Sera, R. Teodorescu, and P. Rodrigues, in *Industrial Electronics, 2007. ISIE 2007. IEEE International Symposium on, Vigo (Spain)*, 4-7 June 2007, pp. 2392–2396, ISBN: 978-1-4244-0755-2.

[9] Arsenal research, an Enterprise of the Austrian research centers, *Datasheet of the Programmable PV Simulator PVAS2*.

[10] "Performance test protocol for evaluating inverter used in grid-connected photovoltaic systems," Sandia National Laboratory, 2004.

Publication 8

On the Impact of Partial Shading on PV output Power

by D. Sera, Y. Baghzouz

On the Impact of Partial Shading on PV Output Power

DEZSO SERA
Institute of Energy Technology
Aalborg University
Pontoppidanstræde 101, 9220 Aalborg
DENMARK
des@iet.aau.dk

YAHIA BAGHZOUZ
Dept. of Electrical & Computer Engr.
University of Nevada, Las Vegas
Las Vegas, NV 89154-4026
USA
baghzouy@unlv.nevada.edu

Abstract: - It is a well-documented fact that partial shading of a photovoltaic array reduces it output power capability. However, the relative amount of such degradation in energy production cannot be determined in a straight forward manner, as it is often not proportional to the shaded area. This paper clarifies the mechanism of partial PV shading on a number of PV cells connected in series and/or parallel with and without bypass diodes. The analysis is presented in simple terms and can be useful to someone who wishes to determine the impact of some shading geometry on a PV system. The analysis is illustrated by measurements on a commercial 70 W panel, and a 14.4 kW PV array.

Key-Words: - photovoltaic systems, effect of shading, modeling and simulation, module layout, power production.

1 Introduction

The photovoltaic (PV) industry is experiencing rapid growth due to improving technology, lower cost, government subsidies, standardized interconnection to the electric utility grid, and public enthusiasm for an environmentally benign energy source [1]-[2]. More precisely, PV usage worldwide has grown between 15% and 40% for each of the past 10 years, while the inflation adjusted cost of PV energy has declined by roughly by a factor of 2 over the same time period [3].

PV system sizes vary from the MW range, in utility applications, down to the kW range in residential applications. In the latter systems, the PV array is typically installed on the roof of a house, and partial shading of the cells from neighboring structures or trees is often inevitable. Then impact of partial shading on PV system performance has been studied at great length in the past [4]-[11]. Some past studies assume that the decrease in power production is proportional to the shaded area and reduction in solar irradiance, thus introducing the concept of shading factor. While this concept is true for a single cell, the decrease in power at the module or array level is often far from linearity with the shaded portion. Other past studies tend to be rather complicated and difficult to follow by someone with limited knowledge on electronic/solid-state physics.

The objective of this study is to clarify the impact of shading on a solar panel performance in relatively simple terms that can be followed by a power engineer or PV system designer without difficulty. First, the circuit model of a PV cell and its I-V curve are reviewed. This is followed by the impact of partial shading on the I-V and P-V curves of a circuit containing two cells with and without bypass diodes. The concept is extended to the circuits with series and parallel submodules. Finally, the impact of shading is illustrated by measurements on a commercial PV panel and a large PV array.

2 V-I Characteristics of a PV Cell

The most commonly used circuit model to describe the electrical behavior of a PV cell is the single diode model as shown in Fig.1 below [9], [12], [13]. The current generated by the cell is expressed by

$$i = I_{ph} - I_o\left(e^{\frac{v+iR_s}{n_s V_t}} - 1\right) - \frac{v+iR_s}{R_{sh}} \qquad (1)$$

where the junction thermal voltage V_t is defined by

$$V_t = \frac{AkT}{q}. \qquad (2)$$

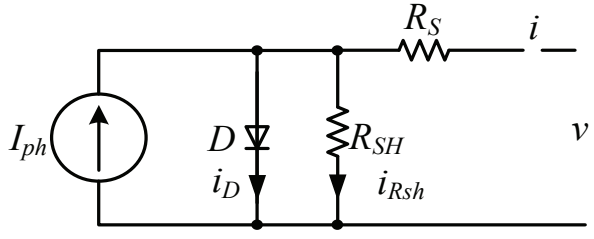

Fig. 1: Equivalent circuit of PV cell using single diode model.

The circuit parameters defined in Equations (1) and (2) are defined as follows:

I_{ph} - photo-generated current,
I_o - dark saturation current,
R_s - panel series resistance,
R_{sh} - panel parallel (or shunt) resistance,
A - diode quality (or ideality) factor,
k - Boltzmann's constant,
q - electron charge,
n^s - number of cells connected in series,
T - cell temperature (in degree Kelvin).

It is a common practice to neglect the term '-1' in Equation (1) since the dark saturation current is very small compared to the exponential term in silicon devices. Fig. 2 below shows typical I-V curves of a crystalline silicon (c-Si) PV cell at different irradiance intensity G at standard temperature condition of 25° C.

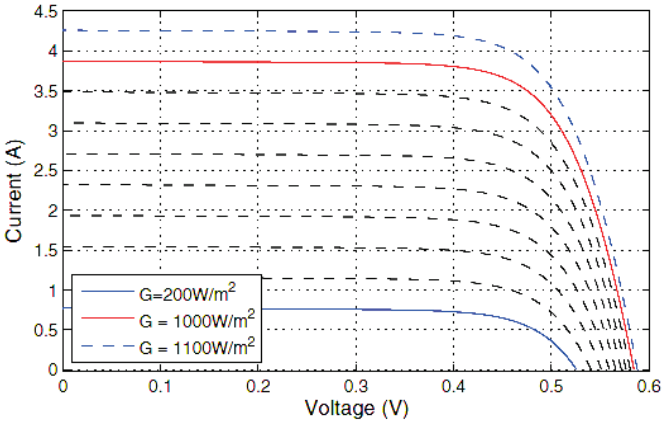

Fig. 2. Forward I-V characteristic of c-Si PV cell at different irradiance intensities.

3 Shading of Series-Connected Cells

Today, commercial c-Si PV panels usually have all their cells connected in series. In order to protect the cells from destructive reverse voltages in case of shadowing or other abnormalities, a number of bypass diodes are utilized. For example, one bypass diode connected in parallel with each set of 18 cells is common practice [11]. In this Section, the operation of the bypass diode is illustrated by a simple example where two series-connected cells, with different irradiation intensities on their surfaces, serve a resistive load as illustrated in Fig. 3 below. It is assumed that the shaded cell irradiation is 25% of the non-shaded cell as indicated by the individual I-V curves in Fig. 4(a).

Two cases are considered: In the first case, the shaded cell has an ideal bypass diode (with negligible forward bias voltage and series resistance) connected in parallel. If one varies the load resistance R_{load} from infinity to zero, the I-V curve of such configuration is shown in red Fig. 4(a). Note that the voltage of the shaded cell falls to zero when the load current exceeds the cell's short-circuit current. Hence, for higher load, the shaded cell is short-circuited and does not contribute any power.

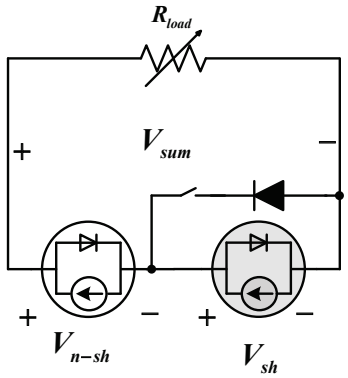

Fig. 3. Two PV cells with different irradiance intensities connected in series (with and w/o bypass diode in parallel with shaded cell).

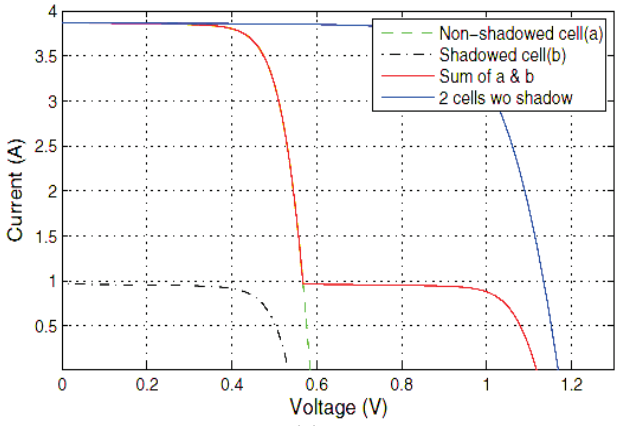

(a)

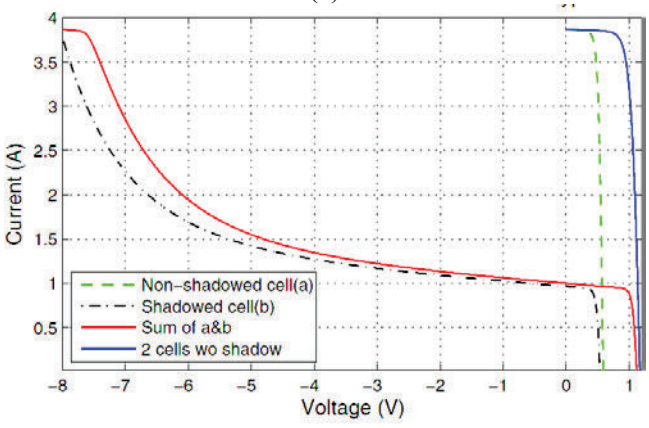

(b)

Fig. 4. I-V characteristic of two PV cells connected in series with different solar irradiance intensities: (a) with and (b) w/o bypass diode in parallel with shaded cell.

The second case considered is when the bypass diode is removed. The resultant I-V characteristics of this configuration are shown in Fig. 4(b). When the load is lower than the shaded cell short-circuit current, the circuit behaves just like the previous case (under the presence of the bypass diode). But as the load is

increased beyond this value, the shaded cell becomes reverse biased and starts to behave like a high resistor. In other words, the shaded cell starts to consume some of the power produced by the non-shaded cell thus resulting in undesirable losses. The reverse-biased region of the I-V curve is obtained by modifying the cell model in Eqn. (1) according to Refs. [9] and [11].

Figure 5 shows the corresponding power-voltage curves for the above two cases, in addition to the case without shading in both cells. Note that without the bypass diode, maximum power is reduced by nearly 50%. On the other hand, the presence of the bypass diode results is a power curve with multiple peaks.

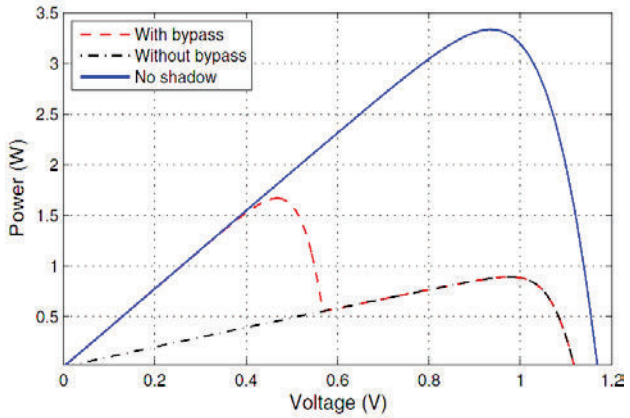

Fig. 5. P-V characteristics of two PV cells connected in series with different solar irradiance intensities (with and w/o bypass diode).

4 Partial Shading of PV Modules

As mentioned in Section 3 above, it is a common practice to use one bypass diode per 18 series-connected cells, which form the so-called submodule [6]. Furthermore, a PV module is likely to contain a number of submodules in series [13], and higher output voltage is obtained by connecting several modules in series to form a PV array. For higher power, a number of PV arrays are connected in parallel. The following material analyzes the impact of shading on part of a module which consists of series as well as parallel submodules that are protected by bypass diodes.

4.1 Partial shading of two series-connected submodules

Consider a module that consists of two series connected submodules (each containing 36 cells) with partial shading as shown in Fig. 6. For illustration, it is assumed that the clear and shadowed areas have a solar irradiance of G_{STD} = 1000 W/m^2 and G_{SH} = 250 W/m^2, respectively. Further, the bypass diodes are assumed to have a forward voltage of V_d = 0.6 V and an on-resistance of R_d = 10 mΩ. Shadowing only two cells can cause a considerable reduction in output power, and the amount of loss greatly depends on which two cells are shadowed. Two cases are considered: Case A where the two shaded cells belong to the same string, and Case B where these cells belong to different strings.

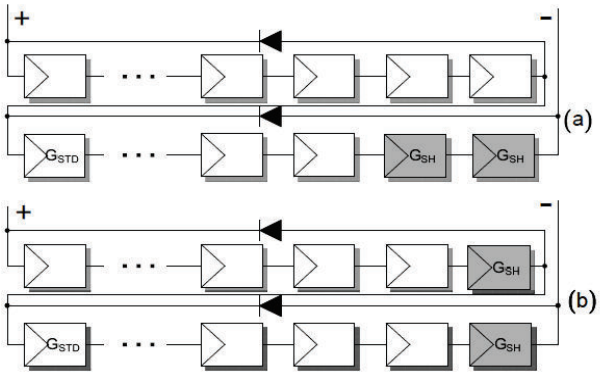

Fig. 6. Series connection of two submodules: (a) two cells shaded in one submodule, (b) one cell shaded in each submodule.

4.1.1 Case A

In Fig. 6(a), the shadowed cell will limit the output current of the submodule as explained in Section 3 above. This has a similar effect as if the whole bottom submodule is shadowed. However, as there is a bypass diode in parallel, the non-shadowed submodule can still produce full power. These remarks are demonstrated by the blue dotted I-V and P-V curves in Fig. 7.

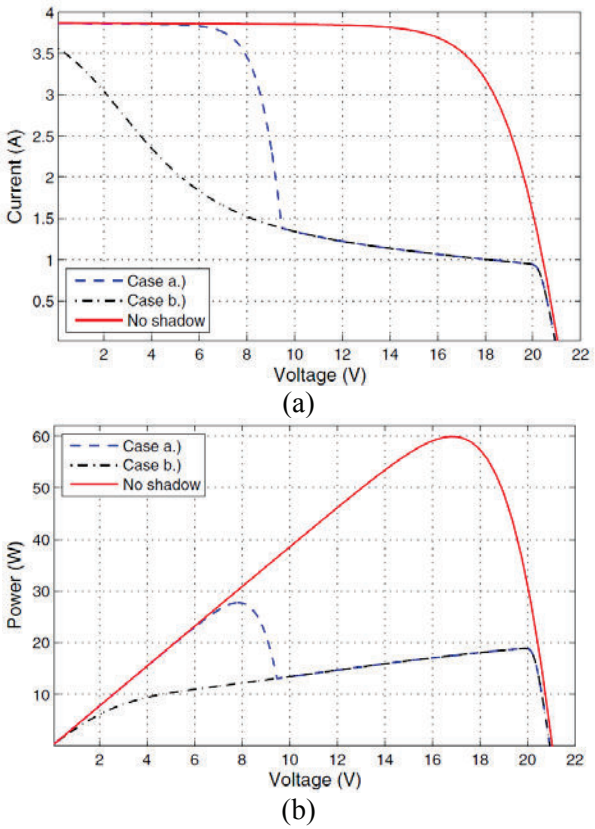

Fig. 7. Characteristics of the two partially shaded series-connected submodules: (a) I-V characteristic, (b) P-V characteristic.

4.1.2. Case B

In Fig. 6(b) both submodules have one shadowed PV cell; hence, their output power will be both limited by the same amount. The bypass diodes will have no effect in this case, and the total power output is almost as low as if the entire string is shadowed. The resulting I-V and P-V curves for this case are shown by the dotted dark curves in Fig. 7(a) and 7(b), respectively.

In summary, although only 2 out of 36 cells are shadowed (that is less than 6% of the total area), the maximum power reduction in Cases A and B are 50% and 70%, respectively. This clearly illustrates that it is erroneous to assume that maximum power production is proportional to the non-shaded area of a PV module.

4.2 Partial shading of two parallel-connected submodules

This configuration considers the same two submodules described in Section 4.2 above with two shaded cells, but connected in parallel, instead of series, as illustrated in Fig. 8 below. Once again, the same two cases are considered. Fig. 9 shows the corresponding I-V and P-V curves the 72-cell module for both cases.

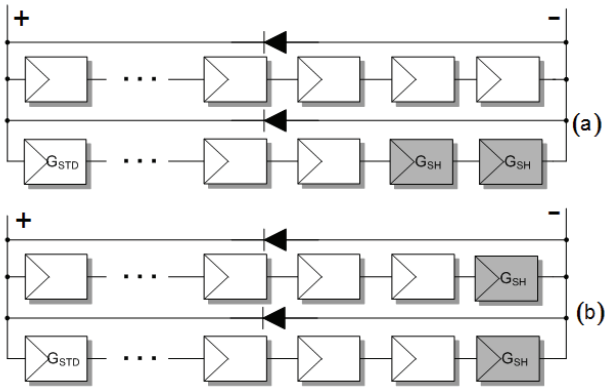

Fig. 8. Parallel connection of two submodules: (a) two cells shaded in one submodule, (b) one cell shaded in each submodule.

Note that the maximum power curve of Case B is the same as that of Case B of the previous section (i.e., max. power reduced by 70%). On the other hand, maximum power in Case A is reduced by only 35% (compared to 50% in Case A of the previous section). This is due to the fact that the cell output current shows a stronger dependency (linear) on irradiation than the voltage (logarithmic).

Alternatively, when two submodules with irradiation intensities are connected together, the relative difference of their maximum power point (MPP) currents is much larger than the relative difference of their MPP voltages. Therefore, in case of the series connection, if one submodule is working at its MPP, the other submodule having the same current works far from its MPP. The opposite is true in the parallel connection (i.e., if one submodule is working at its MPP, the other one sharing the same voltage will work also in the vicinity of its MPP, thus resulting in a higher MPP power).

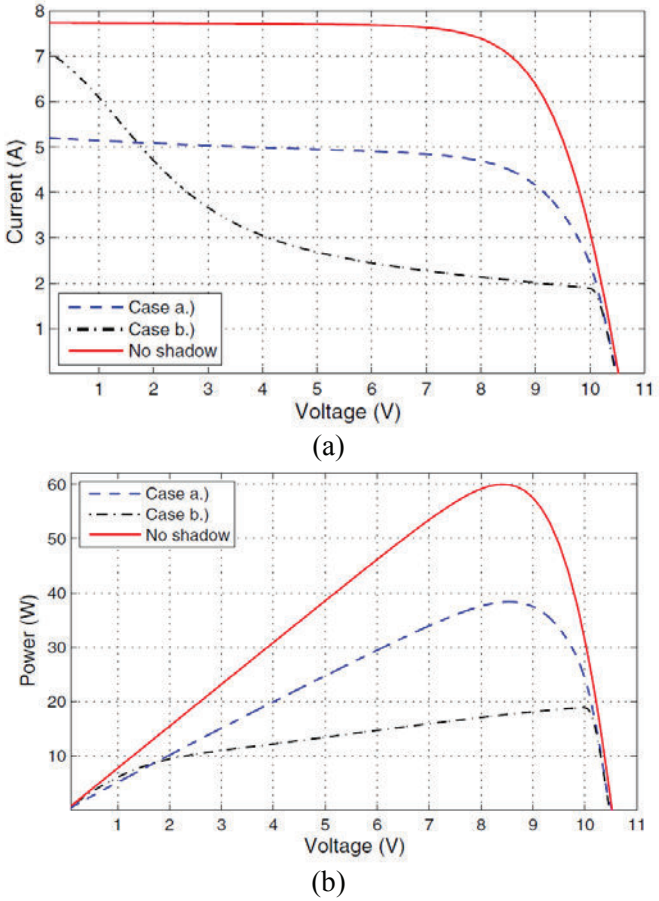

Fig. 9. Characteristics of the two partially shaded parallel-connected submodules: (a) I-V Characteristic, (b) P-V characteristic.

5 Experimental Test

In order to verify some of the simulated curves of the previous section, an experiment was conducted on a Kyocera KC70 multi-crystalline silicone PV panel using a Daystar-100 I-V curve tracer. The electrical specs of the 70 W panel are as follows (at standard temperature conditions):

- short-circuit current: I_{sc} = 4.35 A
- open-circuit voltage: V_{oc} = 21.5 A
- voltage at MPP**:** V_{mpp} = 16.9 V
- current at MPP: I_{mpp} = 14.14 A
- power at MPP: P_{max} = 70 W
- temp. coefficient of I_{sc}: k_t = 3.55 10^{-3} /°C
- temp. coefficient of V_{sc}: k_v = -8.2 10^{-2} /°C.

The Kyocera KC70 photovoltaic panel has the electrical configuration of the cells and bypass diodes identical to the case depicted in Fig. 6. To create a partial shadowing condition, 2 cells belonging to the same submodule were covered with a sheet of cardboard, which makes the shadowing close to 100%, i.e., near zero solar irradiation on the covered area. The measurement results shown in

Fig. 10 below show a good agreement with the predicted curves associated with Section 4.1.1.

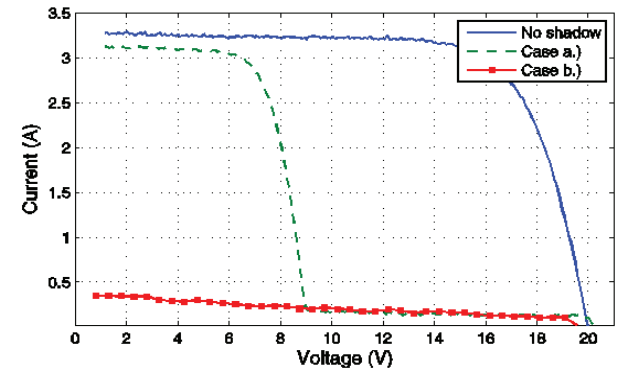

(a)

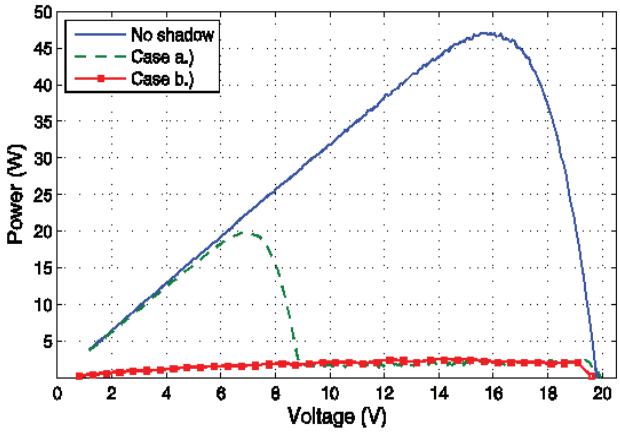

(b)

Fig. 10. Experimental data of Kyocera KC70 PV panel with two shaded cells: (a) V-I characteristic, (b) P-V characteristic.

The next field data involves the impact of partial shading on the performance of a grid-connected, 14.4 kW, 1-axis tracking, PV system that is located in Las Vegas, Nevada. The system consists of 4 identical tracking sub-arrays, as shown in Fig. 11(a), each of which contains two parallel strings of 12 series-connected panels. Herein, each panel is rated at 150 W (each) and consists of 3 series-connected submodules with bypass diodes. Each submodule contains 24 cells connected in series as illustrated in Fig. 11(b). In summary, the array contains 8 parallel strings, each containing 36 submodules and 864 cells.

Fig. 11(c) shows a typical power production curve (in kW) of the array along with the incident solar radiation (in W/m^2) on a clear day. One can immediately note the dip in power production between the hours of 1:00 pm and 3:00 pm on this particular day of 9/11/08. A closer analysis showed that a power pole (only its shadow can be seen in the photo) shaded part of the front sub-array during those hours of that day. Further work will be conducted to estimate the yearly energy reduction due to shading of this structure. The variation of the shadow on the photovoltaic collector will be determined by using techniques such as the one proposed in Ref. [16].

(a)

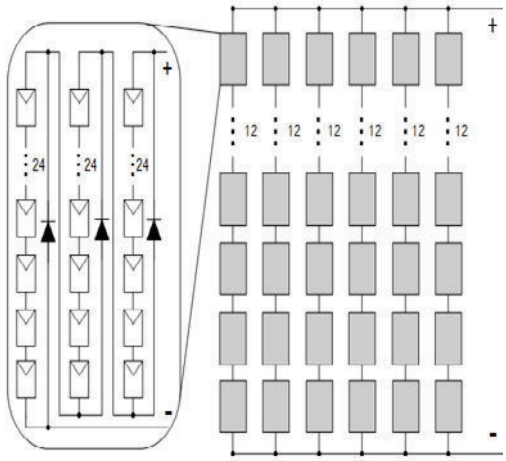

(b)

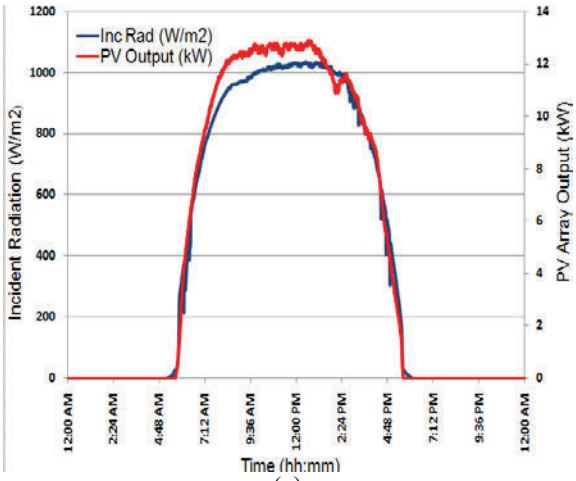

(c)

Fig. 11 14.4 kW grid-connected PV system: (a) actual array, (b) connection diagram, (c) power production on 9/11/08.

6 Conclusion

This paper presented the impact of shading on the I-V and P-C curves of a solar panel, and clarified the basic mechanism that estimates the reduction in output power. Such degradation in maximum power production clearly depends on the shaded area as well as the layout of the submodules and the bypass diodes. The analysis was illustrated by experimental data. It is hoped that this article will be of use to PV system designers when attempting to minimize the impact of shading on system performance.

References:

[1] International Energy Agency, Cost and Performance trends in grid-connected PV systems and case studies, *Technical Report EA PVPS T2-06*, Dec. 2007.

[2] International Energy Agency, Trends in photovoltaic applications - survey report of selected by countries between 1992 and 2005, *Technical Report IEA PVPS T1-15*, 2006.

[3] P.B. Barker and J.M. Bing, Advances in solar photovoltaic technology – an applications perspective, *IEEE Power Engineering Society General Meeting* – June 12-16, 2004, San Francisco, CA.

[4] H. Rauschenbach, Electrical output of shadowed solar arrays, *IEEE Transactions on Electron Devices*, vol. 18, no. 8, pp. 483–490, 1971.

[5] A. Abete, E. Barbisio, F. Cane, and P. Demartini, "Analysis of photovoltaic modules with protection diodes in presence of mismatching," *21st IEEE Photovoltaic Specialists Conference, 1990,* pp. 1005–1010.

[6] A. Kovach and J. Schmid, Determination of energy output losses due to shading of building-integrated photovoltaic arrays using a ray-tracing technique, *Solar Energy*, vol. 57, no. 2, pp. 117–124, Aug. 1996.

[7] N. van der Borg and M. Jansen, Energy loss due to shading in a bipv application, *3rd World Conference on*, in *Photovoltaic Energy Conversion, 2003.* vol. 3, 2003, pp. 2220–2222.

[8] R. Pinkerton, Solar array string characteristics in strange places, *35th Intersociety Conference and Exhibit of Energy Conversion Engineering (IECEC)*, vol. 1, 2000, pp. 681–691.

[9] J. Bishop, Computer simulation of the effect of electrical mismatches in photovoltaic cell interconnection circuits, *Solar cells*, vol. 25, pp. 73–89, 1988.

[10] N. Kaushika and N. Gautam, Energy yield simulations of interconnected solar pv arrays, *IEEE Transactions on Energy Conversion*, vol. 18, no. 1, pp. 127–134, 2003.

[11] V. Quaschning and R. Hanitsch, Numerical simulation of photovoltaic generators with shaded cells, in *Universities Power Engineering Conference*, vol. 30th, 1995, pp. 583–586.

[12] H. Nagayoshi and M. Atesh, Partial shading effect emulation using multi small scale module simulator units, *31st IEEE Photovoltaic Specialists Conference,* 2005, pp. 1710–1713.

[13] A. Woyte, J. Nijsa, and R. Belmansa, Partial shadowing of photovoltaic arrays with different system configurations - literature review and field test results, *Solar energy*, vol. 74, pp. 217–, 2003.

[14] G. Araujo and E. Sanchez, A new method for experimental determination of the series resistance of a solar cell, *IEEE Transactions on Electron Devices,* vol. 29, no. 10, pp. 1511–1513, 1982.

[15] M. Chegaar, Z. Ouennoughi, and A. Hoffmann, A new method for evaluating illuminated solar cell parameters, *Solid-state electronics*, vol. 45, pp. 293–, 2001.

[16] Ike, S.; Kurokawa, K.; Photogrammetric estimation of shading impacts on photovoltaic systems, *31st Photovoltaic Specialists Conference, IEEE*, 3-7 Jan. 2005 Page(s):1796 – 1799.

Publication 9

Photovoltaic Module Diagnostics by Series Resistance Monitoring and Temperature and Rated Power Estimation

by D. Sera, R. Teodorescu, and P. Rodriguez

Photovoltaic Module Diagnostics by Series Resistance Monitoring and Temperature and Rated Power Estimation

Dezso Sera, Remus Teodorescu
Aalborg University, Institute of Energy Technology,
DK-9220 Aalborg, Denmark,
Email: des@iet.aau.dk, ret@iet.aau.dk

Pedro Rodriguez
University of Catalonia, Electrical Engineering Department
Colom 1, 08222, Terrassa-Barcelona, Spain,
Email: prodriguez@ee.upc.edu

***Abstract*—One of the most important parameters, which characterizes a photovoltaic panel health state, is its series resistance. An increase of this, normally indicates bad contacts between cells or panels. An other important property, which characterizes the aging of the panel is the reduction of its MPP power in Standard Test Conditions (STC[1]). Simulation and experimental measurements regarding the determination of a PV panel series resistance, its MPP power in STC, as well as its temperature, are presented in this paper. It is shown that the panel series resistance can be determined experimentally without needing to perform an entire I-V curve scan. The panel MPP power in STC and its temperature - given the irradiance is measured - can be well approximated using the measured I-V curve, and a simple model of the PV panel.**

***Index Terms*—Photovoltaic, modeling, diagnostics, series resistance measurement, temperature estimation, STC power estimation**

I. Introduction

Nowadays the worldwide installed Photovoltaic power capacity shows a nearly exponential increase, despite of their still relatively high cost. [1] This, along with the research for lower cost and higher efficiency devices, motivates the research also in the control of PV inverters, to achieve higher efficiency and reliability. A relatively new tool for increasing the reliability and production of the PV system is to use diagnostic functions, which can warn the user/operator, if there is a fault in the PV array, without the need of disconnecting it from the system, and perform manual measurements. One of the most predominant element in decreasing the PV modules Fill factor (FF), is the series resistance [2], [3]. An other phenomenon, directly related to the ageing of the modules, is the the decrease of the MPP power in Standard Test Conditions, with other words, decrease of power compared to the datasheet. In the present work a simple estimation method for the PV panels series resistance is presented, along with a technique based on a simple model to approximate the panel MPP power in STC. Furthermore, it is shown that in case the irradiation is measured, the panel effective temperature can be estimated relatively precisely, using a simple model.

[1]Standard Test Conditions - The testing conditions to measure photovoltaic cells or modules nominal output power. Irradiance level is $1000W/m^2$, with the reference air mass 1.5 solar spectral irradiance distribution and cell or module junction temperature of 25^oC.

II. PV panel modeling for diagnostics

As mentioned previously, the diagnostic of the panel is partly based on a simple model. The general model based on the Shockley equation, which describes the current-voltage relationship of a standard Silicone-based photovoltaic cell is well known. There are many different approaches reported in the literature for applying this equation to a PV cell, with different degree of details and different types of losses considered. [4]–[8]. However, these models rely on a number of parameters, which are not directly accessible for the user/installer to measure, but they are necessary for creating a good fitting model of the PV cell/panel. There are numerous methods presented in the literature, for extracting the panel parameters ([9]–[13]), but most of them implies complicated equations, 4, 5, or more parameters to determine, and/or numerical methods to find the solutions. Keeping in mind that simple, analytic expressions are desired in case of diagnostics, in the present work a simplified model is used, where the number of parameters is reduced to 3. Starting with the four-parameter single-exponential model, where the module shunt resistance is not considered:

$$\begin{aligned} &v = V_t \ln\left(\tfrac{I_{ph}+I_0-i}{I_0}\right) - iR_s, \quad with \\ &V_t = \tfrac{n_s AkT}{q} \end{aligned} \tag{1}$$

In the above equation, the parameters have the following meaning:

- I_0 - dark saturation current (A)
- n_s - number of cells in series
- q - charge of the electron (C)
- k - Boltzmann's constant
- A - diode ideality factor
- T - temperature (K)
- I_{ph} - photo-generated current (A)

The equivalent circuit of the single-diode model for PV cells is shown on Fig. 1:

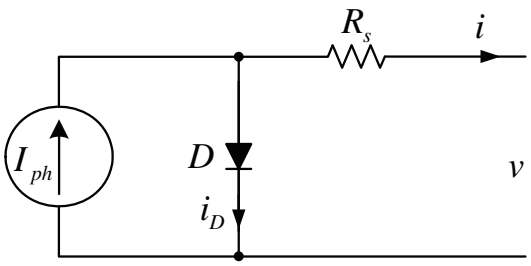

Fig. 1. Equivalent circuit of a photovoltaic cell using the single exponential four-parameter model.

For calculating the panel parameters, some simplification to equation (1) are to be made. As the dark saturation current in silicon devices is very small (and in comparison with the exponential term), it can be neglected. An other simplification, which is necessary to make, in order to obtain simpler and more easily treatable equations is approximating the photo-generated current I_{ph} with I_{sc} ($I_{ph} \approx I_{sc}$). This is a common practice to neglect the difference between the photo-generated current and the short-circuit current, as it is generally very small.

In this case (1) becomes:

$$v = V_t \ln\left(\frac{I_{sc} - i}{I_0}\right) - iR_s \tag{2}$$

Due to the above simplifications, the four-parameter model is reduced to a three-parameter model, and the equation system for determining the panel model parameters can be written as:

$$\begin{cases} V_{oc} = V_t \ln\left(\frac{I_{sc}}{I_0}\right) \\ V_{mp} = V_t \ln\left(\frac{I_{sc}-I_{mp}}{I_0}\right) - I_{mp}R_s \\ \frac{V_{mp}}{I_{mp}} = \frac{V_t}{I_{sc}-I_{mp}} + R_s \end{cases} \tag{3}$$

Where the third equation is coming from the derivative of the power at MPP. In this case it is used the derivative of P_{mp} with current.

Solving the above equation system (3) for V_t, R_s, and I_0, results in:

$$V_t = \frac{(2V_{mp} - V_{oc})(I_{sc} - I_{mp})}{I_{mp} - (I_{sc} - I_{mp}) \ln\left(\frac{I_{sc}-I_{mp}}{I_{sc}}\right)} \tag{4}$$

$$R_s = \frac{Vt \ln\left(\frac{I_{sc}-I_{mp}}{I_{sc}}\right) + V_{oc} - V_{mp}}{I_{mp}} \tag{5}$$

$$I_0 = \frac{I_{sc}}{e^{\frac{V_{oc}}{V_t}}} \tag{6}$$

The above model can be used to estimate different parameters of the panel based on measurements.

III. Series resistance monitoring

As mentioned before, the change in a panel or array series resistance indicates problems related to contacts and/or malfunctioning cells. Thereby the monitoring of this parameter can give important information about the condition of the array. It will be shown later that R_s from (5) is not the real series resistance of the panel, only a model parameter. The same conclusions were reported in [14].

For measuring the panel series resistance, the IEC 60891 standard requires two I-V curve measurement at different irradiance conditions, but at the same temperature and spectrum. The series resistance is calculated than using two working points on each characteristic. There are many alternative methods reported for measuring or estimating a PV panel series resistance. Wagner in [14] uses similar approach as the IEC 60891 standard, but using only one I-V curve. The second is simulated, using a model of the panel. Other methods use the dark curve measurements, as in [15], [16], [17]. Araujo and Sanchez in [11] use the area under the entire measured I-V curve to determine the series resistance. A number of other methods are reported as well, as in [2], [3], [9], and [10].

In this work a simple method, suitable for 'on-line' monitoring is suggested. It uses the slope of the $I - V$ curve in the vicinity of the open-circuit voltage. Similar approaches are reported in [18], but there the slope of the $I - V$ curve around open-circuit is considered the same as the R_s parameter of the model. In references [2], [9], [19] the slope of the $I - V$ curve around open-circuit is considered as an 'open-circuit resistance', and additional terms are used to calculate the series resistance.

According to the equations, the derivative of the voltage with current at open-circuit has the following form:

$$\left.\frac{dv}{di}\right|_{OC} = -\left(\frac{V_t}{I_{sc} + I_0} + R_s\right) \tag{7}$$

It has been found empirically that in case of polycrystalline silicone cells, the real series resistance of the panel can be fairly well approximated with the slope only; in this case (7) becomes:

$$\left.\frac{dv}{di}\right|_{OC} \cong -R_{sPanel} \tag{8}$$

It should be noted that R_{sPanel} is not identical to R_s. The first one is the result based on the slope of the $I - V$ curve, while the latter one is calculated based on the PV model, using datasheet values or measurements. Depending on the panel parameters, R_s can even become negative, [14] while providing good fit of the model with datasheet values. In order to test the validity of (8), a series of measurements have been done on a BPMSX120 PV panel, using a commercial photovoltaic I-V curve tracer, the PVPM 1000C. The datasheet parameters of the panel are the following:

As it can be seen on Fig. 2, both the commercial tracer and our method estimates a series resistance of approximately 2Ω.

TABLE I
PARAMETERS GIVEN IN THE PANEL DATASHEET

I_{sc}	3.87A	short-circuit current
V_{oc}	42.1V	open-circuit voltage
I_{mp}	3.56A	current at maximum power
V_{mp}	33.7V	voltage at maximum power
P_{mp}	120W	maximum power
k_v	$-160 \pm 10mV/^oC$	open-circuit voltage temperature dependence
k_i	$-0.5 \pm 0.05\%/^oC$	short-circuit current temperature dependence

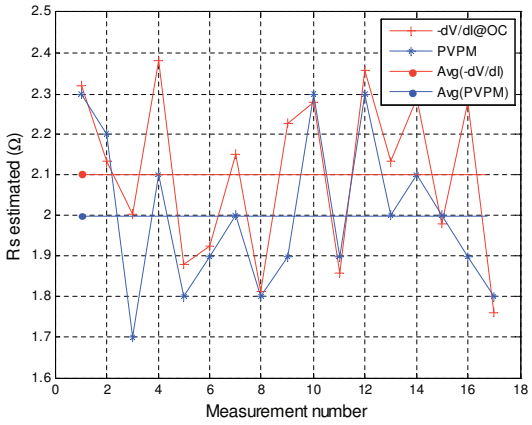

Fig. 2. Estimation of the series resistance for the BPMSX120 PV panel, using a commercial I-V curve tracer, and the slope of the voltage with current around open-circuit.

In order to verify if the above results, an additional resistance of 1Ω has been connected in series with the panel.

From the above graphs it can be seen that the method using dV/dI at open-circuit performs at least as well as the method used by the commercial tracer [14]. When connecting a 1Ω additional resistance in series with the panel, it slightly underestimates the change of resistance, while the PVPM

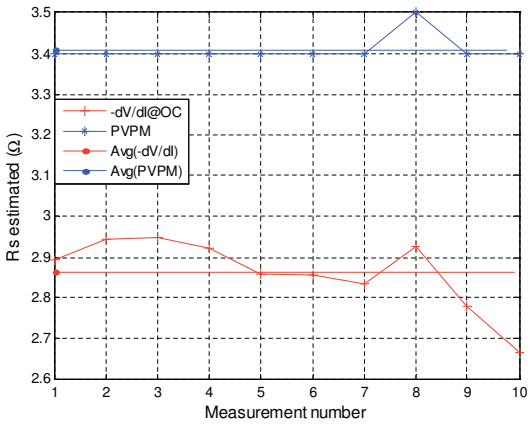

Fig. 3. Estimation of the series resistance of the BPMSX120 PV panel, in case when an additional resistance of 1Ω has been connected in series.

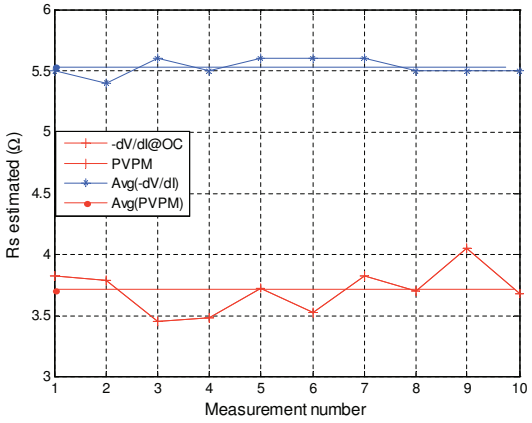

Fig. 4. Estimation of the series resistance of the BPMSX120 PV panel, in case when an additional resistance of 2Ω has been connected in series.

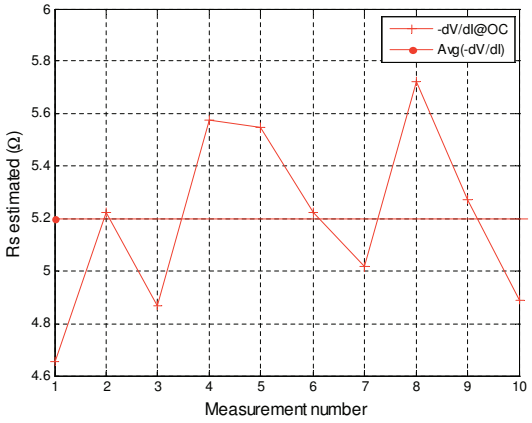

Fig. 5. Estimation of the series resistance of the BPMSX120 PV panel, in case when an additional resistance of 3.3Ω has been connected in series. In this case the commercial tracer did not calculate the series resistance, but the method based on (8) performed well.

overestimates it. As the additional resistance increases, the commercial tracer tends to overestimate the internal series resistance more strongly, while the proposed method decreases its relative error. The main advantage of the proposed method is that it does not require an entire I-V curve of the panel/array, neither a mathematical model.

IV. TEMPERATURE ESTIMATION

Another important information about the PV system state is the PV panel's temperature. Increase of the effective temperature of the modules can indicate bad ventilation, or wrongly connected modules. The temperature can have large variations over the array, therefore it is difficult to measure the array actual temperature. On the other hand, the irradiation is generally stable over the entire array (in case of residential applications, where the area of the array is not very large). The irradiation can be easily measured using a calibrated cell,

or received from satellites [20], [21].

The most affected parameter of the PV panel by temperature is generally the open-circuit voltage, which is easily accessible to measure. Thereby this quantity will be used to estimate the effective temperature of the panel

In STC, the open-circuit voltage can be written as:

$$V_{ocSTC} = V_{tSTC} \ln\left(\frac{I_{scSTC}}{I_0}\right) \tag{9}$$

The value of V_{oc} in STC is known from datasheet value. If one considers that V_t is independent on irradiation, from the above equation follows that the open-circuit voltage depends logarithmically on the irradiation:

$$V_{oc}(G) = V_{ocSTC} + V_{tSTC} \ln\left(\frac{G}{G_{STC}}\right) \tag{10}$$

Adding the temperature dependence to (10), results the expression of the open-circuit voltage in function of the actual environmental conditions, based on STC values.

$$V_{oc}(G,T) = V_{oc}(G) + k_v (T - T_{STC}) \tag{11}$$

According to the above, can be calculated the panel actual temperature, based on measurement of the open-circuit voltage and irradiance, and knowledge of the datasheet parameters, as the open-circuit voltage and its temperature coefficient.

$$T = \frac{V_{oc}(G,T) - V_{oc}(G) + k_v T_{STC}}{k_v} \tag{12}$$

It should be noted that the precision of the above estimation depends on the state of the PV panel. In case it has aged, and its parameters (especially the open-circuit voltage) are changed, the above estimation inherently introduces an error in the temperature estimation. Although in the case of the used panel, which is approximately 12 years old, the open-circuit voltage did not decrease compared to the datasheet value, the authors of the present paper did not find proof that this will not change as the panel further ages. Nevertheless, the method can be used for monitoring changes in the panel/array temperature, and warn the user/operator of the PV system if there is a large or sudden change.

V. Estimation of panel MPP power in STC

The most obvious sign of a panel/array ageing is the decrease of its MPP power. Thereby it is particularly useful to be able to estimate the panel MPP power in STC, based on the actual measurement, and compare it with datasheet values, as it is an important characteristic of the overall health state and performance of the panel/array.

Measuring the entire I-V curve of the panel, and measuring or estimating the temperature as described in the previous paragraph, the measured curve can be translated to Standard Test Conditions, as it is described in the following.

The R_s and V_t parameters by (4) and (5) can be calculated based on the actual measurements, and than translate them to STC. It is known that V_t does not depend on irradiance,

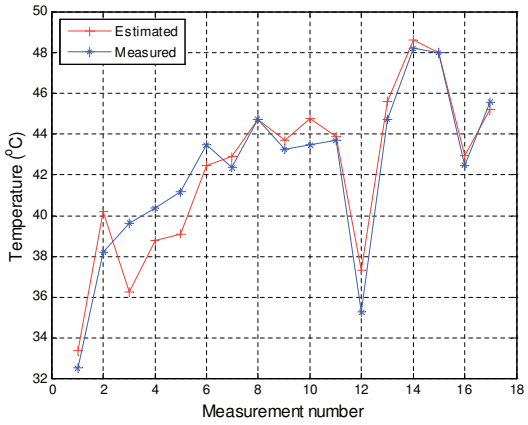

Fig. 6. Estimated and measured temperature of a BPMSX120 PV panel over 17 measurements, in natural environmental conditions. The estimations show a very good agreement with the measurements.

and it is linearly dependent on temperature. R_s on the other hand is considered independent on irradiation and temperature in this case. Taking in consideration the arguments above in paragraph V,the parameters R_{sSTC}, V_{tSTC} can be directly determined, and using similar approach as in (9), (10), and (11), also V_{ocSTC}, can be found. It is well-known that I_{scSTC} is directly proportional with irradiation, while exhibiting a slight increase with temperature, having the temperature coefficient given in datasheet. Based on the above, the following formula can be found for the voltage and current at MPP in Standard Test Conditions:

$$V_{mpSTC} = V_{ocSTC} + V_{tSTC} \ln\left(\frac{V_{tSTC}}{V_{mpSTC} + V_{tSTC}}\right) - \frac{I_{scSTC} V_{mpSTC} R_{sSTC}}{V_{mpSTC} + V_{tSTC}} \tag{13}$$

$$I_{mpSTC} = \frac{I_{scSTC} V_{mpSTC}}{V_{mpSTC} + V_{tSTC}} \tag{14}$$

It can be seen that the expression for V_{mpSTC} is transcendental, thereby no analytical solution can be found for it. Using a simple Newton-Raphson algorithm, the solution can be approximated within a few iteration, with an error smaller than $10^{-}6V$.

A. Test conditions

The measurements presented on Fig.3, 4, 5, 6, and 7 has been produced in the following conditions:

- The panel has been placed horizontally, in order to decrease the cooling by air convection and obtain a more uniform temperature over the panel surface.
- The irradiance sensor has been placed right at the edge of the panel, with the same horizontal orientation as the panel.

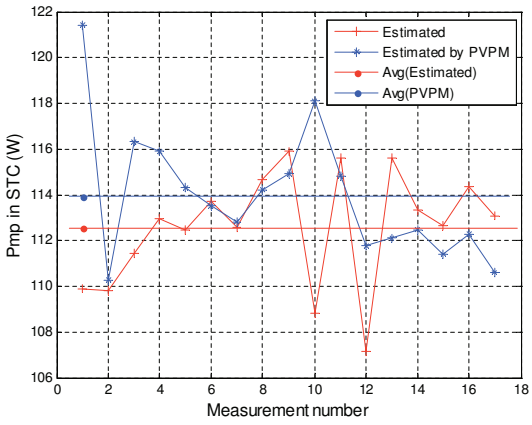

Fig. 7. Estimations of the MPP power in Standard Test Conditions, over a series of 17 measurements, in natural environmental conditions. The estimations by the commercial tracer and by this work show a good fit.

- The temperature sensor has been placed and fixed at the back of the panel, on the geometrical center
- Measurements took place at random irradiation levels, between $500 - 800W/m^2$

VI. Conclusions

Simulation and experimental measurements regarding the determination of a PV panel series resistance, its MPP power in STC, as well as its temperature, are presented in this paper. It is shown that the panel series resistance can be determined experimentally without needing to perform an entire I-V curve scan. The main advantage of the method that it does not require the sweep of the entire $I - V$ curve of the panel, or model calculations. The panel MPP power in STC and its temperature - given the irradiance is measured - can be well approximated using the measured I-V curve, and a simple model of the PV panel.

References

[1] [s.n.], "Trends in photovoltaic applications. Survey report of selected IEA countries between 1992 and 2005," International Energy Agency, Report IEA-PVPS Task 1 T1-15:2006, 2006. [Online]. Available: http://www.iea-pvps.org/products/download/rep1_15.pdf

[2] J. A. d. Cueto, "Method for analyzing series resistance and diode quality factors from field data of photovoltaic modules," *Solar energy materials and solar cells*, vol. 55, pp. 291–, 1998.

[3] ——, "Method for analyzing series resistance and diode quality factors from field data Part II: Applications to crystalline silicon," *Solar energy materials and solar cells*, vol. 59, pp. 393–, 1999.

[4] J. Bishop, "Computer simulation of the effect of electrical mismatches in photovoltaic cell interconnection circuits." *Solar cells*, vol. 25, pp. 73–89, 1988.

[5] H. Rauschenbach, "Electrical output of shadowed solar arrays," *Electron Devices, IEEE Transactions on*, vol. 18, no. 8, pp. 483–490, 1971.

[6] A. Abete, E. Barbisio, F. Cane, and P. Demartini, "Analysis of photovoltaic modules with protection diodes in presence of mismatching," in *Photovoltaic Specialists Conference, 1990., Conference Record of the Twenty First IEEE*, 1990, pp. 1005–1010 vol.2.

[7] W. Xiao, W. Dunford, and A. Capel, "A novel modeling method for photovoltaic cells," in *Power Electronics Specialists Conference, 2004. PESC 04. 2004 IEEE 35th Annual*, vol. 3, 2004, pp. 1950–1956 Vol.3.

[8] A. Burgers, J. Eikelboom, A. Schonecker, and W. Sinke, "Improved treatment of the strongly varying slope in fitting solar cell I-V curves," in *Photovoltaic Specialists Conference, 1996., Conference Record of the Twenty Fifth IEEE*, 1996, pp. 569–572.

[9] D. Chan and J. Phang, "Analytical methods for the extraction of solar-cell single- and double-diode model parameters from I-V characteristics," *Electron Devices, IEEE Transactions on*, vol. 34, no. 2, pp. 286–293, 1987.

[10] M. Chegaar, Z. Ouennoughi, and A. Hoffmann, "A new method for evaluating illuminated solar cell parameters," *Solid-state electronics*, vol. 45, pp. 293–, 2001, oK.

[11] G. Araujo and E. Sanchez, "A new method for experimental determination of the series resistance of a solar cell," *Electron Devices, IEEE Transactions on*, vol. 29, no. 10, pp. 1511–1513, 1982, nG.

[12] M. Alonso-Garcia and J. Ruiz, "Analysis and modelling the reverse characteristic of photovoltaic cells," *Solar Energy Materials and Solar Cells*, vol. 90, no. 7-8, pp. 1105–1120, May 2006.

[13] D. Sera, R. Teodorescu, and P. Rodriguez, "PV panel model based on datasheet values," *Industrial Electronics, ISIE. IEEE International Symposium on*, pp. 2392–2396, 2007.

[14] G. Kuntz and A. Wagner, "Internal series resistance determinated of only one IV-curve under illumination," in *19th Photovoltaic Solar Energy Conference Paris*, 2004.

[15] A. Kaminski, J. J. Marchand, and A. Laugier, "Non ideal dark I-V curves behavior of silicon solar cells," *Solar Energy Materials and Solar Cells*, vol. 51, no. 3-4, pp. 221–231, Feb. 1998. [Online]. Available: http://www.sciencedirect.com/science/article/B6V51-3VHSGC8-1/2/7443fcbccc5258be7ea3df950a2d8224

[16] D. King, B. Hansen, J. Kratochvil, and M. Quintana, "Dark current-voltage measurements on photovoltaic modules as a diagnostic or manufacturing tool," in *Photovoltaic Specialists Conference, 1997., Conference Record of the Twenty-Sixth IEEE*, 1997, pp. 1125–1128.

[17] E. Q. B. Macabebe and E. E. van Dyk, "Extraction of device parameters from dark current-voltage characteristics of PV devices," *Physica Status Solidi (c)*, vol. 5, no. 2, pp. 616–619, 2008. [Online]. Available: http://dx.doi.org/10.1002/pssc.200776834

[18] A. Reis, N. Coleman, M. Marshall, P. Lehman, and C. Chamberlin, "Comparison of PV module performance before and after 11-years of field exposure," in *Photovoltaic Specialists Conference, 2002. Conference Record of the Twenty-Ninth IEEE*, 2002, pp. 1432–1435.

[19] J. P. Charles, G. Bordure, A. Khoury, and P. Mialhe, "Consistency of the double exponential model with physical mechanisms of conduction for a solar cell under illumination," *Journal of Physics D: Applied Physics*, vol. 18, no. 11, pp. 2261–2268, 1985. [Online]. Available: http://stacks.iop.org/0022-3727/18/2261

[20] M. Lefvre, L. Wald, and L. Diabat, "Using reduced data sets ISCCP-B2 from the Meteosat satellites to assess surface solar irradiance." *Solar Energy*, vol. 81, pp. 240–253, 2007.

[21] C. Rigollier, L. M., and W. L., "The method Heliosat-2 for deriving shortwave solar radiation data from satellite images," *Solar Energy*, vol. 77(2), pp. 159–169, 2004.